TESIS DOCTORAL

Modelling and Structural Analysis of historical masonry systems including vaulted structure

tesis doctoral realizada por:

Yohei Endo

dirigida por:

Pere Roca i Fabregat
Luca Pelà

Barcelona, Mayo de 2015

Universitat Politècnica de Catalunya
Departament d´Enginyeria de la Construcció

Modelling and Structural Analysis of historical masonry sytems including vaulted structure

tesis doctoral realizada por Yohei Endo

Mayo ,2015

UNIVERSITAT POLITÈCNICA DE CATALUNYA
BARCELONATECH
Escola de Doctorat

Curso académico: 2014-2015

Acta de calificación de tesis doctoral

Nombre y apellidos
Yohei Endo

Programa de doctorado
Ingenieria de la Construccion

Unidad estructural responsable del programa
Departamento de Ingenieria de la construccion

Resolución del Tribunal

Reunido el Tribunal designado a tal efecto, el doctorando / la doctoranda expone el tema de la su tesis doctoral titulada "Modelling and Structural Analysis of historical masonry systems including vaulted structure"

Acabada la lectura y después de dar respuesta a las cuestiones formuladas por los miembros titulares del tribunal, éste otorga la calificación:

☐ NO APTO ☐ APROBADO ☐ NOTABLE ☐ SOBRESALIENTE

(Nombre, apellidos y firma)	(Nombre, apellidos y firma)	
Presidente/a	Secretario/a	
(Nombre, apellidos y firma)	(Nombre, apellidos y firma)	(Nombre, apellidos y firma)
Vocal	Vocal	Vocal

_____, _____ de _____ de _____

El resultado del escrutinio de los votos emitidos por los miembros titulares del tribunal, efectuado por la Escuela de Doctorado, a instancia de la Comisión de Doctorado de la UPC, otorga la MENCIÓN CUM LAUDE:

☐ SÍ ☐ NO

(Nombre, apellidos y firma)	(Nombre, apellidos y firma)
Presidente de la Comisión Permanente de la Escuela de Doctorado	Secretario de la Comisión Permanente de la Escuela de Doctorado

Barcelona a _____ de _____ de _____

This page is left blank on purpose.

Modelling and Structural Analysis of historical masonry systems including vaulted structure

tesis doctoral realizada por:
Yohei Endo

dirigida por:
Pere Roca i Fabregat
Luca Pelà

This page is left blank on purpose.

ACKNOWLEDGEMENTS

First of all, I would like to express the deepest appreciation to my supervisor Professor Pere Roca, who has shown the attitude and the substance of a genius: he continually and persuasively conveyed a spirit of adventure in regard to research, and an excitement in regard to teaching. Without his supervision and constant help this dissertation would not have been possible. I also would like to show my gratitude to my co-supervisor Dr Luca Pelà, who helped me out to deepen my understanding on numerical analysis and seismic assessment of historical structures.

I would like to thank my committee members, Dr. Climent Molins, Dr. Miquel Llorens and Dr. Ignacio Lombillo, whose work demonstrated to me that concern for global affairs supported by an engagement in comparative literature and modern technology, should always transcend academia and provide a quest for our times.

I thank Dr. Miquel Llorens for providing me valuable information on vaults of Hospital Sant Pau, as allowed us to conduct the study that comprises large part of the present research. In addition, I like to add a thank you to my colleague Ahmed Elyamani, who gave me tutorial of structural-analysis software, DIANA. I also would like to thank a past MSc SAHC student, Juan Arias who helped me for the study of one of vaults of Hospital Sant Pau. I would like to say thank you to a past master student from University of Padova, Alice de Conti, who carried out the study of San Marco church, as has provided useful information to us. I was grateful to attend NIKER project. It not only provided significant knowledge on the seismic assessment of a large-scale church and also made this thesis possible. I would like to show appreciation to the dance school, Seven Dance that has taught me the heart of Latin dance and that also has provided me strong moral support. In the end, I want to thank Nishihara Cultural Foundation, from bottom of my heart, for their financial support throughout this PhD research.

This page is left blank on purpose.

ABSTRACT

The conservation of historic structures has been given special attention due to their cultural, social and economic importance. However they often show considerable structural vulnerability and have been seriously damaged by natural disasters including earthquakes. An excessive loss of architectural heritage has occurred because of earthquakes. A safety assessment and restoration practice on historical structures has been tackled extensively by professionals including architects and engineers. However, structural assessment of historical buildings is a complex task. Complexity comes from insufficient understanding of the characteristic of historical materials, limited knowledge of the seismic response of historical structures and yet-unknown structural deterioration due to the past natural disasters.

Today it is perceived that nonlinear FEM analysis permits detailed study of historical masonry structures. However, in some cases, its application poses difficulties. The difficulties derive from the definition of material properties, the definition of a complex geometry and the analysis procedures. The results depend on the material properties considerably. However, it is not easy to describe appropriately the behaviour of historical materials including masonry in the FEM analysis. The definition of a complex geometry is challenging although the discretisation of accurate geometry is crucial. As for the analysis procedure, one of the difficulties is observed in seismic assessment. FEM-based nonlinear dynamic analysis permits close observation of seismic response of a historical masonry structure but it requires excessive computational effort, for a large-scale structure in particular. On the other hand, pushover can be adopted more efficiently than nonlinear dynamic analysis but the obtained result can be less reliable. All these considerations indicate that the understanding of FEM approaches still needs to be deepened to adopt more accurately and at the same time efficiently for the analysis of historical structures.

The present research discusses the applicability of existing nonlinear FEM approaches to the study of masonry historical structures. The FEM analysis is adopted to the analysis of real and complex structures including mixed steel and masonry vaulted systems belonging to the Hospital de Sant Pau in Barcelona and a large single-nave church damaged by the 2009 Abruzzo earthquake. As a final outcome of the research, the conclusions provided criteria and guidelines for the analysis of these types of structures under vertical loading and seismic forces. The achievement of the research will contribute to both engineers and researchers who are involved in the conservation of historical masonry structures especially by means of FEM analysis.

This page is left blank on purpose.

TABLE OF CONTENTS

This page is left blank on purpose.

TABLE OF FIGURES

LIST OF TABLES

This page is left blank on purpose.

1. INTRODUCTION AND OBJECTIVES

1.1 Introduction

Historic environment such as World Heritage Sites is a central piece of the cultural heritage and great effort has been paid for its conservation. Attractive historic environment draws not only local people but also tourists from all over the world. Thus, today the significance of historic environment is recognised in cultural, social and economic terms. The conservation of historical structures has been given particular attention since they are one of the most principal components of historic environment. However they often show significant structural vulnerability and have been seriously damaged by natural disasters such as earthquakes. In Europe, Friuli, Italy (1976), Athens, Greece (1999) and Abruzzo, Italy (2009) earthquakes have caused a significant loss of architectural heritage. A wide range of safety assessment and restoration practice on historical structures has been tackled by architects, engineers and other professionals. Nevertheless, structural assessment of historical buildings is a complex task. Complexity derives from insufficient understanding of the characteristic of historical materials, limited knowledge of the seismic response of historical structures and yet-unknown structural deterioration due to the past natural disasters.

The consequences of the above-mentioned earthquake in Abruzzo were considered in a European research project, the NIKER project, conducted between 2010 and 2012. Through the project, a new unified methodology was envisaged, oriented to the design of structurally effective and cost-efficient structural seismic protection techniques. Such methodology was aimed to improve the safety level while preserving the artistic and architectural values of the buildings. One of the case studies considered within the present thesis, San Marco church, has been suggested by the works carried out for the NIKER project.

Today it is recognised that nonlinear FEM analysis permits detailed study of historical masonry structures. However, in some cases, its application poses significant difficulties. The difficulties derive from the definition of material properties, the definition of a complex geometry and the analysis procedures. In addition, results of the analysis may be highly influenced by the adopted material properties. It is not straightforward to describe appropriately the behaviour of historical materials including masonry in the FEM analysis. The definition of a complex geometry such as a double-curvature vault is challenging task. In particular, accurate description of the real geometry is essential in order to obtain realistic results. As for the analysis procedure, one of the difficulties is seen in seismic assessment. FEM-based nonlinear dynamic analysis permits close observation of seismic response of a historical masonry structure but it requires very large and often prohibitive computational effort, particularly for large-scale structures. On the other hand, pushover analysis requires significantly less effort than nonlinear dynamic analysis, but the result obtained from pushover is in some cases

insufficiently accurate. All these considerations indicate that, in spite of the availability of sophisticate numerical methods for the study of masonry structures, their practical utilization and applicability to real historical structures is still in need of research and practical experience. Specifically, a mode deep understanding is needed on the more adequate approaches than can be applied to obtain a satisfactory compromise between efficiency and realism.

The present research discusses the applicability of nonlinear FEM approaches to historical masonry structures. The applicability is examined through the study of the structural performance of different masonry systems, including single and double-curvature vaults and large church-type structures, under vertical and seismic loads. The research aims to provide criteria and guidelines for an efficient but sufficiently accurate analysis of historical masonry structures. The research is intended to provide criteria useful for structural analysis to both engineers and researchers involved in the analysis of historical masonry structures.

1.2 Purpose of the thesis

1.2.1 General objective

The general objective of the present research has consisted on the analysis of the applicability of prevalent nonlinear FEM approaches to the study masonry vaulted structural systems. The objective is attained through the application of the FEM approaches to the study of real and complex cases including, in particular, a mixed steel and masonry vaulted system (a pavilion of Hospital de Sant Pau in Barcelona) and a church damaged by a recent earthquake (Church of San Marco in L'Aquila). The numerical methods applied have been chosen among already available advance numerical tools as a compromise of efficiency and accuracy. The study of the selected set of cases is intended to allow the derivation of criteria and guidelines for the application of such approaches to the analysis of historical vaulted masonry structures subjected to gravity and seismic forces.

1.2.2 Specific objectives

The following specific objectives have been considered as a way to achieve the aforementioned general aim:

- Carry out a research of the state-of-art on the different topics relevant for the present research. The topics include masonry mechanical properties, the typology of vertical elements and vaults, structural-analysis techniques and seismic-assessment tools.
- Identify the numerical-analysis strategies to be adopted for the analysis of masonry structures within the present research including geometry modelling approaches, material models and iterative techniques. The techniques to be chosen should provide a satisfactory compromise between efficiency and accuracy in their application to the analysis of large masonry structures.

- Identify appropriate case studies allowing the application of the chosen numerical approaches. The choice will cover different types and scales of structures including vaulted and large-scale church-type structures.
- Apply the chosen numerical approaches to the selected case studies in order to carry out a detailed analysis of their structural response and resistance under different actions, including overloads (in the case of vaulted structures) and earthquake (in the case of the church-type structures).
- Carry out detailed parametric studies using systematically the chosen numerical tools and elaborated numerical models in order to obtain a better insight on the structural response of the selected case studies along with the influence of different mechanical parameters. This study is also aimed to investigate the applicability, efficiency and reliability of the adopted numerical tools.
- More specifically, investigate the applicability, efficiency and reliability of different seismic assessment tools, including limit kinematic analysis and FEM-based approaches such as pushover and nonlinear dynamic analysis.
- Draw conclusions on the applicability and reliability of modeling tools and analysis strategies for the assessment of different types of masonry historical structures under gravity loads and earthquake. Provide general guidelines for an efficient but sufficiently accurate analysis of similar structures. More specifically, provide guidelines on the definition of the geometry, the analysis procedures, the definition of the mechanical properties and other related aspects.

1.2.3 Summary

The work to be carried out in each chapter is presented. In Chapter 1, the general and specific objectives of the present research have been presented. In Chapter 2, the state of art is discussed on masonry mechanics, masonry typologies, structural analysis techniques and seismic assessment tools. In Chapter 3, numerical strategies are discussed regarding FEM modelling and FEM-analysis strategy. The discussions included in Chapter 2, 3 are considered in order to lay-out the studies presented in Chapters 4, 5, 6. In Chapter 4, the FEM analyses on three simple models, including a single Catalan vault supported by two parallel walls is presented. The study covers the parametric study on some of mechanical and FEM mesh parameters and a comparison of seismic assessment tools including pushover and nonlinear dynamic analysis. The findings from this chapter are taken into account for the determination of mechanical parameters and choices of seismic assessment tools for the studies presented in Chapter 5 and 6. In Chapter 5, a selection of Catalan vaults of the pavilions of Hospital Sant Pau in Barcelona are studied. The structures belong to the Santa Maria de la Mercè and the Administration pavilions of the Hospital. The analysis of these structures is rather challenging due to the existing combination of masonry thin-tile vaults and steel profiles. In Chapter 6, the seismic assessment of San Marco church is presented and the results are compared the damage observed in the real structure after the 2009 L'Aquila earthquake. The study focuses on the comparison of seismic assessment tools and the influence of different parameters, with focus on the mechanical parameters of masonry. In this chapter, suggestions for FEM analysis of historical masonry structures are discussed.

As a conclusion from the present research, Chapter 7 provides suggestions for the lay-out of FEM analyses on large historical masonry structures. In the chapter, recommendations for the further research are also discussed.

2. STATE-OF-ART DISCUSSION

2.1 Masonry Mechanics

The word “masonry” denotes a general term that applies to construction using hand-placed units of clay, concrete, structural clay tile, glass block and natural stones (International Code Council 2012). One or more types of masonry units are bonded together with mortar, metal ties, reinforcement and accessories to shape walls and other structural elements. Masonry construction started to be used at least 10,000 years ago for different types of structures such as houses, private and public buildings and historical monuments. One of the earliest monumental public buildings (a massive stone tower) appeared in the Neolithic in Jericho, around 8,000 BC (Wright 2009). The first monumental earth/brick building was constructed in Mesopotamia during 5000 BC. Masonry buildings have been constructed with the materials chosen according to building types, availability, and also the wealth of owners. In this section, masonry mechanics is reviewed. Firstly, the material properties of masonry are discussed. Then, the structural behaviour of masonry under different loading conditions is discussed.

2.1.1 Mechanical properties

Masonry is a composite material in which individual units (stones, bricks or blocks) are embedded in mortar (Macdonald 2007). Mechanical properties of masonry are diversified due to the variety of types of constituent (unit and mortar joint).

In the case of masonry with stone units, all kind of stones have been used (igneous, metamorphic and sedimentary) (Grieve 2008). Among them, sedimentary rocks (specifically sandstones and limestones) have been frequently employed. Bricks shaped usually of fired clay are typically used although those made from dried clay are also utilised in Mediterranean and other countries of hot and dry climate (Adam 1993). The strength of the bricks is influenced by the purity of the clay and the firing temperature (D’Ayala 2004).The mortar joints are prepared by mixing an aggregate, slacked lime or clay, any appropriate additive and water (Grieve 2008). In modern times, portland cement is more widely used. The principal structural function of mortar joints is to connect units together (Macdonald 2007). Mortar joints also prevent concentration of stresses in masonry and distribute compressive stress uniformly (International Code Council 2012). The compressive and bonding strength of the mortar is determined by the proportion of bonding agent/s to sand (D’Ayala 2004).

Mechanical properties of masonry are reviewed through comparison of codes, guidelines and experimental studies carried out by researchers. Codes of Europe, Spain and Italy are referred (CEN 1996, PIET 70 1971, Italian ministry of transport and infrastructure 2009).

2.1.1.1 Mechanical parameters of masonry

The compressive behaviour of masonry is crucial for design and safety evaluation of masonry structures since they are principally stressed in compression (Pina and Lourenço 2006). For instance, in Eurocode 6 (CEN 1996) and Masonry Standards Joint Committee (MSJC) (2002), the compressive strength of the components (unit and mortar) is used to determine the strength of masonry as discussed below.

2.1.1.1.1 Compressive strength

PIET 70 (1971) presents a set of the values of design compressive strength for clay brick masonry and stone masonry, considering the type of unit and mortar. The thickness and consistency of mortar are also taken into account. So as to obtain the characteristic value, the calculation values have to be multiplied by a reduction factor equal to 2.5. For the brick masonry, the presented lowest value is equal to 0.4 MPa and the highest is 5.5 MPa. The former case is composed of hollow clay brick of 2.94 MPa and 1.5 cm lean mortar of M-5 (0.5 MPa). The latter case is composed of solid clay brick of 29.4 MPa and 1 cm fat mortar of M-160 (15.7 MPa). As for the stone masonry, the lowest value is 0.59 MPa and the highest one is equal to 5.9 MPa. The former is sandstone of height of height less than 30 cm and mortar type of M-5. The latter is composed of granite of height more than 30 cm and mortar type of M-80 (7.9 MPa).

In Italian ministry of transport and infrastructure (2009), the values of average compressive strength are presented on the basis of the visual appearance of masonry. For the masonry of solid brick with lime mortar, the lowest value is equal to 1.8 MPa and the highest value is 2.8 MPa. For the stone masonry, the lowest value is equal to 0.6 MPa (rubble stone masonry) and the highest value is 4 MPa (ashlar stone masonry).

On the other hand, different empirical equations have been proposed to determine $f_{ck,}$ the characteristic value of compressive strength of masonry. The equation (2.1)

$$f_{ck} = K * f_b^{0.7} * f_j^{0.3} \ (MPa) \tag{2.1}$$

where:

K is the material factor (0.45 for the sized natural stone and 0.5 for solid brick masonry)

is presented by Eurocode 6 (CEN 1996). Jäger and Pech (2014) made discussion on this equation regarding the methodology and underlying mathematical basis for the anticipated update and adaptation of Eurocode 6 (CEN 1996), comparing with equations presented by other researchers. For instance, referring to Brameshuber et al. (2012), the authors suggested that the material factor, K is to be reduced by 80% for better estimation of characteristic compressive strength of masonry. Geoff (2014) presented different values of experimentally determined compressive strength of bricks, mortar

and masonry, referring to shape factors of units. Then he compared experimentally obtained f_{ck} with ones calculated by means of the equation (2.1) from Eurocode 6 (CEN 1996). As a result, he mentioned that the gradient of the best fit straight line to the two data between experiments and calculated values is 0.92 (Figure 2.1).

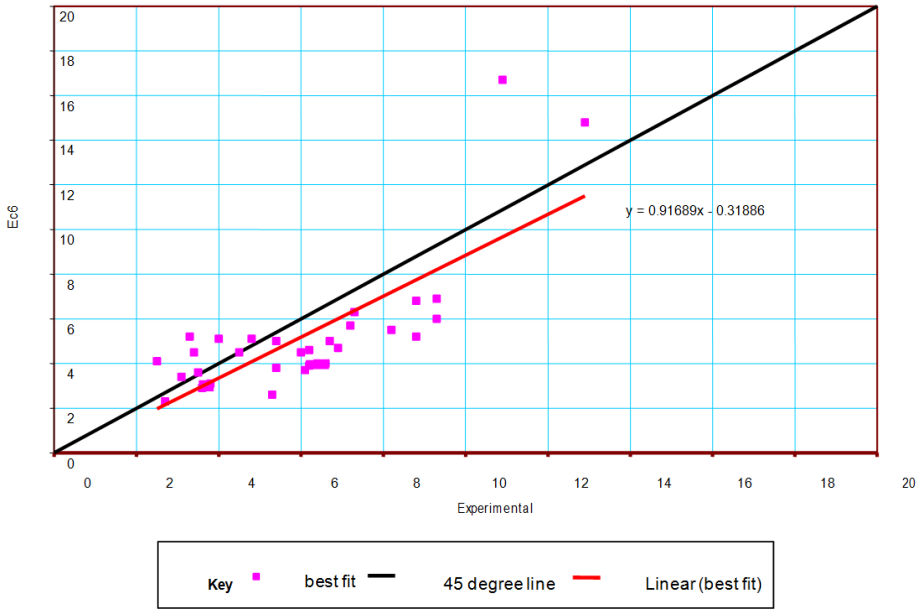

Figure 2.1 - Characteristic compressive strength (Eurocode 6) vs. experimental value (Geoff 2014).

Liberatore et al. (2014) discussed estimation of clay-brick masonry compressive strength based on mortar and unit mechanical parameters. Equations provided by European (CEN 1996) codes and investigators were discussed. Then, the authors presented a set of articles that provide values of compressive strength of masonry, mortar and bricks together with mortar bed joint thickness/ unit height ratio, Young's modulus and the tensile strength of units. They were adopted to the previously-discussed equations. As a result, while the equations show a significant scatter, it was found that some of them seem more appropriate than the others. According to the authors, Eurocode 6 (CEN 1996) provides more suitable results than the other equations.

Dayaratnam (1987) carried out experimental studies on hollow structural clay tiles, and proposed equation (2.2).

$$f_{ck} = 0.275 * f_b^{0.5} * f_j^{0.5} \ (MPa) \tag{2.2}$$

Kaushik (2007) proposed an equation (2.3)

$$f_{ck} = 0.63 * f_b^{0.49} * f_j^{0.32} \ (MPa) \tag{2.3}$$

on the basis of the experiments carried out by the authors. According to the authors, it consistently describes well behaviour of masonry prisms made with low and average compressive strength bricks.

Bennett et al. (1997) suggested that the characteristic strength of a brick masonry prism is conservatively estimated to be 3/10 of the brick compressive strength, using experimental results on hollow structural clay tiles.

A calculation method of effective compressive strength of a masonry specimen presented by Mosalam (2009) is discussed in Section 2.1.2.2.1.

2.1.1.1.2 Tensile strength

Italian ministry of transport and infrastructure (2009) provides average tensile strength, according to visual appearance of masonry.

In Italian ministry of transport and infrastructure (2009), the values of average tensile strength are presented on the basis of the visual appearance of masonry. For the masonry of solid brick with lime mortar, the lowest value is equal to 1.8 MPa and the highest value is 2.8 MPa. For the stone masonry, the lowest value is equal to 0.6 MPa (rubble stone masonry) and the highest value is 4 MPa (ashlar stone masonry).

Considering the values of average compressive strength in the same code as presented in Section 2.1.1.1.1, the ft/fc ratio is equal to 3.4 % for rubble stone masonry, 2.5 % for ashlar stone masonry and 3.3 % for solid brick masonry. Eurocode 6 (CEN 1996) states that tensile strength is not a property normally considered in design process although it can be developed in masonry. Compared to characterisation of compressive strength of masonry, few experimental studies have been carried out on the tensile strength (Backers 1985, Page 1981, 1983, Plujim 1997). The experiments carried out by these authors are discussed in Section 2.1.2. On the other hand, tensile strength of bricks (Schubert 1988, Vermeltfoort 2005, McNary 1985), stones (Augenti and Parisi 2010) and mortar (Suter 1998) has been studied experimentally more widely than that of masonry.

2.1.1.1.3 Young's modulus

Italian ministry of transport and infrastructure (2009) provides the values of average Young's, modulus according to visual appearance of masonry. For the masonry of solid brick with lime mortar, the lowest is 1800 MPa and the highest value is 2400 MPa. As for the stone masonry, the lowest is 690 MPa (rubble stone masonry) and the highest value is 2820 MPa (rectangular ashlar stone masonry).

In Eurocode 6 (CEN 1996) under service conditions and for use in the structural analysis, values are presented as the relationship between masonry compressive strength and Young's modulus as seen in the equation (2.4).

$$E=1000f_{c,}\,(MPa) \tag{2.4}$$

where:

E is the Young's modulus of masonry

In PIET 70 (1971), values are presented as the relationship between masonry compressive strength and Young's modulus as seen in the equation (2.5)

$$E=0.8\alpha f_c\,(MPa) \tag{2.5}$$

where:

α is the coffeicient for Young's modulus

under service conditions. For the calculation of the limit of the resistant capacity instead of equation (2.5), the below equation (2.6)

$$E=0.5\alpha f_c\,(MPa) \tag{2.6}$$

is considered.

For the value of α, for brick masonry, the lowest value is 1125 (hollow brick with mortar of M-5) and the highest is 2500 (solid brick with mortar of M-160 or M-40). For stone masonry, the lowest value is equal to 1125 (rubble stone with mortar type of M-5) and the highest is 3000 (ashlar stone with mortar type of M-160 or M-40).

As a result of monotonic compressive tests on solid clay brick masonry, Kaushik (2007) drew the equation (2.7)

$$E=550f_c\,(MPa) \tag{2.7}$$

to obtain Young's modulus.

2.1.1.1.4 Poisson Ratio

Very few research contributions are found regarding the Poisson ratio of masonry. Augenti and Parisi (2010) acquired the Poisson ratio through monotonic uniaxial compression tests on tuff masonry. A compressive loading was applied along the direction orthogonal or parallel to the bed joint. The value equal to 0.22 (orthogonal) and 0.24 (parallel) were observed as Poisson ratio at one-third of the peak strength. Binda et al. (1998) obtained the Poisson ratio through a flat jack test on brick masonry of Monza bell tower, Italy. The resulted values were between 0.07 and 0.19. A value between 0.1 and 0.2 is suggested as input for numerical analysis (Boothby et al. 2006).

2.1.1.1.5 Shear strength and shear modulus

Italian ministry of transport and infrastructure (2009) presents the value of shear average strength. For the masonry of solid brick with lime mortar, the lowest is 0.06 MPa and the highest value is equal to 0.092 MPa. As for the stone masonry, the presented lowest value is 0.02 MPa (rubble stone masonry) and the highest one is 0.098 MPa (ashlar stone masonry).

Eurocode 6 (CEN 1996) presents the following equation (2.8)

$$f_{vk} = f_{vko} + 0.4\sigma_d \, (MPa) \tag{2.8}$$

where:

f_{vko} is the characteristic initial shear strength, under zero compressive stress

σ_d is the design compressive stress perpendicular to the shear

to estimate the characteristic shear strength, f_{vk} of masonry.

The value of f_{vk0} is between 0.15 and 0.3 MPa. The value of f_{vk} has to be less than the value defined by $0.065 f_b$ or the limit value. The limit value is between 1.0-1.7 MPa according to the type of unit and mortar.

Vasconcelos and Lourenço (2009) investigated the characterisation of the composite behaviour of masonry materials used for the stone masonry walls by means of direct shear tests and uniaxial compressive tests. As a result, for old masonry with weak mortars, a value of 0.05-0.1 MPa is recommended for f_{vk0}. The tangent of the friction angle (multiplier of σ_d) should be reduced to 0.3 (irregular coursed stone) and 0.2 (rubble masonry).

Italian ministry of transport and infrastructure (2009) also presents the values of average shear modulus. For the masonry of solid brick with lime mortar, the lowest is 300 MPa and the highest value is 880 MPa. As for the shear modulus of stone masonry, the lowest is 115 MPa (rubble stone masonry) and the highest value is 470 MPa (rectangular ashlar stone masonry).

In Eurocode 6 (CEN 1996) and MSJC (2002), the shear modulus, G is associated with Young's modulus as seen in the equation (2.9).

$$G=0.4E\ (MPa) \tag{2.9}$$

2.1.1.1.6 Compressive and tensile fracture energy

For characterisation of compressive fracture energy, Augenti and Romano (2007) carried out compression test in the orthogonal/parallel direction of the mortar joints on specimens of tuff masonry. The former test presented 13.16 N/mm and the latter test 7.48 N/mm. Olivito and Stumpo (2001) carried out a test on brick masonry composed of different brick layer (one or two layers) and types of mortar (M-2 [8 MPa] or M-4 [2.5 MPa] according to Italian Ministry of Public works [1987]). As a result, compressive fracture energy is obtained between 1.58 and 3.23 N/mm. As for tensile fracture energy, not so many experimental studies can be found as that of compressive fracture energy (Plujim 1997). The experiment carried out by Plujim (1997) will be discussed in Section 2.1.2.1.1. On the other hand, tensile fracture energy of bricks (Plujim 1992, 1997) and stones (Lourenço et al. 2005) has been studied experimentally more widely than that of masonry.

2.1.2 Structural behaviour

In this section, the behaviour of unit-mortar interface and of masonry as composite material is reviewed respectively. For the behaviour of unit-mortar interface, tension mode (mode I) and shear mode (mode II) are discussed. For the behaviour of masonry, behaviour under uniaxial compression or tension and under biaxial compression/tension is reviewed.

2.1.2.1 Behaviour of unit-mortar Interface

Interface between a unit and a mortar joint is a crucial component of masonry (Mosalam 2009). It may dominate the behaviour of masonry under a loading in certain directions, such us pure tension normal to joint and pure shear parallel to joint. Different shear and tensile loading conditions lead to distinctive failure modes. The corresponding failure modes are individually discussed in this section.

2.1.2.1.1 Tension mode (Mode I)

Tensile strength at the interface is influenced by chemical bond that depends on the absorption rate of the unit. Higher absorption rate causes lower bond strength.

The effective tensile bond strength at the interface due to uniaxial tension can be described by equation (2.10) (Mosalam 2009).

$$f_t = F_u / A_n \ (MPa) \tag{2.10}$$

where:

F_u is the ultimate axial tensile force

A_n is the net bonded area

The net bonded area (A_n) is normally smaller than the whole cross-sectional area of the unit due to the shrinkage of mortar and also the laying process of the units and is centred in the middle of the unit (Figure 2.2).

Figure 2.2 - Typical tensile bond surface (Plujim 1997).

As a result of a displacement control test as shown in Figure 2.3 a, Plujim (1997) presented an experimental tension softening curve for the mode I with fracture energy ranging from 0.005 to 0.02 N/mm for tensile bond strength of 0.3 to 0.9 N/mm^2 (Figure 2.3 b).

Lourenço et al. (1995) described the descending branch of the interface with the following equation (2.11).

$$\frac{\sigma}{f_t} = \exp\left(-\frac{f_t}{G_f^I} w_n\right) \tag{2.11}$$

where

G_f^I is the tensile (Mode I) fractural energy

w_n is the crack band width

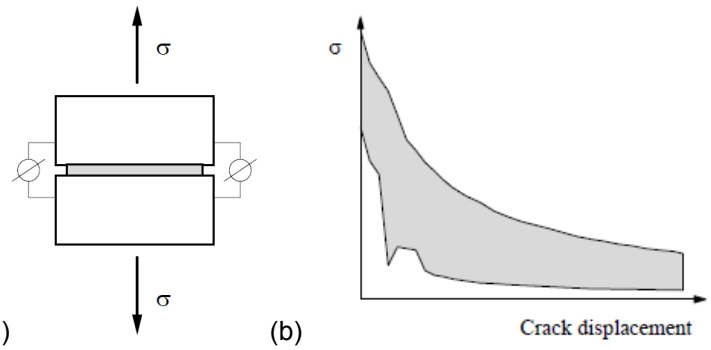

Figure 2.3 - Tensile bond behaviour of masonry: (a) test specimen (direct tension) and (b) stress-displacement relationship given by the experimental study (Plujim 1997).

This equation provides good approximation to the previously-mentioned test results by Plujim (1997).

2.1.2.1.2 Shear mode (Mode II)

Shear strength at the interface is influenced by two factors. The first one is the friction caused by the asperity of the surface between joint and unit. The second is chemical bond between joint and unit (Mosalam 2009). Plujim (1993) carried out the characterisation of the shear behaviour for solid clay and calcium-silicate units through experiments (Figure 2.4)

Based on these results, Lourenço et al. (1995) proposed expression (2.12)

$$\frac{\tau}{c} = \exp\left(-\frac{c}{G_f^{II}} w_s\right) \tag{2.12}$$

where:

c is the cohesion at the interface

G_f^{II} is the shear (Mode II) fractural energy

w_s is the shear crack width

to model the softening behaviour under shear as a relationship between the shear stress and the shear crack width.

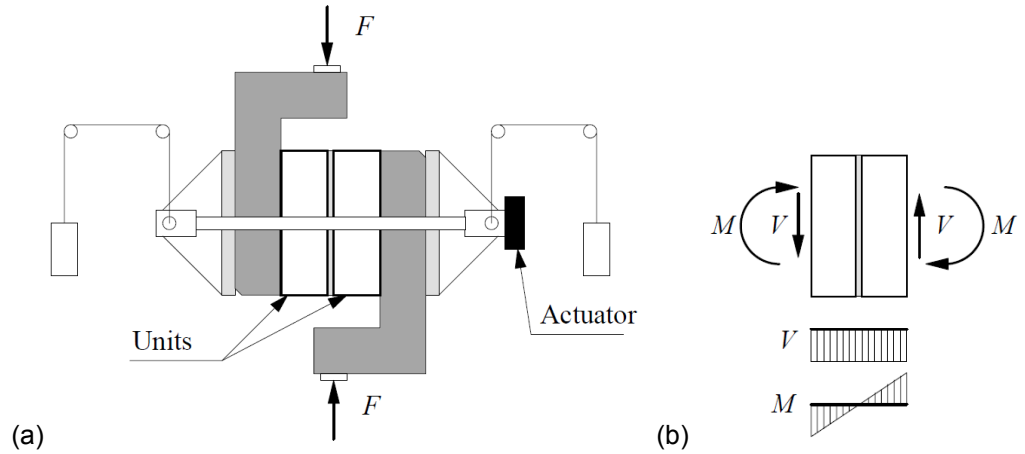

Figure 2.4 - Test set-up to obtain shear bond behaviour: (a) test specimen ready for testing and (b) forces applied to the test specimen during testing (Plujim 1993).

The Mode II fracture energy (G_f^{II}) is equal to the area under the curve showing the relationship between shear displacement and the residual dry friction shear level (Figure 2.5 a). Plujim (1993) found that the value of G_f^{II} is between 0.01 and 0.25 Nmm/mm^2 for an initial cohesion c of a value between 0.1 and 1.8 N/mm^2.

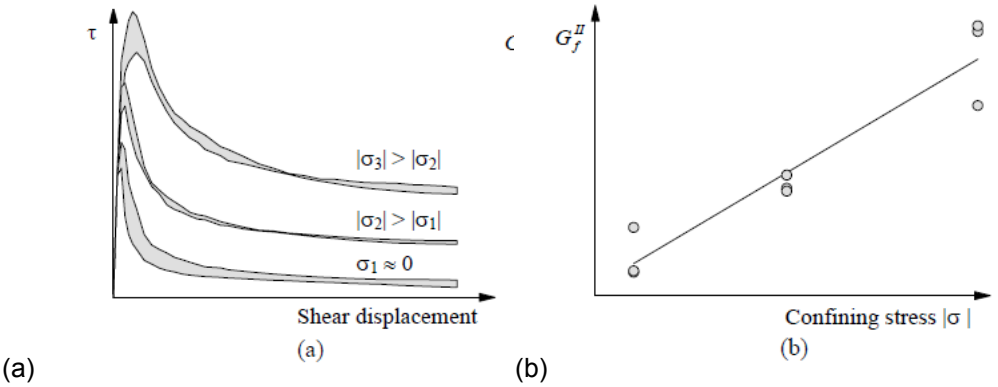

Figure 2.5 - Typical shear bond behaviour of the joints for solid clay units: (a) stress-strain relationship for varied normal stress levels and (b) mode II fracture energy G_f^{II} as a function of the normal stress level (Plujim 1993).

Figure 2.5 b indicates that G_f^{II} is related to the level of confining stress. In Figure 2.6 a, the initial and residual internal friction angle (ϕ_0 and ϕ_r, respectively) associated to the Mohr-Coulomb frictional model is indicated. The value of tan ϕ_0 lays normally between 0.7 to 1.2. The tangent of ϕ_r is normally close to 0.75. The dilatancy angle ψ is defined in Figure 2.6 b. The dilatancy angle is found to be proportional to the confining stress (Figure 2.7 a). In average, the value of tangent of the dilatancy angle results in between 0.2 and 0.7, depending on the unit-surface roughness. Due to either high pressure or increasing slip, tan ψ may be reduced to 0 (Figure 2.7 b). Increasing compression restricts the uplift of bricks while increasing slip grinds down the asperities at the interface.

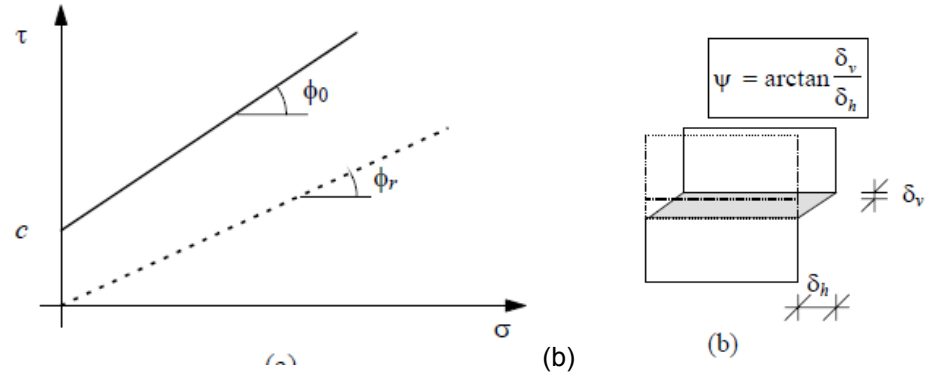

Figure 2.6 - Definition of friction and dilantancy angles: (a) Coulomb friction law, with initial (tan ϕ_0) and residual friction angle (tan ϕ_r) and (b) dilantancy angle from the uplift of adjacent units upon shearing (Lourenço 1998).

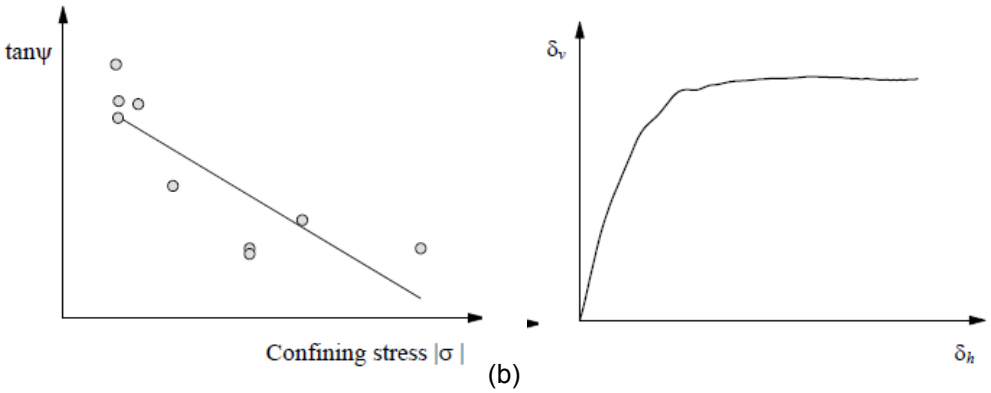

Figure 2.7 - Typical shear bond behaviour of the joints for solid clay units: (a) relation between dilantancy-angle and the level of the confining stress and (b) relation between the normal and shear displacement upon loading (Plujim 1993).

2.1.2.2 Behaviour of masonry as composite material

2.1.2.2.1 Uniaxial compression behaviour

Since the pioneering work by Hilsdorf (1969), it has been generally accepted that the failure of masonry under uniaxial compression is strongly influenced by the difference in elastic properties of units and mortar (Lourenço 1998). Uniaxial compression to masonry causes tri-axial compression in joint and uniaxial compression and biaxial tension in the units as seen in Figure 2.8. Therefore, under uniaxial compression the compressive strength of masonry is influenced by the tensile strength of units. According to Mosalam (2009), the Young's modulus, the Poisson ratio and the thickness of joints and units are also influential on the compressive strength of masonry under uniaxial compression. For the calculation of the compressive strength of masonry, Pande et al. (1994) proposed the following equation (2.13).

$$f_c = \frac{f_t^b}{S_f}\frac{A_n}{A_g} \tag{2.13}$$

where:

f_t^b is the tensile strength of brick unit

S_f is the stress factor (a function of elastic constants and thickness of mortar and units)

A_n is the net sectional area (unit)

A_g is the gross area of (unit)

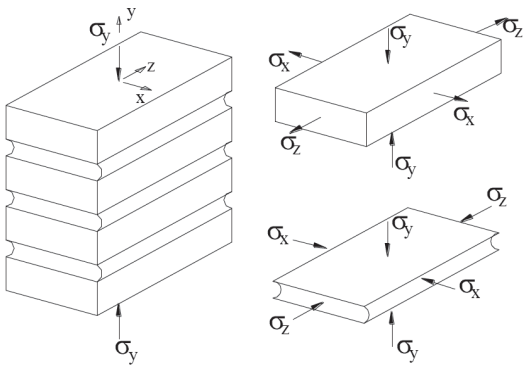

Figure 2.8 - Uniaxial compression mechanism (Mosalam 2209).

Strength and deformation of clay-unit masonry under a uniaxial compressive concentrated load were experimentally studied by McNary and Abrams (1985). The equation (2.14)

$$\Delta\sigma_{xb} = \frac{\Delta\sigma_y[v_b - \frac{E_b}{E_m(\sigma_1,\sigma_3)}v_m(\sigma_1,\sigma_3)]}{[1+\frac{E_b}{E_m(\sigma_1,\sigma_3)}\frac{t_b}{t_m} - v_b - \frac{E_b}{E_m(\sigma_1,\sigma_3)}\frac{t_b}{t_m}v_m(\sigma_1,\sigma_3)]} \quad (2.14)$$

where:

t_b, t_m is the thickness of brick and bed joint

$\Delta\sigma_{xb}$ is the increment of lateral stress in the brick

v_b, is the Poisson ratio of brick

E_b, is the Young's modulus of brick

$v_m(\sigma_1, \sigma_3)$ is the Poisson ratio of the mortar as a function of principal stresses

$E_m(\sigma_1, \sigma_3)$ is the Young's modulus of the mortar as a function of principal stresses

describes an increment of lateral stresses in a brick, $\Delta\sigma_{xb}$ which is caused by an increment of compressive stresses, $\Delta\sigma_y$. Lateral stress in the brick is expressed in a function of material properties of the brick and joint. The Poisson ratio v_m, and Young's modulus of the joint E_m are expressed in a function of the vertical stress, σ_1 and the lateral stress, σ_3.

Failure modes under uniaxial compression also depend on the types of joint (Mosalam 2009). In Figure 2.9 a, compressive strength of type M lime mortar is 17.2 MPa, type S=12.4 MPa, type N=5.2 MPa, type

O=2.4 MPa, as specified by ASTM C270 (2007). In Figure 2.9 b, for masonry prisms of solid soft mud brick is used. f_{mo} denotes the compressive strength of joint. The strength of mortar is $f_{mo,1} < f_{mo,2} < f_{mo,3}$. Both two figures indicate that strong mortar induces a more brittle failure while weak mortar causes ductile failure with slow crack propagation.

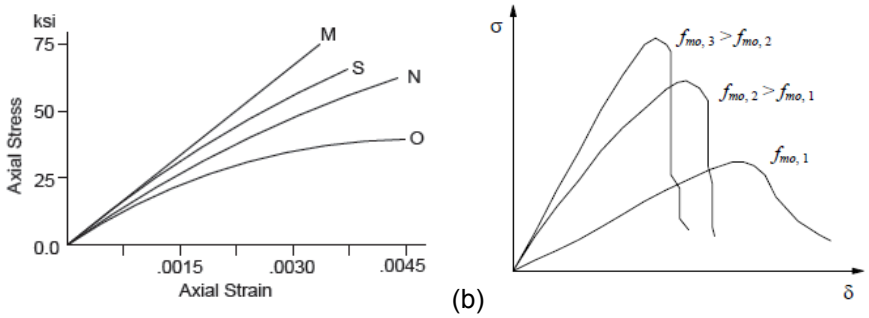

Figure 2.9 - Typical experimental stress-displacement for masonry prisms: (a) Mosalam 2009 and (b) Binda et al. 1998.

2.1.2.2.2 Uniaxial tension behaviour

Backers (1985) carried out two types of direct tension tests with the tensile load applied normal and parallel to bed joints respectively (Figure 2.10). The first test showed that failure occurred due to low tensile bond strength between the units and the joint. As a matter of fact, the tensile strength of the masonry normal to bed joints was approximately equal to the tensile bond strength between the units and the joint. For the second test, two failure modes were observed. Firstly, failure occurred as a stepped crack through head and bed joints (Figure 2.11 a). Secondly, failure occurred as a vertical crack throughout head joints and units (Figure 2.11 b). The author mentioned that this difference in the failure modes was due to different bond strength.

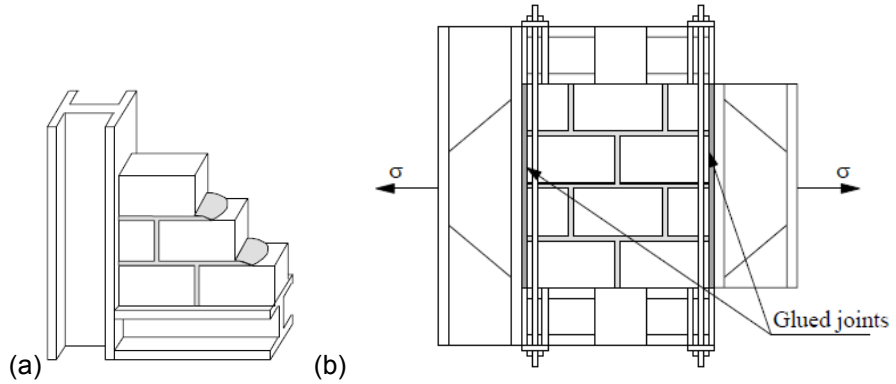

Figure 2.10 - Test set-up for tensile strength of masonry parallel to the bed joints: (a) building of the test specimen and (b) test specimen before 90º rotation and testing (Backers 1985).

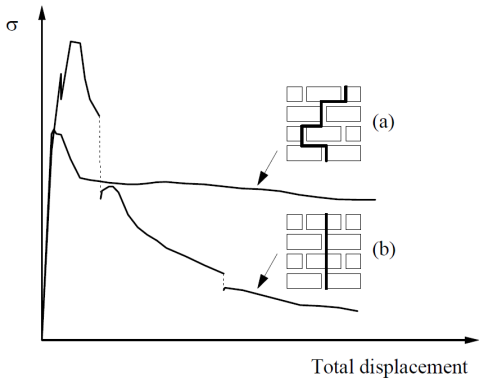

Figure 2.11 - Typical experimental stress-displacement diagrams for tension in the direction parallel to the bed joints (Backers 1985).

2.1.2.2.3 Biaxial compression/tension behaviour

Two types of loading tests are carried out to identify the tensile strength under biaxial loadings: uniaxial compression directed at a certain angle with respect to the bed joints, (Figure 2.12 a) and true biaxial loading at a certain angle with respect to the bed joints, (Figure 2.12 b) (Lourenço 1998).

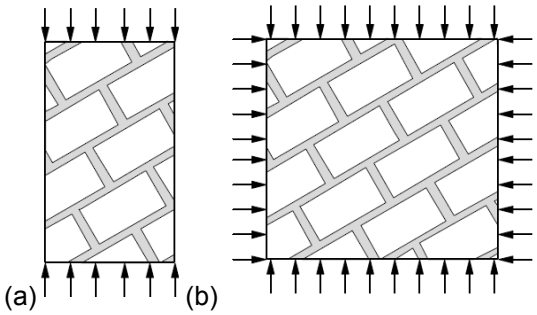

Figure 2.12 - Possible test set-ups for biaxial behaviour: (a) uniaxial loading and (b) biaxial loading (Lourenço 1998).

Experiments carried out by Page (1981, 1983) represented successfully the behaviour of a masonry subjected to biaxial loadings. The test was conducted with half-scale solid clay bricks. Loadings were applied through steel brush platens with three different angles between bed joints and the material axis corresponding to 0, 22.5 and 45 degrees, respectively (Figure 2.13).

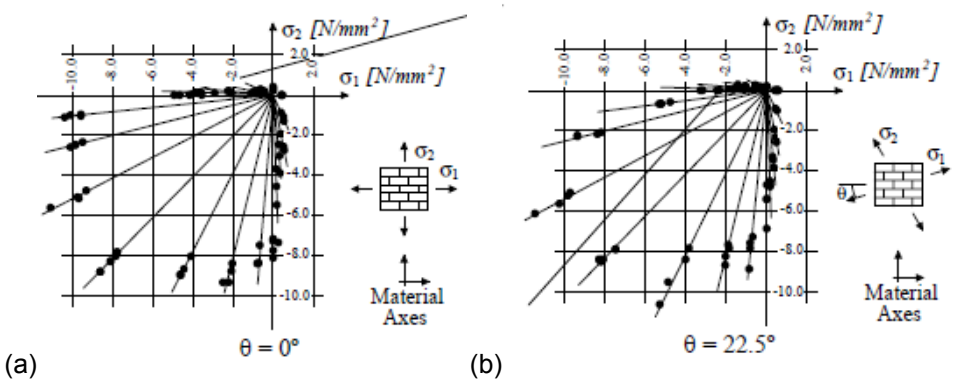

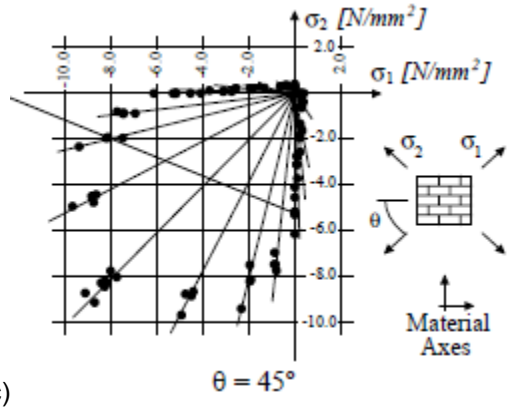

(c)

Figure 2.13 - Biaxial strength of solid clay unit masonry with three different angles between bed joints and the material axis: (a) 0°, (b) 22.5° and (c) 45° (Page 1983).

Dhanasekar et al. (1985) carried out tests on 180 half-scale brick masonry panels. The dimension of the brick was 110x50x35 mm^3 and the composition of the joint was 1:1:6 (cement:lime:sand). Incremental static loads were applied with certain angles to the bed-joint direction (Figure 2.14). The results indicate that nonlinear behaviour occurs due to sliding along the interfaces. Under compression-compression, a change of the tangent modulus was observed as the load increased until failure. Under compression-tension, masonry failed elastically at a low value of the load, showing the brittle character of masonry.

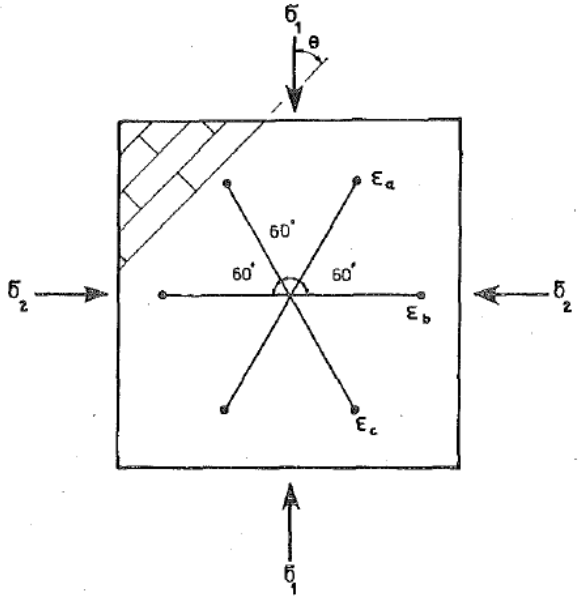

Figure 2.14 - Applied stresses and measured strains (Dhanasekar et al. 1985).

Beyond an elastic range (Figure 2.15), the following equation (2.15)

$$\varepsilon = \frac{\sigma}{E} + \left(\frac{\sigma}{B}\right)^n \tag{2.15}$$

where:

B is the constant with dimension of stress

n is the constant (no dimension)

was proposed by Dhanasekar et al. (1985) to describe a strain-strain curve based on Ramsberg-Osgood relationship. The value of constant B is defined in Table 2.1. It should be noted that the equation is for masonry made of pressed solid bricks.

Table 2.1 - Constants in plastic stress-strain relationship (Dhanasekar et al., 1985).

Direction	*Mean B (MPa)*	*Mean n*
Normal	7.3	3.3
Parallel	8	3.3
Shear	2	4

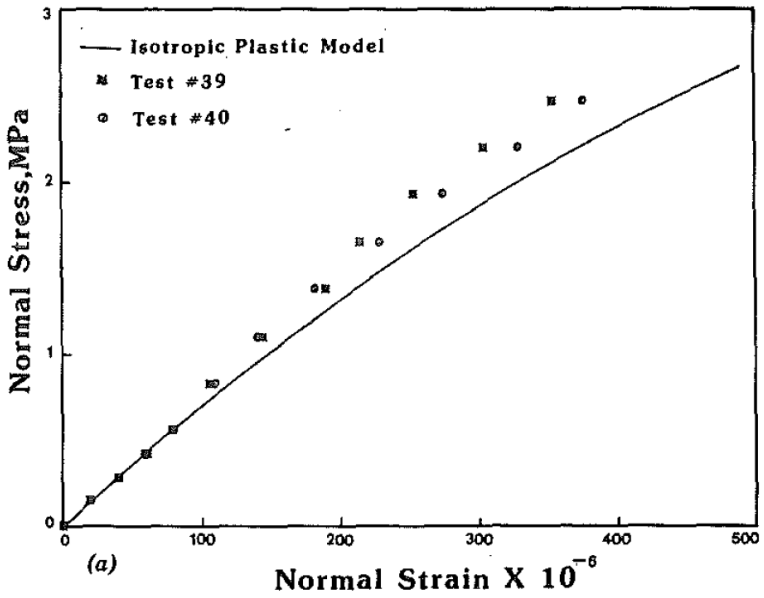

Figure 2.15 - Derived and observed stress-strain curves for panel under biaxial compression-compression (normal stress normal strain case) (Dhanasekar et al. 1985).

2.2 Typology and behaviour of masonry structural elements

Two types of structural elements are discussed in this section, corresponding to vertical structural elements and Catalan vaults. Among different types of vaults, the particular focus on the Catalan vaults is due to the case study objectives in the present research. In the following chapters (Chapter 4, 5) different Catalan vaults are studied by using structural-analysis tools discussed in Section 2.3. For the other types of historical vaults, only the references regarding typologies and experiments are mentioned. Extensive research on the historical progress of studies on masonry arches and vaults have been carried out by Benvenuto (1981), Heyman (1982), Carbone et al. (2001), Boothby (2001) and Huerta (2001). An experiment on a barrel vault model based on an existing two-story masonry building was

carried out by Marini et al. (2008). Theodossopoulos et al. (2002, 2004) carried out static-loading and displacement tests on a ¼ Gothic-cross-vault model based on the church of Holyrood Abbey in Edinburgh, Scotland. D'Ayala and Tomasoni (2008) carried out research on structural behaviour of pavilion vaults by using computational models with adoption of thrust-surface concepts. In this section, firstly, the typology of the vertical structural elements such as walls, pillars and columns is reviewed and their damage mechanisms are discussed. As for Catalan vaults, firstly a review is made on historical approach on understanding of its structural behaviour. Then the example of a recent experiment is presented and discussed.

2.2.1 Typology of vertical structural elements

2.2.1.1 Structural walls

Masonry walls can be classified into load bearing ones, supporting vertical loading and sustaining the vertical load of buildings, and shear walls, providing in-plane strength and contributing to resist the lateral forces caused by wind and earthquake. In the following sections the different types of walls are discussed taking into account the type of masonry that compose it (stone, brick and heterogeneous masonry).

2.2.1.1.1 Stone masonry walls

Investigation on the morphology of stone masonry wall sections in Italy was launched in the early 1990s (Abbaneo et al. 1993, Binda 2000). Abbaneo et al. (1993) and Binda et al. (2003b) classified stone masonry walls into four group, corresponding to one leaf, two leaves, three leaves and dry joint walls (Figure 2.16).

Figure 2.16 - Typical stone masonry sections: one, two, and three leaves (Binda et al. 1999).

During the same period, Giuffré (1993) also studied the mechanical behaviour of stonework masonry typologies. As a result of visual inspection and typology classification, the masonry typologies were reported in the form of a catalogue. The presence of some characteristics including the connection elements is regarded as a critical parameter for the evaluation of the mechanical behaviour of walls.

Da Porto et al. (2003) classified 100 examples of masonry walls in Italy, referring to previous databases of masonry wall classification (De Cesaris 1996, Giuffré 1993, Binda 2000). Accordingly it was reported that the most frequently-observed stone masonry typology is made of two or three leaves which are not interconnected with the external leaves composed of roughly shaped stones bonded in sub-horizontal courses. The average thickness of the observed walls is about 50 cm.

Cardani and Binda (2013) proposed a set of guidelines for the characterisation of the masonry quality for on-site visual inspection. Case-study masonry walls were taken from those including Abruzzo region, Italy that were struck by a severe earthquake in 2009. Masonry walls are classified with regards to the following six factors: the type of masonry units, the shape of the stone elements (regular or irregular), the thickness of the horizontal mortar joint, the horizontality of the courses, the presence of wedges and the type of cross section of the masonry wall (one or multiple leaf). In conclusion, the authors mentioned that the visual inspection of the texture does not fully identify masonry quality. For better understanding of masonry properties in-situ and/or laboratory experiments are required.

2.2.1.1.2 Brick masonry walls

Brick masonry walls are normally composed of several brick layers (one, two or more vertical layers) or by two external leaves with a cavity filled with rubble (D'Ayala 2004).

The characteristic of a brick wall depends on two factors (D'Ayala 2004). As the first factor, integrity and shear resistance of brick masonry walls is influenced by the extent and quality of bond between mortar and bricks. The second factor is the connection between the leaves. The connection between the two leaves is ensured by headers, consisting of bricks placed through the wall at regular intervals. Figure 2.17 presents possible failure patterns under seismic action depending on the sufficiency of the connection between an external and internal leaf (Carocci et al. 2004). When the connection is not sufficient, the external leaf may be detached from the internal leaf.

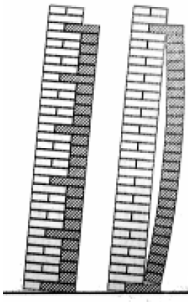

Figure 2.17 - Different configuration of cladding connections and possible failures (Carocci et al. 2004).

Old brick masonries have usually very thick sections (often more than 600 mm) with a much less homogeneous distribution of the bricks in the section than in modern ones (Binda and Saisi 2001). In some cases, only the external leaf is composed of regular bricks while the internal part is composed of

pieces of bricks and large mortar joints. The thickness of joints is usually much lower than that of the brick in a ratio 1-2/5.

Binda et al. (2002) carried out a survey on Milan Roman walls and on Ravenna Byzantine walls. In late Roman architecture and Byzantine construction, the mortar joints were much thicker than in more ancient structures. The walls were classified considering the thickness of the joints (solid wall with thin or thick joints).

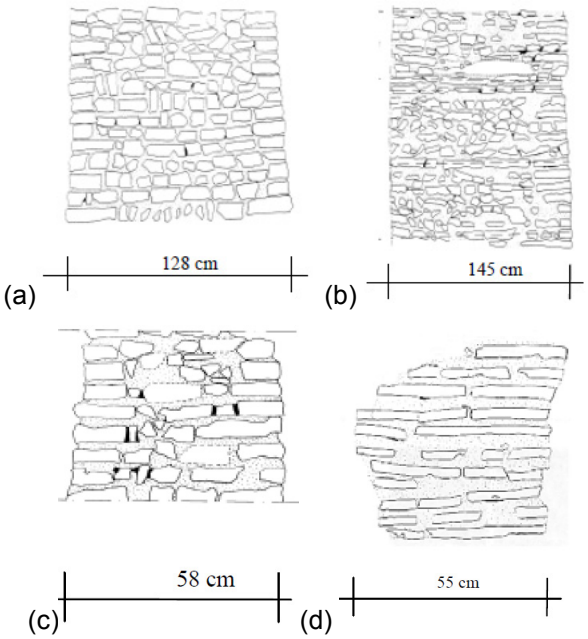

Figure 2.18 –brick masonry classification (NIKER report 2010): (a-b) solid wall with thin joints and (c-d) solid wall with thick joints.

Valluzzi et al. (2009) has presented a classification of brick masonry walls of different structural typologies of historical buildings. The authors sorted out the masonry walls in terms of masonry typology (type of brick) and thickness.

2.2.1.1.3 Mixed brick-stone masonry walls

Mixed brick-stone construction was used for monumental buildings in the Eastern Roman empire (Wright 2009). In some examples, the brickwork is regularly aligned and crossed thoroughly so as to connect the two leaves of the masonry, which improves its seismic behaviour (Figure 2.19). In other cases, the bricks are located irregularly.

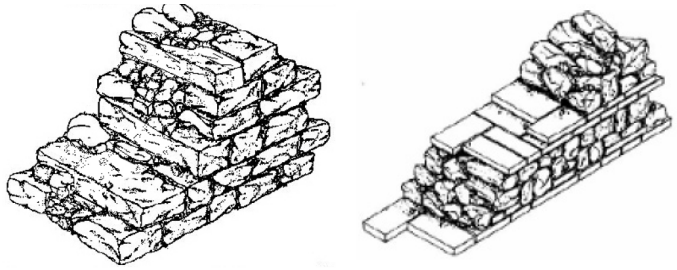

Figure 2.19 – Examples of mixed brick and stone constructions (Ferrini et al. 2003).

2.2.1.2 Pillars and Columns

Historical pillars are normally composed of an external leaf and internal rubble core (Figure 2.20) while the columns are composed of monolithic elements such as large stone blocks (Adam 1993). Columns are in some cases coupled by metal or hard timber pins and bounded with lead (Figure 2.21).

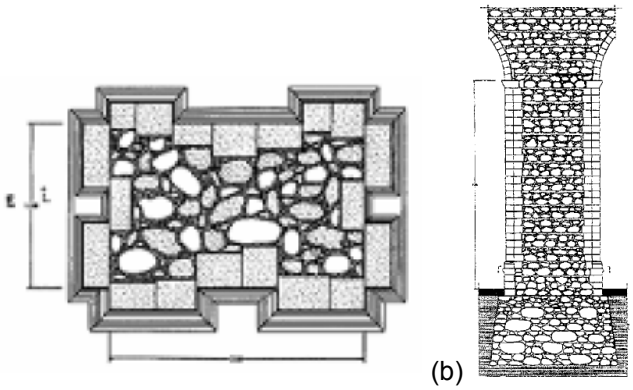

(a) (b)

Figure 2.20 - Example of three leaf stone masonry pillars, Cathedrals of Noto: (a) horizontal section and (b) vertical section (Binda and Saisi 2001).

Figure 2.21 - Details of column drums (NIKER report 2010).

Binda and Saisi (2001) carried out in-situ experiments on pillars in three churches in Italy. Firstly, in the church of S.Nicolò l'Arena, two different typologies were observed for composition of the pillars. Firstly, a pillar is composed of large and regular blocks and filled with rubble masonry made with rather strong mortar. Secondly, it is composed of an internal leaf made of strongly inhomogeneous stone masonry and external leaf of 300-mm-thick masonry made of tile fragments, stones and rather weak mortar. In some cases, the two typologies were seen in the same pillar.

Secondly, in the Cathedral of Noto, the pillars are composed of an external leaf and internal rubble core (Figure 2.20). Their internal courses are rather irregular with thick mortar joints compared to the external courses. However in every two courses of the external leaf (about 50 cm), a course made with small stones and mortar goes through the internal rubble core, as provides certain horizontality to the pillar (Figure 2.20 a). Nevertheless the mortar in the pillar is generally very weak and the bond between the mortar and the stones is limited.

Thirdly, in Crocifisso Church, boring and boroscopy revealed that the pillars are composed a multiple leaf masonry. The external leaf is made of solid stone stones while the internal leaves is a rubble one composed of a rather weak mortar, pieces of calcarenite and travertine (Figure 2.22).

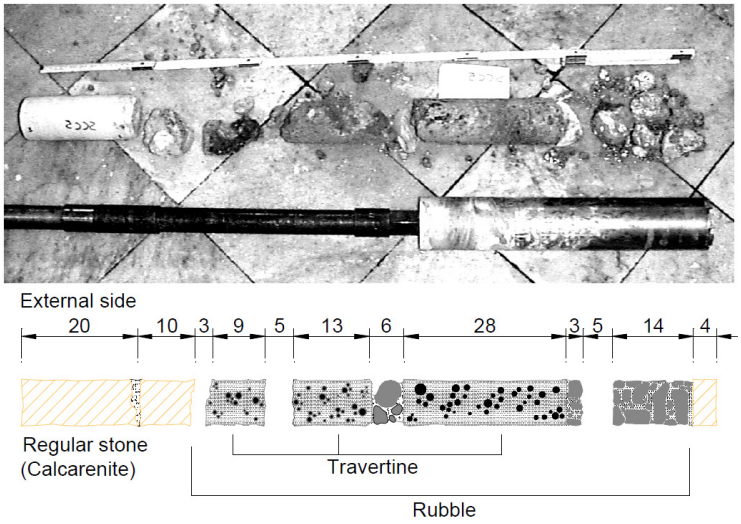

Figure 2.22 – Drilled core of a pillar in Crocifisso Church.

As a peculiar example of a pillar, in case of the Mallorca cathedral in Spain, sonic tomography shows that the section of a pillar are composed of five stones of similar quality, the 5th one, of square shape, located in the center (Figure 2.23a-b) (Roca 2009). The stones rotate 45 degrees at each row to supply satisfactory interlocking (Figure 2.23 c).

(a) 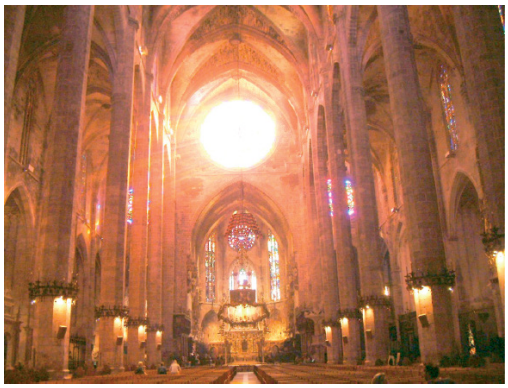 (b) 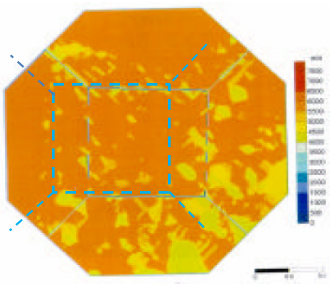

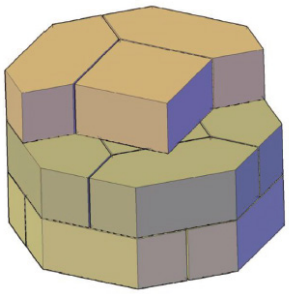

(c)

Figure 2.23 – Mallorca Cathedral: (a) interior view, (b) sonic tomography on one of pillars and (c) arrangement of stone blocks (b from Roca 2009, a.c from González et al. 2008).

2.2.2 Damage and collapse mechanisms of vertical elements under seismic action

2.2.2.1 Collapse mechanisms of walls

After the 1976 Friuli earthquake in Italy, the damage-patterns observed in the affected churches were classified by Doglioni et al. (1994). Typical collapse mechanisms of churches have been later categorised by the Italian Ministry for Cultural Heritage and Activities (2011) for macro elements such as façade, nave, triumphal arch, apse, dome and bell tower. Recently, as part of NIKER project, collapse mechanisms of historical masonry structures have been discussed in a report from the project (NIKER report 2010). A comprehensive web-based catalogue of collapse mechanisms of historical masonry buildings has been also presented for different structural typologies (NIKER catalogue 2013). In this section, both in-plane and out-of-plane mechanisms are reviewed.

2.2.2.1.1 Simple overturning

Simple overturning of an exterior wall is one of the most typical and brittle collapse mechanisms (Figure 2.24). This mechanism may occur when a wall, under seismic actions, has poor connection with orthogonal walls and poor constraints at its bottom. This mechanism involves rigid rotation of the entire or part of a wall around a horizontal hinge. A severe collapse will occur when the wall is free on top and not connected to the orthogonal walls. The simple overturning can occur also when beams or tie beams push the wall outwards during the earthquake. In the case of a multiple-leaf wall, overturning may occur only to the external leaf (Figure 2.25). On site, simple-overturning damage or failure can be identified easily through vertical cracks in the connections with orthogonal walls. This mechanism can be prevented by improving the structural capacity with the insertion of ties or ring beams. However, the intervention with ties or ring beams may result in other mechanisms such as out-of plane bending as discussed below (Section 2.2.2.1.2 and 2.2.2.1.3).

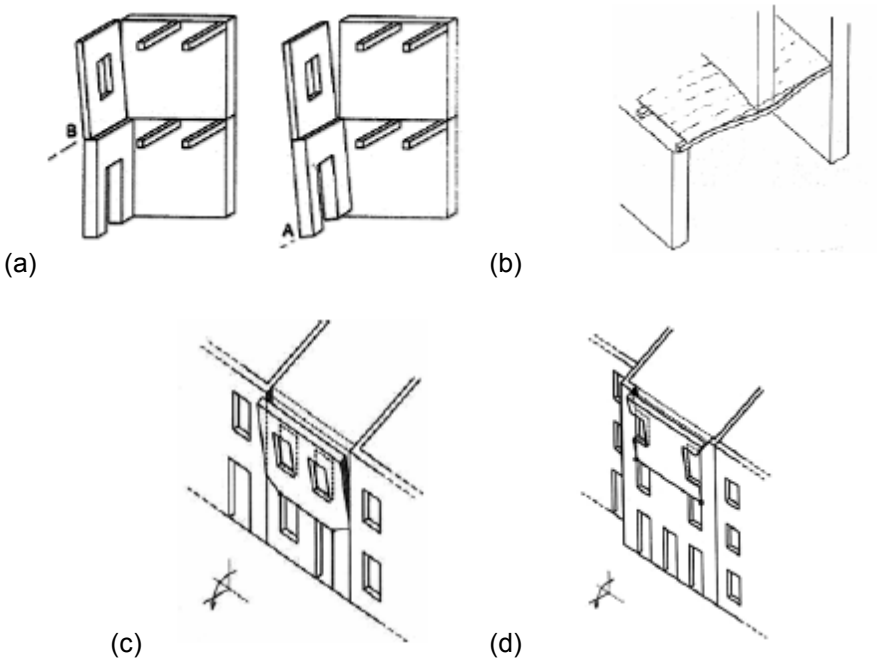

(a) (b)

(c) (d)

Figure 2.24 - Overturning of the whole or part of façade: (a) (Giuffrè 1993), (b) (Borri et al. 2004a) and (c-d) (Doglioni 1999).

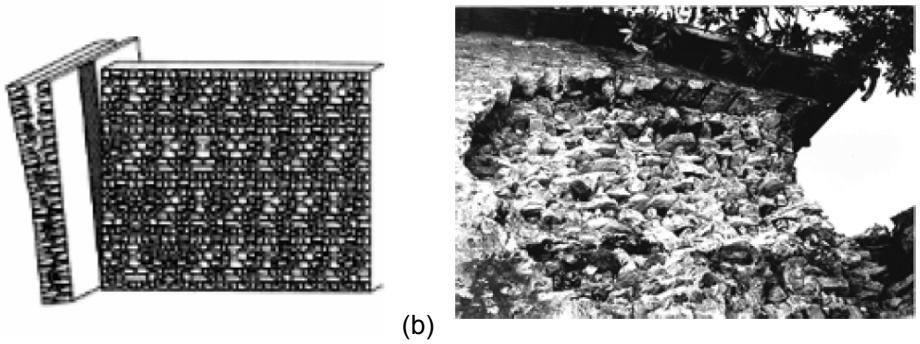

(a) (b)

Figure 2.25 - Overturning of the outer leaf: (a) Borri et al. 2004c and (b) Binda et al. 2006.

2.2.2.1.2 Vertical out-of-plane bending

This mechanism can be seen in a wall constrained at both ends (top and bottom) and free in the middle (Figure 2.26). The mechanism can be caused by the irregular arrangement of tie beams that are installed for prevention of the overturning of the entire wall. This type of overturning may occur only to the external leaf of multiple-leaf walls (Figure 2.27). This failure is frequently seen in buildings intervened with the RC tie beams, particularly when these beams do not cross throughout the transversal span of the building. The mechanism may involve more than one floor. It also happens when ties are placed at the top of the façade.

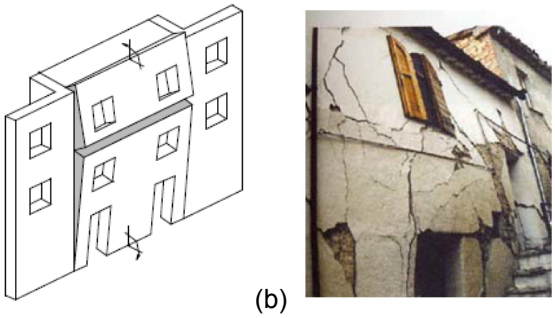

(a) (b)

Figure 2.26 - Separation of wall due to out-of-plane bending: (a) diagram and (b) example (NIKER report 2010).

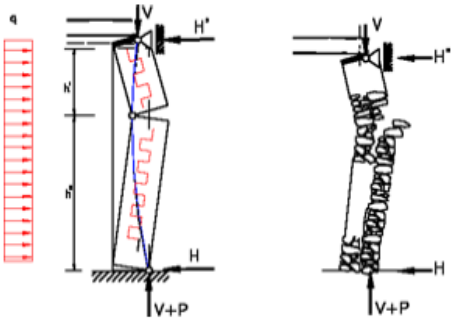

Figure 2.27 - Vertical bending and damage of a multiple leaves wall (Borri et al. 1999).

2.2.2.1.3 Horizontal out-of-plane bending

This failure occurs when a wall is rigidly connected to orthogonal walls in both sides and free in both top and bottom ends. It commonly happens to a wall constrained with ties when the wall is pushed by floors or roof beams. In general it involves an arch mechanism within the wall section caused by out-of-plane actions (Figure 2.28 a). The three-hinge arch mechanism is seen frequently in this failure (Figure 2.28 b-c). Roof beam hammering may produce a partial collapse of a façade if the facade is constructed with low quality of masonry (Figure 2.29).

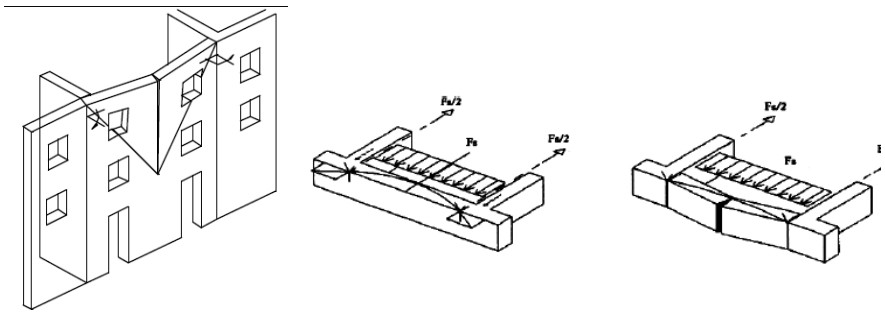

(a) (b) (c)

Figure 2.28 - Arch mechanism: (a) diagram and (b-c) location of hinges (Borri et al. 2004a, b).

(a) (b) (c)

Figure 2.29 – Mechanism involving roof beam hammering ((c) from NIKER report 2010).

2.2.2.1.4 Complex overturning mechanism

This mechanism is observed when a wall experiencing out-of-plane loading rotates with a portion of orthogonal walls (Figure 2.30). The mechanism occurs when a wall has sufficient connections with the orthogonal walls and no constraint at the top. The shape of the mechanism highly depends on the existence of openings and the texture of the masonry. For instance, this mechanism may occur to a wall and its orthogonal walls if they were constructed at the same period with good interlocking. It may also occur in a wall connected to its orthogonal walls by means of strengthening techniques such as steel stitching (Modena et al. 2009).

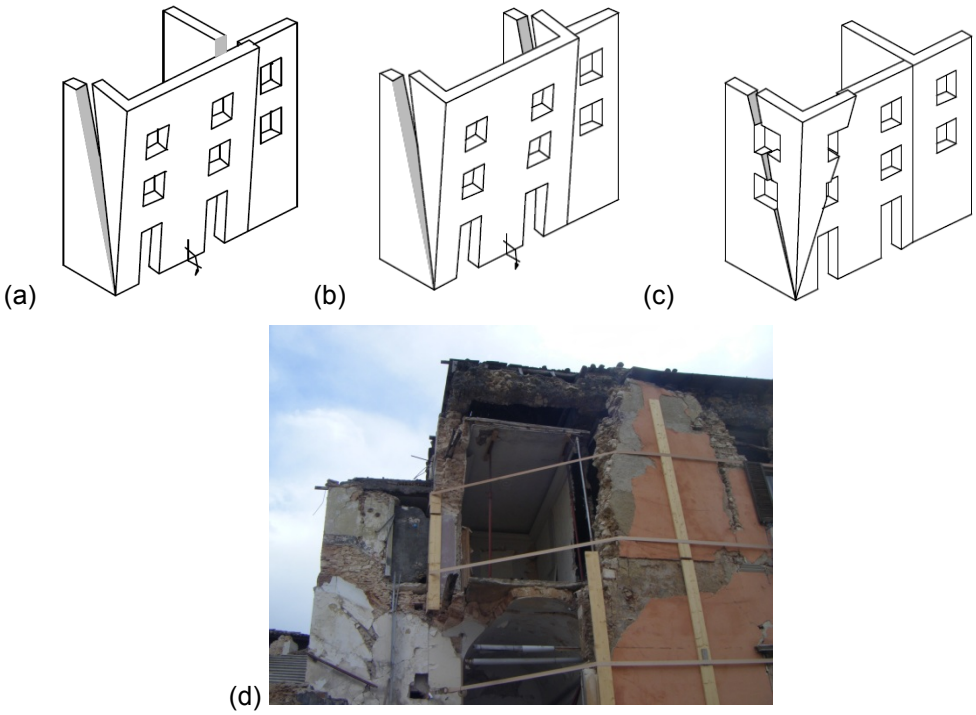

(a) (b) (c) (d)

Figure 2.30 - Complex overturning mechanisms: (a) overturning with one side of a orthogonal wall, (b) overturning with both sides of orthogonal walls, (c) corner failure and (d) corner failure of a building in L'Aquila.

2.2.2.1.5 In-plane mechanisms

In-plane behaviour is caused by forces acting in the plane of a wall. It is usually marked by inclined cracks in an “X” pattern, although this behaviour does not lead often to a full mechanism (Figure 2.31 a). On the other hand, when a full diagonal shear crack appears in a wall, a triangular portion of the wall may separates from the rest, as results in a full mechanism (Figure 2.31 b).

(a)  (b) 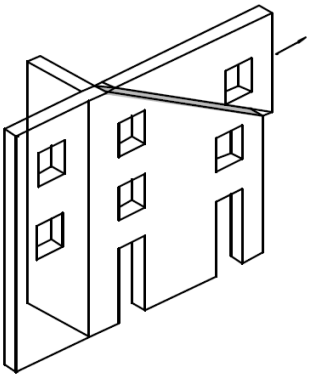

Figure 2.31 – Examples of In-plane failure: (a) X pattern in a wall (Augenti and Parisi 2010) and (b) a triangular section of a wall.

2.2.2.2 Damage mechanisms of pillars and columns

Overturning and crushing at the corner or the bottom of a pillar or columns can occur under seismic action (Corradi et al. 2007). Lateral forces due to seismic actions cause high bending moment. It may result in concentration of local stresses at the bottom of the pillars (Figure 2.32, Figure 2.33). In the case of columns, sliding of drums also may be seen (Figure 2.34) (Konstantinidis 2005).

Figure 2.32 – Local damage concentration due to seismic action, an example of a pillar in L’Aquila Cathedral.

Figure 2.33 – Seismic damaged pillars with emergency measurement in the courtyard of the Spanish fortress in L'Aquila.

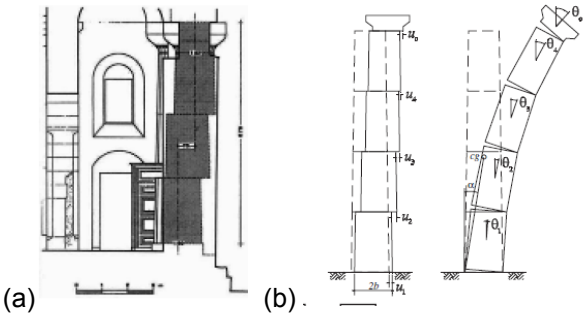

(a) (b)

Figure 2.34 - Failure mechanism of columns: (a) Drum shifted after an earthquake in the 16th century, Cathedral of Syracuse, Italy (Binda et al. 2007) and (b) Diagram showing sliding and overturning of columns (Konstantinidis 2005).

Pillars under dead load experience long-term damage related to creep (Binda et al. 1992). This long-term phenomenon can occur for stresses significantly lower than the than the nominal material strength identified by means of static compression tests. For limestone, creep can start at 45-50% of the nominal strength values. Long-term vertical compression by dead load may also cause lateral deformation (Anzani et al. 1995). This so-called dilatation phenomenon may lead to vertical cracking and may end in the collapse of the pillar or structure (Binda et al. 2001a). This type of phenomenon has been observed for weak masonries or when or the construction technique is poor. Damage can also be coupled with cyclic actions such as wind and temperature variation (Tesarik et al. 2009, Valluzzi 2007).

Massive walls and slender structures like towers can also show long-term behaviour. Examples are found in the study of the collapse of the Civic Tower of Pavia and Noto Cathedral in Italy (Papa and Taliercio 2000, Binda, et al. 1992, 2003a). Anzani et al. (2008) carried out investigation of specimens cut from the walls of the Pavia Tower after its collapse. As a result, the authors drew the formulation of the hypothesis of a collapse due to the long-term behaviour of the material.

2.2.3 Catalan Vaults

2.2.3.1 Introduction

Catalan-vault (also known as Timbrel vault*[1]) construction is a masonry construction technique perfected and widely employed in Catalonia, Spain in the 19th century (Huerta 2003). Today the word "Catalan vault" (*volta catalana* in Catalan) denotes a curvilinear element composed of layers (up to four layers) of tiles (generally, with dimension around 15x30x1.5 cm^3) adhered with mortar (Palizzolo et al. 2008) (Figure 2.35). Its origin is not known (Collins 1968) but the first document on this construction technique can date back to 1382 (Araguas 1999). The peculiar characteristic of Catalan vault comes from low thickness and high loading capacity compared to surface dimensions, quick-setting mortar and the presence of superimposed layers of bricks stuck with mortar (Benfratello et al. 2010). In the 1880s, Raphael Guastavino brought Catalan-vault technique to North America and used it as a construction method for monumental buildings (Collins 1968).

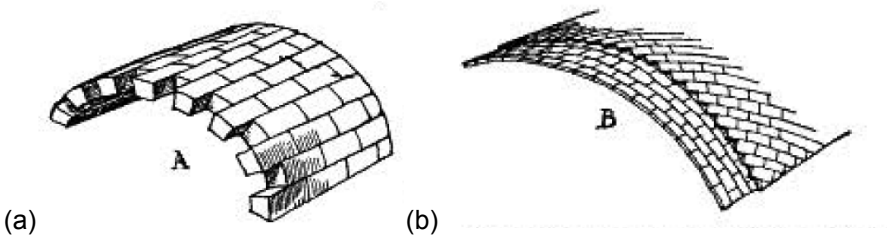

Figure 2.35 – Comparison of stone vault (a) and Catalan vault (b) (Moya 2000).

2.2.3.2 Historical approach to the structural behaviour of Catalan vault

The construction of Catalan vault has been discussed by various authors (Collins 1968, Gulli and Mochi 1995, González 1999, 2005, Huerta et al. 2001, Ramage 2004, Truñó 2004). However, few research contributions have been made on the understanding of its structural behaviour. A comprehensive discussion on the history of Catalan vaults has been presented by Huerta (2003).

One of the earliest documents that made mention of structural design of Catalan vaults, in 1639, is Fray Lorenzo's book (*Arte y Uso de Arquitectura*). He was an architect who built many Catalan vaults in the 17th century. He introduced a law of buttress design for different types of vaults (Table 2.2). He defined the dimensions of two different types of buttresses (uniform wall and wall with counterfort) according to the types of materials and vaults. For the Catalan vault, a buttress with a lesser depth was allowed than for the other types of vaults.

*[1] *In this thesis, the name Catalan vault is used unless there is any specific reason.*

Table 2.2 - Fray Lorenzo's rules for buttress design (Fray Lorenzo 1639).

Type of vault	***Type of buttress***		
	Wall (uniform section)	***Wall with counterfort***	
		Wall depth	***Wall + counterfort depth***
stone vault	1/3	1/6	>1/3
brick vault with radial joints	1/4	1/7	1/3
Brick Catalan vault	1/5	1/8	1/4

In the 18th century, Espie (1754), a French nobleman, stated that Catalan vaults were solid enough to avoid cracks when they were built with good-quality mortar. In turn, D'Olivier (1837) and Fontaine (1865) stated that the structural characteristic of Catalan vaults was similar to that of other conventional vaults. Fontaine carried out an experiment on three continuous Catalan vaults (each spanning 4 m) supported by I-beams spanning 6.25 m at both ends. Failure was seen under a load of 12.3 kN/m^2.

Rafael Guastavino, a Spanish architect, brought the Catalan-vaulting technique to the United States at the end of the 19th century. He refined this construction technique and built various monumental buildings with the so-called 'Guastavino vaulting' technique between 1890 and 1900 in the eastern United States. He also carried out studies on the structural behaviour of the Catalan vault structural system. In his thesis (Guastavino 1893), he explained this construction system by using the term "Cohesive construction", in contrast with the conventional one-layer arched structural system named as "Gravity system". Structural stability of the former was said to be based on the cohesion of materials (Figure 2.36 a). Cohesive-force action appeared due to the mortar between the units. In the latter case the equilibrium of the structure was believed to come from the gravity of each voussoir (Figure 2.36 b). Therefore the structure was kept stable only due to the gravity force while the mortar serves just as a cushion.

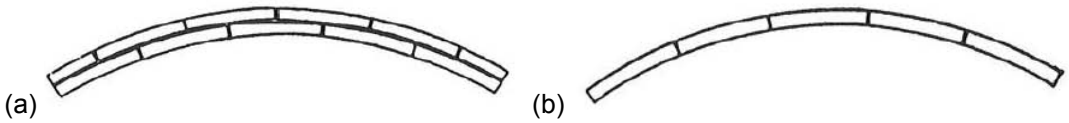

Figure 2.36 - (a) Cohesive construction and (b) Gravity system (Guastavino 1893).

The author carried out an experimental study on specimens of both structural systems (Figure 2.37). For the "Cohesive construction", compressive strength was 14.6 MPa, and the shear strength was 0.85 MPa. Tensile strength was 1.98 MPa. As for the "Gravity system", the tensile strength of the vault was equal to that of the mortar (1.03 MPa). Through this experiment, the author pointed out that the advantage of Catalan vault was confirmed because of this additional tensile strength. However, it has to be noted that the author carried out the experiment on specimens composed of clay brick and portland cement mortar

instead of lime mortar. Hence, the presented values should be higher than for a historical Catalan vault built with lime mortar.

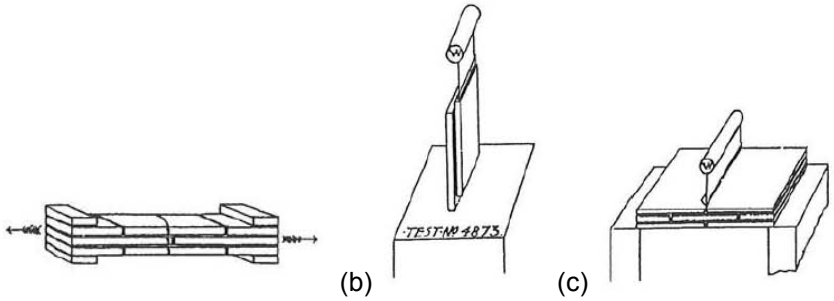

(a) (b) (c)

Figure 2.37 - Experiments carried out by Guastavino: (a) tensile test, (b) shear test and (c) bending test (Guastavino 1893).

In the early 20th century, both graphical analysis and elastic analysis were applied to Catalan vaults. The first graphical approach to Catalan vault was attempted by Eddy (1878). The first attempt of elastic-analysis approach is found in the essay of Guastavino (1983). Although the discontinuity and heterogeneity of masonry were known, the elastic concept was still preferred due to its simple application.

Today it is known that cracking and hinges can be observed in Catalan vaults like in other types of masonry vaults. However, Catalan vault can be constructed without centring or with light supplemental supports due to the cohesiveness (Collins 2004). For the same reason, masons can walk over the vault right after the construction. In summation, the advantage of Catalan vaults to other types of vault can be seen in the construction process. Nevertheless once it is completed, it has to be considered that they may generate cracking and form hinges like other types of masonry vaults. (Huerta 2003).

2.2.3.3 An example of recent experimental research on historical Catalan vaults

Recently, one of the few experiments on a Catalan vault was carried out by Palizzolo et al (2008). A laboratory and in-situ static loading test was carried out on existing vaulted buildings in Palermo, Italy. In Palermo, the Catalan vaults are normally composed of three layers of brick whose dimension is 26x13x2 cm^3. Lime mortar and plaster are used as binder. A description on these tests is also found in the article of Benfratello et al. (2010, 2012). Compression and bending tests were conducted. The compression tests were carried out two samples of two-layers, four samples of three-layers and four samples of four-layers. The thickness of the sample is 45 mm for two layers, 75 mm for three layers and 105 mm for four layers. The observed value of the maximum stress was equal to 1.7 MPa for two layers, 2.5 MPa for three layers and 2.9 MPa for four layers. The three-point and four-point bending test were carried out on three-layer samples. The observed maximum tensile stress was 0.08 MPa.

Then, a static-loading test was carried out. It has to be noted that the building used for the static loading test was different to the building where the samples were taken for the above-mentioned material tests. The test was carried out on a room roofed with three Catalan cross vaults (Figure 2.38 a). The vaults were composed of four layers of tiles. A uniform load (up to 4 kN/m^2) was applied to the squared zone indicated in the Figure 2.38 b. In this test, the vertical displacement was measured at three points (P_1, P_2, P_3 in Figure 2.38 b). P_1 reads 0.627 mm, P_2 0.911 m and P_3 0.784 mm, respectively. Detailed discussion on the results from this experiment is pending.

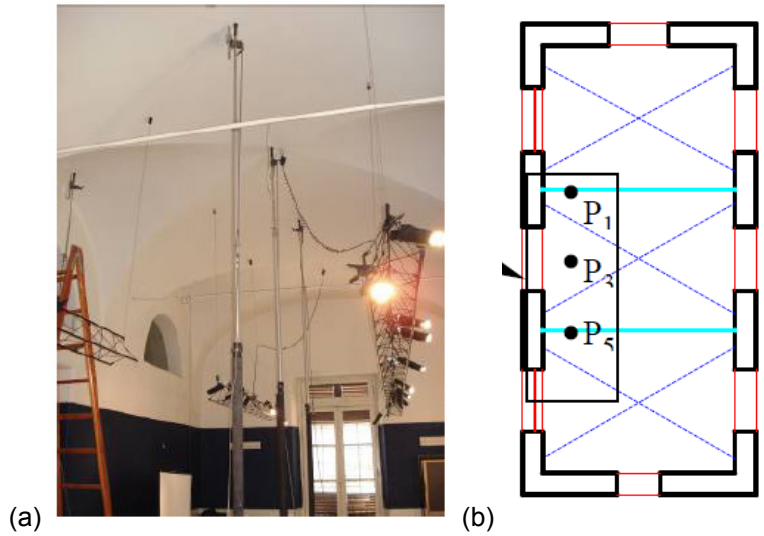

(a) (b)

Figure 2.38 - (a) Photo of the vault and (b) sketch of the vault plan (Palizzolo et al. 2008).

2.3 Structural Analysis techniques

2.3.1 Limit analysis

2.3.1.1 Introduction

In 1676 Robert Hooke found that the ideal shape of an arch ring is the form of the inverted catenary which is obtained though hanging uniformly-distributed weights from a chain. He described this concept in his publication as: *"Ut pendet continuum flexile, sic stabit contiguum rigidum inversum"*- -As the continuous flexible hangs downward so will the continuous rigid stand upward inverted (Hooke 1676). Nearly at the same time Gregory (1697) independently discovered and developed a notion similar to Hooke. He stated that only the shape of inverted catenary is correct for an arch. He added that an arch of any other shape is stable in case a catenary can fit within its thickness. This inverted catenary principle was employed for the design and assessment of arched masonry structures in the 18th and 19th century. For instance, Poleni (1743) carried out the study of the dome of St. Peter through hanging strings. During the same period, based on the inverted catenary principle, graphically oriented procedures were developed by various researchers such as la Hire in the 18th century and Rankine in the 19th century. In the middle 19th century, the theory of thrust line was established by Moseley (1835) and was given a sophisticated mathematical treatment by Milankowitch (1907). In practice up to the

early 20th century, the safety assessment of arches was done through graphical analyses; an arch was regarded as safe in case a thrust line could be drawn within the boundary of the arch (Huerta 2008). In the late 20th century, the theory of limit analysis of masonry arches was developed principally by Heyman (1966). His theory is discussed in Section 2.3.1.2.

Recently a number of proposals are made for analysis of 3-dimentional vaulted structural systems, based on Heyman's limit analysis. O'Dwyer (1999) proposed the analysis of curved shell structures by decomposing curved masonry shell structures into a system of arches in equilibrium. Ochsendorf and Block (2008a) proposed a method based on the reciprocal relationship between the geometry and the in-plane internal forces of networks of Williams (1986). Andreu et al. (2007) developed a computational technique where masonry structures are modelled as 3-dimensional catenary networks. In this section, these three recent analysis tools are discussed after short review of the limit analysis of Heyman (1966).

2.3.1.2 Limit Analysis (Heyman 1966)

Heyman (1966) proposed a formulation for the limit analysis of masonry arches. According to Heyman's formulation, the limit theorems of plasticity can be applied to masonry structures when the following three hypotheses are satisfied: (1) masonry has null tensile strength, (2) friction between voussoirs is sufficient to prevent failure due to sliding of one voussoir relative to another and (3) masonry has infinite compressive strength. On the basis of the three hypotheses, three theorems are applicable, corresponding to the lower-bound, upper-bound and uniqueness ones. They are described as follows.

According to the lower-bound theorem collapse does not occur when a statically admissible state of equilibrium can be identified (Figure 2.39 a). This occurs when a thrust line can be determined, in equilibrium with the external loads, which lies within the boundaries of the structure. The external loads are a lower-bound of the actual ultimate loads (that causes collapse). The lower-bound theorem supports a so-called static approach for the safety assessment of masonry structures.

According to the upper-bound theorem, the arch will collapse when a kinematically admissible mechanism can be found, for which the work developed by external forces is positive or zero. In other words, if a mechanism is assumed by locating arbitrarily a sufficient number of hinges, the loads which result from equating the work of external forces to zero is an upper-bound of the actual ultimate load (Figure 2.39 b). The application of the upper bound theorem enables to apply a so-called kinematic approach to the study of masonry buildings.

Under the uniqueness theorem, the arch is at the point of collapse if a both statically and kinematically admissible collapsing mechanism is found (Figure 2.39 c). In other words, the collapsing configuration will be reached if a thrust line can be found causing as many hinges as needed to develop a mechanism. Hinges appear where a thrust line becomes tangent to the boundaries of the arch. When this occurs, the

load is the true ultimate load, the mechanism is the true ultimate mechanism, any other thrust lines are not possible.

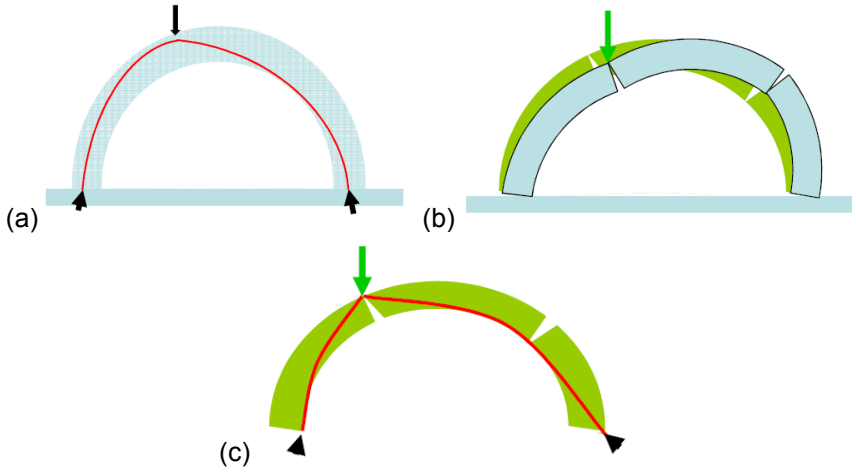

Figure 2.39 - Safe-theorem diagrams: (a) lower-bound theorem, (b) upper-bound theorem and (c) uniqueness theorem.

2.3.1.3 Advanced analysis tools based on limit analysis of Heyman (1966)

2.3.1.3.1 Method of O'Dwyer (1999)

O'Dwyer (1999) extended a thrust-line theory into 3-D shell structures by discretising them into systems of arches in equilibrium. These systems are named a force network models. The force network model is based on three assumptions: (1) the forces in the network model cannot be tensile, (2) the forces meeting at each node in the network-model must be in equilibrium with the external loads applied at that node and (3) all the nodes in the network must lie within the envelope of the structure.

The preparation of the force network model is made up of seven steps as follows: (1) identify principal structural actions (Figure 2.40 a, b), (2) choose a mesh pattern and density (Figure 2.40 c), (3) discretise external loads, (4) formulate constraints on node heights, (5) formulate the vertical equilibrium constraints, (6) linearise the equilibrium constraints and (7) use repeatedly linear programming solution to solve the non-linear programming problem. The author provides a case study of a barrel vault subjected to gravity and an imposed concentrated load and compares his solution (Figure 2.41 a) with the shape given by cloth membrane analysis (Figure 2.41 b).

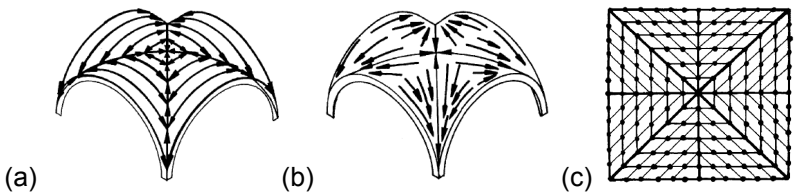

Figure 2.40 - (a, b) Two possible load paths for a groined vault and (c) Groined vault mesh pattern capable of representing the structural actions identified in Figure 2.40 a, b (O'Dwyer 1999).

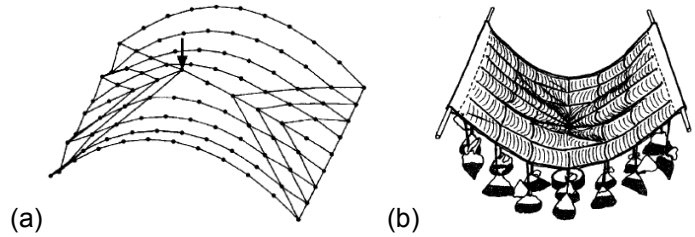

(a) (b)

Figure 2.41 - (a) Optimised three-dimensional shape of the force network for a barrel vault and (b) shape given by the cloth membrane analysis (O'Dwyer 1999).

Simple application is one of the advantages of this method. Discretisation of loads and structural discontinuity can be incorporated in an effortless manner by this stress-modelling method. However, results are heavily influenced by discretisation patterns. Moreover, this methodology is time-consuming since nonlinear problem is resolved by a simple linear programming problem repeatedly.

2.3.1.3.2 Method of Ochsendorf and Block (2008a,b)

Ochsendorf and Block (2008a) proposed a method where limit analysis is applied to 3-D structures. They developed a methodology (so-called thrust-network analysis) for the analysis of three-dimensional structures so as to acquire lower-bound solutions for masonry vaults with complex geometries. This methodology extends the above-discussed method of O'Dwyer (1999) by adding the reciprocal relationship between the geometry and the in-plane internal forces of networks of Williams (1986). This relation between the geometry of a network and its internal forces was first demonstrated by Maxwell (1864). Figure 2.42 demonstrates this relationship: the internal force equilibrium of one grid (left in Figure 2.42) is represented by the geometry of the other grid (right in Figure 2.42) and vice versa. In other words, the equilibrium of a node in one of them is assured by a closed polygon in the other and vice versa.

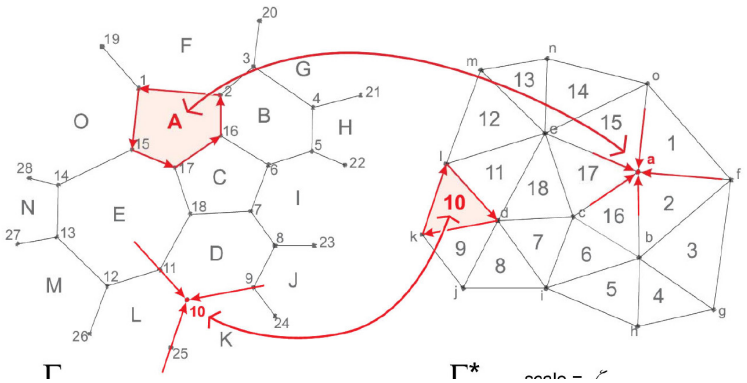

Figure 2.42 – Diagram by reciprocal relationship between the geometry and the in-plane internal forces of networks presented by Bow (2014).

The procedure consists of the following steps: (1) defining a solution envelope (2) choosing a force pattern Γ (3) generating a reciprocal force diagram Γ^* (4) attributing weights (5) updating the force

diagram (6) identifying an equilibrium solution G (Figure 2.43). As a case study, the authors carried out an equilibrium analysis of a groin vault under self-weight (Figure 2.44). It is found that possible horizontal thrust values at the corners range from 21% to 32% of the total weight of the vault.

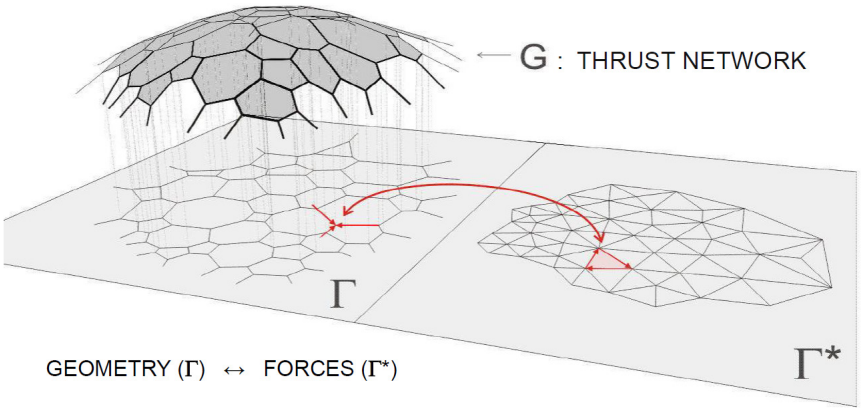

Figure 2.43 - Thrust network diagram: geometry Γ and forces Γ^* (right) (Ochsendorf and Block 2008b).

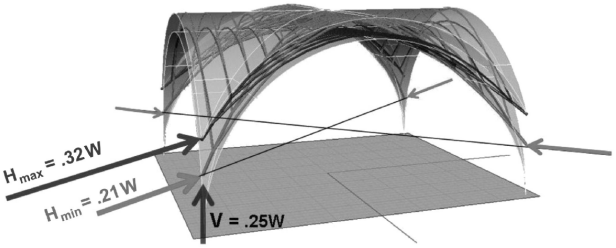

Figure 2.44 - Possible thrust network patterns with: min (21%) and max (32%) horizontal thrust (Ochsendorf and Block 2008b).

As an advantage of the methodology, different force patterns between the maximum and minimum case can be prepared and compared easily. The model of a vault can have continuous edge supports or just corner supports, as is determined by the curvatures of the vault or by the existence of cracks. Moreover, imposed loads such as fillings can easily be integrated by adding loads to the affected nodes. Problems can be resolved as a one-step linear optimisation. As a disadvantage, all the possible force patterns and diagrams have to be taken into account until the absolute minimum and maximum values of thrust can be identified.

2.3.1.3.3 Method of Andreu et al. (2007)

Andreu et al. (2007) proposed a new limit analysis methodology by applying a cable network system. The method is applicable to complex structures such as domes and vaults (i.e. 3-D curved structure) This technique can be used to assess the safety of 3-D masonry structures (lower-bound theorem) and define the ultimate capacity (uniqueness theorem).

In this method, firstly a catenary-element model is prepared (Figure 2.45). Then, safety assessment and evaluation of the ultimate capacity are carried out by using the model. The authors present a case study consisting of one of the towers located in the façade of Barcelona Cathedral. Wind analysis was carried out on the tower (Figure 2.46). Ties and monolithic tracery panels were included in the model as stiff braces.

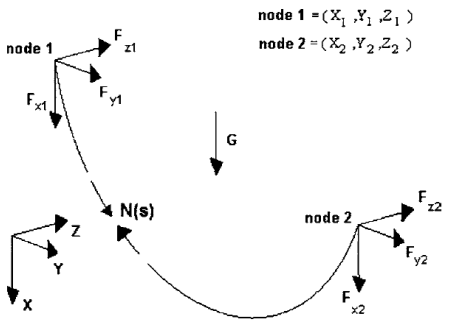

Figure 2.45 - Catenary element (Andreu et al. 2007).

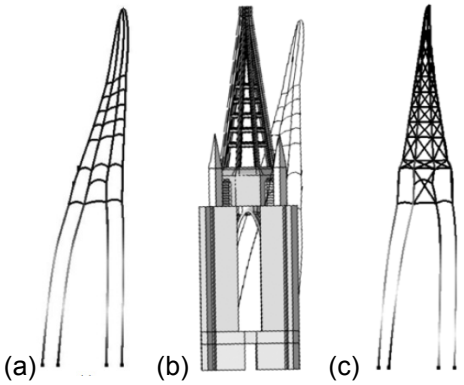

Figure 2.46 - Funicular model (a, b) for wind load without stiff braces (c) with stiff braces simulating the stiffening action of tiles and monolithic tracery panels (Andreu et al. 2010).

As an advantage of this methodology, modelling process is simple and complex material parameters are not required. Therefore the analysis can be done relatively easily. The ultimate capacity of the structure is easily estimated by applying the uniqueness theorem. Since the number of degrees of freedom is limited, the analysis is conducted with high computational efficiency. Additionally, since the method is based on a direct physical analogy with a catenary, it is unlikely that the result includes a large number of errors. However, load paths in the structure should be anticipated in advance to the analysis. Thus the method requires the sufficient understanding of the structural behaviour and the catenary principles. Furthermore, the preparation of cable network is time consuming especially when the structure has a complicated shape.

2.3.2 FEM Analysis

Today, FE method offers a huge variety of possibilities for the simulation of historical masonry structures in terms of detailed nonlinear analysis (Roca et al. 2010). Among the variability of FEM

analysis techniques, adequate tools should be chosen considering cost, need for experienced users/engineers, the level of accuracy required, the availability of input data, need for validation and the use of the results (Lourenço 2002). Today two modelling approaches are mainly used for FEM analysis of masonry structures, namely the micro- and macro-modelling ones (Rots 1991). The former approach represents individually each components of masonry: i.e. unit (brick block etc) and mortar. The latter approach smears out masonry in a homogeneous continuum. FEM strategies for historical masonry structures (including modelling approaches) are discussed in Chapter 3. In this section, macro-modelling approach oriented especially to masonry vaulted structures is reviewed looking to its application to the case studies dealt with in following chapters.

Developments on nonlinear analysis of historical vaulted structures have been limited due to the difficulties caused by their curved, two-dimensional and spatial character. The study of the domes of San Marco Basilica (Venice, Italy) by Oñate et al. (1995) is seemingly a pioneering work. A set of vaults were represented with a continuum damage model for masonry and concrete, considering the effects of mechanical and other (physical, chemical, biological) deterioration. As a result the safety condition of the system of vaults was characterised (Figure 2.47).

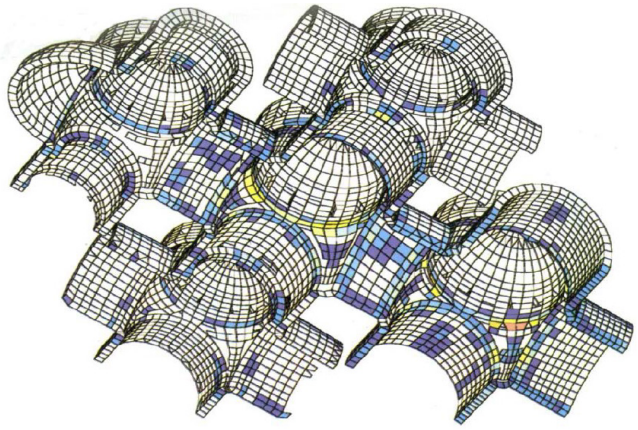

Figure 2.47 - Study of Saint Marco's domes in Venice by a continuum damage model (Oñate et al. 1995).

Croci et al. (1998a) conducted FE analysis of Cathedral of Sta. María, in Vitoria, Spain. It started with the analysis of the main transverse sections of the nave and nave vaults. Then incremental strategy was adopted considering cracking due to tension or shear stresses as well as the equilibrium second-order effects. He also carried out similar analyses such as the study of the collapse of Beauvais Cathedral (Croci et al. 1998b) and the study of the effects of the earthquake of September 1997 on the Basilica of Assisi (Croci 1998). Barthel (1993) developed detailed FE models and analysed gothic cross-vaults. The models were represented as combination with partial constitutive models enabling the simulation of masonry cracking as well as sliding between arch-voussoirs joints. Cauvin et al. (1993, 1995) conducted studies on Gothic cross vaults using both limit analysis and FEM nonlinear analysis. This method was

successfully adopted to the study of the central nave of Reims Cathedral. A formulation for the study of masonry spatial and curved shells was proposed by Lourenço (1997). It included the constitutive equations based on plasticity, as resulted in the stimulation of the response of materials in combination with joint elements allowing the representation of block sliding.

The combination between creep phenomena, geometric effects and construction process was investigated in Mallorca Cathedral (Roca et al 2012, 2013, Pelà et al. 2014) due to the remarkable deformed condition of its structural system. The authors proposed a FE model able to account for construction processes through sequential-evolutionary analyses, with the description of masonry mechanical damage and long-term deformation. The analysis measured the evolution of deformation to assess the long-term stability of a representative bay subject to constant vertical loading. According to the outcomes of the research, significant further progress of the lateral deformation of the piers might bring stability problems, but the building seems at present far from this concerning condition.

Saloustros et al. (2015) also used an advanced FE analysis to study the deformation and existing damage in the church of the Poblet Monastery. The model included the actual-deformed 3D geometry of a representative bay to include the effect of real deformation in the analysis. The analysis considered different scenarios, like gravitational loading, settlements, past earthquakes and reported structural alterations, to understand the possible causes of the present damage and deformation in the structure.

Advanced nonlinear FEM analyses permit an accurate study of the response of the structure. However, FEM models may be very sensitive to changes in boundary conditions, load history and may predict the formation of cracks in unexpected locations (Huerta 2003). According to Boothby et al. (2006), the solutions provided by an initial FEM model must always be validated against known information on the structure such as testing results, crack location and/or other damage. During the validation process an initial model may probably need to be refined in terms of boundary conditions and material properties. It is also important to study the influence of the different parameters on the results through a parametric study.

2.3.3 DEM analysis

The discrete element method (DEM) is a method that models materials as an assemblage of distinct blocks interacting along the boundaries. The pioneering work is found in Cundall and Hart (1971). According to these authors, the name “discrete element” can be applied to a computer approach when the two conditions are satisfied. Firstly, the method permits finite displacements and rotations of discrete bodies, including the complete detachment. Secondly, it is able to recognise new contacts between blocks automatically as the calculation progresses.

The formulation was initially directed to the study of jointed rock and later was extended to other

engineering applications. It required a detailed study of contact between blocks or particles, such as soils and other granular materials (Ghaboussi and Barbosa 1990). Finally, it has also been adopted to the modelling of masonry structures (Pagnoni 1994, Lemos 1998, Sincraian 2001). It is common in the application of the discrete element method to masonry to idealise the material as a discontinuum where joints are modelled as contact surfaces between different blocks. This approach allows us to model various types of nonlinear behaviour, including large displacements. The method suits the study of failures in both quasi static and dynamic ranges.

Rocking motion of stone blocks (Peña et al. 2007), static and dynamic analysis of load bearing walls (Pagnoni 1994, Baggio and Trovalusci 1995, Schlegel and Rautenstrauch 2004), stone bridges (Lemos 1995, Bicanic et al. 2001), columns and architrave (Papastamatiou and Psycharis 1993, Psycharis et al. 2003), arch and pillar (Pagnoni 1994, Pagnoni and Vanzi 1995, Lemos 1998) are typical examples of the application of DEM analysis. However, the analysis of complex structures is still a controversial topic in DEM. Computational viability of analysis may limit severely the number of block elements that can be included in a model. Models prepared to simulate the response of real structures may result in too coarse or unrealistic discretisation or 2D, and specially, 3D real masonry structures.

DEM can ideally simulate structural behaviour of blocky structures such as systems composed of columns and arches. The analysis of large structures may encounter difficulties related with the size of DEM elements (Lemos 2007). In principle, the element sizes should be equal to the real dimensions of the masonry units; however, this may be impractical for large structures. Therefore, a simplified modelling strategy is normally used, with the element sizes becoming larger than the real ones. In this case, additional judgment is required so as to adjust deformability of joints and blocks.

2.4 Seismic assessment tools

Three different seismic assessment tools are considered for its possible application to the case studies included in the present research. These methods, discussed in the following sections, are kinematic limit analysis, pushover analysis and nonlinear dynamic analysis

2.4.1 Kinematic limit analysis

As discussed in Sections 2.2.2.1, it emerges that to many historical masonry structures, partial collapses occur due to the loss of equilibrium of parts behaving as rigid blocks. The vulnerability to local mechanisms is incremented by the lack of efficient connections among elements, like for instance among perpendicular walls. Consequently, the structure can be ideally divided into macro-elements with an almost independent structural behaviour. Verifications of damage and collapse regarding chosen local mechanisms can be performed by means of the limit equilibrium analysis based on the kinematic approach. By applying the principle of virtual work for a chosen mechanism, it is possible to estimate the

seismic capacity in terms of maximum force (linear kinematic analysis) and ultimate displacement (non-linear kinematic analysis) (Italian ministry of transport and infrastructure 2009). Each approach is explained as follows.

2.4.1.1 Linear kinematic analysis

The objective of linear kinematic analysis is to identify, for each kinematic admissible mechanism, the collapse coefficient c, defined as the seismic acceleration normalised according to acceleration of gravity g. To determine the horizontal load multiplier c that activates the local damage mechanism, it is necessary to apply the forces to a rigid block: the dead load of the blocks applied at their centre of gravity; the vertical loads carried by the block. The multiplier c is determined by applying the virtual work principle: equating the total work done by the external forces to the internal forces applied to the system corresponding to the virtual work.

2.4.1.2 Nonlinear kinematic analysis

Under linear kinematic analysis, the collapse coefficient c, that induces the loss of equilibrium, is obtained by evaluating the rotations between the blocks due to the kinematic mechanism. On the other hand, under nonlinear kinematic analysis the seismic performance of the structure is analysed until the collapse (c=0) by increasing the displacement of a control point and applying the principle of virtual works to the corresponding configurations. The curve obtained through the incremental kinematic analysis can be transformed into the equivalent SDOF system capacity curve. A direct comparison between the displacement ultimate capacity and the displacement spectrum demand can then be done.

2.4.2 Pushover analysis

2.4.2.1 Pushover analysis with invariant forces. Conventional approach

Today pushover analysis (inelastic static analysis) is one of the main approaches used for seismic assessment of historical masonry structures, as discussed in Section 2.4.4. Detailed description of history of development of pushover analysis is discussed by Elnashai (2001). One of the pioneer works on pushover analysis was carried out by Gulkan and Sozen (1974). They used a SDOF model in order to represent a MDOF structure equivalently. Simplified inelastic analysis procedures have been also proposed by Saiidi and Sozen (1981) and Fajfar and Fischinger (1988). The development of pushover analysis on MDOF systems is more recent. Krawinkler (1995) proposed a method in which shape vectors were established according to normalised displacement profiles at the first estimate of the target displacement level. However, this author mentioned that pushover analysis with invariant forces cannot detect changes caused by higher mode effects in the inelastic dynamic characteristics. The same mention is found in Bracci et al. (1997) as well. Kim and D'Amore (1999) made a comparison between pushover analysis and nonlinear time-domain dynamic analysis. In conclusion, it was stated that pushover analysis did not represent the same results predicted by nonlinear dynamic analysis with the

accelerograms generated from a set of different earthquake records. Interaction between inelastic MDOF structures of continuously-changing dynamic characteristics under various frequencies from a set of natural records cannot possibly be simulated by a single pushover analysis under a predefined and fixed lateral load or displacement vector.

To overcome limitations of pushover analysis including those mentioned above, advanced pushover analysis techniques have been developed (FEMA 440 (Federal Emergency Management Agency 2004), Aydinoglu 2003, Papanikolu and Elnashi 2005). Adaptive pushover analysis (APO) and multi-mode pushover (MMP) analysis are discussed in the following sections.

2.4.2.2 Adaptive pushover analysis

Adaptive pushover analysis (APO) uses the first mode and considers softening in the capacity curve that reflects a reduction in stiffness, which, in turn, results in a change in the mode shape (Federal Emergency Management Agency 2004). Under APO, lateral loads are adopted in proportion to the amplitude of a transforming first-mode shape. Early discussion on APO is also found in Krawinkler and Seneviratna (1998). Different methodologies of APO have been proposed in accordance with different load updating methods. Bracci et al. (1997) and Lefort (2000) proposed a method where the load is updated according to load-equilibrium patterns. According to the method proposed by Gupta and Kunnath (2000), a load pattern is updated constantly depending on the instantaneous dynamic characteristics of the structure and a site specific spectrum. At each load step, eigenvalue analysis is conducted. The force pattern for each mode is determined by multiplying the storey weight with the modal participation factor, mode shape and spectrum amplification. Then pushover analysis is conducted for each mode. The identified responses are combined using SRSS rule and then added to the previous load step. Albanesi et al. (2002) proposed that the force pattern is determined according to the inertial properties and the kinematic energy of the structure generated by strong motion. Antoniou (2004b) proposed two methods for load updating: total updating and incremental updating.

The total updating method replaces a totally new loading pattern at each step. The load vector P_t at a given step t is obtained by replacing fully the existing balanced loads (load vector at a previous step) with a newly derived load vector. The load vector P_t is calculated as the product between the current total load factor λ_t, the current normalised modal scaling vector $\bar{F}_t$ and the nominal load vector P_0, as shown in the equation (2.16).

$$P_t = \lambda_t \bar{F}_t P_0 \tag{2.16}$$

The incremental updating method increments the loading pattern at each step to that of the previous step. The load vector P_t at a given analysis step t is obtained by adding to the load vector of the previous step P_{t-1} (existing balanced loads) a newly derived load vector increment. This increment is calculated as

the product between the current load factor increment $\Delta\lambda_t$, the current modal scaling vector $\bar{F}_t$ and the nominal load vector P_0, as presented in the equation (2.17).

$$P_t = P_{t-1} + \Delta\lambda_t \bar{F}_t P_0 \tag{2.17}$$

The incremental updating method is preferred to the total updating method since the former updating method may cause instability to the analysis, according to the author.`

2.4.2.3 Multi-mode pushover analysis

Another recently-discussed tool of advanced pushover analysis is multi-mode pushover analysis (MMP). MMP considers the influence of higher modes on response quantities by combining peak response quantities obtained in separate pushover analyses for the first several modes with a combination method such as a SRSS combination (Federal Emergency Management Agency 2004). One of the pioneering works was carried out by Sasaki et al. (1998). They carried out pushover analyses separately for the first several modes in order to identify if higher modes had effect on causing collapsing mechanisms. Black and Aschheim (2000) carried out pushover analysis individually for the first two modes. Then the peak displacements and inter-story drifts from those analyses were combined by square-root-of-the-sum-of-the squares (SRSS) combinations. They observed significant divergence between the peak inter-story drifts and the SRSS estimation. Chopra and Goel (2002) described a method where pushover analyses are conducted independently for each mode (the first three or five modes).The procedure is explained as follows. Pushover analysis is carried out for each mode using invariant lateral load patterns associated with the each mode shape and capacity curves from each analysis are plotted separately. Then, the capacity curves of each mode are converted to a bilinear curve of a capacity diagram of the corresponding SDOF system. Peak inelastic displacement of the equivalent SDOF system of each mode is calculated for a given earthquake using the bilinear curve. Peak inelastic response quantities of interest (inter-story drifts and plastic hinge rotations) are calculated individually for each mode. Finally, according to the SSRS rule, peak response quantities from each mode are superposed. This MMP procedure is equivalent to response spectrum analysis (RSA) when MMP is carried out on elastic systems (Chopra and Goel 2002). This method was successful in estimating floor displacement and storey drift correctly but not plastic hinge rotations when it was adopted to a nine-storey steel moment-frame structure. Subsequently Chopra and Goel (2004) proposed an “improved” version of MMP. In this method, the P-Δ effect in all the modes is taken into account. In this method, plastic hinge rotation according to the estimated inter-storey drifts and assumed inelastic mechanism. For this application, the authors suggested to use the CQC (complete quadratic combination) rule for the superposition of the response values from the analysis of each mode instead of the SRSS rule. This improved method still lacks accuracy in estimating plastic hinge rotation and may overestimate the rotation in the lower stories and underestimating it in the upper stories. Jan et al. (2004) proposed a procedure where the first two modal pushover analyses are combined. Hernández-Montes

et al. (2004) proposed an energy-based pushover technique in order to overcome a problem regarding reversals of the higher mode pushover curves that were observed in the application of the method proposed by Chopra and Goel (2002).

2.4.3 Nonlinear dynamic analysis

Nonlinear dynamic analysis (NDA) using a set of ground motion records with a detailed structural model theoretically can produce results with relatively low uncertainty (Federal Emergency Management Agency 2004). However application of nonlinear dynamic analysis still remains a challenge. This may be due to the complexity of time-integration algorithms, difficulties in damping representation and the effect of both of the above on results, especially in terms of acceleration and force-related quantities (Elnashai 2002) and uncertainty associated principally with the lack of data on actual component behaviour, especially at high ductility (Federal Emergency Management Agency 2004). Moreover, the diversity of ground motion leads to significant dispersion in results. Through the application of a series of nonlinear dynamic analyses for increasingly larger intensities of ground shaking, it has been found that the dispersion of results increases with higher shaking intensity and with greater elasticity (Vamvatsikos and Cornell 2002). It is advisable to adopt this analysis method only when the other analysis methods including nonlinear static analysis fail in representing sufficiently reliable results (Italian ministry of transport and infrastructure 2009).

2.4.3.1 Solution of equation of motion

A comprehensive discussion of the application of NDA is found in Chopra (2001). The dynamic analysis aims at describing the displacement-time history of a system subject to time-domain loads. The history of displacements of the selected degrees of freedom is calculated by solving the equations of motion of the structure.

The equation of motion for a linear SDOF system subjected to external force is a second order differential equation (2.18).

$$m\ddot{u} + c\dot{u} + ku = p(t) \tag{2.18}$$

In this equation, m, c and k are the mass, damping and stiffness of the system, respectively. $p(t)$ is an applied force.

The equation of motion is solved by one of four methods presented below. Firstly, the classical solution is a complete solution of the linear differential equation of motion. It is an analytical time-domain solution and is useful for solving differential equation for free vibration and for excitation such as harmonic, step and pulse forces. Secondly, the Duhamel's integral represents an applied force as a sequence of

infinitesimally short impulses. It is also a time-domain method. Duhamel's integral can be alternative to the classical solution when the applied force is described by a simple function that permits analytical evaluation of the integral. Thirdly, the transform methods such as Laplace and Fourier transforms are powerful tools for the solution of linear differential equations, particularly the equation of motion for a linear SDF system. It is the frequency-domain method.

However, these three methods are limited to linear systems and cannot consider the inelastic behavior of structures if the ground shaking is intense. Hence, a fourthly presented method, numerical time-stepping methods such as Newmark's method is considered a practical approach for such systems. In the following case-study chapters, a numerical method (Newmark's method) is used. The Newmark's method assumes a linear variation of the acceleration over the time step. The Newmark's method is based on the following two equations (2.19) and (2.20).

$$\dot{u}_{i+1} = \dot{u}_i + \Delta t(1-\gamma)\ddot{u}_i + \gamma\,\Delta t\ddot{u}_{i+1} \quad (2.19)$$

$$u_{i+1} = u_i + \Delta t\dot{u}_i + \Delta t^2(0.5-\beta) + \Delta t^2\ddot{u}_{i+1} \quad (2.20)$$

These equations are controlled by parameters β and γ. These parameters define the stability and accuracy characteristics of the method. The typical value for γ is ½ and that for β is between 1/6 and 1/2. Newmark's equations with β=1/4 and γ=1/2 describe a case with constant variation of the acceleration, equal to the average acceleration over a time step (Figure 2.48 a). Those with β =1/6 and γ=1/2 correspond to the assumption of linear variation of acceleration over a time step (Figure 2.48 b). The latter is used for the nonlinear dynamic analyses (NDA) presented in following chapters.

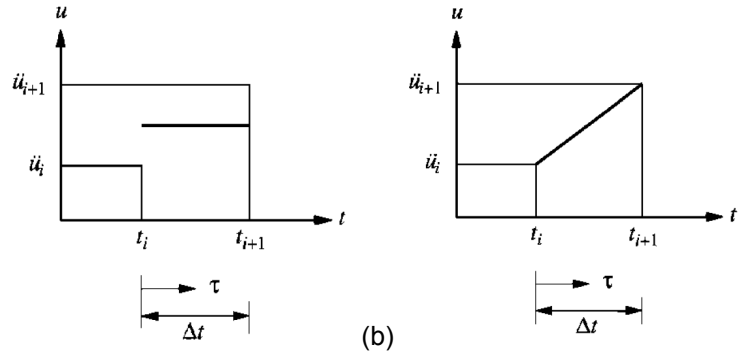

Figure 2.48 - (a) constant average acceleration and (b) linear variation of acceleration (Chopra 2001).

2.4.3.2 Adoption of damping model

The nonlinear dynamic analyses presented in following chapters have been carried out by adopting a Rayleigh damping model. Rayleigh damping is characterised by the two constants a_0 and a_1 (Bathe 1996), defined as

$$a_0 = 2\ \omega_1\ \omega_2\ \beta \tag{2.21}$$

$$a_1 = 2\ \beta \tag{2.22}$$

For a given damping coefficient ζ. ω_1 and ω_2 are the two lowest frequencies of the structural system. The Rayleigh damping parameter β is determined according to equations (2.23) and (2.24).

$$\beta = \frac{(1-\alpha)\zeta}{\omega_2 - \alpha\omega_1} \tag{2.23}$$

$$\alpha = \frac{\omega_1}{\omega_2} \tag{2.24}$$

2.4.4 Comparison of seismic assessment tools

Limit analysis is frequently used for safety analysis and for the design of strengthening (Binda et al. 2001b, Ramos and Lourenço 2004). One of the advantages of this method is that it can be carried out without requiring excessive computational effort. However, it can only be used to examine the ultimate state condition, and the choices of mechanisms to be analysed depend on the practitioner's experience (Cennamo et al. 2011). The determination of the most vulnerable mechanisms may not be simple when a large variety of mechanisms are possible in the structure (Boscato et al. 2014). In many cases, limit analysis predicts an ultimate capacity similar to that yielded by FEM pushover analysis (Milani et al. 2012, Betti et al. 2010, 2012). Boscato et al. (2014) have presented a case where overturning of a façade is predicted better by limit analysis than by nonlinear dynamic analysis (NDA).

Nonlinear static (pushover) analysis, normally based on macro-modelling, is one of the commonly used tools for seismic assessment (Pelà et al. 2009, Milani et al. 2012). Nevertheless, it has been reported that it may not simulate properly the out-of-plane behaviour of structures (Lourenço et al. 2011). The distribution pattern of the seismic equivalent load is an influential factor and it needs to be chosen carefully, according to the performance of the structure. Frequently-used distribution patterns are those defined in proportion to the mass of the structure (Betti et al. 2011, Casarin et al. 2008) and to the first modal shape (Betti et al. 2008, Lourenço et al. 2012). According to Galasco et al. (2006), the former load distribution induces more extensive damage while the latter can cause more damage on higher parts of the structure. Some authors (Krawrinkler and Seneviratna 1998) recommend to compare the results of pushover analysis with more accurate approaches (such as NDA) especially when the effect of the higher modes is dominant.

Eurocode 8 (CEN 2004) suggests the adoption of the N2 method proposed by Fajfar and Fischinger

(1987), which combines pushover analysis with the capacity spectrum approach. This method correlates the displacement capacity of the structure to the displacement demand of the expected earthquake. For symmetrical structures, good performance has been observed. Although attempts have been made for asymmetrical frame buildings (Fajfar 2002, Fajfar et al. 2005), further research is still required for other typologies. For highly irregular structures, the Italian Ministry for Cultural Heritage and Activities (2011) suggests the use of adaptive pushover analysis, in which the force distribution pattern is updated at each load step. Adaptive procedures are still under research (Galasco et al. 2006). Lourenço et al. (2011) applied a method where the load distribution pattern proportional to the first modal shape is updated as a function of the existing damage.

Although pushover analyses with predefined invariant forces have been used frequently for seismic assessment, it is known that there are limitations. For instance, they cannot detect changes caused in nonlinear dynamic characteristics due to higher mode effects (Krawinkler 1995). Considering disadvantages of invariant-force pushover analysis, advanced pushover analysis (i.e. MMP and APO) have been discussed (FEMA 440 (Federal Emergency Management Agency, 2004), Aydinoglu 2003 and Papanikolaou and Elnashi 2005). MMP has been developed by various researchers such as Sasaki et al. (1998), Reinhorn (1997), Chopra and Goel (2002), and Jan et al. (2004). It permits the consideration of higher modes in pushover analysis. When MMP is applied to elastic models, it should be equivalent to response spectrum analysis (Chopra and Goel 2002). One of the defects of this method is that the sequence of damage development is not observed since only the final deformed shape is presented by superposition of the deformed shape from each mode. In addition it still lacks accuracy in estimating plastic hinge rotation. It may lead to overestimate the rotation in the lower stories and underestimate it in the upper stories when adopted for a multi-story RC frame building (Chopra and Goel 2004). Almost in parallel with MMP, APO also has been developed by different investigators such as Bracci et al. (1997), Albanesi et al. (2002) and Antoniou (2004a, b). This method can consider damage occurring in the course of the analysis by updating force distribution patterns. APO considers the state of local resistance and of inelasticity at the current step and updates the lateral load distributions accordingly (Papanikolaou and Elnashi 2005). However, updating methods and frequency of load update are still under research.

Alternative approaches to pushover analysis are response spectrum analysis (Apostolopoulos et al. 2008, Cennamo et al. 2010, Cagnan 2012, Pelà et al. 2013a) and nonlinear dynamic analysis in the time-domain (NDA) (Pelà et al. 2013b, Lourenço et al. 2011, Milani et al. 2012). With a set of carefully chosen ground records, NDA offers accurate evaluation of structural seismic response. However, its practical use still encounters difficulties due to its complexity and high computer effort demand (Mwafy et al. 2001). According to Casolo and Uva (2013), NDA is suggested to be used when detailed vulnerable assessment is required. For analysis of complex buildings, partial models are frequently used, involving, for instance, a bell tower or a single façade (Boscato et al. 2014, Bayraktar et al. 2012).

2.5 Discussion

In the state-of-art discussion, four topics have been dealt with. Firstly, as masonry mechanics, the mechanical property and the structural behaviour have been reviewed. Secondly, the typology and behaviour of vertical elements and Catalan vaults have been discussed. Thirdly, structure-analysis techniques (Limit analysis, FEM analysis and DEM analysis) have been reviewed. Fourthly, seismic assessment tools (kinematic limit analysis, pushover analysis and nonlinear dynamic analysis) have been discussed. The discussions will be taken advantage of especially for the structural analysis discussed in Chapter 4, 5, 6.

2.5.1 Masonry mechanics

2.5.1.1 Mechanical property

In Section 2.1.1, different mechanical parameters have been discussed including compressive strength, tensile strength, Young's modulus, shear strength and shear modulus. European (CEN 1996), Spanish (PIET 1971) and Italian (Italian ministry of transport and infrastructure 2009) codes have given a good insight on the values of mechanical property which will be employed in the present research. In European code (CEN 1996) the compressive strength of a unit and mortar is used to calculate the characteristic value of masonry compressive strength. Spanish code (PIET 1971) presents a set of design values of compressive strength for clay brick masonry and stone masonry, considering the type of unit and mortar. The thickness and consistency of mortar are also taken into account. Italian code (Italian ministry of transport and infrastructure 2009) presents the recommended average values of mechanical property of both stone and brick masonry according to their visual appearance. In addition to the codes, some articles including discussions on masonry parameters have been also reviewed. Kaushik (2007) carried out on uniaxial compression test on clay brick masonry. He also presented and compared equations of different researchers and codes. As a result, he proposed his equation to calculate compressive strength and Young's modulus of clay brick masonry. Some researchers (Jäger and Pech 2014, Liberatore et al. 2014, Geoff 2014) have discussed the adequacy of equations including that of the code of Eurocode 6 (CEN 1996), applying the experimentally determined values of units and mortar to these equations and comparing them with also the experimentally obtained values of masonry.

2.5.1.2 Structural behaviour

The behaviour of unit-mortar interface and of the masonry as composite material has been reviewed.

The unit-mortar interface dominates the behaviour of masonry under pure tension loading normal to joint and pure shear one parallel to joint. Tension and shear mode (mode I and mode II) has been discussed. In case of mode I, tensile failure has been reviewed and in case of mode II, sliding failure has been discussed.

For the behaviour of masonry as a composite material, uniaxial compression or tension behaviour and biaxial compression/tension behaviour has been discussed. Uniaxial compression loading to masonry results in uniaxial compression and biaxial tension in a unit and tri-axial compression in joint. Therefore it can be said that, under uniaxial compression, the compressive strength of masonry is dependent on the tensile strength of units. Failure modes under uniaxial compression partially depend on the strength of mortar. Strong mortar causes rather brittle failure while weak mortar ends in ductile failure with slow crack propagation. Under uniaxial tension loading, masonry behaves as linear elastic material. Tensile failure is characterised by splitting along the interface. According to the direction of the loading (a load applied normal or parallel to bed joints), different types of failure are observed. From the load applied normal to bed joints, failure occurs due to low tensile bond strength between the units and the joint. The tensile strength of the masonry normal to bed joints is nearly same as the tensile bond strength between the units and joint. From the load applied parallel to bed joints, two different failure modes can be observed. In the first case, a stepped crack through head and bed joints is observed as failure. In the second case, a vertical crack throughout head joints and units is seen. Under biaxial compression/ tension behaviour, nonlinear behaviour is observed due to sliding along the interfaces. Under compression-tension, masonry fails elastically at a low value of the load.

2.5.2 Typology and behaviour of masonry structural elements

2.5.2.1 Vertical elements

Vertical structural elements (walls, pillars and columns) have been reviewed in terms of its typology and structural behaviour under seismic action.

As for walls, stone, brick and mixed brick-stone masonry walls have been discussed. For stone masonry walls, classifications were made by researchers considering factors including the presence of connection elements, shape of the stone elements, average dimension of stones, thickness of the bed joint, horizontality of the courses, and type of cross section of the masonry wall. As for brick masonry walls, it has been mentioned that their characteristic is influenced by the extent and quality of bond between mortar and bricks and the connection between the leaves. Old brick masonries have usually very thick sections (more than 600 mm in many cases) with a much less homogeneous distribution of the bricks in the section than in modern ones. For mixed brick-stone masonry walls, in some examples, the brickwork is regularly located and crossed thoroughly to connect the two leaves of the masonry, as improves the behaviour under seismic action. In others, the bricks are aligned irregularly.

Historical pillars typically consist of an external leaf and internal rubble core while columns are composed of monolithic elements such as large stone blocks. As a peculiar example of a pillar, in the Mallorca cathedral in Spain, the section of a pillar consist of five stones of similar quality, the 5th one, of square shape, placed in the centre. The stones rotate 45 degrees at each row to provide sufficient interlocking.

As for structural behaviour of a masonry wall under seismic action, both out-of-plane and in-plane mechanisms have been discussed. Typical collapse mechanisms of churches have been categorised by the Italian Ministry for Cultural Heritage and Activities (2011), considering macro elements such as façade, nave, triumphal arch, apse, dome and bell tower. Recently, as part of NIKER project, collapse mechanisms of historical masonry structures have been discussed in a report from the project (NIKER report 2010). A comprehensive web-based catalogue of collapse mechanisms of historical masonry buildings has been also presented for different structural typologies (NIKER catalogue 2013). In case of churches which will be studied extensively in Chapter 6, the collapse mechanisms involving a façade are the most representative. Triumphal arches, domes and vaults are also vulnerable members.

Failure of a pillar is mostly overturning due to the out-of-plane bending. For columns, drum shifting can occur. The long-term phenomenon can also lead to the collapse for both pillars and columns. The long-term high compressive load causes the vertical cracks, as may end in the collapse as a result of the crack propagation. It has been discussed that a slender structures such as towers also show similar long-term behaviour.

2.5.2.2 Catalan vaults

Among different types of vaults, the particular focus on the Catalan vaults is due to the case study objectives in the present research. In the following chapters (Chapter 4, 5) different Catalan vaults will be studied. In the 18th century, some stated that Catalan vaults were solid enough to avoid cracks when they were built with good-quality mortar. However, cracking and hinges are observed in Catalan vaults like in other types of masonry vaults. On the other hand, Catalan vault can be constructed without centring or with light supplemental supports due to the cohesiveness. Therefore, the advantage of Catalan vaults to other types of vault can be seen in the construction process. Nevertheless, once it is completed, they should be considered to generate cracking and form hinges like other types of masonry vaults.

2.5.3 Structural-analysis techniques

2.5.3.1 Limit analysis

Discussions have been made on three recently-proposed structural analysis techniques for three-dimentional vaulted structural systems. They were developed, based on limit analysis of Heyman (1966).

Firstly, O'Dwyer (1999) proposed an analysis method for curved shell structures by decomposing curved masonry shell structures into a system of arches in equilibrium. Simple application is an advantage of the method. Discretisation of loads and structural discontinuity can be incorporated easily. On the other hand, results heavily depend on discretisation patterns. In addition, this methodology is

time-consuming because nonlinear problem is solved by a simple linear programming problem repeatedly.

Secondly, Ochsendorf and Block (2008a) proposed a method based on the reciprocal relationship between the geometry and the in-plane internal forces of networks of Williams (1986). As an advantage of the methodology, different force patterns between the maximum and minimum case can be prepared and compared in a straightforward manner. The model of a vault can have continuous edge supports or just corner supports. Imposed loads such as fillings can easily be integrated by adding loads to the affected nodes. Moreover, problems can be resolved as a one-step linear optimisation. As a disadvantage, all the possible force patterns and diagrams have to be considered until the absolute minimum and maximum values of thrust can be identified.

Thirdly, Andreu et al. (2007) developed a computational technique in which masonry structures are modelled as three-dimensional catenary networks. As an advantage of this methodology, modelling process is simple and complex material parameters are not required. The ultimate capacity of the structure is easily estimated by applying the uniqueness theorem. Because the number of degrees of freedom is limited, the analysis does not require high computational effort. In addition, since the method is based on a direct physical analogy with a catenary, the result would not include a large number of errors. As a disadvantage, load paths in the structure should be known in advance to the analysis. In other words, the method requires the sufficient understanding of the structural behaviour and also the catenary principles.

2.5.3.2 FEM analysis

For FEM analysis, macro-modelling approach oriented especially to masonry vaulted structures has been reviewed. Although nonlinear FEM analyses may permit an accurate study of the response of the structure, FEM models can be very sensitive to some factors including changes in boundary conditions, load history and may predict the formation of cracks in unexpected locations. The solutions provided by an initial FEM model must always be validated against known information on the real structure such as experimental results, crack locations and/or other damage. Through the validation process, the initial model may probably need to be updated. It is also important to study the influence of the different parameters on results through a parametric study. FEM strategies for historical masonry structures will be discussed in Chapter 3.

2.5.3.3 DEM analysis

DEM can ideally simulate structural behaviour of blocky structures such as systems composed of columns and arches. The analysis of large structures may pose difficulties relevant to the size of DEM elements. Principally, the element sizes should be same as the actual dimensions of the masonry units but this may be impractical for large structures. Therefore, a simplified modelling strategy is usually

considered, with the element sizes becoming larger than the real ones. In this case, additional judgment is necessary so as to adjust deformability of joints and blocks.

2.5.4 Seismic-assessment tools

Three seismic assessment tools (kinematic limit analysis, pushover analysis and nonlinear dynamic analysis) have been discussed. For pushover analysis, advanced techniques such as adaptive and multi-mode pushover analysis have been also reviewed.

Limit analysis is frequently used for safety analysis and for the design of strengthening. As one of the advantages of this method, it can be carried out without requiring excessive computational effort. However, it can only examine the ultimate state condition and the choices of mechanisms to be analysed are dependent on the practitioner's experience. The determination of the most vulnerable mechanisms may not be easy when a large variety of mechanisms are possible in the structure. It is typical that limit analysis predicts an ultimate capacity similar to that yielded by FEM pushover analysis.

Pushover analysis is one of the frequently used tools for seismic assessment. Nevertheless, it has been reported that it may not show adequately the out-of-plane behaviour of structures. The distribution pattern of the seismic equivalent load is a dominant factor so its choice should be done carefully, considering the behaviour of the structure. Commonly-used distribution patterns are those defined in proportion to the mass of the structure and to the first modal shape. The former load distribution pattern leads to more extensive damage while the latter one can end in more damage on higher parts of the structure.

Although pushover analyses with predefined invariant forces have been used frequently for seismic assessment, there are limitations. For instance, it is known that they cannot detect changes caused in nonlinear dynamic characteristics due to higher mode effects. Considering disadvantages of invariant-force pushover analysis, advanced pushover analysis (i.e. multi-mode pushover analysis and adaptive pushover analysis) have been discussed.
It is advisable to compare the results of pushover analysis with more accurate approaches (such as nonlinear dynamic analysis) especially when the effect of the higher modes is dominant. It is said that with a set of carefully chosen ground records, NDA provides accurate evaluation of structural seismic response. Nevertheless, its practical use still poses difficulties due to its complexity and high computer effort demand. NDA is suggested to be used when detailed vulnerable assessment is necessary. For analysis of complex buildings, partial models are commonly used, involving, for instance, a bell tower or a façade.

2.6 Conclusions

Discussions in the state-or-art discussions will be taken advantage of in the following chapters (Chapter 4, 5, 6). As masonry mechanics, the mechanical property and the structural behaviour have been reviewed. The mechanical parameters of masonry of the case study buildings in Chapter 4, 5, 6 will be determined considering these discussions. The typology and behaviour of vertical elements and Catalan vaults have been discussed. The results obtained from structural analysis will be discussed considering the findings in these sections. In addition, mechanisms to be analysed by kinematic limit analysis will be chosen taking advantage of these discussions. Three structure-analysis techniques (Limit analysis, FEM analysis and DEM analysis) have been reviewed. Considering the advantages and shortcomings of each technique, limit analysis and FEM analysis will be employed. Especially, FEM analysis based on macro modelling will be regarded as the principal technique since case study structures are complex and in a large scale. Three seismic-assessment tools (kinematic limit analysis, pushover analysis and nonlinear dynamic analysis) have been discussed. Pushover analysis and nonlinear dynamic analysis will be considered the principal tool. Pushover analysis will be used since it can represent structural behaviour with sufficient accuracy without requiring extreme computational effort. As for the lateral load distribution patterns, different ones will be applied and compared including those defined in proportion to the mass of the structure and to the first modal shape. Adaptive and multi-modal pushover analysis will be adopted as well. Nonlinear dynamic analysis will be also used since it represents structural behaviour more accurately than pushover analysis although it requires higher computational effort than pushover analysis. Kinematic limit analysis will be used due to its simple application and compared with the results obtained from pushover and nonlinear dynamic analysis.

3. NUMERICAL STRATEGIES ADOPTED FOR THE PRESENT RESEARCH

In this chapter, numerical strategies used for following case-study chapters are reviewed. The topics are composed of two themes: FEM-modelling strategies and analysis procedures. Discussions on the FEM modelling strategies deal with micro/macro-modelling approaches, types of finite element, numerical integration scheme and material behaviour including cracking. Discussions on the analysis strategies deal with iterative techniques, line search method, force/displacement control and convergence criteria. The discussions in this chapter are taken advantage of for the FEM analyses carried out in the present research.

3.1 FEM-modelling strategies

3.1.1 Modelling approaches

In accordance with level of accuracy and simplicity required, one of the following modelling strategies is chosen: (a) detailed micro-modelling, (b) simplified micro-modelling and (c) macro-modelling (Figure 3.1) (Lourenço 2002). Masonry shows distinct directional properties due to mortar joints that act as planes of weakness. Therefore for detailed analysis of masonry, it is necessary to include a representation of units, mortar and unit/ mortar interface, as is realised by the micro modelling approach. The macro-modelling approach, on the other hand, is applicable when the structure is composed of solid walls with sufficiently large dimensions for which the assumption of a homogeneous material is acceptable at a macroscopic level. The two approaches are discussed in the following sections.

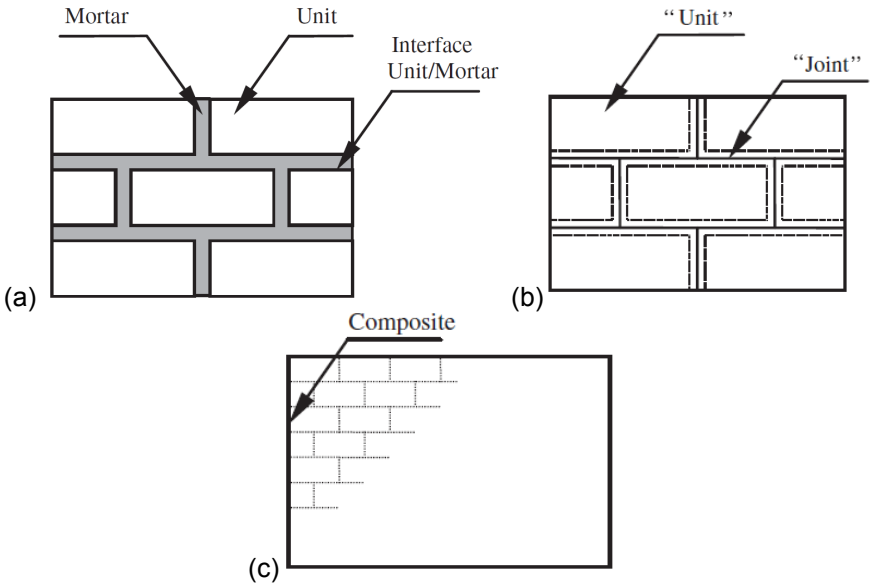

Figure 3.1 - Modelling strategies for masonry structures: (a) detailed micro-modelling, (b) simplified micro-modelling and (c) macro-modelling (Lourenço 2002).

3.1.1.1 Detailed micro-modelling approach

Page (1978) is considered to be the first person that attempted to apply micro-modelling approach to masonry structures. Under his approach, nonlinear behaviour was described in an unsophisticated way as a material showing brittle behaviour in tension and hardening in shear/compression.

Detailed micro models represent units and mortar with continuum finite elements while unit-mortar interface is represented with interface elements. This approach take into account Young's modulus, Poisson's ratio and, optionally, inelastic properties of both unit and mortar. The interface includes a potential crack/slip plane with initial dummy stiffness to avoid interpenetration of the continuum. This permits the combined action of unit, mortar and interface to be studied under a magnifying glass (Zucchini and Lourenço 2002).

The nonlinear behaviour of the interfaces has been studied in detail by means of such models (Rahman and Anand 1994, Lourenço and Ramos 2004) and the individual fracture of mortar and bricks (Guinea et al. 2000). Drougkas et al. (2014) proposed a detailed micro-modelling approach in which units, mortar and their interface are modelled as separate parts for the estimation of the compressive strength and the Young's modulus of the masonry composite.

The detailed micro modelling is appropriate for small structural elements showing strongly heterogeneous states of stress and strain (Berto et al. 2002). However, it is usually not feasible, due to the computer effort demand, to carry out failure analysis of large and/or geometrically complex structures with this approach (Reyes et al. 2009).

3.1.1.2 Simplified micro-modelling approach

The detailed micro-modelling approach can represent behaviour of masonry with sufficient accuracy as discussed above. On the other hand, it may be considerably impractical to analyse a complicated structure with this approach due to its computational effort. Simplified micro-modelling may provide more accurate results than macro-modelling with less computational effort than the detailed micro-modelling (Lofti and Shing 1994, Lourenco 1994, Lourenço and Rots 1997, Sutcliffe et al. 2001).

Lourenço (1998) proposed a model that can represent cracking, crushing and shearing failure (Figure 3.2). Material properties of the model were determined, based on laboratory tests discussed by him in the same paper (Figure 3.3). This approach is suitable for small structures experiencing considerably diverse stress and strain. Although it is time consuming, it allows us to comprehend behaviour of each component: mortar, unit and their interface. It is mentioned that it is complicated to update contact behaviour between the elements during the analysis and accommodate large displacements.

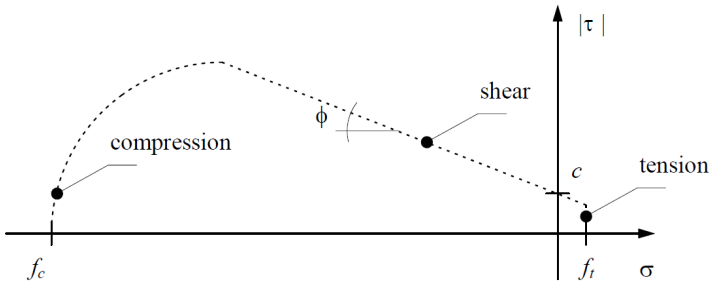

Figure 3.2 - Interface model for masonry (plane stress representation) (Lourenço 1998)

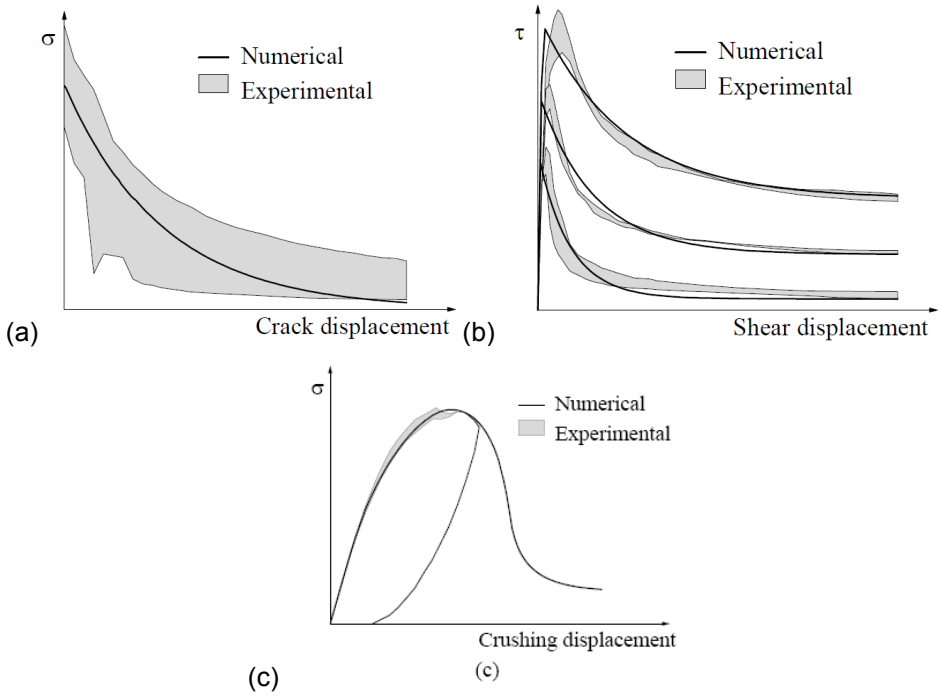

Figure 3.3 - Behaviour of the model for (a) uniaxial tension, (b) shear and (c) uniaxial compression (Lourenço 1998).

Gambarotta et al (1997a, b) proposed a simplified micro-modelling approach based on damage models for the study of the seismic response of brick masonry shear walls. In this approach, masonry is regarded as a set of inelastic blocks connected by potential fracture/slip lines at joints. Expanded units are used to represent continuum elements. The behaviour of mortar joints and unit-mortar interfaces is described in interface elements. The authors prepared a model in which brick units are modeled with four or eight-node iso-parametric elements while mortar joints are modeled by four-node interface element (Figure 3.4). Failure criteria of the interfaces in tension include sliding and cracking (Figure 3.5). Comparison was made between experiments and analysis of rectangular shear walls experiencing a horizontal force at the top.

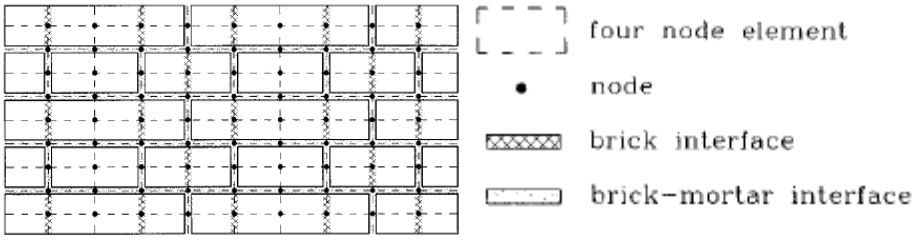

Figure 3.4 - Finite element composite model of the masonry (Gambarotta et al. 1997a).

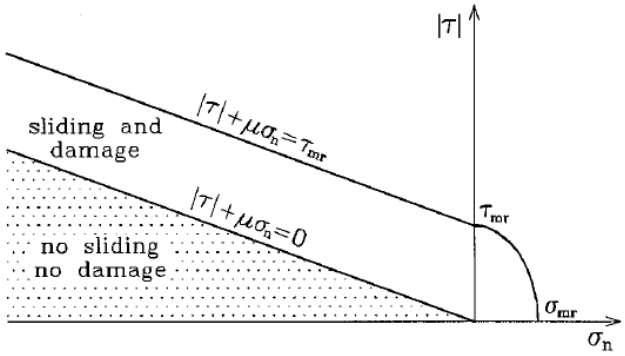

Figure 3.5 - Limit strength domain and elastic domain of the mortar joint in the (σ_n, $|\tau|$) plane (Gambarotta et al. 1997a).

3.1.1.3 Macro-modelling approach

This approach does not differentiate between individual units and joint. Instead, it considers masonry as homogeneous continuum. This approach is practical when a compromise between accuracy and efficiency is required.

Lourenço (1997) developed this approach by using plate and shell elements. The author combined a concept of plasticity with anisotropic material behaviour by applying different hardening/softening behaviour in each material axis. A Rankine-like yield surface for tension and a Hill-like yield surface in compression were adopted (Figure 3.6). As a result, the model showed different behaviour along each direction. Implementation of this model ended in satisfactory results in terms of collapse loads and reproduced behaviour. As a matter of fact, Pelà et al. (2013c) proposed a macro-model, based on continuum damage mechanics, for the in-plane analysis of masonry structures. The orthotropic behavior of the material is simulated by means of an original methodology, resulting from the concept of mapped tensors from the anisotropic field to an auxiliary workspace (Pelà et al. 2011). Thanks to appropriate mapping of Rankine and Drucker-Prager criteria in the anisotropic space, it was possible to reproduce the anisotropic failure envelopes of different types of masonry. The constitutive model makes use of two scalar damage variables which monitor the damage under tension and compression. The model is able to capture the stiffness, the strength and the inelastic dissipation in each material direction.

The macro-models have been extensively employed to analyse the seismic response of complex masonry structures such as arch bridges (Pela' et al. 2009), historical buildings (Mallardo et al. 2008)

and mosques and cathedrals (Roca et al. 2004, Martínez et al. 2006; Murcia-Delso et al. 2009). The macro-modelling approach has been used extensively for the seismic analysis of large-scale historical masonry structures, as discussed in Section 2.4.4.

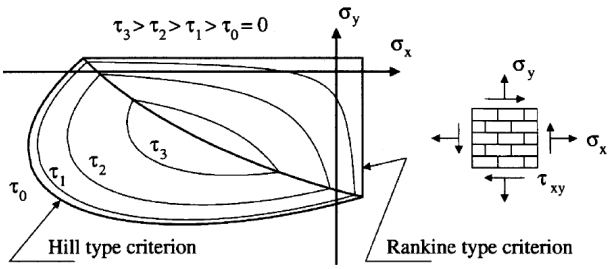

Figure 3.6 - Continuum failure surface for masonry (plane stress representation) (Lourenço 2002).

3.1.2 Choices of finite element types

In the thesis, shell, beam and interface elements are combined for modelling of the different case studies. Discussions on finite element types are found in some books (Zienkiewicz and Tayler 2005, Bathe 1986, 1996, de Borst et al. 2012, Krenk 2009) and in an article of Dvorkin and Bathe (1984).

3.1.2.1 Shell elements

In the present research, shell elements are principally used to represent sufficiently wide structural elements such as walls and vaults (Dvorkin and Bathe 1984, Manie and Kikstra 2012).

For the adopted curved shell elements, the local axes are defined as seen in Figure 3.7. The local z direction is perpendicular to the element plane. Local element $\bar{x}$ axis directs from the first to the second node of the element. The local y axis is perpendicular to the $z\bar{x}$ plane. The local x axis is perpendicular to the yz plane.

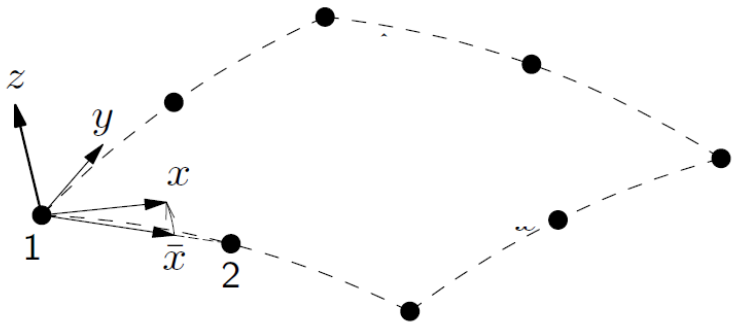

Figure 3.7 – Definition of local axes for shell elements.

Two types of curved shell elements are adopted. Firstly, s, a three-node triangular and four-node curved quadrilateral shell element are considered (Figure 3.8 a b). The following strain and stress distribution

are adopted. The strain ε_{xx}, the curvature κ_{xx}, the moment m_{xx}, the membrane force n_{xx} and the shear force q_{xz} are constant in local x direction and vary linearly in local y direction. The strain ε_{yy}, the curvature κ_{yy}, the moment m_{yy}, the membrane force n_{yy} and the shear force q_{yz} are constant in local y direction and vary linearly in local x direction.

Secondly, a six-node triangular and eight-node quadrilateral curved shell element are considered (Figure 3.8 c d). The following strain and stress distribution are adopted. The strain ε_{xx}, the curvature κ_{xx}, the moment m_{xx}, the membrane force n_{xx} and the shear force q_{xz} vary linearly in local x direction and vary quadratically in local y direction. The strain ε_{yy}, the curvature κ_{yy}, the moment m_{yy}, the membrane force n_{yy} and the shear force q_{yz} vary linearly in y direction and vary quadratically in local x *direction*.

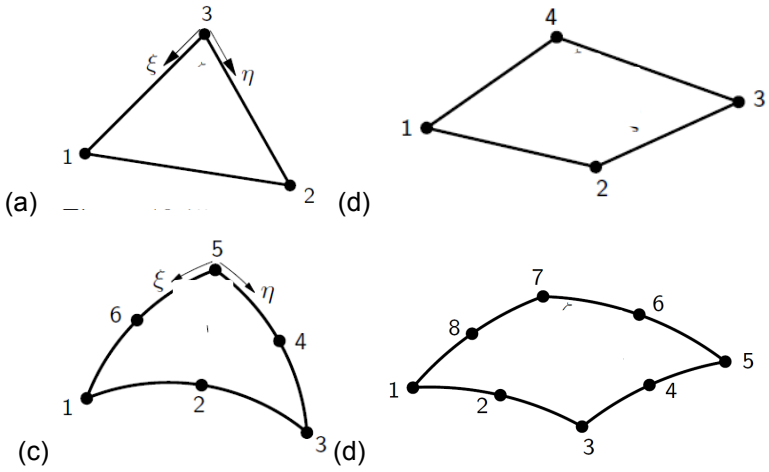

Figure 3.8 – Shell element types: (a) triangular 3-node, (b) quadrilateral 4-node curved, (c) triangular 6-node, (d) quadrilateral 8-node shell element (Manie and Kikstra 2012).

3.1.2.2 Beam elements

Beam elements are used to represent linear structural elements including arches and columns. Two types are considered, including a straight three dimensional two-node element and a curved three dimensional three-node element. Both elements are numerically integrated over its cross section and along its axis (de Borst et al. 2012, Krenk 2009, Manie and Kikstra 2012).

The straight three dimensional two-node element keeps its cross-sections plane and perpendicular to the slope of the beam axis (Figure 3.9 a). As a result, shear deformation along the axis is not taken into account in this element. The strains vary linearly along the center line of the beam.

For curved three dimensional three-node element, the normal strain ε_{xx} varies linearly over the cross-section area and the transverse shear strains remain constant (Figure 3.9 b). Shear deformation

is taken into account in this element, as opposite to the former straight two-node beam element. The displacement and rotation of the normal beam axis are individually interpolated from the displacement and the rotation in each node. One of the advantages of this element is that it can represent a curved shape. .

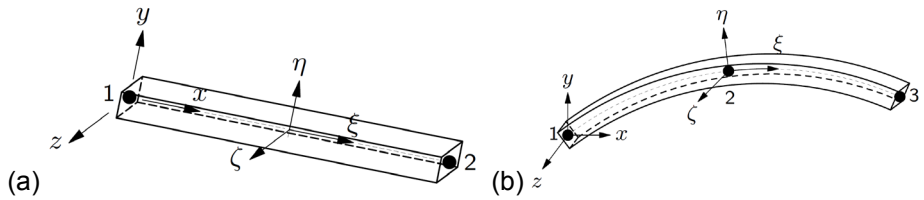

Figure 3.9 – Beam element types: (a) straight 2-node 3D and (b) curved 3-node 3D beam element (Manie and Kikstra 2012).

3.1.2.3 Interface elements

For representation of interface behaviour, three interface elements are considered, corresponding to the following three types of interface element (de Borst et al. 2012, Zienkiewicz and Tayler 2005, Manie and Kikstra 2012).

Firstly, a 6-node line interface element is used between two lines in a curved shell configuration. The local x axis defines the direction from the node 1 to 2 of the element as seen in Figure 3.10 a. The local y axis is perpendicular to the local x axis. The local z axis is in the thickness direction of the interface. The element is based on quadratic interpolation.

The second is a 4-node interface element between two lines in a curved shell configuration (Figure 3.10 b). For the local x,y and z axis, the same scheme as the 3+3 interface element is. The element is based on linear interpolation.

Thirdly, a 2-node interface element is an interface element between two nodes in a three-dimensional configuration (Figure 3.10 c). The local x axis is defined in the direction along nodes 1 and 2 of the element. The interface plane is defined perpendicular to the direction of the x axis.

These three different elements are chosen according to the type of adjacent FEM elements: e.g. for the interface between two eight-node quadrilateral shell elements, a 3+3 node line interface element is adopted.

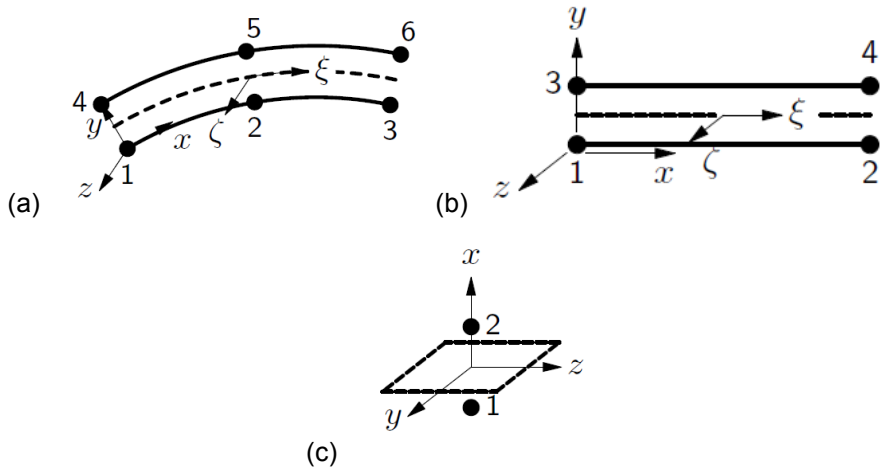

Figure 3.10 – Interface element types: (a) 3+3 node line interface element, (b) 2+2 node line interface element and (c) 1+1 node interface element (Manie and Kikstra 2012).

3.1.3 Choice of the order of numerical integration

The choice of the order of numerical integration is significant for two reasons (Bathe 1996). Firstly, higher computational effort is required with higher-order integration. Secondly, solutions are sensitive to an integration order, especially in three dimensional analyses. In the present research two integration schemes are considered, namely Gauss and Simpson integration. In the former scheme, all the integration points are located in the interior of elements. On the other hand, in Simpson scheme, integration points are positioned on the boundary and also the interior of elements. Gauss integration is preferred for analysis of solids (Bathe 1986). Simpson integration is more preferred for beams, plates and shells (de Borst et al. 2012). This integration scheme is also appropriate for interface elements. Bathe (1996) made a suggestion for an appropriate number of integration points over the area for quadrilateral shell elements as follows: 2x2 for four-node elements, 3x3 for eight- and nine-node elements and 4x4 for 16-node elements.

3.1.4 Representation of cracking behaviour

Numerical modelling of cracking in reinforced concrete launched in the late 1960s with pioneering articles of Ngo and Scordelis (1967) and Rashid (1968). They introduced smeared and discrete crack concepts. In the smeared cracking approach, a cracked element is considered continuum with a change in material behaviour from isotropic character to orthotropic one. Criteria for crack propagation and prediction of its direction are based on failure criteria described in terms of stresses or strains. In the discrete approach, on the other hand, each crack is represented by discontinuity in meshes. A crack occurs as a node separation on the side of adjacent elements, when the nodes' principal tensile stresses reach the material tensile strength. Criteria for crack propagation and direction are based on energy criteria. In the 1970s, investigations of the smeared cracking approach were carried out extensively so as to reproduce stress-strain characteristic of concrete that were identified experimentally. Today still this approach is preferred due to the high computational effort required by the discrete approach (Nuroji

et al. 2010). Comprehensive discussions on constitutive models are found in the papers of de Borst (1997), Giordano et al. (2002) and Jiarsek et al. (1998), the reports by Hube and Mosalam (2009) and Nuroji et al. (2010) and the PhD thesis of Rots (1988). In this section, both concepts are discussed and compared.

3.1.4.1 Smeared cracking

Smeared crack concepts can be broken into fixed and rotating smeared crack concepts (Rots 1988). Under a fixed concept, the orientation of a crack is fixed during the entire computational process or updated in a stepwise manner. On the other hand, a rotating concept permits the orientation of a crack to co-rotate with the axes of principal strain. In this section firstly the two fixed crack concepts are reviewed: total strain and multi–directional fixed crack concept. Then, also rotational crack concept is discussed.

3.1.4.1.1 Fixed total strain cracking

This model was first proposed by Vecchio and Collins (1986) in two dimensional modified compression field theory. Later, it was extended to three dimensions by Selby and Vecchio (1993). For this model, stress-strain relationships are evaluated in a fixed coordinate system that is determined once cracking initiates. A strain vector, ε in the global coordinate system xyz at iteration $i+1$, for a nonlinear static loading, is described with the strain increment $\Delta\varepsilon$ according to the equation (3.1).

$$\varepsilon^{i+1} = \varepsilon^{i} + \Delta\varepsilon^{i+1} \tag{3.1}$$

This constitutive model describes stresses as a function of strains. This notion is known as hypo-elasticity (softening elasticity) when the loading and unloading behaviour is along the same stress–strain path. Figure 3.11 shows the two extreme of unloading/reloading types: elastic and secant.

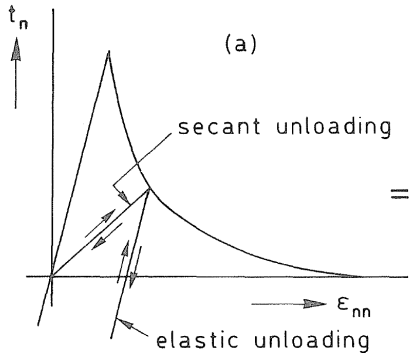

Figure 3.11 – Secant and elastic unloading in elastic-softening behaviour: normal stress against total strain (Rots 1989).

For elastic unloading, the crack closes (more technically speaking, the crack becomes inactive) immediately after a strain reversal. Then rigorously it returns to elastic behaviour. As for secant

unloading, the crack normal strain is reversible. Upon reaching the origin of the diagram (thus, ε_{nn}=0 in Figure 3.11), the crack becomes inactive. Then elastic behavior is recovered. For both elastic and secant cases, it is assumed that an inactive crack opens again when the stress normal to it goes beyond the stress which existed upon closing. In the present research, the secant unloading is considered for the simulation of loading/unloading behaviour.

3.1.4.1.2 Fixed multi-directional crack

The first proposal of the fixed multi–directional crack model was made by Litton (1975). This method is based on the concept of decomposition of the total strain increment into an elastic strain increment $\Delta\varepsilon^e$ and a crack strain increment $\Delta\varepsilon^{cr}$ according to the equation (3.2).

$$\Delta\varepsilon = \Delta\varepsilon^e + \Delta\varepsilon^{cr} \tag{3.2}$$

$\Delta\varepsilon^{cr}$ can also be decomposed into multiple increments, as shown in the equation (3.3).

$$\Delta\varepsilon^{cr} = \Delta\varepsilon_1^{cr} + \Delta\varepsilon_2^{cr} + \ldots \tag{3.3}$$

$\Delta\varepsilon_1^{cr}$ is the global crack strain increment due to a primary crack, $\Delta\varepsilon_2^{cr}$ is the global crack strain increment due to a secondary crack and so on. According to this decomposition, it is possible to include also thermal, and creep strains in strain increments (Hube and Mosalam 2009).

Once a crack starts, the crack is considered to be located perpendicular to the direction of the principal tensile stress. The fixed multi-directional concept controls the formation of subsequent cracks via the threshold angle. When the angle of inclination between existing crack(s) and the current direction of principal stress goes beyond the value of a certain threshold angle, a new crack starts to appear.

As a limitation of this concept, it has been discovered that maximum allowable tensile stress may become larger than input tensile strength. Under the concept, it is considered that the successive initiation of cracks occurs if the following two conditions are satisfied at the same time. As the first condition, the principal stress violates the stress condition, as is governed by a tension cut-off criterion as explained in Section 3.1.5.1. As the second one, the angle between the existing crack and the principal tensile stress exceeds the threshold angle, as discussed above. As a result, according to Rots (1988), it is possible that tensile stress temporarily becomes three times greater than tensile strength while the threshold angle condition is not violated yet.

3.1.4.1.3 Rotating crack

Cope et al. (1980) proposed a concept in which the axes of material orthotropy co-rotate with the axes of principal strain. However, their approach was criticised by Bazant (1983). As one of the issues, the

rotation of principal stress did not coincide the rotation of principal strain due to the assumption of material orthotropy. The rotating crack formulations proposed by Gupta and Akbar (1984) overcome this deficiency. Applications with fixed and rotating cracks were systematically examined by Rots (1988). His Ph. D. dissertation is regarded as a standard reference for modern smeared crack formulations (Jirasek and Zimmermann 1998).

The rotating total strain crack concept uses the coaxial stress-strain approach, in which the stress-strain relationships are evaluated in the principal directions of strains, coinciding with the direction of a crack (Hube and Mosalam 2009). On the other hand under the rotating concept considering the threshold angle for multi-directional cracks to vanish, a new crack arises at the beginning of each step of the incremental process. It is possible to regard rotating multi-directional cracking as equivalent to a collection of fixed tiny cracks of different orientation (Rots 1989).

3.1.4.2 Discrete cracking

A pioneering work in this approach is found in the paper of Ngo and Scordelis (1967). The discrete crack model represents strain discontinuity on elements by means of node separation. It occurs when the principal tensile stress reaches tensile strength at a nodal point. However the node separation at the side of element does not necessarily agree with the true direction of the crack, as may ends in excessive extension of the crack propagation (Nuroji et al. 2010). Under the approach proposed by Nuroji et al. (2010), two adaptions are proposed and applied to the existing discrete crack model. Firstly, rotation of the element edge before node separation is adopted. Secondly, dragging of the node along the crack line is considered. By the two procedures, crack patterns during propagation are better predicted along the proper crack line according to the principal stresses. According to the method proposed by Cervera et al. (2003), a stabilised mixed displacement/pressure method is proposed to the solution of incompressible J_2-plasticity and damage problems with strain localisation. These procedures make a discrete problem stable and free of pressure oscillations and volumetric locking. As a result, solutions become practically mesh independent.

3.1.4.3 Comparison between smear and discrete crack concept

In the smeared cracking model, re-meshing or topological redefinition are not necessary for representation of cracks. This makes the method computationally convenient. However, the assumption of displacement continuity contradicts with the nature of actual geometrical discontinuities that occur across a crack. This continuity in meshes may cause stress locking (Rots 1991). In addition, solutions depend on the shape and size of mesh (Giordano et al. 2002). Mesh size dependency can be improved to some extent by relating the parameters of a constitutive model to the size of each finite element through a material characteristic such as the fracture energy (de Borst et al. 1993). In addition, a fixed crack model overestimates stiffness of the structure (de Borst 1997). In spite of these limitations,

Giordano et al. (2002) stated that the smeared cracking model is able to represent reasonable solutions as long as adequate material parameters are adopted.

As for the discrete crack model, unlike smeared cracking approach strain discontinuity caused by cracking is physically represented. In this sense, the discrete crack approach reflects the ultimate damaged state more closely than the smeared cracking model (Hube and Mosalam 2009). However, this approach does not fit the nature of the finite element method (continuity). Moreover the node separation may be not similar to the real direction of crack, and result in an erroneous estimation of the crack propagation (Nuroji et al. 2010). According to Cervera et al. (2003), the existing discrete model still lacks accuracy in prediction of stress and strain fields around crack tips. Today still the smeared approach is preferred over the discrete one because the latter requires high computational effort for analyses of large scale structures (Giordano et al. 2002).

3.1.5 Description of material behaviour in tension, compression and shear

Material description in tension, compression and shear is discussed. For tension and compression behaviour, uniaxial stress-strain relationship and failure criteria are discussed. For shear behaviour, shear retention parallel to a crack is discussed. The material description discussed here is embedded into the aforementioned crack concepts for a formulation of an adequate constitutive model.

3.1.5.1 Tension behaviour

3.1.5.1.1 Failure criterion

For tension failure criterion, a tension cut-off condition is defined in the principal stress space. When the combination of principal stresses violates this condition, it is considered that a crack starts to appear. In other words a uniaxial tensile strength involves the tension cut-off and as a result, a maximum stress condition is reduced. This approach is justified unless tensile cracking is not accompanied by significant lateral compression (Kupfer et al. 1969). Two failure criteria in tension are considered in the present research: constant or linear tension cut-off. The former is based on Rankine's criterion (Figure 3.12a). The latter is based on a Mohr-Coulomb's criterion (Figure 3.12 b).

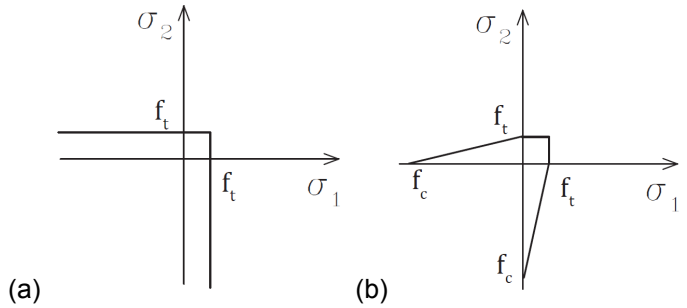

Figure 3.12 – Tension cut-off: (a) constant and (b) linear.

Rankine's failure criterion in tension (constant tension cut-off) assumes that failure occurs when the maximum principal stress reaches a value equal to the tensile strength obtained from a uniaxial tension test. In the principal stress plane, this criterion is as described in the equation (3.4).

$$\sigma_{1,2} \leq f_t \tag{3.4}$$

where

$\sigma_{1,2}$ is the principal stresses and f_t is the tensile strength.

Mohr-Coulomb criterion in tension (linear tension cut-off) assumes that a crack arises when the maximum principal tensile stress exceeds the value defined in the equation (3.5) (3.6).

$$\sigma_1 \leq f_t(1 + \frac{\sigma_2}{f_c}) \tag{3.5}$$

$$\sigma_2 \leq f_t(1 + \frac{\sigma_1}{f_c}) \tag{3.6}$$

where

f_c is the compressive strength.

3.1.5.1.2 Uniaxial stress-strain relationship

Linear tension softening function is adopted for uniaxial stress-strain relationship of masonry (Figure 3.15).

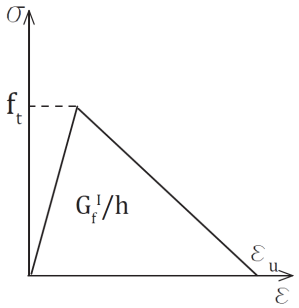

Figure 3.13 –Linear tension softening function.

This function is based on the material tensile strength f_t and the fracture energy G_f^I. When the tensile strain is larger than the ultimate strain ε_u in the equation (3.7),

$$\varepsilon_u = 2G_f^I / hf_t \tag{3.7}$$

the material loses its entire tensile capacity. This ultimate strain depends on the crack band-width h expressed as $h = \sqrt[3]{V_e}$ where V_e is the volume of the finite element.

3.1.5.2 Compression behaviour

3.1.5.2.1 Failure criterion

For failure criterion in compression, the Drucker–Prager's failure criterion is considered. It is a pressure-dependent model for determining whether a material fails or experiences plastic yielding (Figure 3.13).

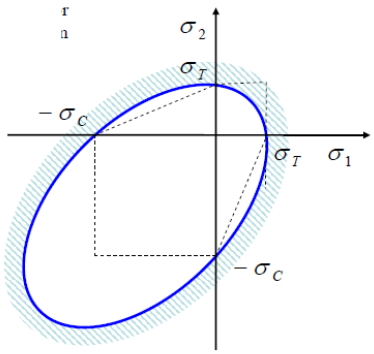

Figure 3.14 – A section of Drucker-Prager's failure criterion.

This criterion is described in the equation (3.8).

$$\sqrt{J_2(\sigma)}A + BI_1 \tag{3.8}$$

Constants A and B are determined as shown in equations (3.9) and (3.10),

$$A = \frac{2}{\sqrt{3}}\left(\frac{\sigma_t \sigma_c}{\sigma_t + \sigma_c}\right) \tag{3.9}$$

$$B = \frac{1}{\sqrt{3}}\left(\frac{\sigma_t - \sigma_c}{\sigma_t + \sigma_c}\right) \tag{3.10}$$

where (σ_t, σ_c) are the yield stresses obtained from uniaxial tension and compression test respectively .

Invariants J_2 and I_1 are expressed in equations (3.11) and (3.12).

$$J_2 = \frac{1}{3}(\sigma_1^2 + \sigma_2^2 - \sigma_1\sigma_2) \tag{3.11}$$

$$I_1 = \sigma_1 + \sigma_2 \tag{3.12}$$

3.1.5.2.2 Uniaxial stress-strain relationship

For compressive uniaxial stress-strain relationship, a parabolic function introduced by Feenstra (1993) is considered (Figure 3.15).

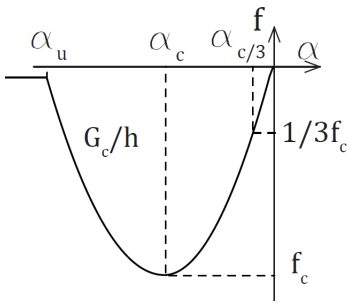

Figure 3.15 – Parabolic compressive function.

The strain $\alpha_{c/3}$, at which one-third of the maximum compressive strength fc is reached, is defined by equation (3.13).

$$\alpha_{c/3} = -\frac{1}{3}\frac{f_c}{E} \tag{3.13}$$

where E is Young's modulus.

The strain α_c, at which the maximum compressive strength fc is reached, is described by equation (3.14).

$$\alpha_c = -\frac{5}{3}\frac{f_c}{E} = 5\alpha_{c/3} \tag{3.14}$$

Both $\alpha_{c/3}$ and $\alpha_c$are irrespective of the size of a finite element or compressive fracture energy, G_c. Finally, the ultimate strain α_u, at which the material is completely softened in compression, is described by equation (3.15).

$$\alpha_u = \alpha_c - \frac{3}{2}\frac{G_c}{hf_c} \tag{3.15}$$

In the equation h is the crack band-width, as defined in Section 3.1.5.1.2.

The numerical model utilised in the present research have considered a fixed smeared cracking model with a Rankine failure criterion in tension and a plasticity model with Drucker-Prager failure criterion in compression. For a smeared cracking model, the total-strain crack model may describe material behaviour more accurately due to the two limitations of the model to be used in this study. Firstly, tensile stress temporarily may become larger than the tensile strength, as discussed in Section 3.1.4.1.2. Secondly, the plasticity model to be used in this research considers the compressive fracture energy infinite. This may end in insufficiently accurate description of the material behaviour in compression. The plastic yielding continues once the material reaches its maximum allowable compressive stress governed by Drucker-Prager failure criterion. The total-strain crack model, on the other hand, does not hold these limitations since it is controlled by a uniaxial equation both in tension and compression. However it can be more costly. Since most of the case-study structures are in a large scale (i.e. an entire single-nave church), this crack model is principally used in spite of this disadvantage to the total-strain crack model.

3.1.5.3 Shear behaviour

Once a crack starts to appear, shear behaviour parallel to a crack is considered under smeared crack approach (Rots 1989). A constant value used to be assumed for the crack shear modulus D^{II}_{secant}. This assumption resulted in a linear ascending relation between shear stress and shear strain across the crack. It allowed shear stress to increase indefinitely and as a result allowed the principal stresses in the cracked elements to rotate continuously.

So as to avoid this inadequate behaviour, once a crack appears, crack shear modulus D^{II}_{secant} is considered to be reduced from elastic shear modulus, G (Cedolin and Dei Poli 1977, Kolmar and Mehlhorn 1984, Rots et al. 1984). This reduction is described by shear retention factor, β. The calculation of D^{II}_{secan} as a function of β is indicated in equation (3.16).

$$D^{II}_{secant} = \frac{\beta}{1-\beta} G \tag{3.16}$$

Two options are considered in the present research: full shear retention and constant shear retention factor. Full shear retention factor ($\beta = 1$) considers that the elastic shear modulus G is not reduced. This indicates that the secant *crack* shear stiffness D^{II}_{secant} is infinite. In turn, constant shear retention factor ($0 < \beta < 1$) assumes that the elastic shear stiffness is reduced once a crack appears. In the present research, the latter assumption is used. For smeared crack concept, the value of a shear retention factor has to be chosen carefully. When relatively high value is adopted, results may become too stiff. A value nearly equal to 0 is suggested by Rots et al. (1985).

3.1.6 Representation of interface behaviour

For the representation of the interface behaviour, two different models are considered in this research: composite interface model and Coulomb friction model (Figure 3.16) (Lourenco and Rots 1997, Van Zijl 2000). The composite interface model is adequate to simulate fracture, frictional slip and crushing along interface between two elements. It is based on multi-surface plasticity, including the Coulomb friction model combined with a tension cut-off and an elliptical compression cap. Softening performs in all three modes and is preceded by hardening in the case of the cap mode. On the other hand, the Coulomb friction model describes frictional behaviour of the interface and tension cut-off (Figure 3.16 b). The interface behaviour between unit and mortar has been discussed in Section 2.1.2.1.2.

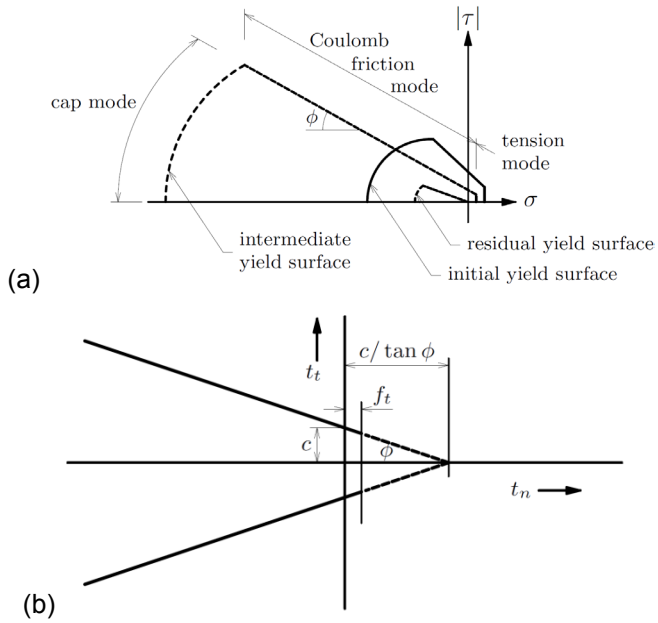

Figure 3.16 – (a) Composite interface model and (b) Coloumb friction model (Manie and Kikstra 2012).

3.2 Analysis-procedure strategies

In this section, different analysis strategies are discussed including iterative techniques. Comprehensive discussions are found in some books (Zienkiewicz and Tayler 2005, Bathe 1986, 1996, de Borst et al. 2012, Krenk 2009).

3.2.1 Iterative techniques

Various iterative techniques are considered, including full Newton-Raphson method, modified Newton-Raphson method and quasi Newton method. The full Newton-Raphson method updates stiffness matrix after each iteration process (Figure 3.20 a). Although fast convergence is observed, each iteration is costly. The modified Newton-Raphson iteration updates stiffness after each step (Figure 3.20 b). During iteration, the same stiffness matric is adopted. Convergence may be slower than

the full Newton-Raphson method and at the same time the iterations are less costly. The quasi Newton method uses the secant stiffness built from the last two converged steps for the following step (Figure 3.20 c). The result may be less accurate and slower than the full Newton-Raphson method but the analysis can become more stable and robust. One of the disadvantages is that potential bifurcation and equilibrium branches can be missed unlike with the full Newton-Raphson method.

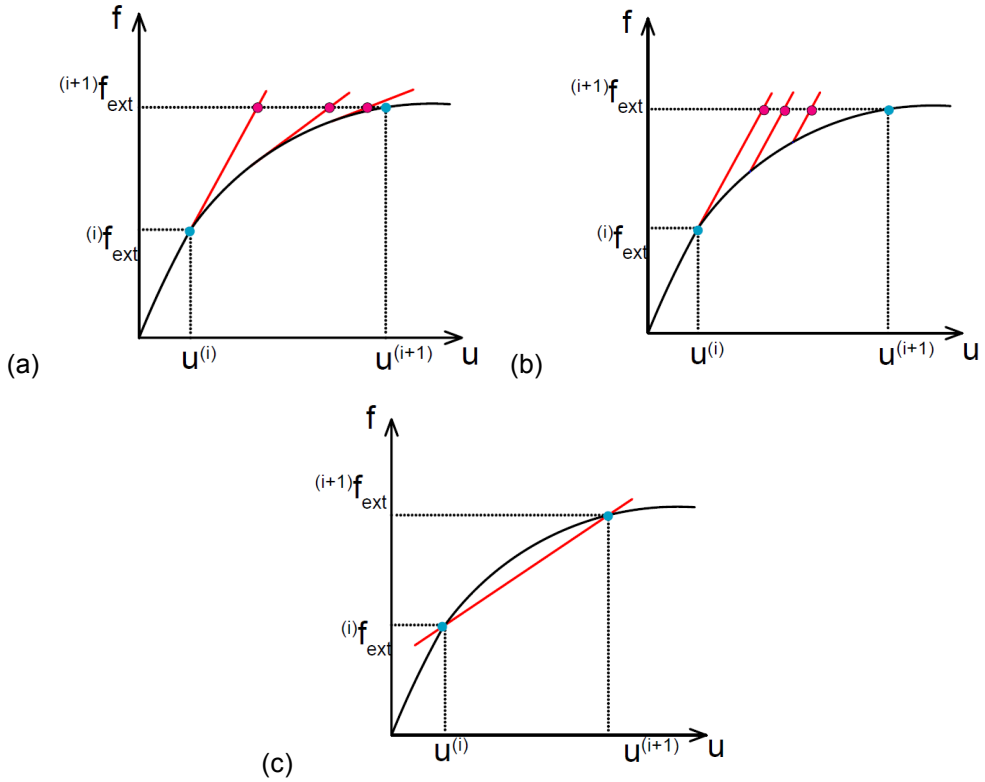

Figure 3.17 – Iterative technique: (a) full Newton-Raphson method. (b) modified Newton Raphson method and (c) quasi Newton method.

3.2.2 Line search

A line search technique can increase a convergence rate (Bathe 1996). This method is especially efficient when a current solution is far from a converged solution. It is particularly useful to solve problems involving plasticity as well as large displacements.

The line search technique applies an improvement to the original incremental displacement vector $d\tilde{u}_{j+1}$ by scaling it with a multiplier η_{j+1}, as shown in the equation (3.17).

$$du_{j+1} = \eta_{j+1}\, d\tilde{u}_{j+1} \tag{3.17}$$

The parameter u_j stands for the total displacement after iteration j at a certain load step. The displacement increment in iteration $j+1$ is given by du_{j+1}, such that $u_{j+1} = u_j + du_{j+1}$. The multiplier η represents the derivative of the potential energy which denotes the difference of the external (δW_{ext}) and the internal virtual work (δW_{int}) as described in the equation (3.18).

$$\eta = \frac{\partial \Pi}{\partial u} = \delta W_{ext} - \delta W_{int}. \tag{3.18}$$

According to de Borst et al. (2012), the line search is only useful when inaccurate tangential stiffness is predicted. Hence, under the full Newton-Raphson method, it does not save any computational effort. It is also mentioned that line search can improve the performance of the modified Newton-Raphson method but that still it does not compete with the full Newton-Raphson method.

3.2.3 Increments and control of a solution

Two different incremental approaches are considered, respectively corresponding to displacement and load control. In addition, the arch length method, which is able to adapt the step size according to the results of a current step, is also considered. The load control is carried out by prescribing loads directly to a structure (Figure 3.18 a). As a disadvantage, this method may not go over limit points (Figure 3.19). The displacement control is carried out by prescribing displacements to the equivalent load points of the structure (Figure 3.18 b). In this case, reactions are considered corresponding forces. The displacement control can overcome the limit points but cannot go beyond turning points (Figure 3.19).

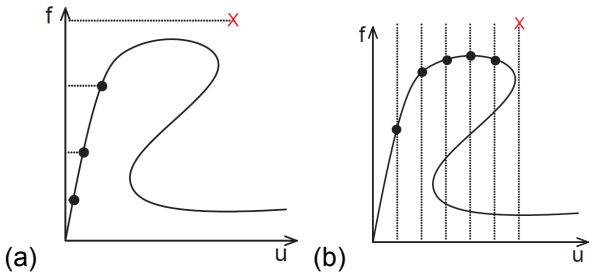

Figure 3.18 – (a) Load control and (b) displacement control.

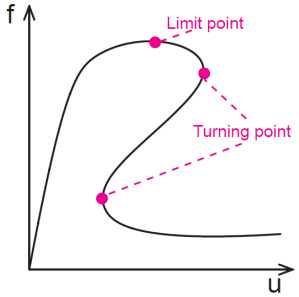

Figure 3.19 – Limit points and turning points.

By using the arc-length control, both limit points and turning points can be overcome (de Borst e al. 2012) (Figure 3.19). Arc-length methods have been developed on the basis of the notion that the 'length' of the combined displacement–load increment has to be controlled during equilibrium iterations (Riks 1979). The general procedure is described as follows (Krenk 2009). This procedure seeks for an adjacent point on an equilibrium path, at a certain distance given from the previous converged step. Distance is measured from both displacement and force in a given norm. Efficiency of the method may depend on adequacy of chosen distance norm (Figure 3.20).

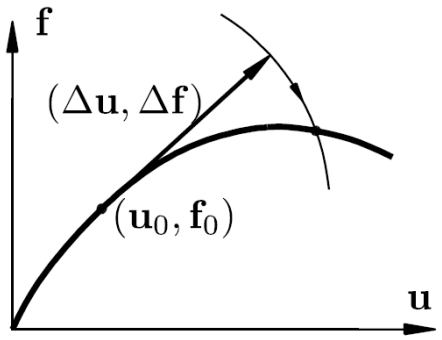

Figure 3.20 - Arc-length control (de Borst e al. 2012).

Although arc-length control can overcome both limit points and turning points, there are some disadvantages to direct load and displacement control (Bathe 1996). Firstly, sometimes direct load control represents more accurate results than arc-length control. Under arc-length control, a specific load is only used at the initiation point. Then, at each converged step, lower value is observed than the actual values. As a result, this method does not provide a solution with a specific load or a displacement. Secondly, arc-length control sometimes ends in negative values as is often seen in snapback through analysis. Too small or too large radius ends in drift-back of load-displacement relation.

According to Dall'Asta and Zona (2002), the displacement control is more suitable than the other two methods (load control and arc-length control). It is said that arc-length control method may be applicable after the displacement control fails. However there are cases where load control has to be used to solve a problem (de Borst et al. 2012) for instance, creep problems. .

3.2.4 Convergence criteria

The iteration process stops when convergence is observed. It also stops when a specified maximum number of iterations are reached or the divergence is detected during the iteration. For convergence criteria, force, displacement and energy norms are used. The choice of the norm and its convergence tolerance value has to be determined in accordance with the type of analysis (de Borst et al. 2012). For instance, the displacement norm is not effective in analysis with a large number of prescribed displacements. On the other hand, the force norm is not effective for analysis of a very flexible structure

since that sort of the structure generates little internal forces. The value of the convergence tolerance must be considered properly. A too loose convergence could result in inaccurate and unreliable answers. On the other hand, a too strict convergence tolerance sometimes hardly improves the results while it increases required computational effort drastically.

4. CASE STUDY 1: SIMPLE MODELS

4.1 Introduction

In this chapter, the studies focus on deepening the understanding on influence of different parameters and also on analysing the adequacy of the proposed numerical tools for seismic assessment. So as to limit complexity of the analyses, simple models are chosen consisting at most of a combination of one horizontal element (a vault) and the vertical elements that support it (walls). Firstly, the influence of mechanical and numerical parameters is studied through structural models based on a vault of the Lio Palace in Barcelona. In this building, there are two rooms roofed with Catalan vaults. One of the rooms, composed of four double-curvature vaults, is studied. A set of parametric studies are carried out by applying vertical static loads. Using the model with the properties identified through the parametric study, seismic assessment is also carried out by pushover analysis and linear kinematic analysis. Secondly, a comparison of seismic assessment tools is done on a simple structure models. Three different tools for seismic assessment, namely nonlinear dynamic analysis, invariant-force pushover analysis and advanced pushover analysis (adaptive pushover analysis and multi-mode pushover analysis are considered for comparison. Simple masonry structures are chosen based on examples available in the literature and tested experimentally. Laboratory-built prototypes (a one-storey box structure and a cross vault supported by piers) are studied. The examples are subjected to simple accelerograms (different to the ones applied in the experiments) in order to compare results between different methods. Findings from this chapter are considered for the preparation of models and the analysis of the rest of case studies presented in the thesis.

4.2 Study of influence of parameters

4.2.1 Description of the structure

Lio Palace (*Palau Lio* in Catalan) is located at the heart of the historic centre of Barcelona. It was built in the 16th century as the palace of the Marques de Lio. Today it is used as a museum of historical costumes. It is a three-story building and includes two rooms roofed with Catalan vaults in the ground floor. One is composed of five single-curvature Catalan vaults in a row (Figure 4.1 a). The other is made up of four double-curvature vaults (Figure 4.1 b). In this study the latter room is used. The vaults are supported by the perimeter walls and the pillar in the centre of the room. Four arches rise from the head of the pillar form the edges of each vault. The vault is 5x5 m^2 in plan. Its thickness is 0.11 m. The rise/span ratio at the edge of the vault is 0.17 (0.85/5). The walls and the pillar are 3 m high. The distance between the floor and the centre of the vault is 4.1 m. The thickness of the wall is 0.7 m and the diameter of the pillar is 0.36 m. The section of the arch is 0.12x0.34 (height x width) m^2. The masonry of the vaults is composed of clay bricks and lime mortar while the masonry of the walls is composed of

sandstone and lime mortar. Today cracks are seen in one of the arches and between the wall and the vault (Figure 4.2).

(a)  (b) 

Figure 4.1 – Catalan vaults in Lio Palace (a) room of five Catalan vaults and (b) room of four Catalan vaults.

Figure 4.2 – Cracking observed in one of the vaults.

4.2.2 Parametric study on a double-curvature vault of Lio Palace

4.2.2.1 Outline of the parametric study

A first parametric study is done on a chosen single vault of the four vaults that composed of the roof. One of the four double curvature vaults is taken out for parametric study. The models are assessed by applying vertical loads statically. Two different load cases are considered. For the first load case, gravity is applied. For the second load case, distributed load over the vault is applied till the analysis stops due to failure. In the analyses, the following parameters are invariable: compressive strength (f_c) (4 MPa), Young's modulus (E) (2000 MPa) tensile fracture energy (G_{fi}) (5.8 N/m), the density of masonry (1800 kg/m^3 for brick masonry and 2000 kg/m^3 for stone masonry) and Poisson ratio (0.2). These values are chosen considering typical ones for historical masonry structures. Detailed discussion on masonry mechanical parameters has been made in Chapter 2. As for the failure criteria, the Drucker-Prager model is adopted in compression and the Rankine criteria with fixed multi–directional cracking in tension. The failure criteria and cracking model for numerical analyses has been discussed in Section 3.1.4 and 3.1.5.

In total, 11 FEM analyses are carried out. The combination of parameters in each analysis is listed in Table 4.1. Studies are carried out on parameters regarding the material, parameters regarding the FEM calculation technique (FEM parameters) and supporting conditions of the vault. The only parameter analysed regarding the material is the tensile strength. Three different tensile strength values are compared: 0.2 MPa (5% of f_c), 0.12 MPa (3% of f_c) and 0.04 MPa (1% of f_c). Three FEM parameters are also examined: type of shell element, number of integration points and element size. The choices of the parameters are determined on the basis of the discussions on numerical strategies included in Chapter 3. Two shell elements are compared, corresponding to 6-node triangular or 8-node quadrilateral elements. Five different sizes of the elements for the vault are compared: 670, 340, 220, 170 and 130 mm (length of the side). This corresponds to the following number of elements: 64, 256, 576, 1024 and 1600. Four different number of integration points in the thickness of shell elements (3, 9, 11 and 21) are examined. Just three points is obviously a very small number, but it is also analysed because some software packages use it by default. Then two supporting conditions of the vault are compared: fixed supports at the four corners of the vault and two parallel walls.

Table 4.1 – List of the analyses.

case	**1**	**2**	**3**	**4**	**5**	**6**	**7**
support	Fixed supports	Fixed supports	Fixed supports	Fixed supports	Fixed supports	Fixed supports	Fixed supports
f_t(MPa)	5%	5%	5%	5%	5%	3%	1%
FEM shell	quadrilateral	triangular	quadrilateral	quadrilateral	quadrilateral	quadrilateral	Quadrilateral
Integ. Points	11	11	11	11	11	11	11
element size (mm)	125	125	312	208	155	125	125

combination	**8**	**9**	**10**	**11**
support	Fixed supports	Fixed supports	Fixed supports	2 walls
f_t(MPa)	5%	5%	5%	5%
FEM shell	quadrilateral	quadrilateral	quadrilateral	quadrilateral
Integ. Points	3	9	21	11
element size (mm)	125	125	125	125

4.2.2.2 Reference case (case1)

The case 1 is regarded as the reference case. The FEM model is presented in Figure 4.3. Combination of the parameters is presented in Table 4.1. A load-deflection curve is presented at the middle of the vault (Figure 4.4). The ultimate load capacity is 4.02 kN/m^2 and the ultimate displacement capacity is

8.75 mm. The principal tensile strain distributions at the bottom surface is presented in Figure 4.15 a, and that at the top surface is in Figure 4.15 b.

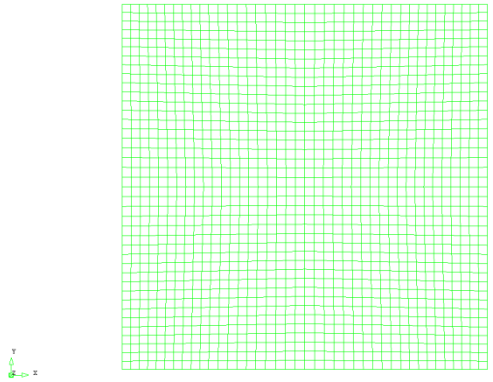

Figure 4.3 – FEM model composed of 4000 8-node quadrilateral elements.

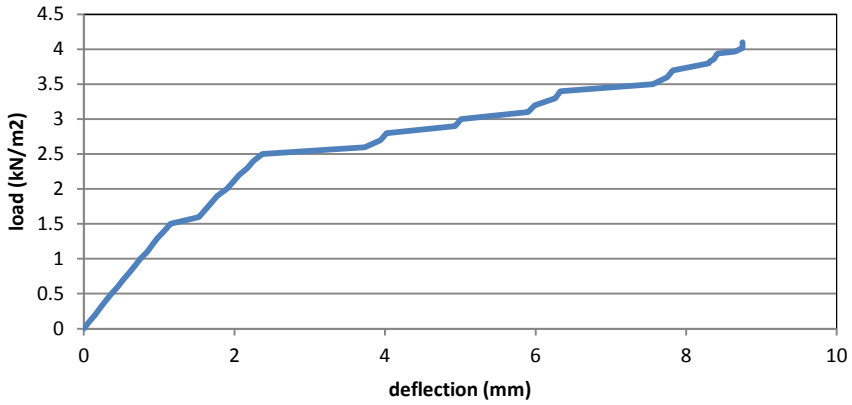

Figure 4.4 – Load-deflection curve, control node at the middle of the vault, reference case.

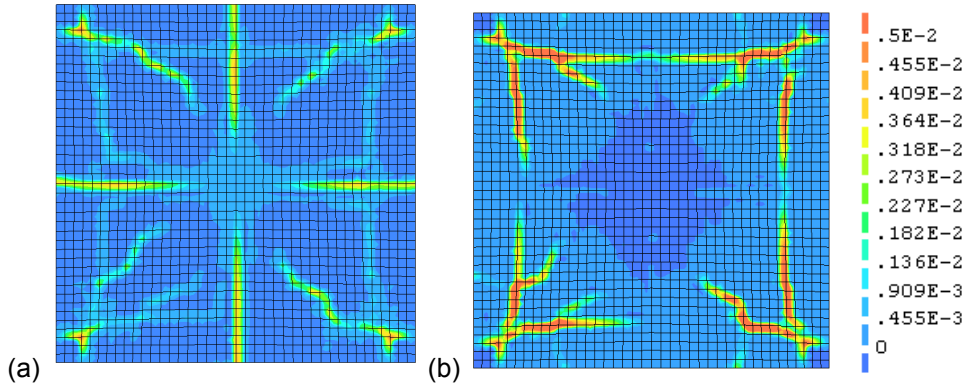

Figure 4.5 – Ultimate principal tensile strain distributions, reference case: (a) bottom surface and (b) top surface.

4.2.2.3 Shell element types (case 2)

The reference case (a model of composed of 8-node quadrilateral elements) is compared with the vault modelled with 6-node triangular elements (case 2). The results are similar when the load-deflection

curves and principal tensile strain distributions are compared (Figure 4.7). However, quicker convergence is seen for the analysis of model of 8-node quadrilateral than that of 6-node triangular elements. As a result, the model of 8-node quadrilateral elements will be used for the further analyses.

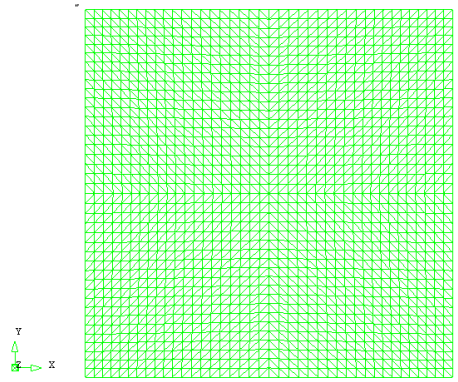

Figure 4.6 – FEM model composed of 3200 6-node triangular elements.

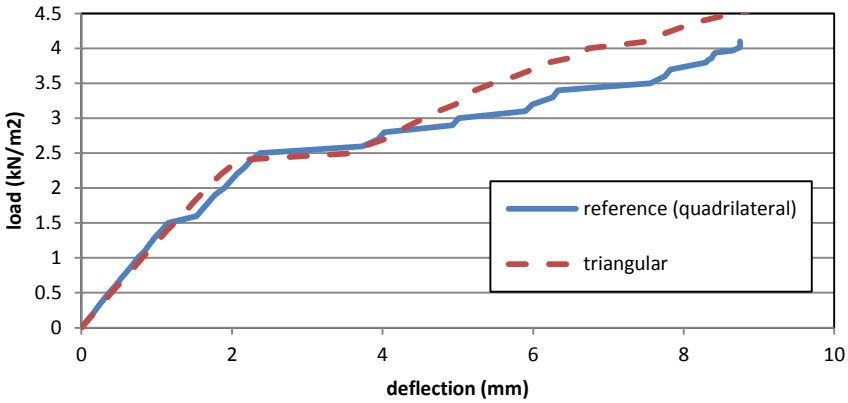

Figure 4.7 – Load-deflection curves comparison of triangular and quadrilateral shell elements, control node at the middle of the vault.

4.2.2.4 Number of elements (case 3-5)

Different numbers of elements over the vault are compared as follows: 312 mm (case 3: 16x16 elements), 208 mm (case 4: 24x24 elements) and 155 mm (case 5: 32x32 elements) with the reference case (125 mm, 40x40 elements). The case 3 and 4 do not indicate damage as clearly as case 1 and 5. On the other hand, case 1 and 5 show similar distribution of damage. The ultimate load capacity of each case is as follows: 3.22 kN/m^2 (case 3), 4.35 kN/m^2 (case 4) and 3.35 kN/m^2 (case 5) while that of the reference case is equal to 4.01 kN/m^2.

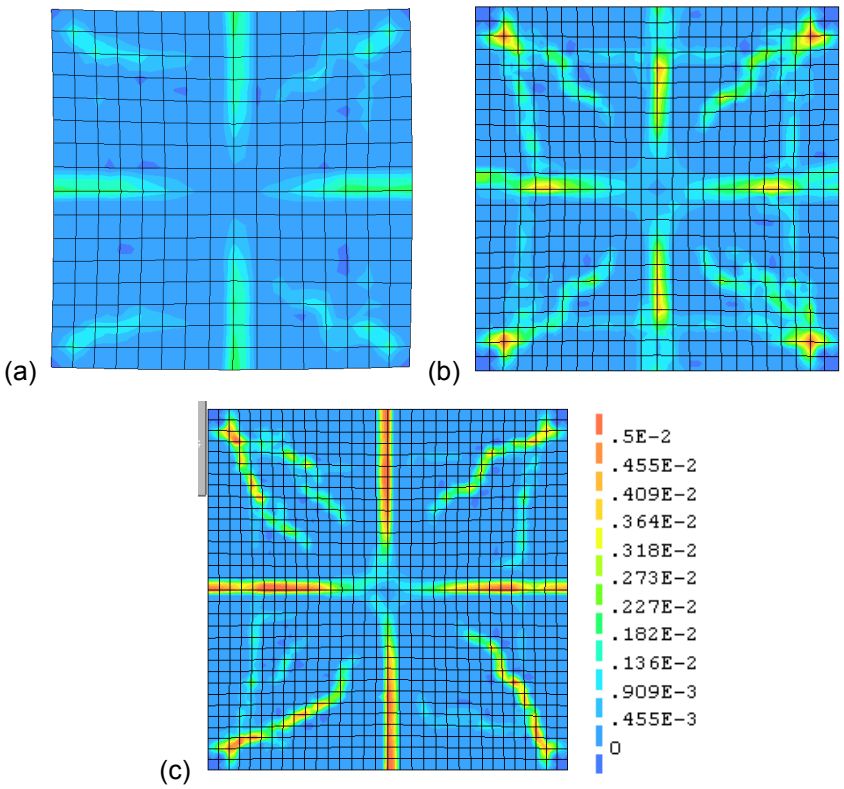

Figure 4.8 – Ultimate principal tensile strain distributions of different number of elements, at the bottom surface: (a) 256 (case 3), (b) 576 (case 4) and (c) 1024 elements (case 5).

4.2.2.5 Tensile strength (case 6-7)

Influence of tensile strength is compared: 3% of f_c (case 6) and 1 % of f_c (case 7) with the reference case (5% of f_c). Tensile fracture energy is linearly proportional to the value of the tensile strength. For the reference case (f_t =5 % of f_c), the value is equal to 5.8 N/m as mentioned in Section 4.2.2.1. Accordingly, for the case 6 (f_c =3% of f_c), it is equal to 3.5 N/m and for the case 7 (f_t=1% of f_c), it is equal to 1.2 kN/m. The case of 3% of f_c represents the load capacity equal to 2.52 kN/m^2 and the displacement capacity equal to 7.66 mm. When the reference case and the case 1 are compared, the load capacity is decreased by 37.5 %. The analysis of the case of 1% of f_c stops during the application of the self-weight. It is probably due to the low value of tensile strength and tensile fracture energy.

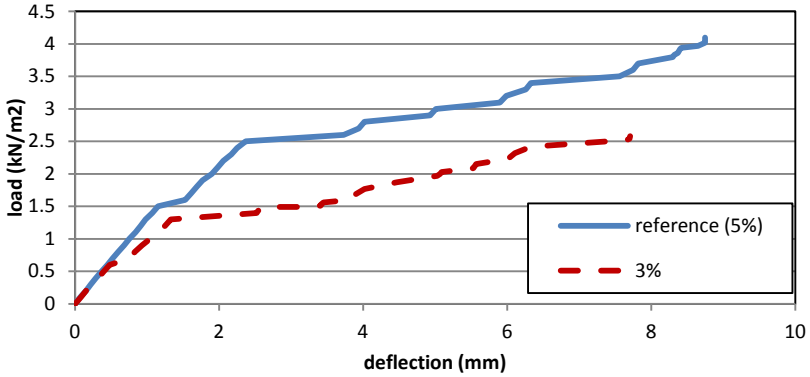

Figure 4.9 –Load-deflection curves control node at the middle of the vault, different values of tensile strength.

4.2.2.6 Integration points (case 8-10)

For a number of integration points, case 8 to 10 are compared: 3, 9 and 21 points, compared with 11 points (reference case). The case 8 (3 points) provides brittle response. The ultimate load capacity is equal to 2.36 kN/m^2 and the displacement capacity is 1.93 mm. The case 9 (9 points) and case 10 (21 points) represent a load-deflection curve similar to that of the reference case (11 points). With 21 points, slightly higher displacement capacity is observed than the reference case. However it required more computational effort than the other cases. The ultimate load capacity and corresponding deflection (at the centre of the vault) of each case is as follows: 2.36 kN/m^2 and 1.93 mm (case 8), 3.81 kN/m^2 and 8.85 mm (case 9) and 4.48 kN/m^2 and 12.1 mm (case 10).

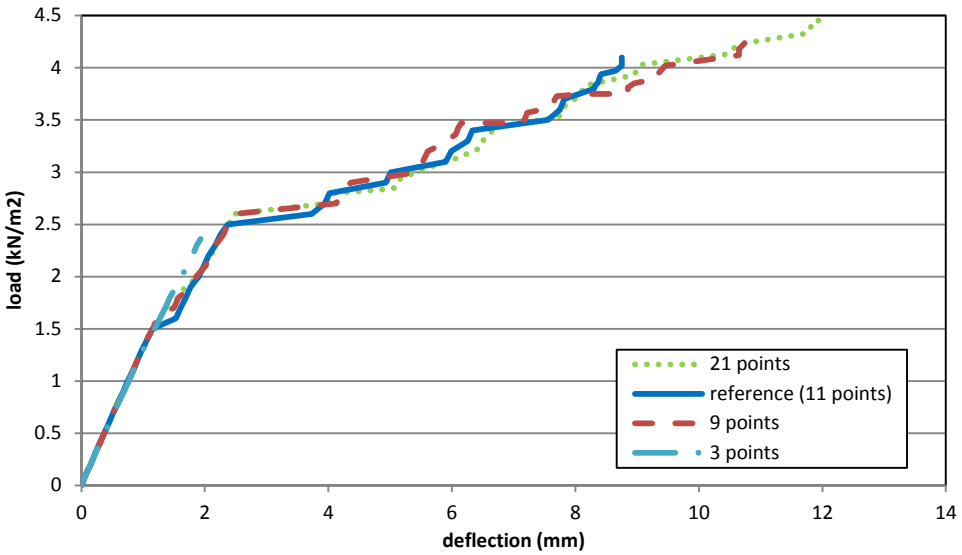

Figure 4.10 – Load-deflection curves, control node at the middle of the vault, different numbers of integration points.

4.2.2.7 Different support (case 11)

The reference case (a vault supported by fixed support at four corners) is compared with a vault supported by two parallel walls (case 11) (Figure 4.11). The thickness of the wall is 0.7 m. It is the same as that of the perimeter walls in the real structure. The walls are modelled with 6-node triangular

elements and 8-node quadrilateral elements. The integration points in thickness is 11. The number of elements of the vault are 1600 (40x40). The entire number of elements are 4000.

Lower load capacity (2.9 kN/m^2) is observed than the reference case (decreased by 27.5 %). On the other hand, higher value of deflection (14.9 mm) is identified (increased by 70 %). At the ultimate state, evident damage is observed, at the middle of the vault parallel to the walls (Figure 4.13). Also visible damage appears diagonally over the vault.

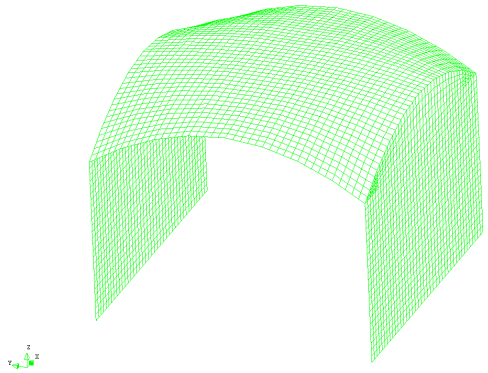

Figure 4.11 – FEM model.

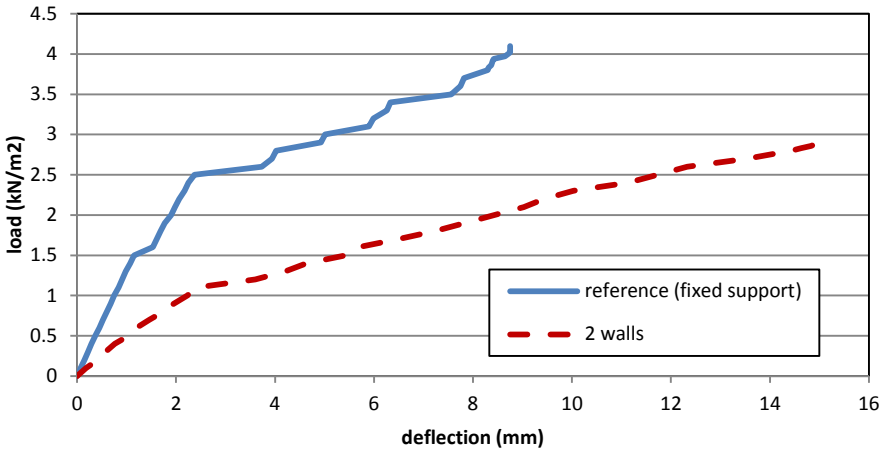

Figure 4.12 – Load-deflection curves, control node at the middle of the vault, different vertical support types.

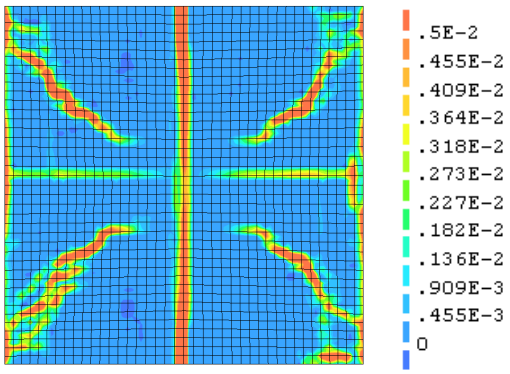

Figure 4.13 – Ultimate principal tensile strain distributions, at the bottom surface, 2-wall model (case 11).

4.2.3 Structural assessment of roof composed of multiple vaults from Lio Palace

In this section, the entire roof of the room, comprising four double curvature vaults, is studied. First, static analysis is carried out by applying a uniform load or concentrated load. Seismic analysis is done by means of pushover analysis. Linear kinematic analysis is also carried out and compared with FEM analysis.

4.2.3.1 Description of the model

A FEM model is prepared in accordance with the findings in the parametric studies of the Section 4.2.2. The same combination of mechanical parameters and failure criteria as the reference model of the previous parametric study is adopted, as mentioned in Section 4.2.2.1. Thus, compressive strength is 4 MPa. Young modulus is 2000 MPa (500 times fc). Tensile strength is 0.2 MPa (5% of fc). Tensile fracture energy is 5.8 N/m. The Drucker-Prager model is adopted in compression and the Rankine criteria with smeared cracking in tension. The pillar and the arches are discretised with 2-node curved beam elements. The length of the element is 100 mm. The walls are modelled with quadrilateral 8-node curved shell element and the vaults with triangular 6-node curved shell element. The side length of both elements is 100 mm. The number of integration points in thickness is 11. The number of nodes is 23753 and that of elements is 10454 (Figure 4.14).

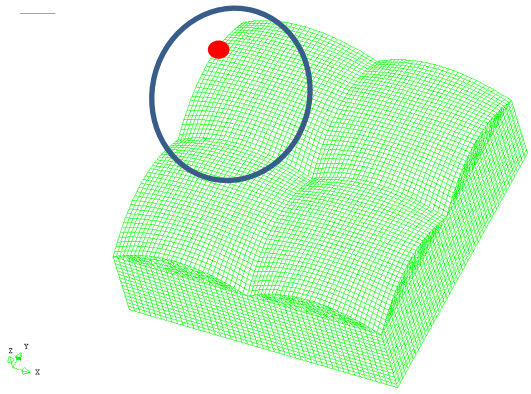

Figure 4.14 – FEM model.

4.2.3.2 Capacity assessment under a uniform load over one of the four vaults

A uniform live load is applied over one of the vaults (blue circle in Figure 4.14). The node at the centre of the vault experiencing the loading is chosen for the vertical displacement of the presented load-deflection curves. At the load of 6.4 kN/m^2, a short horizontal branch is observed (Figure 4.15). At this load, more distributed damage appears over the vault where a uniform load is applied. The maximum load is 9.5 kN/m^2. The corresponding deflection at the centre of the vault is 21.2 mm. More intense damage is found in the loaded vault although damage is visible all over the four vaults (Figure 4.16). In addition, concentration of damage is observed in the middle of two arches supporting the loaded vault, as would indicate appearance of a hinge in them.

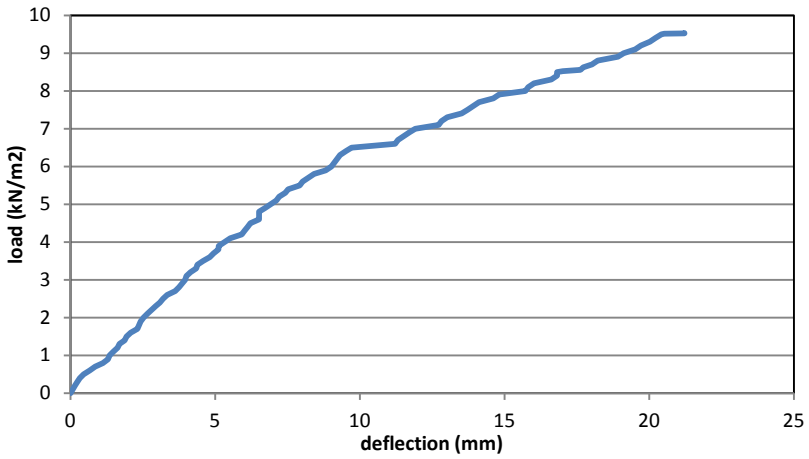

Figure 4.15 – Load-deflection curve, control node at the centre of the vault, uniform load over a vault.

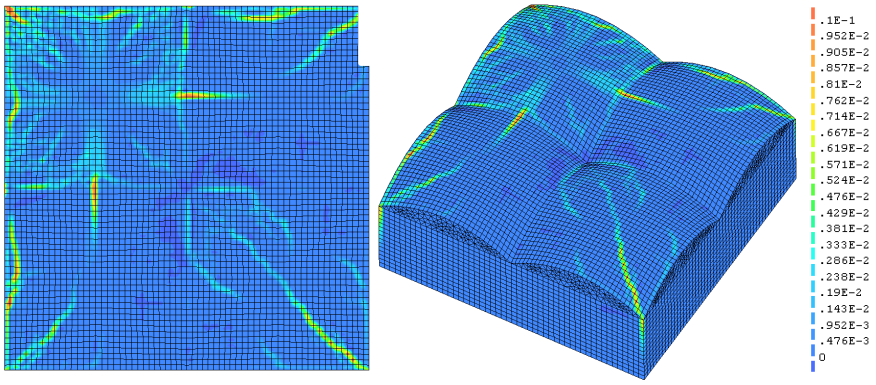

Figure 4.16 – Principal tensile strain distribution at ultimate state under a uniform load over a vault, at the bottom surface.

4.2.3.3 Capacity assessment under a uniform load over four vaults

A uniform load is applied over the four vaults. A horizontal branch appears at the load of 3.8 kN/m^2 (Figure 4.17). At this load, damage starts to propagate around one of the corners of each vault (at the corner of the room). The maximum load is 4.9 kN/m^2. The corresponding deflection at the centre of the vault is 11.2 mm. Severe damage is observed around the aforementioned corners (Figure 4.18). Concentration of damage in the middle of the arches would indicate appearance of a hinge.

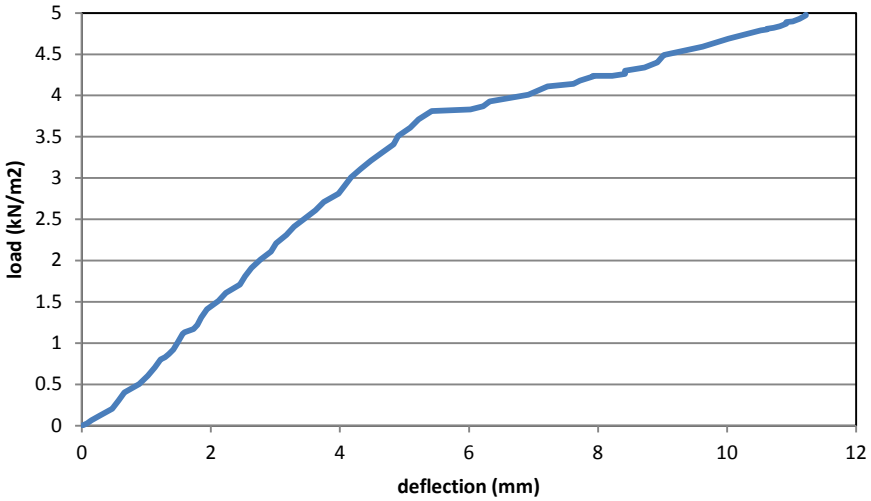

Figure 4.17 – Load-deflection curves, control node at the centre of the vault, uniform load over four vaults.

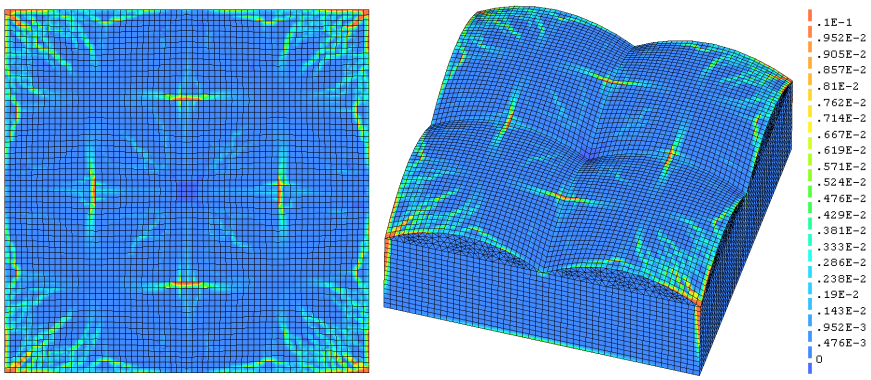

Figure 4.18 – Principal tensile strain distribution at ultimate state under the concentrated load at the bottom surface.

4.2.3.4 Capacity assessment under a concentrated load

A concentrated load is applied to one fourth point of the vault (red point in Figure 4.14). The maximum load is 30.9 kN (Figure 4.19). The corresponding deflection at the centre of the vault is 0.68 mm. Concentration of damage is seen around the loaded point (Figure 4.20).

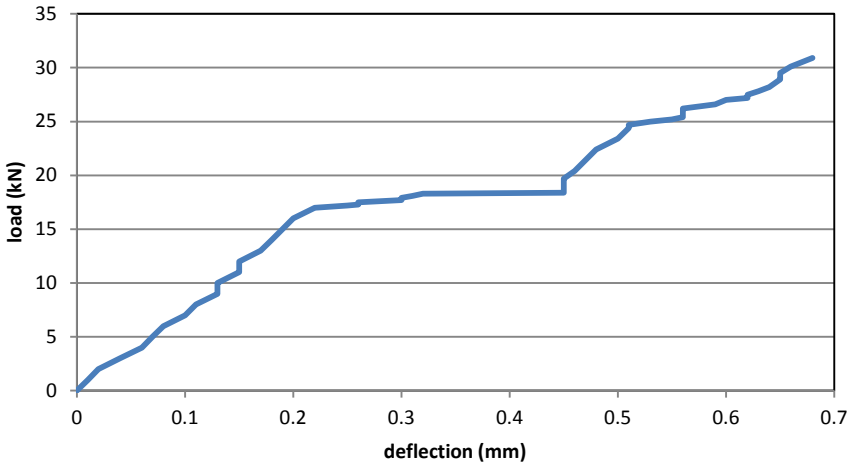

Figure 4.19 – Load-deflection curves, control node at the centre of the vault, concentrated load.

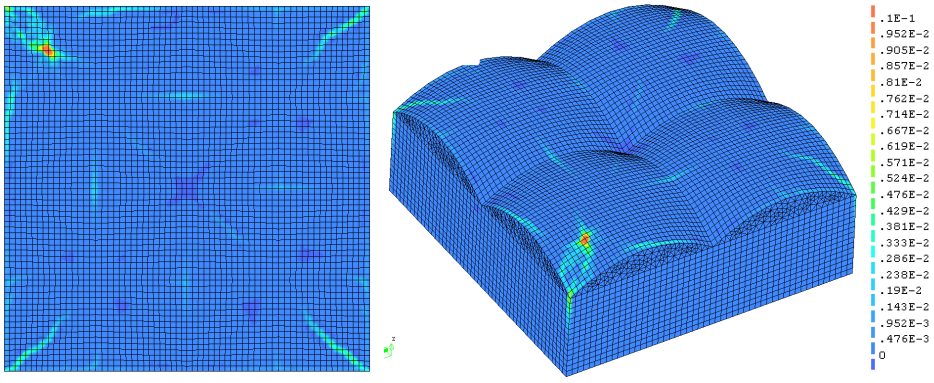

Figure 4.20 – Principal tensile strain distribution at ultimate state under the concentrated load at the bottom surface.

4.2.3.5 Seismic assessment by pushover analysis

For seismic assessment, the previous model is modified. The arches supporting the vaults are modelled with quadrilateral 8-node curved shell elements instead of beam elements. This procedure permits clearer visualisation of locations of hinges in the arch. The Number of element is 8882 and nodes 25292 (Figure 4.21).

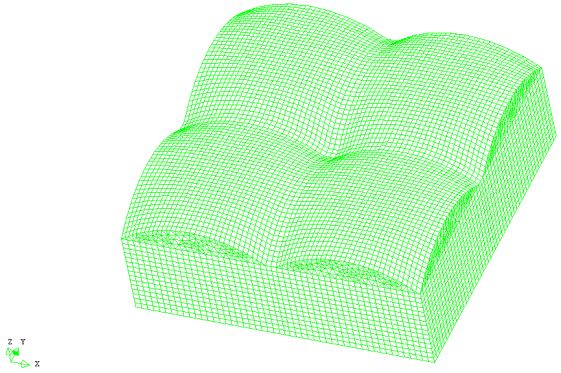

Figure 4.21 – Modified model.

During the application of the gravity forces, cracks already appear in the connection between the arches and the vault and between the wall and the vault. Then, lateral force proportional to the masses of the model is applied. In the load-deflection curve, two horizontal branches are seen (Figure 4.22). At the first phase, the maximum base shear coefficient is 0.105g and the corresponding displacement at the top of the wall is 0.55 mm. Damage runs through the corner of walls and indicates separation of the wall from perpendicular walls and the initial overturning of the walls (Figure 4.23 a). Then at the second branch (with the maximum base shear coefficient 0.13g, and corresponding displacement 0.98 mm), noticeable damage appears diagonally on the vaults (Figure 4.23 b). These damage patterns develop till the ultimate state and no new pattern of damage is observed (Figure 4.23 c). The ultimate load capacity is 0.184g and the corresponding displacement capacity at the top of the wall is 1.39 mm. It has to be mentioned that neither diagonal cracks in vaults nor vertical cracks between the walls are not observed in the real structure

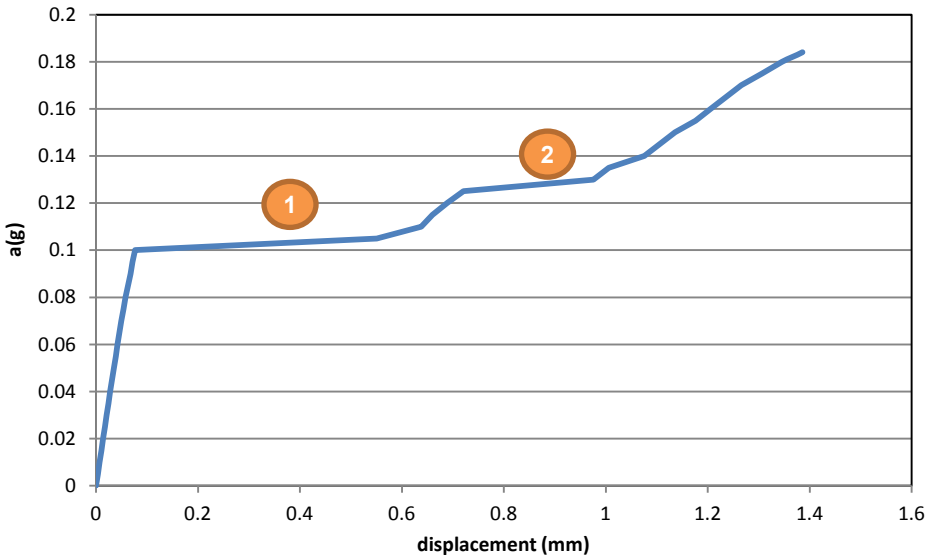

Figure 4.22 – Load-displacement curve, control node at the top of the wall, pushover analysis.

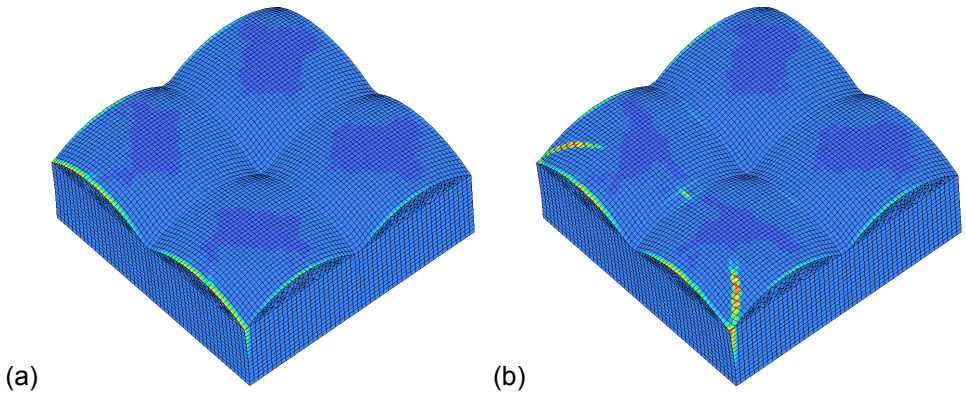

(a) (b)

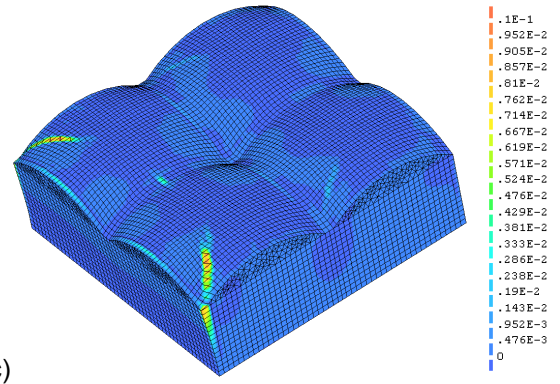

(c)

Figure 4.23 – Damage distribution: (a) first phase, (b) second phase and (c) ultimate state.

Linear kinematic analysis (LKA) is carried out for the prediction of the wall overturning (Figure 4.24). The calculation is done with the following values: weight of the wall (W) equal to 483 kN., wall dead load (N) of 1300 kN., The height of the wall (H) is equal to 3 m. and the depth of the wall (b_1) is 0.7 m. The position of the centre of the weight (Z) is 1.5 m (Z) and 0.35 m (b_2). Subsequently the activation coefficient α_0 is 0.135g. In FEM analysis, the mechanism is activated at 0.183g. Difference is seen by 33.3 %.

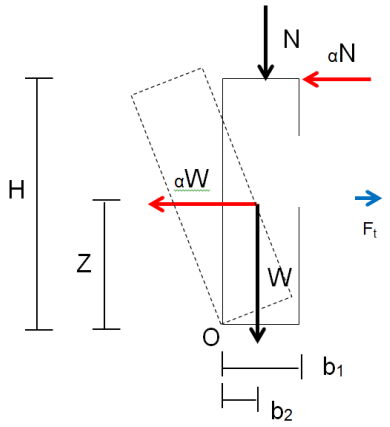

Figure 4.24 – Limit analysis, overturning of the façade.

4.3 Comparison of seismic assessment tools

4.3.1 Methodologies

In the examples presented in this section, different seismic assessment tools are compared, including invariant-force pushover analysis (IPO) adaptive pushover analysis (APO), multi-modal pushover analysis (MMP) and nonlinear dynamic analysis (NDA). Discussions on these seismic assessment tools have been made in Section 2.4.

Different IPO methods are compared according to a force distribution pattern: mass-proportional (mass IPO), first-mode force distribution (1st-mode IPO), first-mode with consideration of mass distribution

(1^{st}-mode*mass IPO) and force distribution patterns according to the first and last peaks of NDA. The latter are called the 1^{st}-peak IPO and last-peak IPO respectively. The mass IPO is a force distribution pattern proportional to masses of the structure. The 1^{st}-mode IPO is a force distribution proportional to the first mode. The displacement of each node of the first mode is obtained through an eigenvalue analysis. Forces are applied to each node in proportion of the corresponding displacement. The 1^{st}-mode*mass IPO is a force distribution proportional to the first mode with consideration of distribution of masses. It is prepared by multiplying the force of each node from the first mode (obtained from the 1^{st} mode IPO) with the weight of masses of each node. The 1^{st}- and last-peak IPO make use of internal force distribution patterns from NDA. They are prepared by considering the internal force distribution at the moment of the 1^{st} and last local peaks of the time history of the displacement. They are studied so as to examine and compare the responses obtained from pushover analysis with these force distribution patterns. Methodologies of IPOs have been discussed in Section 2.4.2.1 As for MMP and APO, discussions are found in Section 2.4.2.2. For MMP, the method proposed by Chopra and Goel (2004) is adopted. As for APO, a method proposed by Antoniou (2004b) is considered. An actual application method of both advanced pushover techniques is presented in Section 4.3.3.2 where they are applied to one of the case study buildings.

These analysis method are adopted to analyse firstly, a single vertical element model (a cantilever), then multiple vertical elements (one-storey box structure) and finally a combination of horizontal and vertical elements (cross vault supported by two parallel piers).

4.3.2 Cantilever

4.3.2.1 Description of the model

A brick masonry cantilever specimen (0.2x0.2x1 m^3 [WxDxH]) is assumed. It is discretised with 4-node curved quadrilateral shell elements. The number of nodes and elements are 156 and 125 (Figure 4.25). The number of integration points in thickness is 11. Compressive strength is 4 MPa, tensile strength 0.2 MPa and Young modulus 2 GPa. Tensile strength is taken as 5 % of compressive strength and the Young's modulus is 500 times compressive strength. For tensile fracture energy, 50 N/m is assumed. These values are assigned according to the parametric studies carried out in Section 4.2 and Chapter 6. Poisson ratio is 0.2 and the density is 1800kg/m^3. For the failure criteria, Rankine criteria in tension and Drucker-Prager in compression are applied. These failure criteria are determined on the basis of the discussions in Chapter 2 and Section 4.2. The Rayleigh damping model is assumed with a_0 is 14.5 and a_1 is 0.0001 according to the equation (2.38), (2.39) in Section 2.4.3.2. IPOs and NDA are adopted to the model and compared.

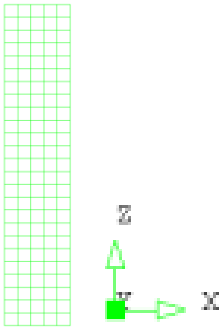

Figure 4.25 – FEM model of a cantilever.

Before the results obtained from the analyses are discussed, force and displacement application methods are compared. To make discussions simple, a cantilever of the same dimension is modelled with 2-node 3 dimensional beam elements in this comparison. The comparison is made by three analyses. As the first analysis, a lateral uniform load (12.5N/m^2) is applied to the model (force application). As a result, a deformed shape is obtained. As the second analysis, the displacements obtained from the deformed shape are applied to each node (displacement application). As a result, the reactions from each node are identified. Unexpectedly these observed reactions are not identical to the uniform load used for the first analysis. Regardless of this finding, as the third analysis, these reactions are applied to the model. Consequently, the same deformed shape is observed as the first analysis. This analysis comparison would indicate that applying displacements to all the nodes of the FEM model do not necessarily properly represent the same force distribution pattern as the force application. Considering this finding, in this thesis, the pushover analyses are carried out by applying forces.

4.3.2.2 Application of seismic assessment tools

The shell-element cantilever model is analysed by IPOs and NDA. For NDA, the accelerogram shown below is applied (Figure 4.27). In Figure 4.28, the time history is presented. For IPO, three invariant force distribution patterns are compared: mass IPO, 1st mode IPO, 1st-mode*mass IPO and 1st- and last- peak IPO. The analyses are conducted in the X direction. The shape of the first mode is shown in Figure 4.26. The mass participation factor for the 1st node is 61.2 %.

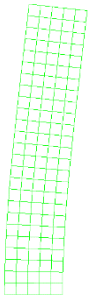

Figure 4.26 – first-mode shape.

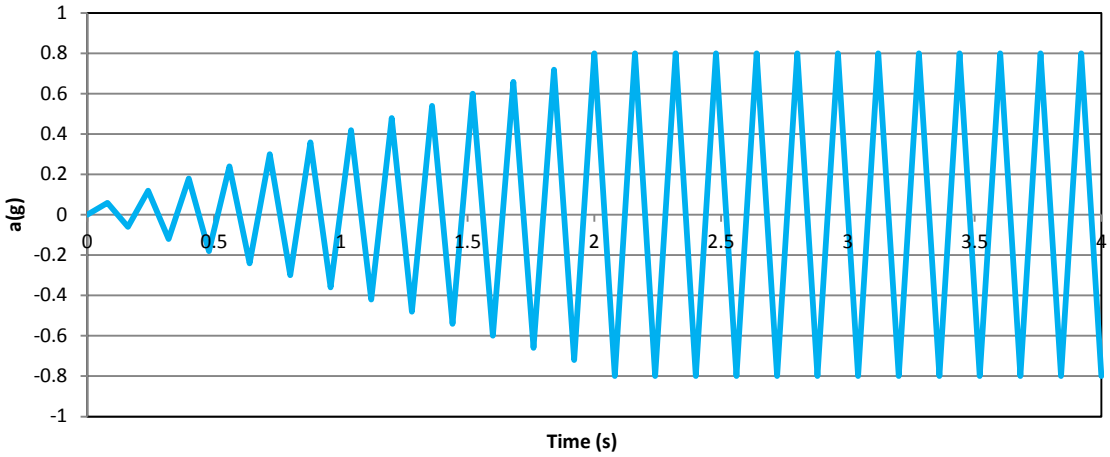

Figure 4.27 – Adopted accelerogram.

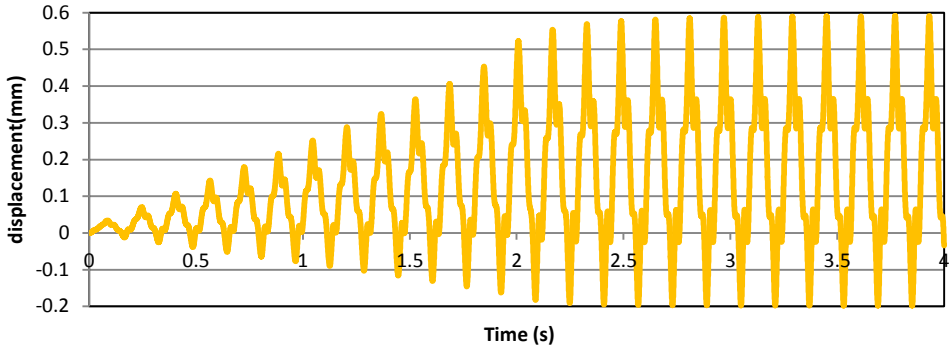

Figure 4.28 – Time history of the displacement at the top of the cantilever.

In Figure 4.29, the load-displacement curves from pushover analyses and the envelope of the base shear force and the displacement (V-δ relation) from NDA are compared. The mass IPO fits the best to the V-δ relation although NDA shows much higher ductility than pushover analyses. When the ultimate displacement capacities are compared between the pushover analyses, the 1st mode IPO predicts closer value to NDA than the mass IPO. Both 1st- and last-peak IPO shows similar load capacity to the mass IPO. The 1st peak IPO uses an internal force distribution pattern at 0.26 seconds of NDA and the last peak IPO uses that at 3.9 seconds. The last-peak IPO shows slightly higher displacement capacity than the mass IPO and the 1st-peak IPO shows higher displacement capacity than the mass IPO. In spite of slight difference in load and displacement capacity it must be mentioned that these three IPOs (mass, 1st and last peak) show nearly the same results. The ultimate tensile strain distribution patterns are presented in Figure 4.30.

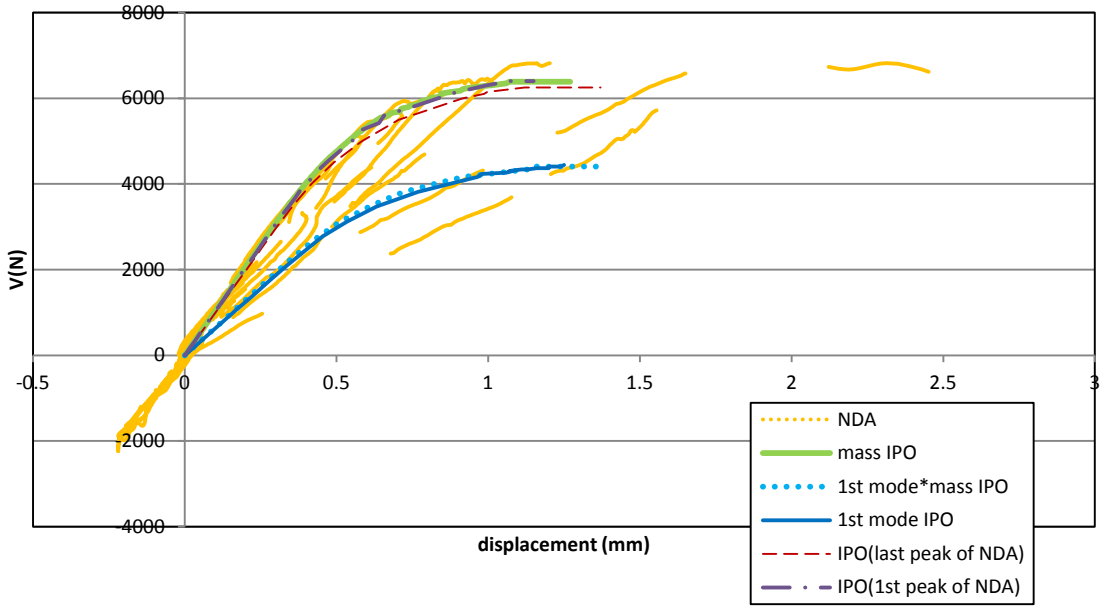

Figure 4.29 – Load-displacement curves and displacement-base shear force relation.

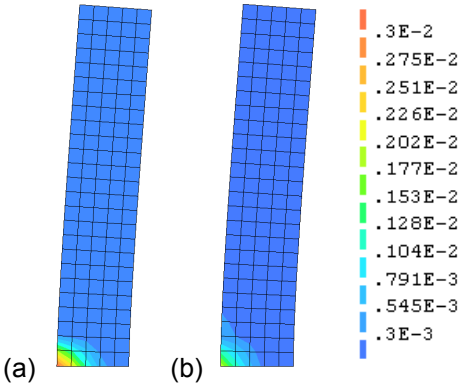

Figure 4.30 – Ultimate tensile strain distributions of: (a) mass IPO and (b) 1st mode IPO.

Force distribution patterns are compared between the pushover analyses and the state at the first and the last peak from the time history of the base acceleration of NDA (Figure 4.31). They are normalised so that the sum of the values of the forces is equal in each case. The mass IPO distributes forces equally along the height while the 1st mode and 1st mode*mass IPO show concentration of forces in the upper part of the structure. The internal force distribution at the first peak of NDA shows a similar shape to the mass IPO. The internal force distribution at the last peak of NDA shows large force values at the upper part of the structure than that at the first peak.

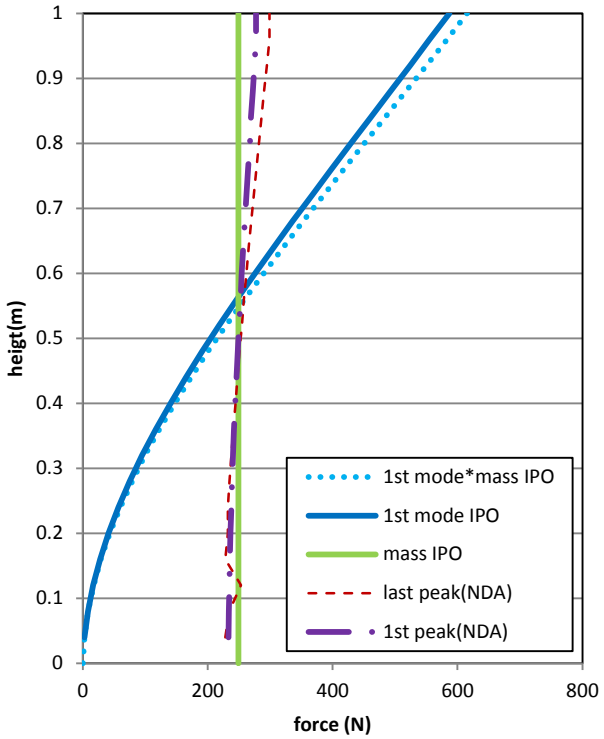

Figure 4.31 – Comparison of normalised force distribution patterns.

4.3.3 One storey box structure

4.3.3.1 Description of the model

A stone-masonry four-wall box structure is studied (Figure 4.32 and Figure 4.33). The model is prepared according to a shaking-table test carried out at the “Laboratório Nacional de Engenharia Civil” (LNEC), in Lisbon, within the European Project “ECOLEADERLIS – Enhancing Seismic Resistance and Durability of Natural Stone Masonry” (Ramos et al. 2005). The masonry is composed of limestone units and lime mortar joints. The tests included application of a sequential of ground motions intensities up to 0.25 g. The state after the shaking table tests is presented in Figure 4.34. Cracks between the widths of 0 to 1 mm are shown in the figure. Damage is concentrated in the southern wall over a large opening. Diagonal crack around the windows of the eastern and western walls are seen. Damage also appears in the connections of walls.

It must be noted that the FEM analyses discussed in this section does not exactly correspond to the experiment carried out in the laboratory in two points. Firstly, some of the material properties are assumed, as discussed below since not all of them have been presented by the authors. Secondly, the accelerogram adopted for NDA is different from that used for the shaking-table test. It is also the due to the insufficient information.

Figure 4.32 – Specimen built in the laboratory (Ramos et al. 2005).

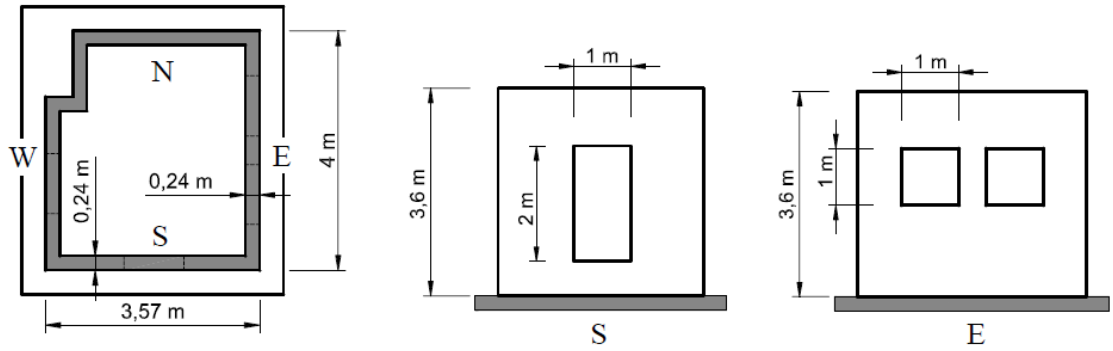

Figure 4.33 – Geometry of the box structure (Ramos et al. 2005).

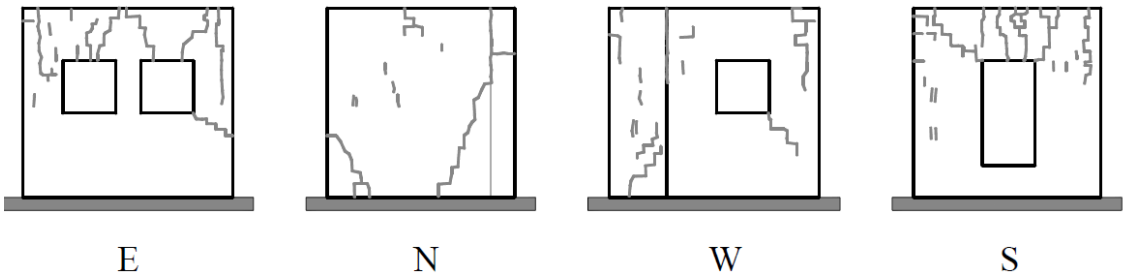

Figure 4.34 – Crack patterns observed after the shaking table tests (Ramos et al. 2005).

The FEM model is seen in Figure 4.35. The thickness of the walls is 24 cm. The density is 2300 kg/m^3. Poisson ratio is 0.2. Young's modulus is 5 GPa. These three values have been presented in their paper. Since the other values were not provided in the paper as mentioned above, they are assumed on the basis of typical properties for similar masonries: compressive strength is 4 MPa, tensile strength is 0.2 MPa and tensile fracture energy is 50 N/m. Discussion on masonry properties is found in in Section 4.2.2. For the failure criteria, Rankine criteria in tension and Drucker-Prager in compression are applied also according to the discussions in Section 4.2.2. The structure is modelled with 4-node curved shell elements. The number of nodes and elements is 1275 and 1197. The Rayleigh damping model is applied for NDA:. a_0 is 5.536 and a_1 is 0.0004 according to the equation presented in Section 2.4.3.2.

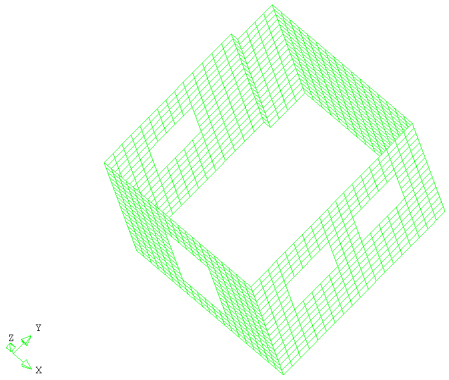

Figure 4.35 – FEM model of the box structure.

4.3.3.2 Application of seismic assessment tools

NDA and pushover analyses are compared. The analyses are carried out in the longitudinal (Y) direction. For NDA, a simple accelerogram presented in Figure 4.37 is applied. It must be noted that this accelerogram is not the same one used for the shaking table test as mentioned above. Three IPO (mass, 3rd mode, 3rd mode*mass IPO and 1st- and last peak IPO) are compared in addition to APO.

For 1st- peak IPO, the internal force distribution of the first peak in the time history of the displacement at 0.021 seconds in Figure 4.38 is considered and for the last peak IPO at 1.78 seconds (the last peak in the time history). For APO, two different loading patterns are considered: 3rd mode APO and mass-3rd APO. From NDA, the time history of the displacement is obtained (Figure 4.38). The third mode is mode with longer period in the Y direction and therefore this mode is the one considered for the pushover analyses (Figure 4.36). The 3rd mode is considered instead of the 1st mode since the 3rd shows much higher partition factor (38.2 %) than the 1st one (0.6e-3%).

As for APO, two different load distribution patterns are considered. Firstly, the load distribution pattern proportional to the 3rd mode is incremented. The load pattern is updated every 12.5 kN of base shear force (i.e. V=12.5, 25, 37.5 kN and so on). The method is adopted according to Antoniou (2004b). It is called 3rd-mode APO in this chapter. Second method is proposed and provisionally adopted by the author. In this method the loading pattern according to the masses of the structure is incremented till the structural element of interest is considered to reach the first nonlinear stage. Specifically, the base shear force equal to 250 kN is considered in this case. At this point, the southern wall reaches the first nonlinear stage, as the mass-IPO shows in Figure 4.39. Then, from that point on, the load pattern proportional to the 3rd mode shape is incremented. The load pattern is updated every 12.5 kN of base shear force. It is called mass-3rd APO. The purpose of this method is to combine the effect of the load proportional to masses of the structure and to the third mode.

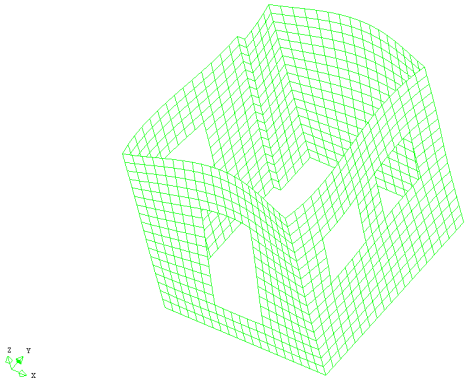

Figure 4.36 – Shape of the fundamental mode in the Y direction.

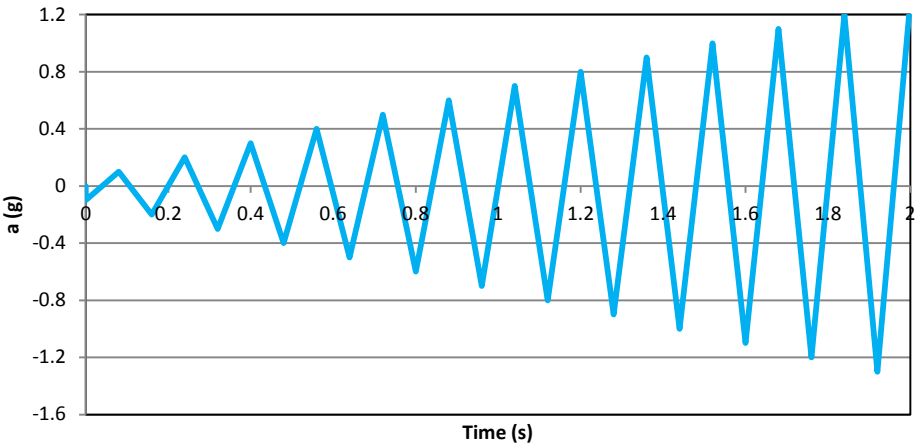

Figure 4.37 – Adopted accelerogram.

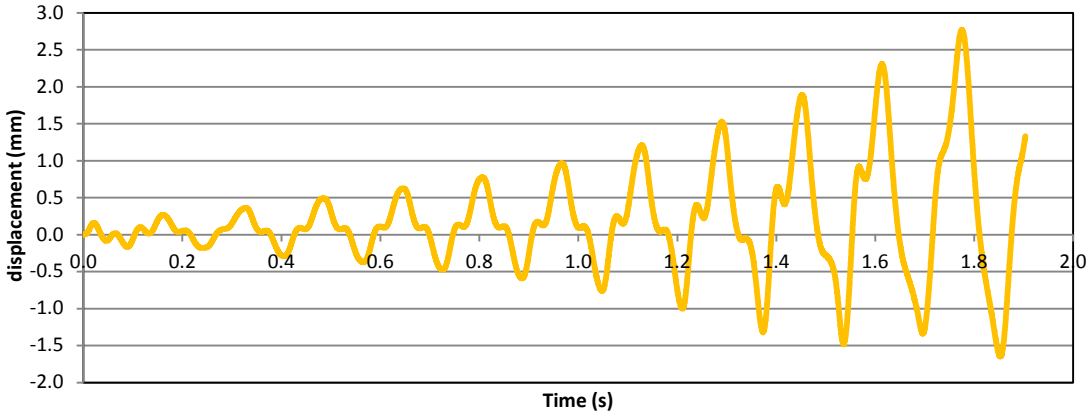

Figure 4.38 – Time history of the displacement at the top of the wall.

When the envelope of the peaks resulting in the NDA is compared with the load-displacement curves from pushover analyses, mass IPO fits the best with NDA although the 3rd -mode IPO predicts closer displacement capacity (Figure 4.39). 3rd APO shows higher displacement capacity than the 3rd mode IPO. Mass-3rd APO represents similar displacement capacity to the mass IPO although it shows lower load capacity.

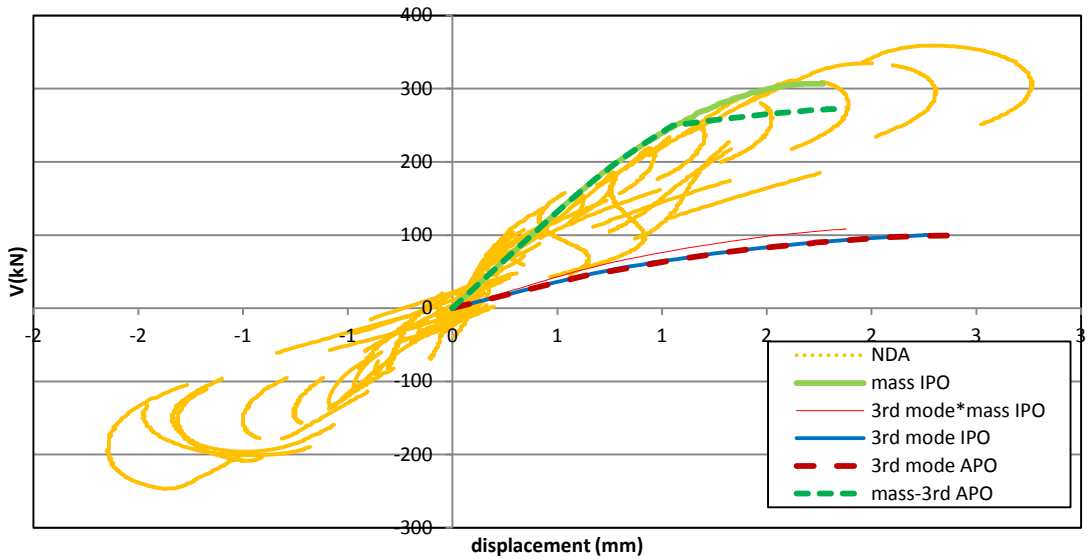

Figure 4.39 – Load-displacement curves and displacement-base shear force relation, at the top of the wall

The ultimate tensile distribution patterns from the pushover analyses are compared with tensile distribution pattern at 1.78 seconds. Although the accelerogram is different from the one used for the shaking-table test, comparable damage to the real structure is observed: especially the damage above the opening in the southern wall and damage appearing diagonally around the opening of the eastern wall (Figure 4.40). The mass IPO shows damage in the eastern wall (Figure 4.41 a). The 3rd mode and 3rd mode*mass IPOs show concentration of damage in the southern wall (Figure 4.41 b-c). The mass-3rd APO shows damage in the southern and eastern wall (Figure 4.41 d). Thus, among the pushover analyses, the mass-3rd APO shows more similar damage pattern to NDA than the other pushover methods.

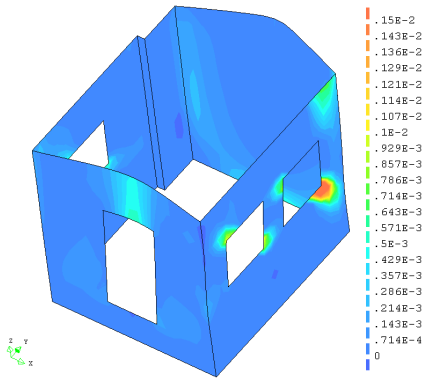

Figure 4.40 – Tensile strain distributions of NDA at 1.78 seconds.

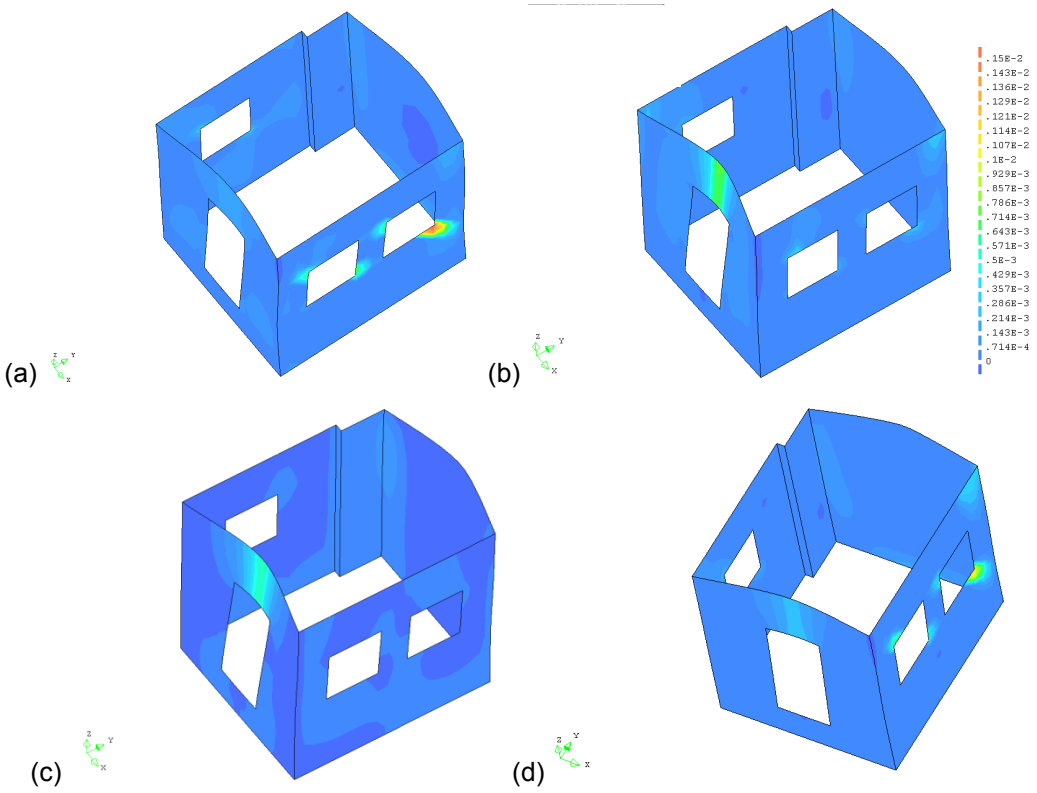

Figure 4.41 – Ultimate tensile strain distributions of: (a) mass IPO, (b) 3rd mode IPO, (c) 3rd mode*mass IPO and (d) mass-3rd APO

Force distribution patterns from pushover analyses are compared (Figure 4.42 a). They are normalised so that the sum of the values of the forces is equal in each case. The mass IPO distributes forces uniformly along the height except for the region around the height of 2 m. that includes the openings in the eastern and western walls. On the other hand, the 3rd mode and 3rd mode*mass IPO show concentration of forces in the upper part of the structure. In Figure 4.42 b, the ultimate force distribution patterns from the pushover analyses are compared with internal force distribution patterns from NDA (those used for the 1st and last peak IPO) (Figure 4.42 b). The internal force distribution at the 1st peak of NDA shows a similar shape to the mass IPO. The internal force distribution at the last peak of NDA shows more force concentration in the upper part of the structure than that at the first peak.

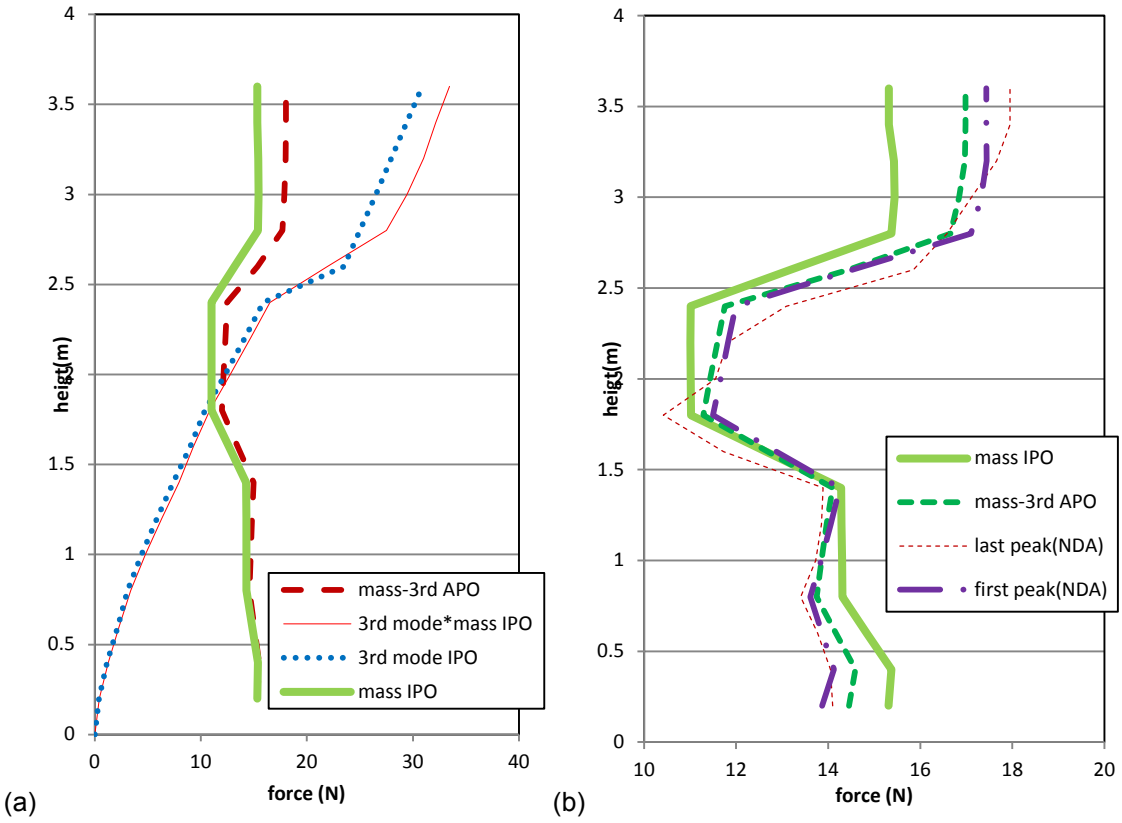

Figure 4.42 – Comparison of normalised force distribution patterns between: (a) pushover analyses and (b) pushover analyses and NDA.

MMP is also applied to the same model. The method proposed by Chopra and Goel (2004) is adopted. The first seven modes with higher participation factor in Y direction (mode 3, 9 10. 11 23, 38 and 39) are considered. Superposition of responses from each mode is done by the SRSS rule. Load-displacement curves from each pushover analysis are compared with the envelope of the peaks of the NDA curve (Figure 4.39). Comparison of the maximum response values between NDA, mass IPO and MMP is presented in Table 4.2. MMP shows closer estimation of displacement capacity to NDA than mass IPO, while mass IPO shows closer estimation of the capacity of the base shear force than MMP. In fact, the response values of MMP are closer to those of the fundamental mode (3^{rd} mode) (2.28 mm and 99.91 kN). The participation factor of the 3^{rd} mode is 38.2%. On the other hand, the participation factor of the other modes (9, 10, 11, 23, 36, 39) is less than 10 %. It is supposed that MMP is more effective when the set of chosen modes has larger overall participation factor.

Table 4.2 – Comparison of maximum responses from different analysis tools.

Assessment tool	Displacement (mm)	V (kN)
NDA	2.76	356.00
MMP	1.94	85.31
mass IPO	1.76	306.0
3^{rd}-mode IPO	2.28	99.9

4.3.4 Cross vault

4.3.4.1 Description of the model

A cross vault structure is analysed. The vault typology selected is based on a vault built and experimentally analyzed by the Research on Restoration of the Hellenic Ministry of Culture (DTRR/HMC) in collaboration with the Laboratory of Earthquake Engineering of National Technical University of Athens (LEE/NTUA) in 2007 (Miltiadou-Fezans 2008). The specimen consists of a cross vault which rests on two parallel piers. The piers are composed of three-leaf stone masonry. The masonry of the external leafs is composed of travertine stones and lime mortar. The masonry of the internal leaf is composed of rubble stones and lime mortar. The masonry of the vault is composed of solid bricks and lime mortar. It was built according to the typology and the properties of the materials of the masonry of Katholikon of Dafni Monastery in Greece. However, due to the size of the shaking simulator (4x4 m^2), the specimen was built in a reduced scale of 2:3 (Figure 4.43). The plan of the specimen is 2.71x 2.60 m^2. The height of the piers is 2.60 m and the total height of model is approximately equal to 2.85 m. The thickness of the piers is 0.45 m. The thickness of the vault is 20 cm.

4-node curved quadrilateral shell elements are used. The number of nodes and element is 2474 and 2956 (Figure 4.44). The mechanical parameters of masonry values presented in Table 4.3 are determined on the basis of the experiments carried out on specimens composed of the same materials as the cross-vault structure (Vintzileou et al. 2008). Due to insufficient information on some material properties in the reference paper, some values have been assumed to carry out the analyses. For the failure criteria, Rankine criteria in tension and Drucker-Prager in compression are applied according to the discussions in Section 4.4.2. For NDA, a Rayleigh damping model is assumed with a_0 equal to 4.2638 and a_1 equal to 0.0005 according to the equation (2.38), (2.39) presented in Section 2.4.3.2.

Figure 4.43 – Specimen built in the laboratory.

Table 4.3 - Mechanical properties for FEM analysis.

	stone masonry	brick masonry
Density (kg/m^3)	2000	1800
Compressive strength (MPa)	4	4
Young's modulus (MPa)	500×fc	500×fc
Tensile strength (MPa)	5%fc	5%fc
Poisson ratio (-)	0.2	0.2
Fracture energy (N/m)	50	50

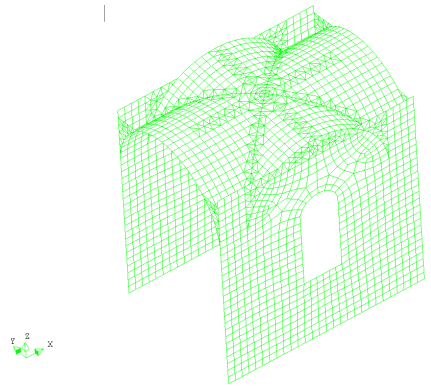

Figure 4.44 – FEM model of a cross vault.

4.3.4.2 Application of seismic assessment tools

Three invariant force distribution patterns (mass, 1st mode and 1st mode*mass IPO) are compared. The analyses are carried out in the transversal (Y) direction. The first mode is shown in Figure 4.45. The participation factor is 67.0%. The accelerogram in Figure 4.46 is applied for NDA. The time history of the displacement at the top of the wall is presented in Figure 4.47.

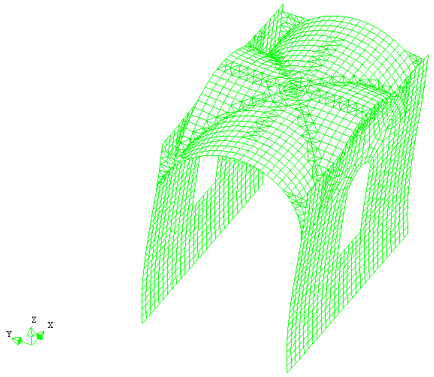

Figure 4.45 – First mode shape.

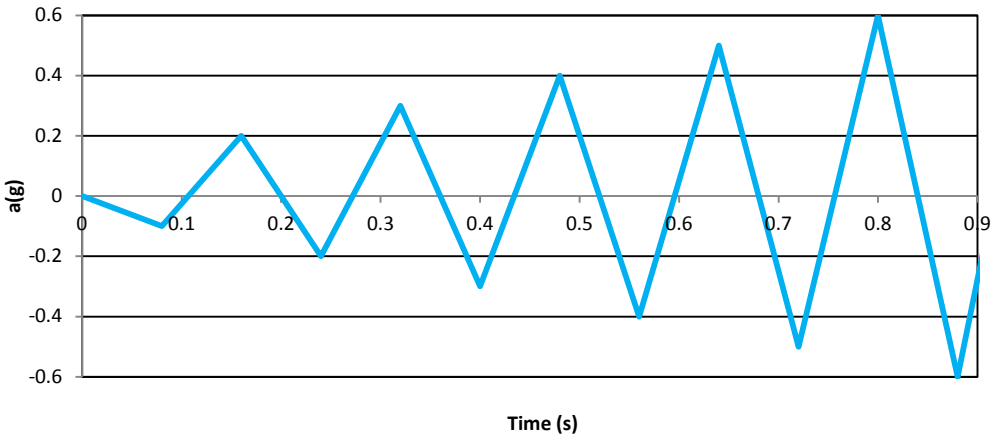

Figure 4.46 – Accelerogram.

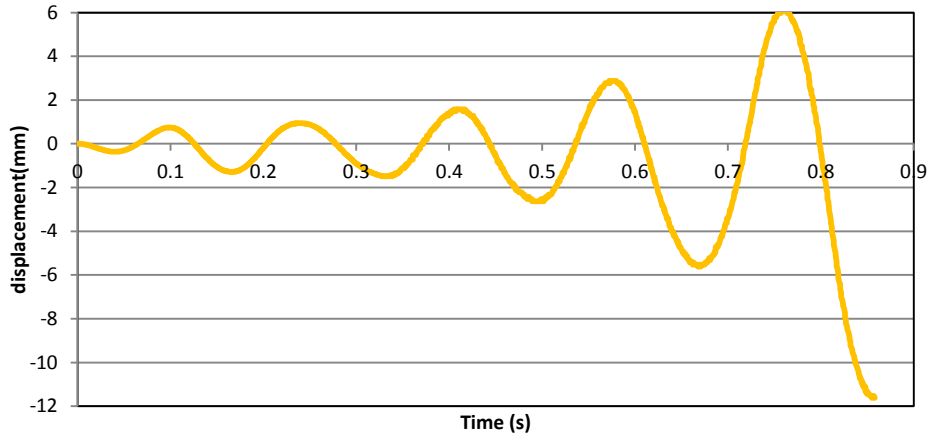

Figure 4.47 – Time history of displacement at the top of the wall.

When the load-displacement curves from pushover analyses are compared with the V-δ relation, mass IPO provides a curve with a similar shape to the NDA envelope (Figure 4.48). Mass IPO 0 shows closer load capacity to NDA than the other two IPO methods. On the other hand, the three IPOs show much lower displacement capacity than NDA-Tensile strain distributions from NDA and pushover analyses are compared. They show similar damage patterns, showing damage in the vault and at the bottom of the model, although NDA presents a higher damage intensity (Figure 4.49 and Figure 4.50).

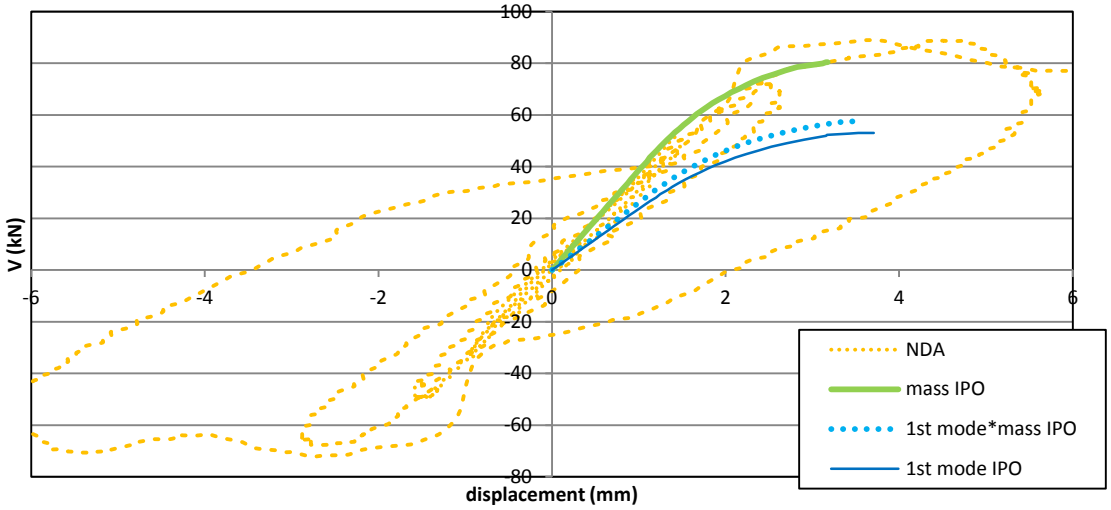

Figure 4.48 – Load-displacement curve at the top of the pier.

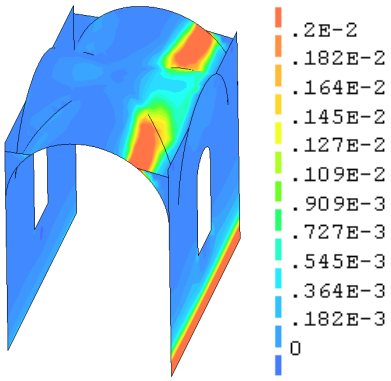

Figure 4.49 – Tensile strain distributions of NDA at 0.828 seconds.

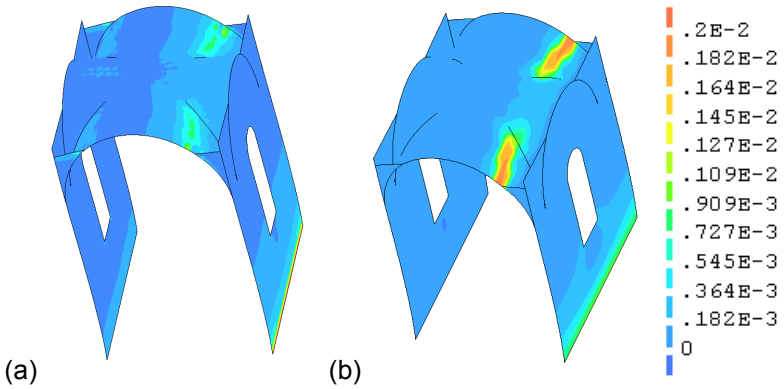

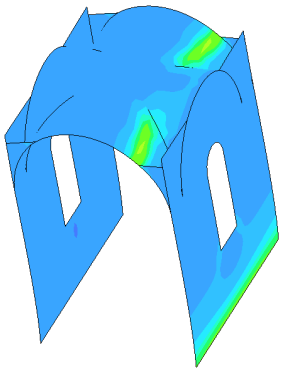

(c)

Figure 4.50 – Ultimate tensile strain distributions of: (a) mass IPO, (b) 1st mode IPO and (c) 1st mode*mass IPO.

Force distribution patterns from pushover analyses are compared (Figure 4.51 a). They are normalised so that the sum of the values of the forces is equal in each case. The mass IPO shows slightly higher values at the upper part of the structure due to the existence of the vault and fillings. The 1st mode IPO shows high concentration of forces in the upper part of the structure. The 1st mode*mass IPO also shows similar shape of the force distribution pattern to the 1st mode IPO although the effect of masses is considered in the 1st mode*mass IPO. In Figure 4.51 b, the ultimate force distribution patterns from pushover analyses are compared with internal force distribution patterns from NDA at 0.028 seconds (the first peak in the time history of the base acceleration) and at 0.83 seconds (the last peak in the time history). The internal force distribution at the first peak of NDA shows a similar shape to mass IPO. The internal force distribution at the last peak of NDA shows higher forces in the upper part of the structure than that at the first peak.

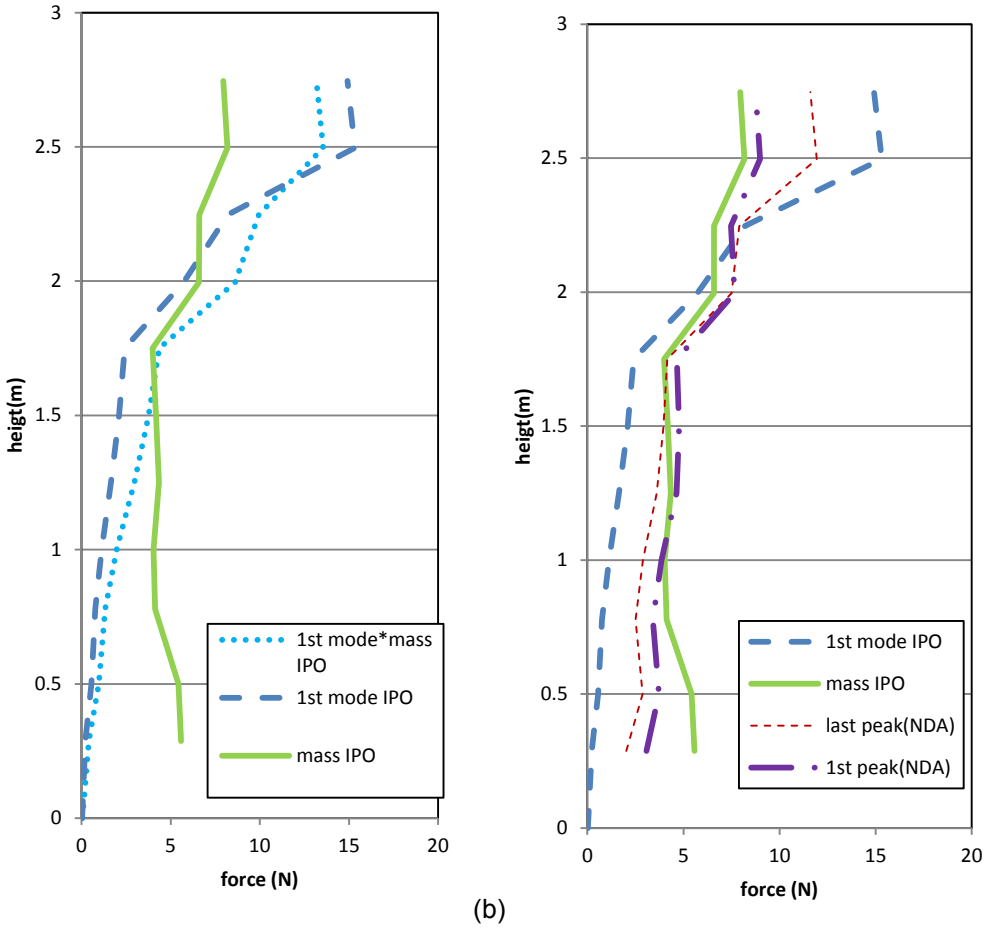

Figure 4.51 – Comparison of force distribution patterns from: (a) pushover analyses and (b) pushover analyses and NDA.

4.4 Discussions

4.4.1 Influence of different parameters on a single Catalan vault

Using one-vault models, the following parameters have been examined: tensile strength, FEM element types, size of FEM elements, number of integration points, and supporting element of the vault. Comparison of shell elements (6-node triangular and 8-node quadrilateral shell elements) has been made. Both models represent similar results. However, the model of 8-node quadrilateral shell elements shows quicker convergence than that of 6-node triangular elements. Decreasing the size of the element (312x312, 208x208, 155x155, 125x125 mm^2) has resulted in showing location of damage more clearly. The model with element size of 125x125 mm^2 has shown similar damage pattern to that with 155x155 mm^2: the dimension of the vault is 5x5 m^2 in plan and its thickness is 11 cm. Decrease of tensile strength (5%, 3%, 1% of f_c) has ended in decrease of load capacity. It has to be noted that tensile fracture energy is linearly proportional to the value of the tensile strength. Increase of integration point (3, 9, 11, 21 points) has resulted in significant increase of the capacity. Convergence of the behaviour has been observed with 9 points. It has been observed that elastic stiffness is not influenced by number of

integration points. Two different types of the support of the vault have been compared: fixed supports at the four corners of the vault and 2-parallel walls. With the 2-wall supports, lower load capacity has been observed than the fixed support case although higher value of deflection has been observed.

4.4.2 Behaviour of a room of four Catalan vaults

The behaviour of complex structure involving four vaults has been studied under a vertical load and also seismic load. As for the vertical load, a uniform load has been applied on one of the four vaults or the entire four vaults, respectively. A concentrated load has been also considered at the one-fourth point of the vault. With the uniform load applied to one of the four vaults, the observed capacity has been equal to 9.5 kN/m^2. With the uniform load applied to the four vaults, the capacity has been reduced to 4.9 kN/m^2. With the concentrated load, the observed capacity has been equal to 30.9 kN. Seismic assessment has been carried out by pushover analysis. The used loading pattern is proportional to the masses of the structure. In the ultimate state (0.183g), overturning of the wall with part of the vaults is observed. Linear kinematic limit analysis (LKA) is carried out for the wall overturning. The seismic coefficient α_0 is equal to 0.135g. Difference from the FEM analysis is rather noticeable (by 33.3 %). It is believed that the difference comes from the consideration of the tensile strength. Thus, in the kinematic limit analysis, the wall is regarded as an independent structural component but in FEM analysis the wall is connected to the orthogonal walls and also the vault. As a matter of fact, a parametric study on the FEM model has been carried out. Two cases of lower tensile strength (1% and 0.5% of f_c) were assumed than the reference case (5% of f_c.) It has to be noted lower tensile fracture energy was considered according to the lower tensile strength as the aforementioned parametric studies of the one vault models. As a result, lower capacities (0.165 g for 1% of f_c and 0.135 g for 0.5% of f_c) have been identified with the same collapse mechanism as the reference case (overturning of the wall). This parametric study supports that higher capacity has been observed in FEM analysis than LKA due to the consideration of tensile strength.

4.4.3 Comparison of seismic assessment tools

Three cases (a cantilever, a box structure and a cross vault) have been analysed with the aim of comparing different seismic assessment tools. The seismic assessment tools have been compared are NDA, IPO (mass, 1st mode and 1st mode*mass IPO) APO and MMP.

It has been found that internal force distribution patterns from NDA are close to force distribution patterns used for the mass IPO in the elastic range. However, once the structure reaches nonlinear stage, the forces become more concentrated to the upper part of the structure than described by mass IPO. It has been also found that the mass IPO shows linear elastic stiffness and load capacity closer to NDA analysis than for the 1st mode IPO. On the other hand, no IPOs have predicted displacement capacity similar to NDA.

For APO, two different methods have been adopted to the model of the box structure: the 1st APO and mass-1st APO. The 1st APO has shown higher displacement capacity than the 1st mode IPO. The mass-1st APO shows similar displacement capacity to mass IPO although it has attained lower load capacity. When damage patterns at the ultimate state have been compared among IPOs, APOs and NDA, NDA and the mass-1st APO have shown damage both in the longitudinal wall and transversal walls while IPOs have shown damage only in the longitudinal wall. Thus, among the pushover analyses, only the mass-1st APO has shown a damage distribution similar to NDA.

MMP has been applied to the same box-structure model. The first seven principal modes have been considered. The resultant values of MMP have been rather close to the values from the IPO of the 3rd mode and improvement has not been observed compared to the other IPOs. The participation factor of the 3rd mode is 38.2%. On the other hand, the participation factor of the other modes (modes 9, 10, 11, 23, 36, 39) is less than 10 %. MMP would be more effective for a set of modes with larger participation factor.

4.5 Conclusions

As the conclusion of this chapter, combination of parameters applicable to the further study of the thesis is presented. As for the number of integration points in thickness of shell elements, 11) is adequate for this type of shell structure). 8-node quadrilateral elements are preferred to 6-node triangular shell elements considering their convergence rate.

A comparison of seismic assessment tools has been carried out. When the results obtained from IPOs have been compared with those from NDA, they have shown limitations in terms of the prediction of capacities and mechanisms. More advanced pushover analysis tools (APO and MMP) also have been adopted. However, improvement of the results has not been seen, compared to IPOs. Further research and practice are necessary for their practical application. For the rest of the case studies in this thesis, NDA will be regarded as the reference case for its accuracy of the representation of seismic behaviour. Limit analysis and mass IPO will be also adopted and compared with NDA.

5. CASE STUDY 2: CATALAN VAULTS OF HOSPITAL SANT PAU

5.1 Purpose of the study

A structural assessment of a set of vaults belonging to two buildings of Hospital Sant Pau (the Nostra Sra. De la Mercé Pavilion and the Administration building) is carried out.

The historical part of Hospital Sant Pau has been inscribed to World Heritage site. The Mercé Pavilion is composed of seven bays roofed with Catalan vaults in the central part. Its structural configuration is more complicated than the previous case study (Lio Palace) due to the existence of horizontal and vertical steel members supporting the vaults. The Administration building also includes Catalan vaults confined with horizontal steel profiles. The Administration building includes, in particular, a large space covered with two single Catalan vaults spanning 9x9 m^2. In this building, the steel is located only horizontally to confine the vaults while the vaults are vertically supported on brick masonry load bearing walls.

The objective of the study is to prepare and test a FEM model capable of representing the structural behaviour of the systems characterised by combination of masonry vaults and steel members, the latter used to confine and, in some cases, to support the former.

Whenever possible, some validation of the models has been carried out by comparison of FEM results with experimental results consisting on static or dynamic load tests actually performed in the buildings. The material properties of the Catalan vaults and walls were estimated based on laboratory compression tests carried out on a sample of bricks and penetration tests carried out in situ by means of the Windsor penetrometer.

In fact, several dynamic tests and a static-loading test were carried out on pavilions. The static loading test was conducted on another pavilion (Sant Rafael Pavilion) which has quasi equal structural configuration to that of Mercè Pavillion. Nonlinear static analysis is conducted by applying a uniform live load. Seismic assessment is also carried out by pushover analysis. The work presented here was partially carried out during the restoration works of the pavilions of the Hospital of Sant Pau.

5.2 Description of the structure

5.2.1 Description of Hospital Sant Pau

In 1901, LLuis Domènech i Montaner was committed with the design of the large hospital complex that is today known as Hospital de la Santa Creu i de Sant Pau in Barcelona, Spain (Figure 5.1). His proposal for the buildings of the hospital was strongly based on two contemporary concepts related to the

architectural hygiene of hospitals. Firstly, as a way to improve recovery rates and decrease mortality, patients were supposed to breathe pure air. Secondly, it was also important to group patients according to types of illness and to separate them from one another. Domènech i Muntaner attained the first requirement by providing sufficient volume and effective ventilation to the buildings. The latter was achieved by designing the hospital as a set of numerous different individual pavilions, part of which were designed and built by him until 1913. Domènech i Muntaner enjoyed an almost absolute freedom in the design, construction and decoration of the pavilions. Today the Hospital Sant Pau is regarded as one of the major examples of the Catalan Modernism which flourished in Barcelona in the early 20th century. The historical part of the complex was inscribed as UNESCO World Heritage Site in 1997. The buildings show genuine structural features, as will be described in the following section.

The complex has actually been used as a hospital until recent time. Due to the need for additional space and more modern facilities, the construction of a new hospital complex was decided in 1990. The moving of the hospital to the new premises allowed the restoration of the modernist buildings and their adaptation to new uses. At present, most of the buildings are intended to host offices of international organisations. The restoration of the modernist pavilions has motivated comprehensive studies on their structure and architecture oriented to respectful conservation and rehabilitation interventions. In most of the pavilions, additions implemented during the 20th century, such as intermediate stories and partition walls, have been removed in order to recover the original spaces and construction features designed by Domènech i Muntaner. More information on history of Hospital Sant Pau is presented by González et al. (2012).

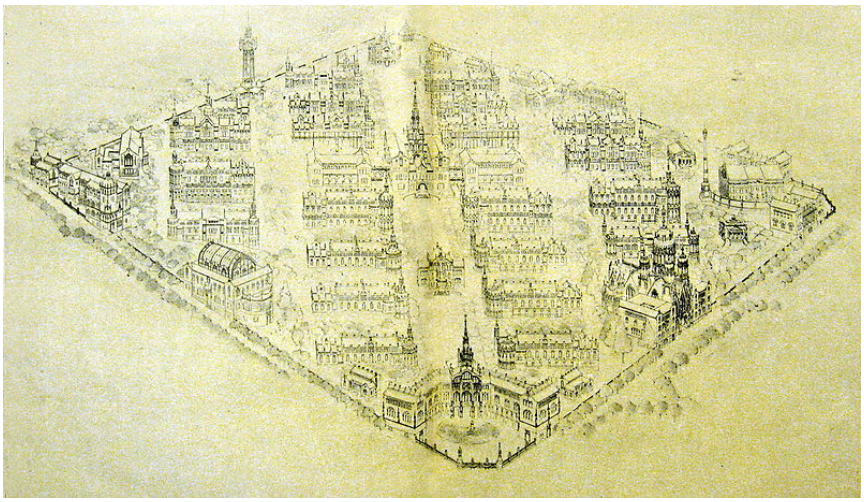

Figure 5.1 - Original drawing showing the general plan and distribution of the pavilions envisaged by Domènech i Montaner.

5.2.2 Description of the structure

The structure of the buildings analysed, namely the Mercé pavilion and the Administration pavilion, are discussed in the following sections. More information on the structure of some of the pavilions of the Hospital complex can be found in the report of BOMA (2007, 2008), the article of González (2005), González et al. (2011) and Casals et al. (2011) and the master thesis of Arias (2013). In the following sections, so as to avoid the redundancy, only the name of the pavilion is used to indicate it: e.g Mercè is used instead of Ntra. Sra. De la Mercé pavilion.

5.2.2.1 Mercé Pavilion

Mercé is one of the eight pavilions located in the centre of the site (Figure 5.1). The exterior of the building is seen in Figure 5.2 a, b. The building is composed of four parts: entrance area (corresponding to zone 1 in Figure 5.3 a), dome area (zone 2), central area (zone 3) and back area (zone 4). The entrance area has an irregular shape. It is composed of the basement, ground and first floor. The dome area consists of the underground and ground floor. Originally the ground floor was shielded with a double shell dome. The central area is composed of the underground and ground floor. The back area is composed of the basement, ground and first floor. The basement and ground floor are covered with suspended domes.

This research focuses on the central area. The central area is composed of seven two-story vaulted bays (Figure 5.3 a-b). The dimension of the bay is 3*9 m^2 in plan. The height of the wall is 4 m at the underground floor and 7.5 m at the ground floor. Each bay has two windows in the ground floor at both ends (Figure 5.3 d). The dimension of the upper window is 3x2 m^2 and that of the lower is 1.1x2.5 m^2. The ceiling and the floor slab of the ground and underground floor is composed of double- and single-curvature Catalan vaults respectively (Figure 5.3 c-d). In this thesis, the single-curvature vault is named Lower vault and the double-curvature vault is named Upper vault in accordance with their location. For both the vaults and walls, the masonry is composed of clay bricks and lime mortar. Steel profiles are installed inside of the walls and arches and at bottoms of the vaults. It is supposed that these steel members absorb the normal and bending forces caused by the arches and vaults. However, today the steel profiles in both Lower and Upper vault show serious corrosion in various places (Figure 5.4).

(a)   (b)

Figure 5.2 - Mercé Pavilion: (a) façade and (b) side.

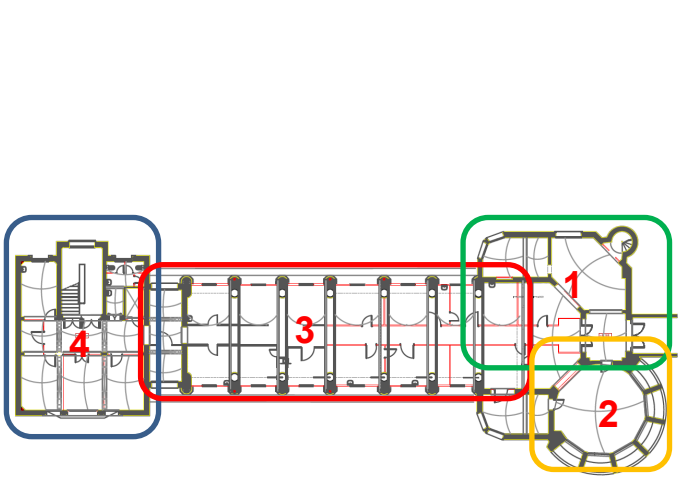

(a)

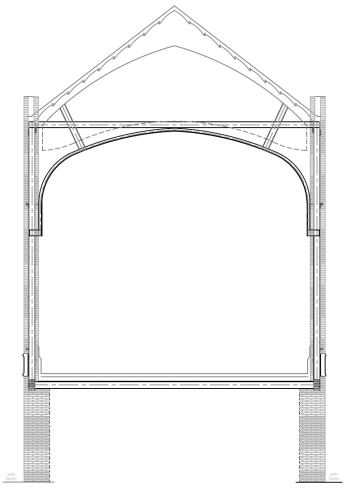

(b)

(c)   (d)

Figure 5.3 - (a) Plan of ground floor, (b) diagram of section and (c) Lower vault and (d) Upper vault after the restoration.

.

 

Figure 5.4 – Corrosion of steel profiles embedded in masonry vaults before the restoration works.

As mentioned above, the Lower vault is a single curvature one (Figure 4, b). Its transverse span is 3 m and its maximum rise is 0.35 m, thus showing a rise/span ratio of 0.116. I-beam steel profiles (IPN 240) are placed longitudinally along the springing of the vaults to support them (Figure 5.5). These profiles are connected to a couple of vertical U-shaped steel profiles (UPN 200) embedded in the façade wall. The vault is composed of three layers of solid bricks bonded with lime mortar. The first layer (from the intrados of the vault) is 40 mm thick and the second and third layers are 20 mm thick. The thickness of the mortar beds is 5 mm. The total thickness of the vault is 90 mm.

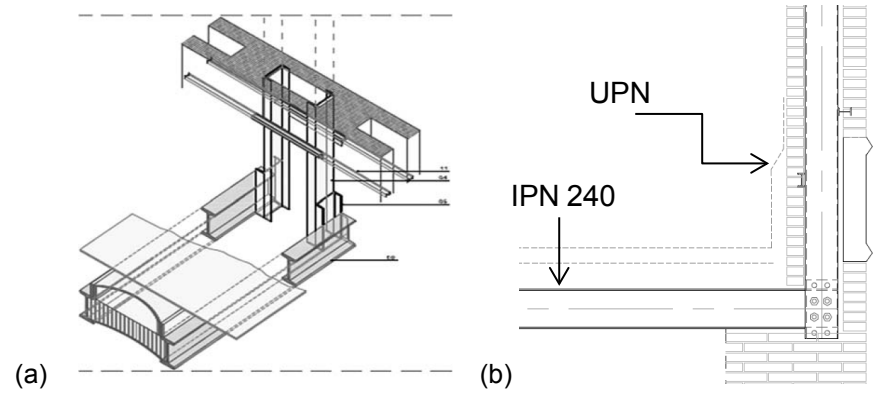

Figure 5.5 – Steel profiles, lower vault: (a) support detail (González et al. 2011). and (b) section.

The Upper vault is a double-curvature one with a span of 9 m in the longitudinal direction of the vault and a span of 3 m in its transverse direction (Figure 5.3, b). The rise at the perimeter of the vault is 0.4 m (with rise/span ratio of 0.133) in the transversal direction and 0.8 m (with rise/span ratio of 0.0889) in the longitudinal direction. The maximum rise, at the centre of the vault, is 1.05 m. Like the lower one, the vault is composed of three layers of solid bricks bonded with lime mortar. As in the previous case, the first layer is 40 mm thick and the second and third layers are 20 mm thick. The thickness of the lime mortar beds is 5 mm. The total thickness of the vault is 95 mm since the intrados is covered with 5 mm-thick tiles as seen in Figure 5.4.

As in the lower one, the Upper vault is supported on steel profiles. In the case of the upper vault, however, the supporting system is more complex and redundant, and involves not only the existing steel structure but also the upper masonry arches that shape the roof of the building. The vault is directly supported on two different steel members. On the one hand, the vault is supported, along its lateral sides, over curved T profiles shaped as an arch. On the other hand, the vault is also supported, at mid-span of its lateral sides, on two horizontal U-shaped steel profiles (UPN 200). These horizontal profiles are, in turn, supported on steel pillars embedded in the façade walls. The horizontal profiles are also suspended, at a certain distance from their connection to the pillars, from diagonal steel profiles (also UPN 200 ones) that hang from the upper masonry arches (Figure 5.6, b-c). The diagonal profiles are also connected to the arched T profiles on which the vault is partly supported. The masonry arches

that support the roof and also sustain the vault through the diagonal profiles are made of a brick masonry hollow box showing a width of 60 cm and a variable depth measuring 24 cm at the bottom and 100 cm at the top (Figure 5.6, a). Figure 5.6, d, corresponding to a construction stage, helps understand the important role of the steel skeleton of the structure and the only secondary role of the masonry façade walls.

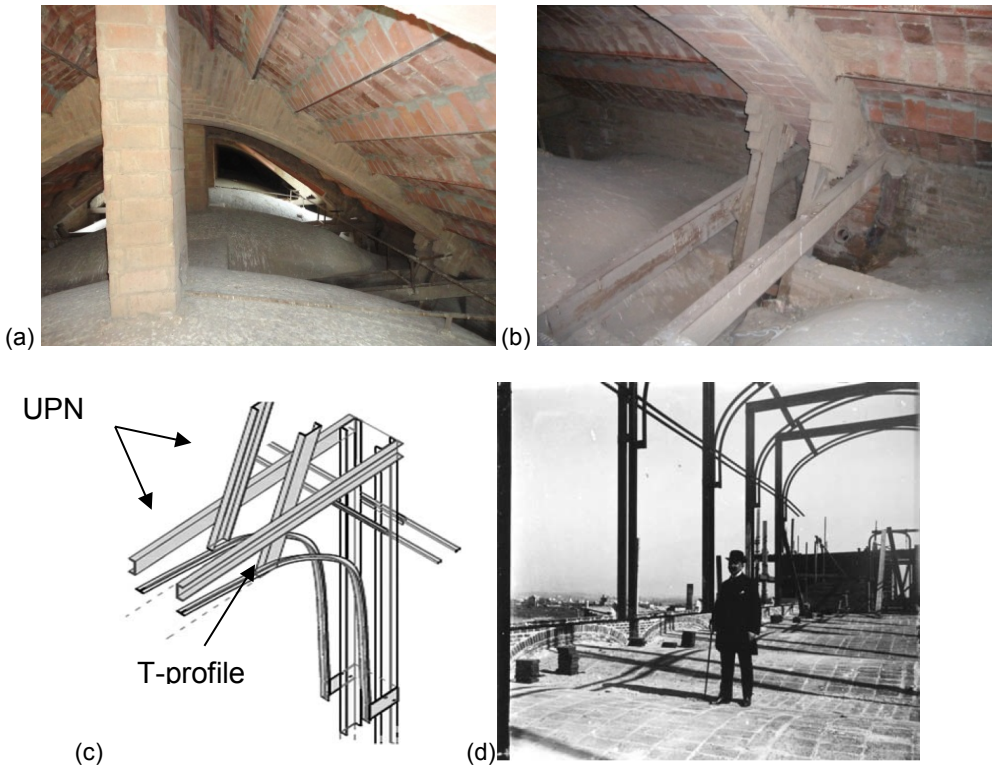

Figure 5.6 – Upper vault: (a) masonry arches shaping the roof, (b) horizontal and diagonal UPN profiles in which the vault is partly supported, (c) details of the steel structure that supports the vault, (d) steel skeleton of one of the pavilions visible during the construction. ((c) and (d) from Gonzales et al. 2011).

5.2.2.2 Administration building

This building is situated at the entrance of the site of the Hospital of Sant Pau. It is the biggest building in the hospital and its prominent appearance gives the visitors a splendid impression of the complex (Figure 5.7 a). In the building, there are 130 Catalan vaults. Their intrados are decorated with tiles (Figure 5.7 b). In the Administration building, most of the steel profiles are only located horizontally and are used to retain the thrust of the vaults, while, unlike in the other pavilions, the vaults themselves are supported on masonry load-bearing walls (Figure 5.7 d). The building is symmetric in plan (Figure 5.7 c). It is composed of five parts: central body (corresponding to zone 1 in Figure 5.7 c), east and west middle body (corresponding to zones 2, 4) and east and west extreme body (corresponding to zone 3, 5). This is a four-storey building composed of the basement, ground, first and second floor. In both the vaults and walls, also in the Administration building, masonry is composed of clay bricks and lime mortar. In this

research, three double-curvature vaults are studied: Small, Intermediate and Large vault. Each is explained as follows (Figure 5.7 e).

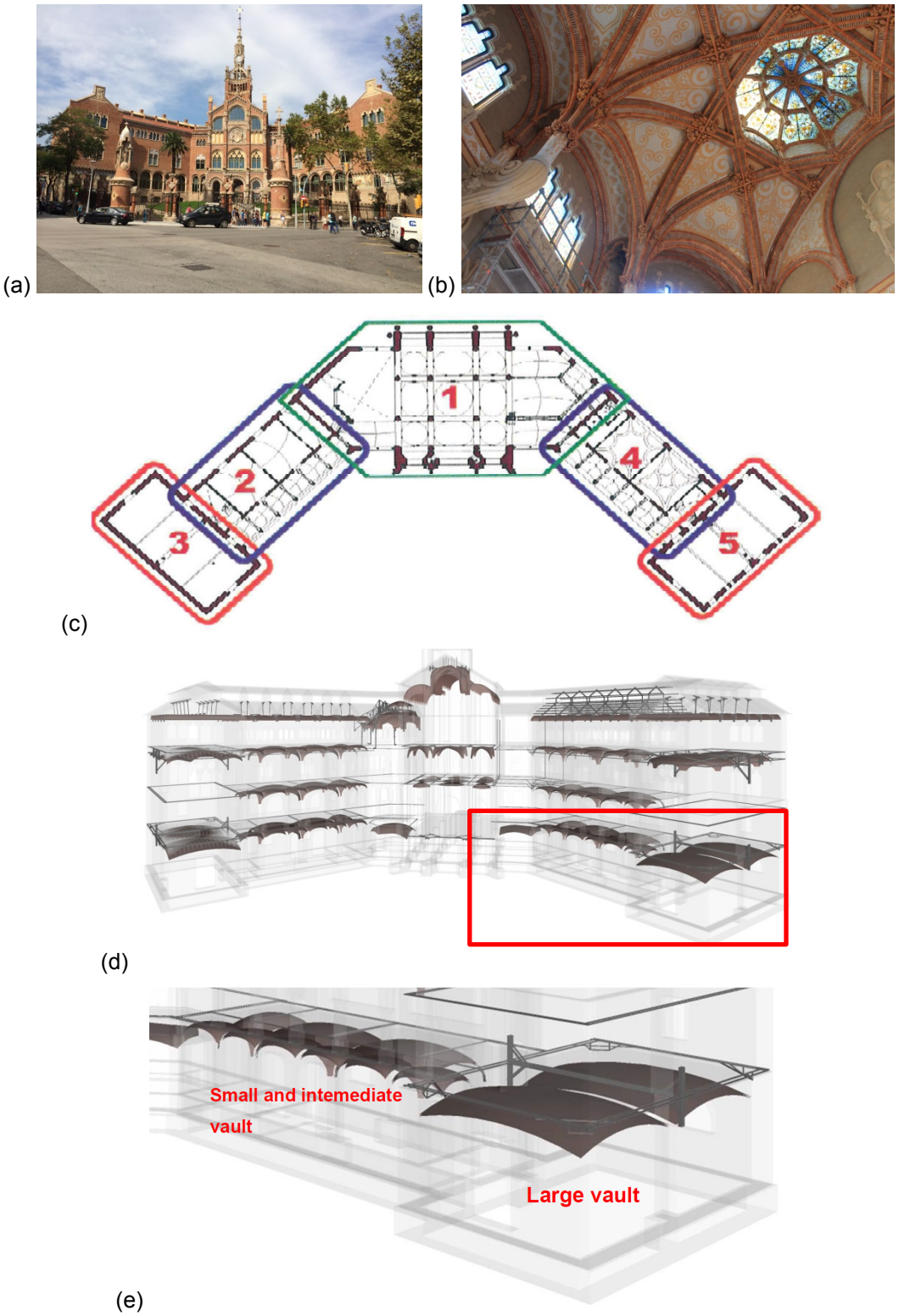

Figure 5.7 – Administration building: (a) façade, (b) vault decorated with tiles (c) diagram (d) 3D view (BOMA 2007) and (e) basement floor of west middle and extreme body

5.2.2.2.1 Small vault

The Small vault to be analysed is located on the basement floor of the west middle body (zone 4) (Figure 5.7 c, e). Six vaults of the same dimension are located in a row and this space is used as a corridor giving access to rooms of the Intermediate vaults and also the Large vaults (Figure 5.8). Each vault is 3.12x3.12 m^2 in plan. The thickness of the vault is 12 cm. The rise at the perimeters of the vault is 0.6 m. The height of the wall is 4.6 m and its thickness is 35 cm. There are two steel profiles of IPN 80 located along the longitudinal perimeters the slab (Figure 5.7 e).

Figure 5.8 – Small vaults in a row, Administration building.

5.2.2.2.2 Intermediate vault

The Intermdeiate vault to be analysed is located on the basement floor of the west middle body (zone 4) (Figure 5.7 c, e and Figure 5.9). There are two vaults of the same dimensions on this floor. There is a wall between the two vaults. The thicknes of the vault is 12 cm. Its plan is 6.7x6.2 m^2. The rise at the perimeters of the vault is 11 cm. The height of the wall is 3.9 m. Its thickness is 70 cm for the external wall and 35 cm for the wall between the two vaults. There are two steel profiles IPN 80 surrounding horizontally along the perimeters of the slab (Figure 5.7 e).

Figure 5.9 – One of the intermediate vaults, Administration building.

5.2.2.2.3 Large vault

The Large vault is located in the room of the basement floor of the west extreme body (zone 5) (Figure 5.7 c, e). There are two vaults of the same dimension in the room. Between the two vault, there is an arch (Figure 5.7 a). The dimension of each vault is 8.8x8.8 m^2. The thickness of the vault is 8 cm. The rise at the perimeters of the vault is 8.6 cm. The thickness of the wall is 76 cm. Its height is 4.3 m (Figure 5.10 a). There are two steel profiles of IPN 100 surrounding horizontally along the perimeters of the slab (Figure 5.7 e). Two steel profiles of UPN 200 located in the arch in the middle of the room. At the corners of the room, there is a steel confinement composed of IPN 100 as shown in Figure 5.7 e and Figure 5.10 b.

(a)  (b) 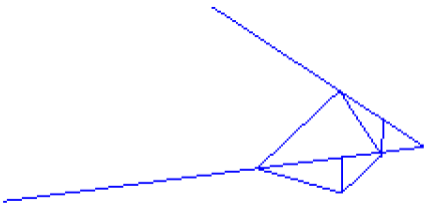

Figure 5.10 – One of the large vaults, Administration building: (a) vault decorated with tiles and (b) diagram of the steel confinement at the corner of the room.

5.3 Experimental studies

5.3.1 Mercé Pavilion

5.3.1.1 Material tests

A penetrometer test was carried out so as to examine the compressive strength of mortars in Mercé in September, 2011. The test was carried out by means of a Windsor pin penetrometer. The penetration test by means of pin penetrometers has been regulated by the American Society for Testing and Materials (ASTM) C-803 (2010). The test procedure is explained as follows (Windsor Pin system, 2010). First, a pin is shot to the mortar joint to be tested. It has to be confirmed that the penetrometer is perpendicular to the test surface. After the pin is removed from the surface, a hole remains. The value of the compressive strength is determined by measuring the depth of the hole and referring to the strength table provided by the manufacturer of the penetrometer. The test has to be repeated seven times. As a result, the compressive strength of mortars has been determined as Table 5.1. The values are very limited except for Upper vault. It has to be mentioned that the measurement was carried out at the extrados of the Upper vault. Therefore it is suspected that its high compressive strength is due to an original finishing or later repair with a kind of mortar different to lime mortar.

Separately, the strength of brick was examined by compression test on samples at a laboratory of Polytechnic University of Catalunya (Barcelona, Spain) in September, 2011. They are taken from Mercé. Bricks were cut in half and faced with mortar. Then they were cured till the mortar obtained the strength necessary to perform the test. From the results, the average compressive strength is 20 MPa (Table 5.2).

Table 5.1 – Compressive strength of mortar estimated by Windsor penetration tests

Location	Strength (MPa)
Upper Vault	15.8
Lower Vault	2.3
External wall	4.6
Load-bearing wall	2.2
Shear wall	1.3
Non load-bearing wall	2.1

Table 5.2 – Compressive strength of bricks tested in laboratory

sample name	dimension (cm)	failure load (kN/m2)	compressive strength (MPa)
3915.7A	14.3x14.7	448.2	21.3
3915.7B	14.5x14.8	389.1	18.1
3915.8A	14.6x14.5	394.5	18.6
3915.8B	14.2x14.4	423.8	20.7
3915.9A	14.9x14.7	334.1	15.3
3915.9B	14.6x14.8	375.7	17.4
3915.10A	14.0x14.1	358.8	18.2
3915.11A	13.9x14.5	466.8	23.2
3915.11B	14.6x14.0	512.6	25.1
average	-	-	20.0

5.3.1.2 Static loading test

A static loading test was carried out on another pavilion (Sant-Rafael Pavilion) in March, 2010 (Bernuz-Fernández Arquitectes SLP, 2010). The structure of Mercé and Sant Rafael are very similar. Sant Rafael also includes seven bays composed of Lower and Upper vaults of the same dimensions as in Mercé (Figure 5.3 a, Figure 5.12 a). During the load test, a loading/unloading procedure was carried out with water tanks placed in the marked area on the slab over the Lower vault. A load up to 4 kN/m^2, was applied for the first 24 hours (Figure 5.12 b-c). The transition of the deflection was measured for 48 hours at the chosen points (Figure 5.12c). The maximum deflection was 0.86 mm and 1.64 mm (at the middle part of the vault: point 1 and 6), 2.14 mm and 1.19 mm (at the middle of steel profiles: point 2 and 5) and 1.91 mm and 1.64 mm (at the centre of the vault: point 3 and 4), respectively (Figure 5.12 c-d). It has been reported that no cracking appeared during the test.

It is reported that during the test, props were located underneath the middle part of the I-beams (corresponding to the part where water tanks were put) (Figure 5.11). Supposedly the props were put for two purposes. Firstly, they were supposed to constrain the steel profiles so only the deformation of the vault could be observed from the test. Secondly, steel members that support the vaults present significant corrosion that might have caused deterioration of their capacity. The props were located underneath them so as to avoid risks due to the test. At any rate it is not very typical to carry out a static loading test on a structure with props installed. Besides, deformation of the steel profiles was observed in spite of the placement of the props. It has to be commented that the test results have become rather ambiguous due to these props. In Section 5.4.1, comparison of the results between this static loading test and FEM analysis is made. For the comparison, the effect of these props is considered under two different hypothesis.

Figure 5.11 –Props supporting the Lower vault.

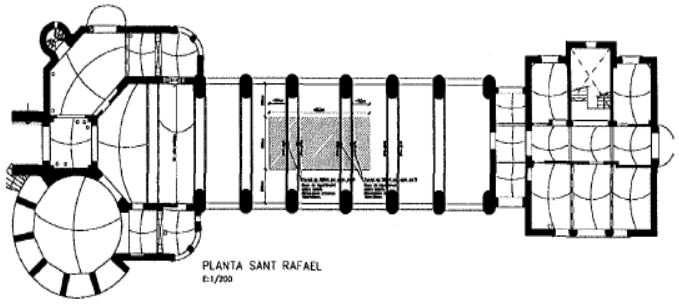

(a)

(b)

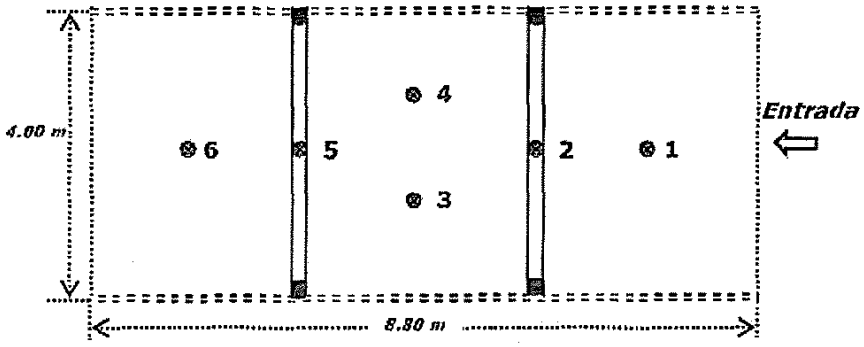

(c)

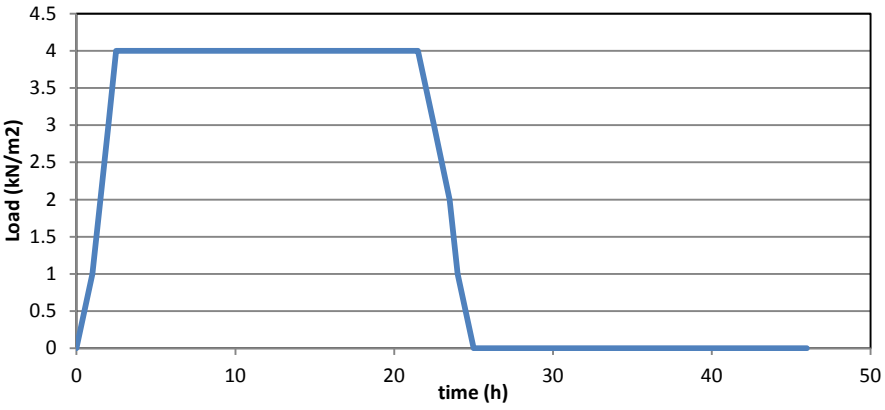

(d)

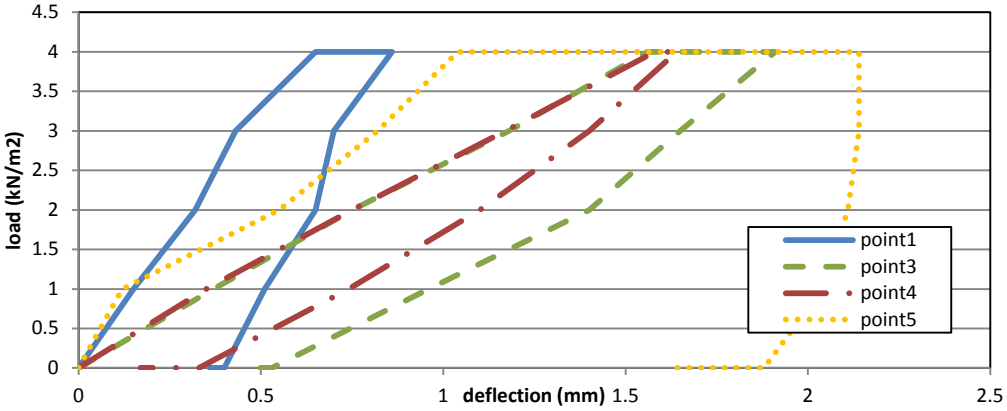

(e)

Figure 5.12 - Sant Rafael Pavilion: (a) loaded area, (b) water tanks on the slab, (c) measured points in loaded area, (d) loading/unloading process and (e) load-deflection relation at different measured points.

5.3.2 Administration building

5.3.2.1 Intermediate vault

5.3.2.1.1 Dynamic identification

A vibration test was carried out on site (Llorens 2013). The excitation was caused by an impact hammer. The vibration was measured by piezoelectric accelerometers. The experiment was repeated four times. The shown result in Table 5.3 is calculated from the average of four experiments.

Table 5.3 – Eigenvalues from the experiment.

	1st	2nd	3rd
Frequency (Hz)	16.99	24.238	38.802

5.3.2.1.2 Static loading test

A static loading test was carried out on one of the intermediate vault in Administration building in September, 2010 in the similar procedure as the Lower vault in Sant-Rafael Pavilion (Cocta, s.a. 2010). A loading/unloading procedure with water tanks was carried out on the entire slab up to 4 kN/m^2 for the first 24 hours (Figure 5.13 a, c). The transition of the deflection was measured for 48 hours at the chosen points (Figure 5.13 b).

The maximum deflection at point 1, 2 and 4 is 1.2 mm, 1.5 mm and 0.4 mm, respectively (Figure 5.13 b, d). It is reported that no cracking appeared during the test.

(a) 

(b) 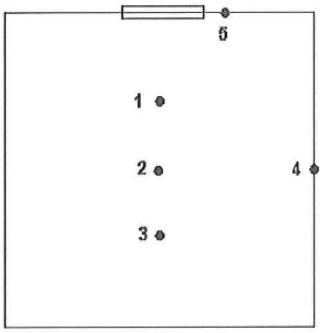

(c) 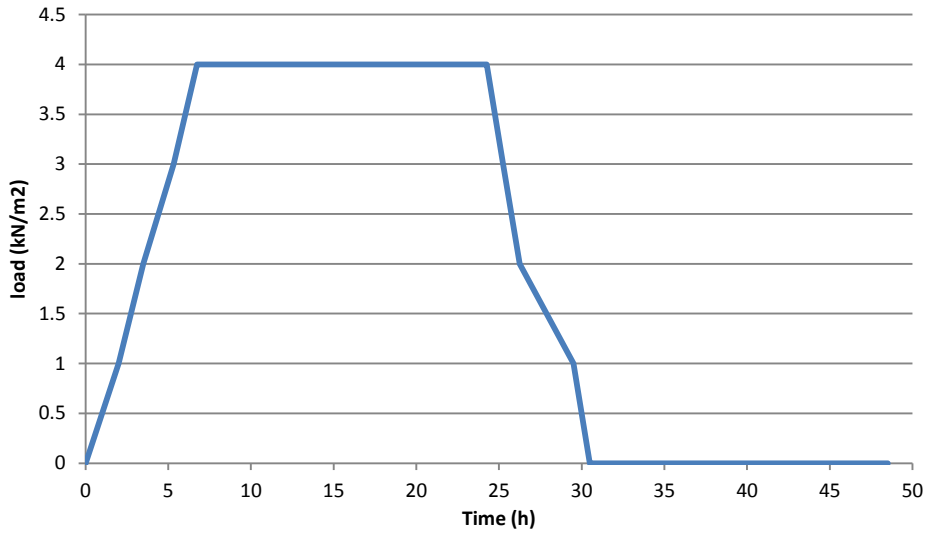

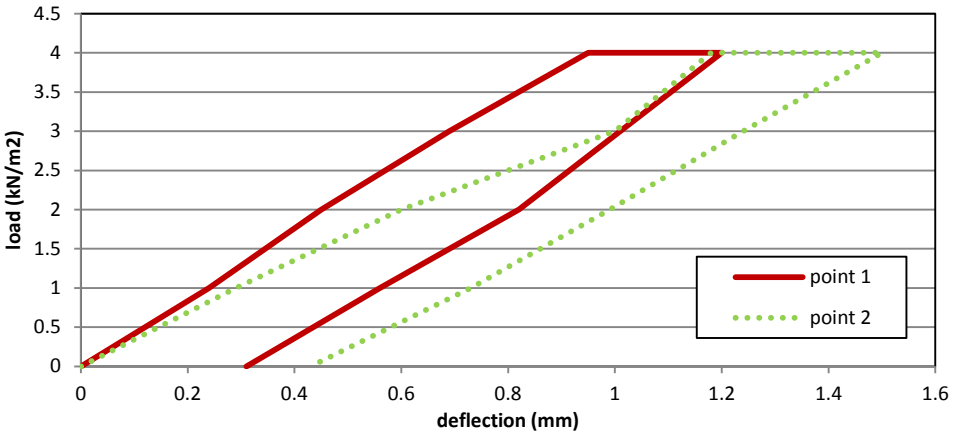

(d)

Figure 5.13 – Intermediate building, Administration building: (a) water tanks on the slab, (b) location of accelerometers (c) loading/unloading process and (d) load-deflection relation at different measured points.

5.3.2.2 Small vault

5.3.2.2.1 Dynamic identification

A vibration test was carried out on site (Llorens 2013). The result is shown (Table 5.4). The experiment has been carried out in the same procedure discussed in Section 5.3.2.1.1.

Table 5.4 – Eigenvalues from the experiment.

Mode	1st	2nd	3rd	4th	5th	6th	7th	8th
Frequency (Hz)	23,908	28,317	32,437	37,453	41,414	44,353	47,490	50,461

5.4 Structural analysis of the vaults of Mercé pavilion

The Lower vault, Upper vault and a typical bay in the Mercé are studied. They are analysed individually. For the Lower vault, firstly comparison of the behaviour between the real structures and FEM models is done by taking advantage of the results from the static loading test discussed in Section 5.4.2. Then capacity assessment under a uniform live load is conducted. For the Upper vault, capacity assessment under a uniform live load is carried out. For a typical bay, seismic assessment is carried out by means of pushover analysis. The analyses are carried out considering geometrical nonlinearity.

5.4.1 Lower vault

5.4.1.1 Model description

The material properties of brick masonry and steel are assumed as indicated in Table 5.5. The compressive strength of masonry is assumed considering the values of compressive strength of bricks and mortar discussed in Section 5.3.1. Tensile strength is taken as 5 % of compressive strength and Young's modulus is taken as 500 times the compressive strength. For the tensile fracture energy, 50 N/m is assumed. The last three values are assigned according to the parametric studies carried out in Chapter 6. For the failure criteria, Rankine criteria in tension and Drucker-Prager in compression are

applied. These failure criteria are determined on the basis of the discussions in Chapter 3 and 4. Parameters of steel are determined as specified in the recommendation for historical steelworks by the British constructional steelwork association (Bates 1991). Von Mises yield criterion is assumed for failure criterion. Friction behaviour between steel and vault is considered in this study. For this behaviour, the Coulomb friction model is considered. Detailed discussion on frictional behaviour is found in Chapter 3. Since information is limited on the frictional behaviour in a masonry-steel contact, the frictional parameters are assumed in accordance with the conventional ones for friction between concrete and steel. It is considered that the friction angle is 26.5º ($\tan\phi = 0.5$) (PCI Industry Handbook Committee 2004). Values of 200 MPa/mm for normal linear stiffness and 100 MPa/m for shear linear stiffness are assumed. These values are determined on the basis of preliminary studies carried out on models of the Lower vault. It has been found that too low value of normal linear stiffness (0.2 MPa/mm) introduces inadequately high displacement capacity and on the other hand, a too high value (2000 MPa/mm) causes a brittle failure before a mechanism is observed. It was assumed that normal linear stiffness is twice as large as shear linear stiffness in those analyses. For the value of cohesion, 0.4 and 0.1 MPa are compared. The former value is decided considering the one for the friction between masonry and steel (Virdi et al. 2013). The latter is determined from a more conservative viewpoint with very limited cohesion between steel profiles and a masonry vault.

Table 5.5 – Material properties

Property	Brick masonry	Steel
Tensile strength (MPa)	0.2	100
Compressive strength (MPa)	4	280
Young's modules (MPa)	2000	200000
Density (kg/m^3)	1800	7850

Two different models have been considered for the analysis. The first model represents a single-curvature vault supported on the IPN 240 profiles. Both vault and I-beams are discretised with 8-node quadrilateral curved shell elements (Figure 5.14). The number of elements is 4224 and the number of nodes is 12953. The number of integration points of shell elements in thickness is 11 according to the discussion in Chapter 4. The model is restrained by fixed supports at the end of the I-beams: the supports are applied to the node at the centre of the section. Since in the real structure there are adjacent vaults on the both sides, the transversal movement of the vault is restrained. Interface elements are adopted along the connections between the vault and the steel. A 3+3 node line interface element is used.

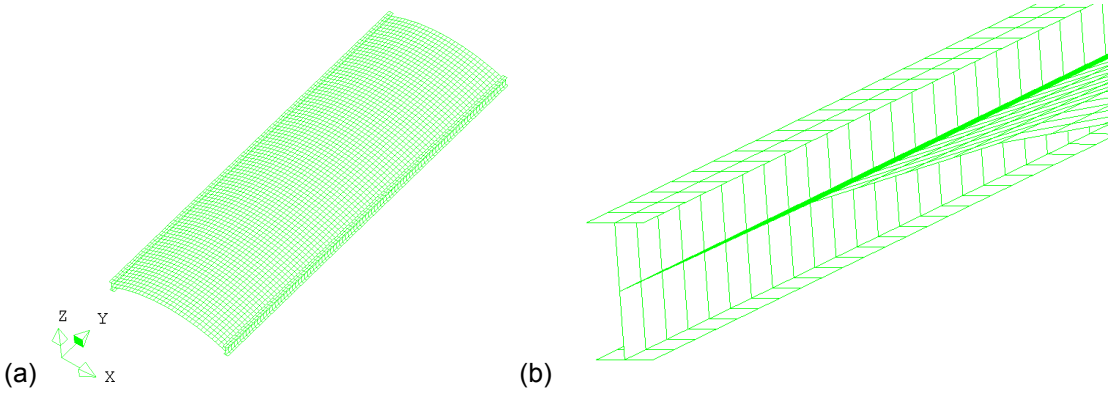

Figure 5.14 – FEM model of the vault (1st model): (a) entire model and (b) I-beam.

The second model is based on the 1st model but includes the additional structural elements existing over the vault. Slab, longitudinal beams and wallets are added to the 1st model (Figure 5.15). The thickness of the slab is 10 cm. That of the wallets is 2.5 cm. These wallets are located every 37.5 cm. The thickness of the longitudinal beams at the edges of the vault is 35 cm. Number of nodes is 32351 and that of elements is 13580. In this model, the steel profiles (IPN 240) are modelled with 3-node curved beam elements instead of 8-node curved shell elements since it facilitates the modelling of wallets and longitudinal beams and also the visualisation of the entire model. A 1+1 node line interface element is used.

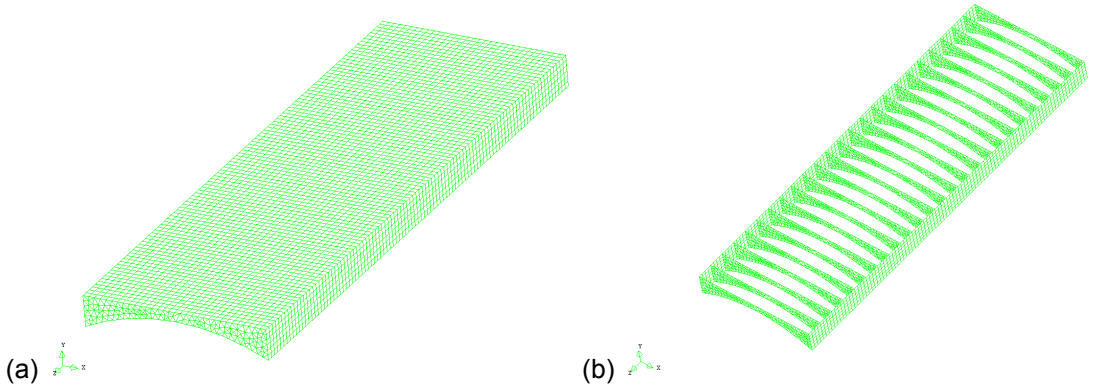

Figure 5.15 –FEM model of the vault and the slab (2nd model): (a) entire model and (b) wallets and longitudinal beams.

5.4.1.2 Comparison with experiments

The experiment discussed in Section 5.3.1 is simulated using the two FEM models. The same loading/unloading process is adopted (Figure 5.12 d). The load is applied on the corresponding location (the middle of the vault or slab, comprising 4x3m^2, Figure 5.16). As discussed in the previous section, props were located underneath the steel profiles during the test. Since, in fact, those profiles deflected during the test, it is assumed firstly assumed that the props did not actually constrain their vertical deformation. Therefore, and as a first hypothesis, the props are not considered. As for the cohesion of the masonry-steel contact, the value of 0.4 MPa is adopted to the 1st model. For the 2nd model, 0.1 MPa and 0.4 MPa are compared.

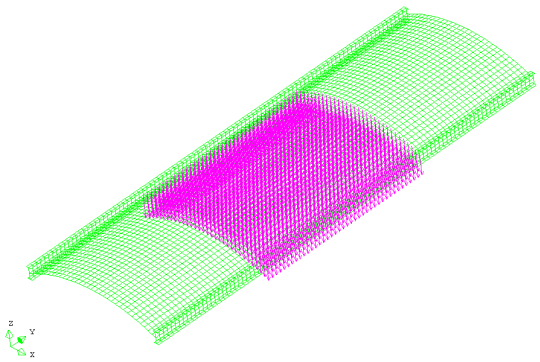

Figure 5.16 – Loading area (2nd model).

Regarding the 1st model, the numerical response obtained shows a lower stiffness compared with the load-deflection relation obtained experimentally (Figure 5.17 a). As for the 2nd model, with the cohesion equal to 0.4 MPa, the load-deflection relation from FEM analysis shows good agreement with that from the experiments (Figure 5.17 b). When the maximum deflection at the middle of the steel profiles is compared, this model also shows a similar value compared with the experiment: 1.67 mm (the average deflection of point 2 and 5 from the experiment) and 2.2 mm (FEM analysis). When 0.1 MPa is assumed for the cohesion, the stiffness is reduced significantly.

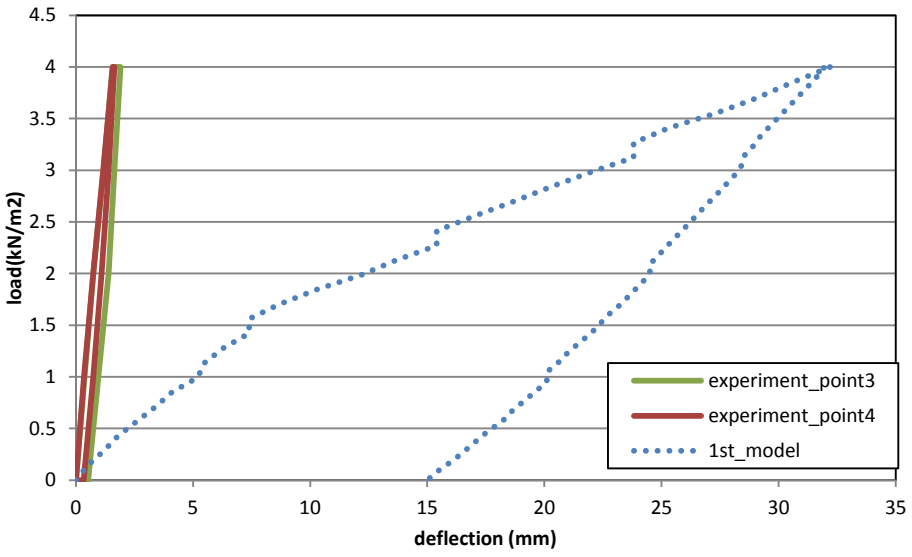

(a)

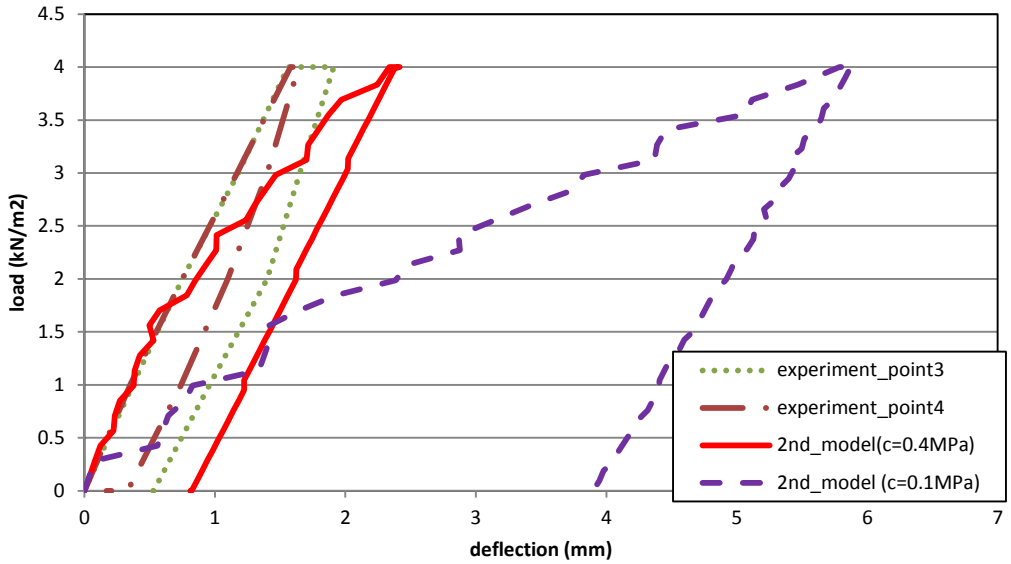

(b)

Figure 5.17 - Load-displacement relations, comparison between experiment and FEM results: (a) 1st model and (b) 2nd model.

As a second step, another assumption is made regarding the role of the props. In this case, it is assumed that the props actually limited the deflection of the steel profiles, so that these had their deflection totally restrained. In the model, the vertical displacement of the profiles is restrained by means of pin supports. Both the 1st and 2nd models are studied. It is considered that the cohesion is equal to 0.4 MPa. In this case, the 1st model experiences a deflection of 0.4 mm at the centre of the vault, while 2nd model shows a deflection of 0.22 mm at the same point. The experiment showed a relative deflection of 0.11 mm at the centre of the vault with respect to the profiles. The average deflection at the centre of the vault was 1.78 mm (point 3 and 4) and that at the middle of the steel was 1.67 mm (point 2 and 5). Also under this assumption, the 2nd model provides closer values to the experimental results than the 1st model.

As a summary of this section, it is supposed that the 2nd model is more reliable than the 1st model. As for the cohesion, the value of 0.4 MPa provides a closer value of the deflection measured in the experiment than 0.1 MPa.

5.4.1.3 Assessment of the capacity under a uniform live load

Since through the comparison with experimental results discussed in Section 5.4.1.2, the 2nd model with the cohesion equal to 0.4 MPa has shown similar behaviour to the real structure in the experiment. Therefore using the same 2nd, the ultimate capacity of the vault is examined (Figure 5.18 a). In this study, the uniform live-load is applied on the entire surface of the slab and increased gradually up to failure. At a life load of 4.0 kN/m^2, sliding between the vault and the I-beams occurs. At the same time damage over the slab becomes evident. At the ultimate state, the maximum deflection at the centre of the vault is 39.1 mm and the ultimate capacity is 13.7 kN/m^2. Then an analysis is carried out with applied

conventional safety factors over the dead load (1.35) and over the live load (1.5) and also with reduced values of the material properties (with factors of 2.5 and 1.15 applied respectively over masonry and steel. In this case the maximum acceptable live load is equal to 9.37 kN/m^2. At the ultimate state significant damage is seen is seen at the connection between the slab and longitudinal beams (Figure 5.18 b). Noticeable damage appears transversally around the middle of the vault (Figure 5.18 c).

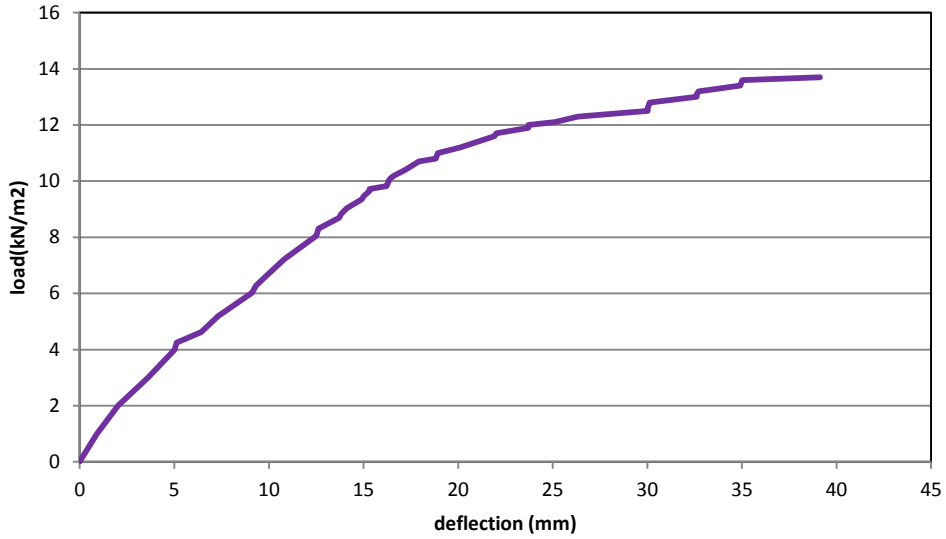

(a)

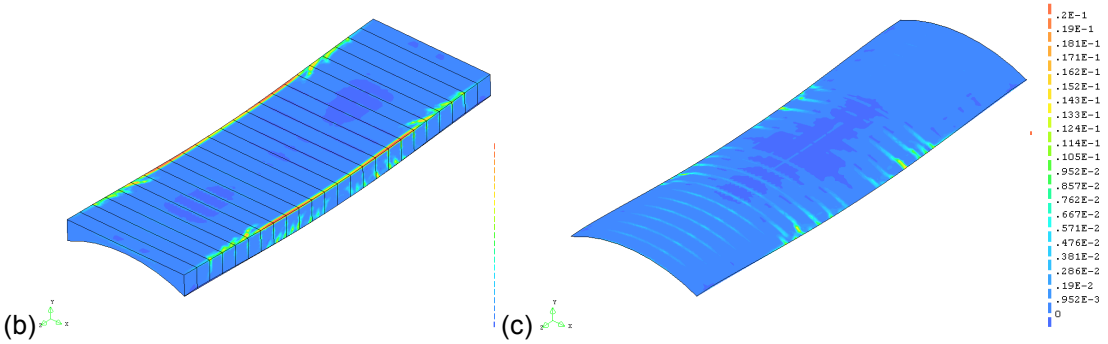

Figure 5.18 –1st model of the lower vault (c=0.4 MPa) (a) load-deflection curve as a relationship between the live load applied and the deflection at the centre of the vault, and (b-c) principal tensile strain distribution at the ultimate condition, 2nd model.

From more conservative (and possibly more realistic) viewpoint, the ultimate capacity of the cases of cohesion equal to 0.1 MPa is also studied. Both 1st and 2nd models are analysed. As for the 1st model, the maximum obtained live load capacity is equal to 10.4 kN/m^2. The corresponding deflection at the centre of the vault is 113.2 mm (Figure 5.19). Damage starts to propagate from the connections between the steel profiles and the vault. This damage develops till the end of the analysis (Figure 5.20). At the ultimate state, it would indicate the failure of the vault. When the same safety factors as the previous analysis are considered, the resulting acceptable load capacity is 4.3 KN/m^2. As for the 2nd model, sliding starts under self-weight. Correspondingly, transversal damage across the middle of the intrados

of the vault also appears. The maximum load is 13.2 kN/m^2 and the corresponding displacement is 82.5 mm (Figure 5.19). At the ultimate state, damage also appears in the middle of the longitudinal masonry walls (Figure 5.21). Significant damage is seen at the connection between the slab and longitudinal beams. Noticeable damage appears transversally around the middle of the intrados of the vault. When the safety factors over the loads and material properties are considered, the maximum acceptable live load is equal to 5.6 kN/m^2. In all the cases, the steel yield limit is reached at the end and mid-span sections of the steel profiles.

It must be noted that this load has been obtained assuming that the vaults and the steel beams can work together, according to the frictional laws adopted. However, since there is no experimental evidence on the combined action of steel profiles and vaults, from an engineering point of view it may be preferable to ignore this combined work and assume conservatively that all the load is resisted by the steel profiles. Under this assumption, the resulting capacity is significantly smaller than that predicted by the FEM analyses. Accepting this conservative approach requires an appropriate strengthening solution to grant the viability of the new uses foreseen for the building.

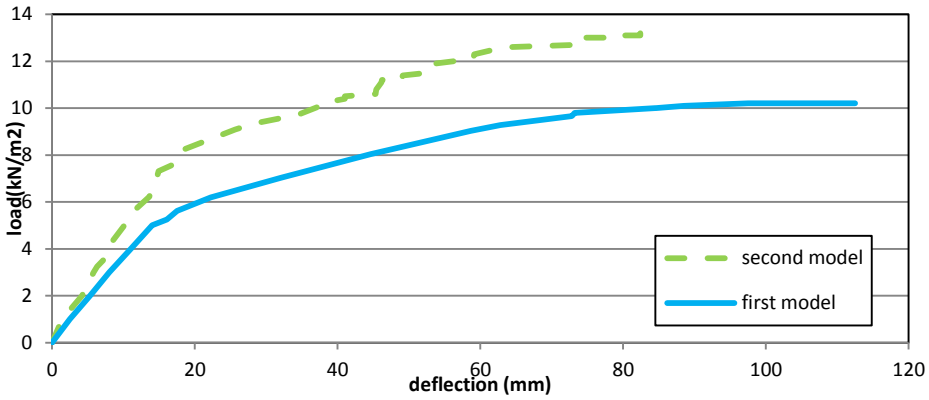

Figure 5.19 – Load-deflection curves as a relationship between deflection at the centre of the vault and applied uniform live load.

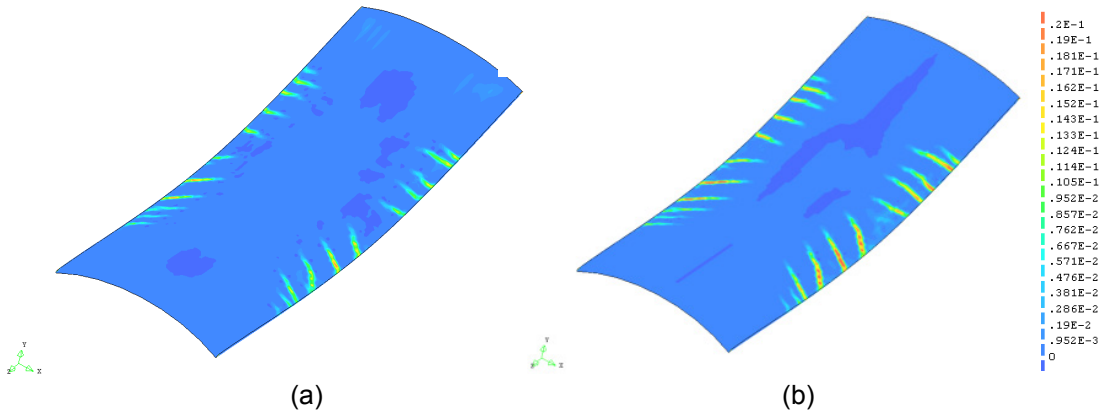

(a) (b)

Figure 5.20 – Deformation (amplified) and principal tensile strain distribution close to the ultimate condition. 1st model of the lower vault (c=0.1 MPa), vault extrados (a) and intrados (b).

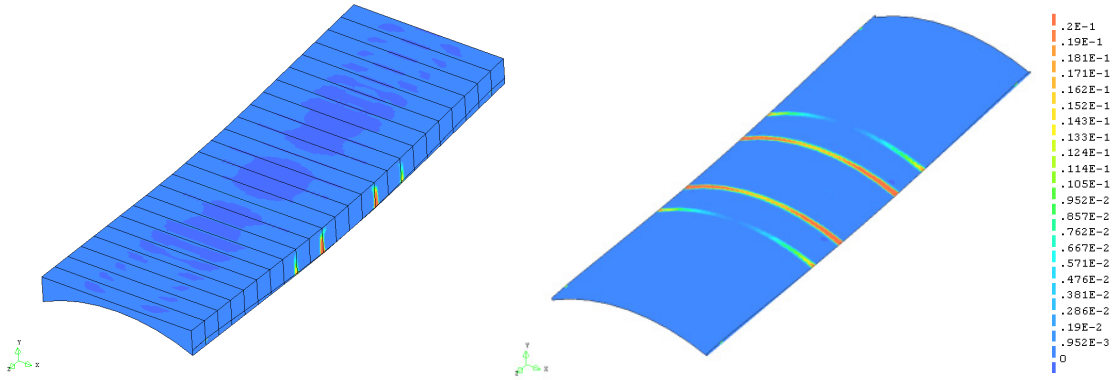

(a) (b)

Figure 5.21 – Principal tensile strain distribution close to the ultimate condition. 2nd model of the lower vault (c=0.1 MPa), entire model (a) and vault intrados (b).

5.4.2 Upper vault

5.4.2.1 Description of the model

The model prepared for the upper vault includes the vault with the steel profiles and the masonry arch (Figure 5.22). The steel framework and the masonry arches are modelled with 3-node beam elements. The number of nodes is 12,697 and that of elements is 5,044. The same material and interface properties described in Section 5.4.1.1 are assumed. As in the previous case, the Coulomb friction model is adopted to model the contact between the T-steel profiles and the vault. The model is restrained by pin supports at the ends of the T-profiles. A distributed uniform live load is applied all over the vault and is increased till failure is observed.

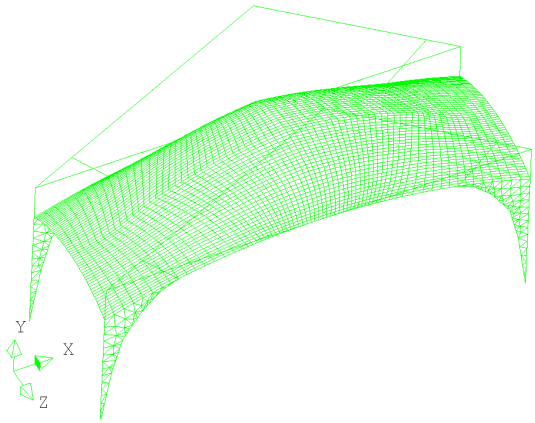

Figure 5.22 – FEM model of the upper vault.

5.4.2.2 Assessment of the capacity under a uniform live load

Damage in the vault starts to appear longitudinally both in the intrados and the extrados at a load of 4.5 kN/m^2. In the extrados, no other damaged regions are observed (Figure 5.23). The end of the analysis is reached for a maximum load of 9.4 kN/m^2. The displacement at the centre of the vault at ultimate load is

8.7 mm. When the safety factors over the loads and materials are considered, the resulting maximum live load is equal to 2.5 kN/m^2.

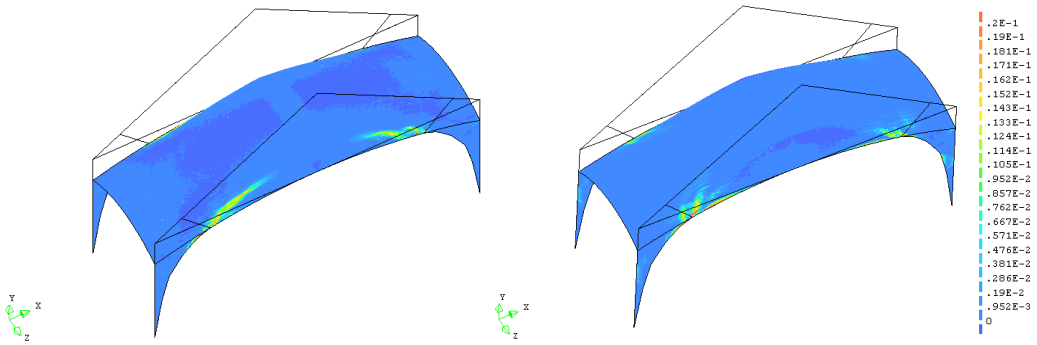

(a) (b)

Figure 5.23 – Principal tensile strain distribution close to the ultimate condition. The upper vault, vault extrados (a) and intrados (b).

5.4.3 Typical bay

5.4.3.1 Model description

The seismic behaviour of a typical bay is herein studied. The numerical model is prepared by adding the walls to the 2nd model (Figure 5.24). The lower portion of the structure including the Lower vault is not considered in this model. Since the lower part includes massive masonry piers, it is considered that it is laterally much stiffer than the upper part. Therefore, fixed constraints are applied at the bottom of the walls. Transversal movement of the bay is restrained since there are adjacent bays on both sides. The walls are modelled with 8-node quadrilateral and 6-node triangular curved shell elements. The number of nodes is 31980 and that of elements is 8820. Pushover analysis is carried out by applying horizontal loads proportional to masses of the model. The horizontal loads are increased till the analysis is stopped due to failure.

It has to be mentioned that to calibrate the seismic capacity more properly, the other parts of the building (entrance, dome and back area) should have to be included. Those parts would help to hold the lateral movement of the central area (typical bays). However, a simplified analysis involving only the typical bay is conducted as a first approach to the study of the seismic capacity of the central area of the building.

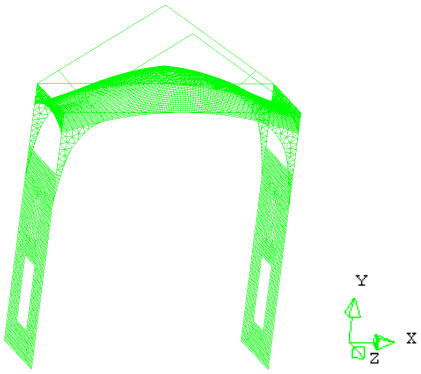

Figure 5.24 – FEM model of a typical bay.

5.4.3.2 Seismic assessment (pushover analysis)

The analysis shows the first appearing damage at the corners of the vault and the connection between the vault and steel profiles at a load of 0.075g (Figure 5.25 a). At the ultimate state (0.095g), in addition to this damage, the failure of part of the vault close to the walls is observed (Figure 5.25 b). Longitudinal cracking on the vault is also observed. The horizontal displacement at centre of the vault is 36.6 mm. The ultimate acceleration obtained from the pushover analysis is rather low. However, as mentioned above, the other parts of the building (entrance, dome and back area) are not included in this model. If they were included, a higher seismic capacity would be expected due to their retaining effect.

(a)

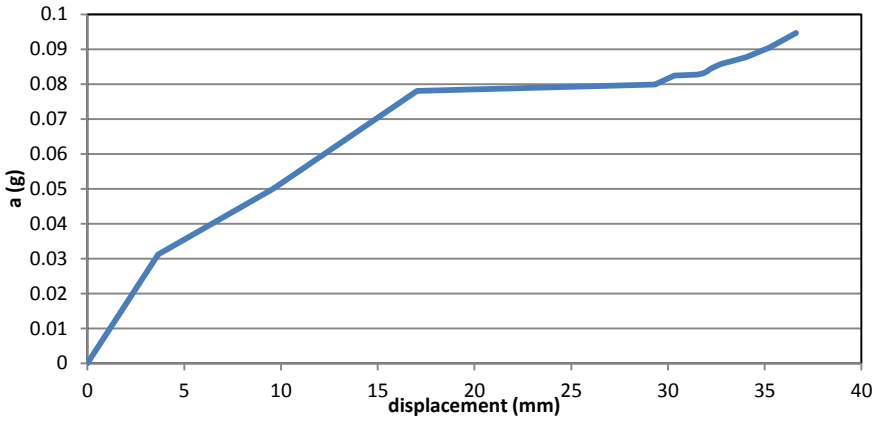

(b)

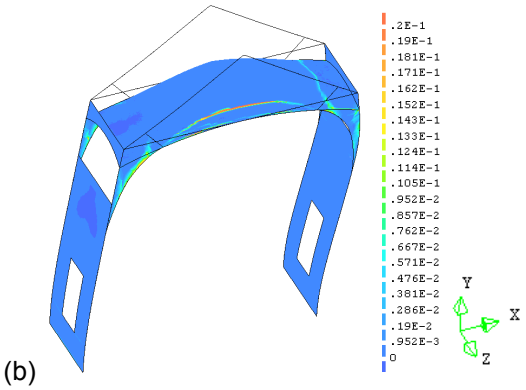

Figure 5.25 - (a) Acceleration-displacement curves at the centre of the vault and (b) ultimate principal tensile strain distributions.

5.5 Structural analysis of the vaults of the administration building

5.5.1 Introduction

The vaults identified as Small, Intermediate and Large ones in the Administration building are studied. Their location and configuration, including the dimensions of the vaults and steel profiles have been specified in Section 5.2.2.2. The models prepared represent the vault, walls, slab, wallets and steel profiles (Figure 5.26). The thickness of the slab and wallets is 10 cm. The locations of the wallets are presented in Figure 5.26 b, d, f. They are studied individually. For the Small vault, firstly comparison of the behaviour between the real structures and FEM models is done by taking advantage of the results from the dynamic identification test discussed in Section 5.4.3. Then capacity assessment under a uniform live load is conducted. For the Intermediate vault, first comparison of the behaviour between the real structures and FEM models is made by referring to the results from the static loading and dynamic identification test. Then capacity assessment under a uniform live load is carried out. For the Large vault, first, capacity assessment under a uniform live load is conducted. Then a parametric study on the influence of existing structural elements (slab, wallets and steel profiles) is done.

The same material properties as in Mercé are assumed for the brick masonry and steel profiles. In this model, the Coulomb friction model is considered for the masonry-masonry contacts between slab and wallets and also between the wallets and the vault. The discussion on frictional behaviour of masonry has been made in Section 2.1.2.1 and its simulation in numerical analysis has been discussed in Section 3.1.6. In the lack of more specific evidence, the values used for numerical analysis by Lourenço and Rots (1997) are taken advantage of. Therefore a friction angle of 36.9^{o} (equal to 0.75 by $\tan\phi$) is adopted. The values adopted for the normal and shear linear stiffness are respectively of 100 MPa/mm and 50 MPa/mm.

Taking advantage of the vaults' symmetry, only one-fourth of them are modelled by adopting appropriate boundary conditions. As for Mercé pavilion, the walls, slabs. vaults and wallets are modelled with curved 8-node quadrilateral and 6-node triangular elements. The steel profiles are modelled with 2-node straight beam elements. Interface element is 2x2 node line-shell elements. For the Small vault model, the number of nodes is12352 and that of elements is 13320 (Figure 5.26 a, b). For the Intermediate vault model, number of nodes is18828 and that of elements is 19688 (Figure 5.26 c, d). For the Large vault, number of nodes 4937 and that of elements is 5582 (Figure 5.26e, f). The original model of the Large vault was prepared by Arias (2013).

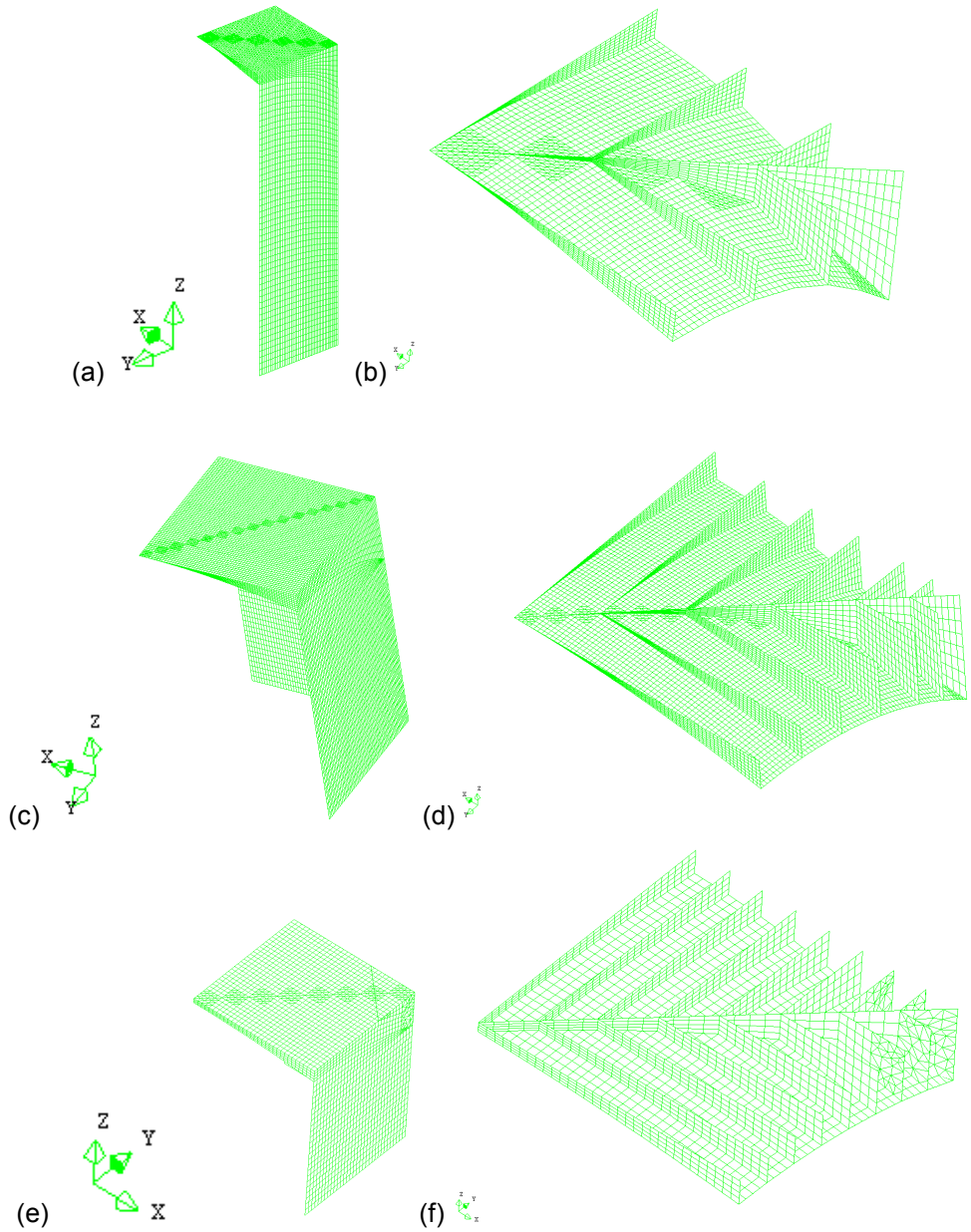

Figure 5.26 – FEM model of vaults in the Administration building: (a,b) model of small vault, (c,d) model of intermediate vault and (e,f) model of large vault.

5.5.2 Small vault

5.5.2.1 Comparison with experiments

Eigenvalues obtained from the experiment discussed in Section 5.3.2 is compared with those from FEM analysis. Good agreement is observed between them (Table 5.6).The error is within 1.5-2% except for the 4th mode. Consequently it is considered that this model can be used for capacity assessment without requiring any modification.

Table 5.6 – Eigenvalues comparison between experiments and FEM.

Mode	1st	2nd	3rd	4th	5th	6th	7th	8th
Experiment (Hz)	23.91	28.32	32.44	37.45	41.41	44.35	47.49	50.46
FEM (Hz)	24.49	-	31.99	39.99	-	43.72	47.09	-
Error (%)	-2.36	-	1.40	-6.34	-	1.45	0.85	-

5.5.2.2 Assessment of the capacity under a uniform live load

A uniform live load is applied on the entre slab and increased till failure. Sliding of the slab occurs at a load of 36 kN/m^2. The ultimate deflection is 9.9 mm at the centre of the vault and 39.0 kN/m^2 (Figure 5.27). When the safety factors (for dead load, live load and materail properties) are considered, the load capacity is equal to 23.9 kN/m^2. At the ultimate state, failure is observed along the connection between slab and walls, between vault and walls, and also around the centre of the vault (Figure 5.28). The distribution pattern of the damage is asymmetric along the diagonal wallets. This lack of symmetry is due to the existence of two steel profiles of IPN 80 only in the longitudinal direction. Higher damage is seen on the side where the steel profiles are not installed.

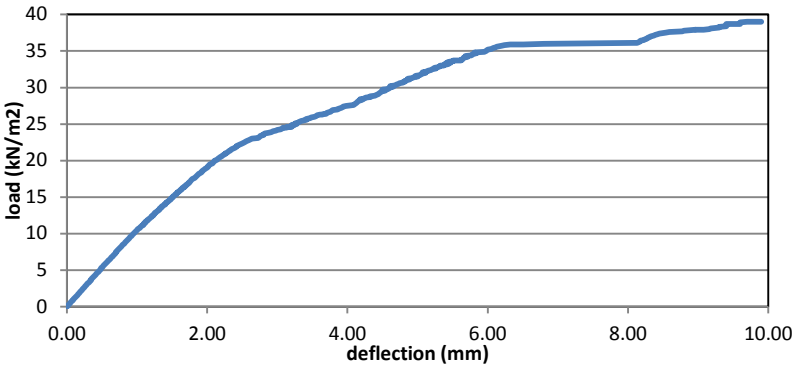

Figure 5.27 – Load-deflection curves, Small vault, at the centre of the vault.

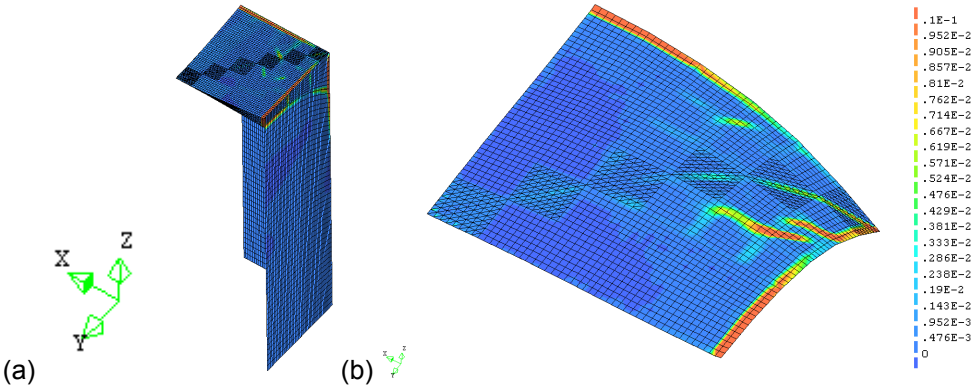

Figure 5.28 – Ultimate principal tensile strain distributions, Small vault: (a) the entire model and (b) vault of the entire model.

5.5.3 Intermediate vault

5.5.3.1 Comparison with experiments

5.5.3.1.1 Dynamic identification

Eigenvalues obtained from the above-discussed experiment (Section 5.3.2) are compared with those from FEM analysis. A good agreement is observed with an error of about 1% (Table 5.7).

Table 5.7 – Eigenvalues comparison between experiments and FEM.

Mode	1st	2nd	3rd
Experiment (Hz)	16.99	24.238	38.802
FEM (Hz)	16.82	24.01	38.37
Error (%)	1.01	0.95	1.13

5.5.3.1.2 Static loading test

Using the same model, the static loading test discussed in Section 5.3.2 is simulated. The deflection-loading relation at the ¼ of the span of the vault is presented. It is close to the experiment (Figure 5.29). From the two comparisons, it is considered that this model can be used for capacity assessment without any modification.

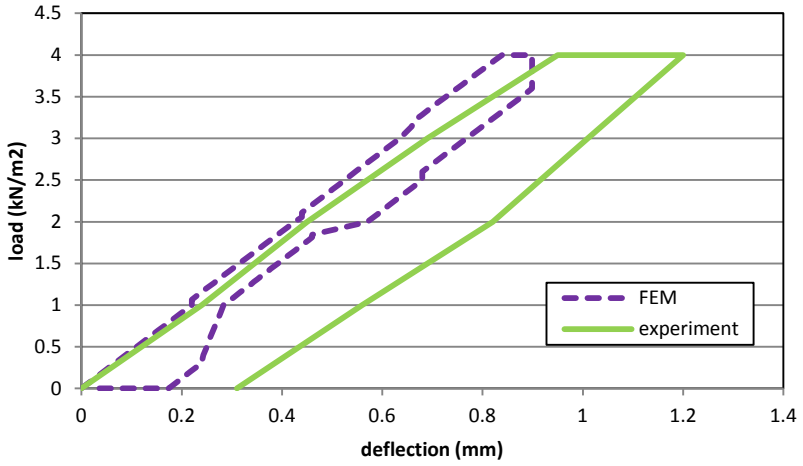

Figure 5.29 – Comparison of load-deflection relation, at ¼ of the span of the vault.

5.5.3.2 Assessment of the capacity under a uniform live load

Sliding of the slab occurs at the load of 6.5 kN/m^2. The ultimate deflection is 12.5 mm and the load capacity is 9.73 kN/m^2 (Figure 5.30). Whith the safety factor, the maximum acceptable live load is equal to 4.73 kN/m^2. At the ultimate state failure is observed at the connection between slab and walls and also around the centre of the vault (Figure 5.31). The damage distribution is not symmetric along the diagonal wallets because the thickness of the walls is different (35 and 70 cm). High concentration of damage in the vault appears on the side close to the thinner wall. Unlike in the case of the Small vault, not so much damage is observed in the connections between the vault and walls.

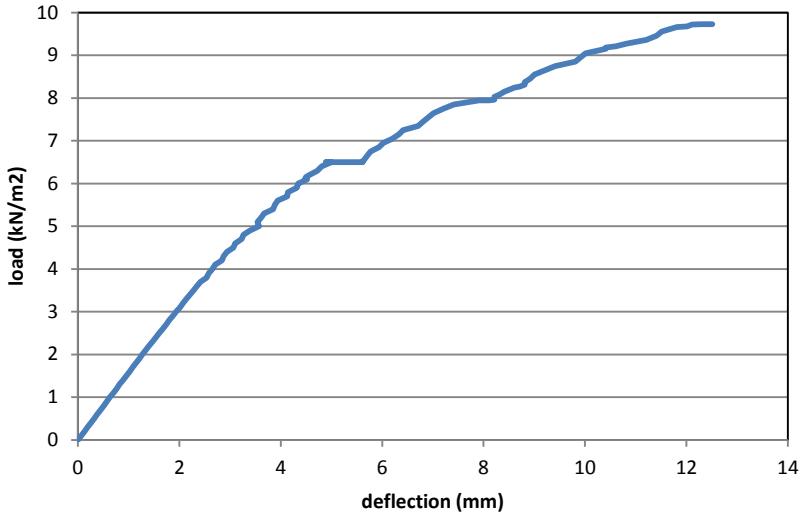

Figure 5.30 –Load-deflection curve at the centre of the vault.

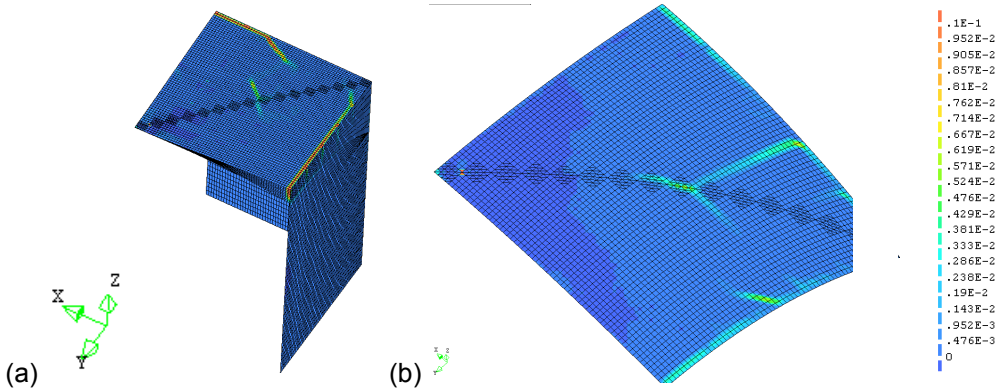

Figure 5.31 –Principal tensile strain distributions, Intermediate vault: (a) entire model and (b) vault of the entire model.

5.5.5 Large vault

5.5.5.1 Assessment of the capacity under a uniform live load

As for the large vault, first damage appears at connections between the vault and central wallets at a load of 3.03 kN/m^2. This corresponds to change of the stiffness in the load-deflection curve (Figure 5.32). Sliding of the slab also occurs at a load of 7.65 kN/m^2. After this, extensive damage is observed over the entire vault. The ultimate deflection is 46.5 mm at the centre of the vault and the ultimate load capacity is 8.97 kN/m^2. At the ultimate state, a concentration of damage at the connection between slab and walls and also around the centre of the vault is observed (Figure 5.33). It is observed that both intrados and extrados of the vault are sufficiently damaged unlike the small nor intermediate vault. It is probably due to the confinement of the steel profiles as discussed in Section 5.2.2.2.3. The steel confinement allows the vault and the other masonry structural elements (wallets, slab and walls) to work together more effectively than steel profiles just horizontally placed. When the same safety factors are considered, the maximum acceptable live load is equal to 4.83 kN/m^2.

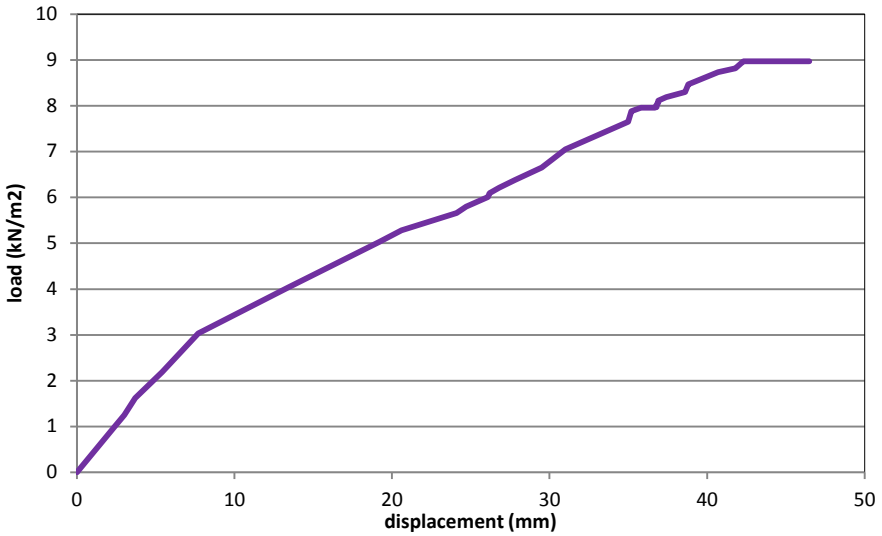

Figure 5.32 – Load-deflection curve, Large vault, at the centre of the vault.

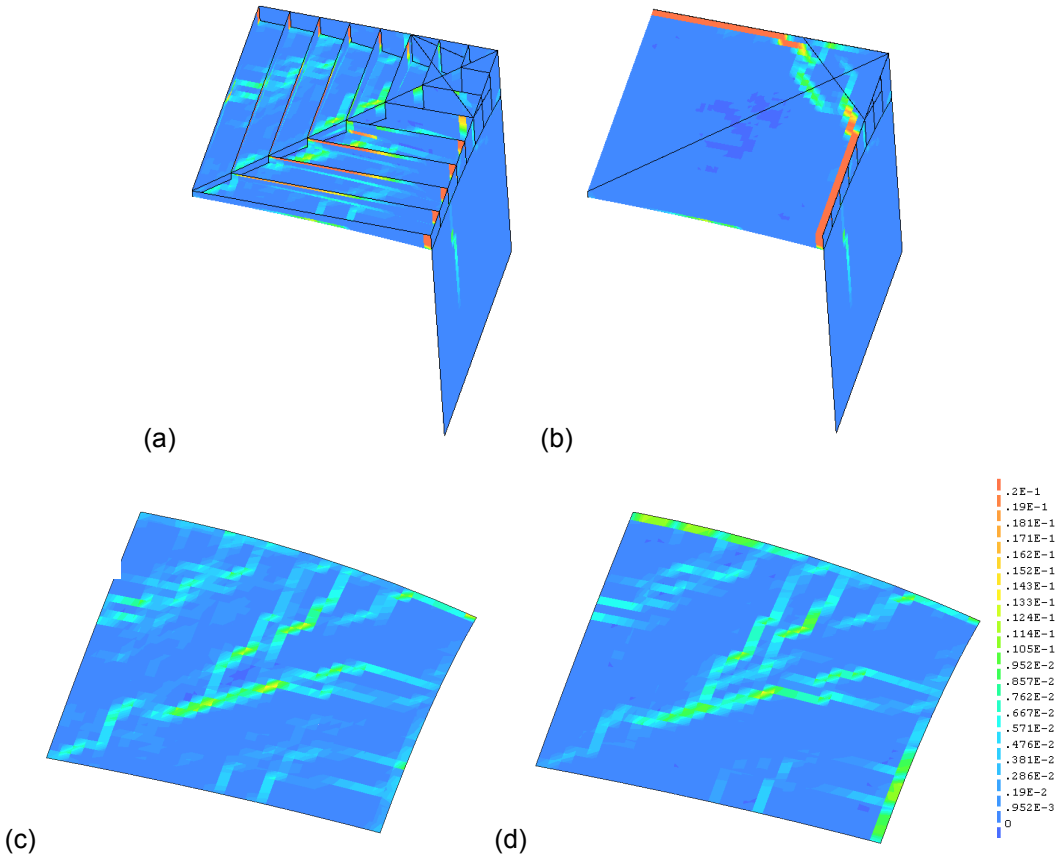

Figure 5.33 – Principal tensile strain distributions, large vault close to the ultimate condition), (a) the entire model without the slab (b) the entire model, (c) vault of the entire model (extrados) and (d) vault (intrados).

Parametric study is carried out on different configurations of large vault models. Three models are compared (model a-c). Model_a is the same one used in the above-discussed capacity assessment. It is

composed of the vault, walls, steel profiles, wallets and slab. Model b is prepared by removing the slab from model a, Model c is made by removing the slab and wallets from model_a.

Comparison of the load-deflection curves is presented in Figure 5.34. As expected, removal of the structural elements decreases the load capacity and stiffness. Removal of the slab (from model_a to model_b) decreases the capacity around by 33.3 %. Different pattern of damage distribution is seen from model_a (Figure 5.34, Figure 5.35 a-b). Model_a shows damage over the entire vault as discussed above while model_b shows damage propagated from the connection between the vault and walls. Removal of wallets (from models_b to model_c) decreases the capacity by 50 %. However, model_b and _c show similar damage patterns (damage propagated from the connections between the vault and walls) in spite of the difference of damage intensity (Figure 5.35). Considering the difference of the damage distribution patterns, the inclusion of the slab has particularly significant influence on the behaviour of this structure.

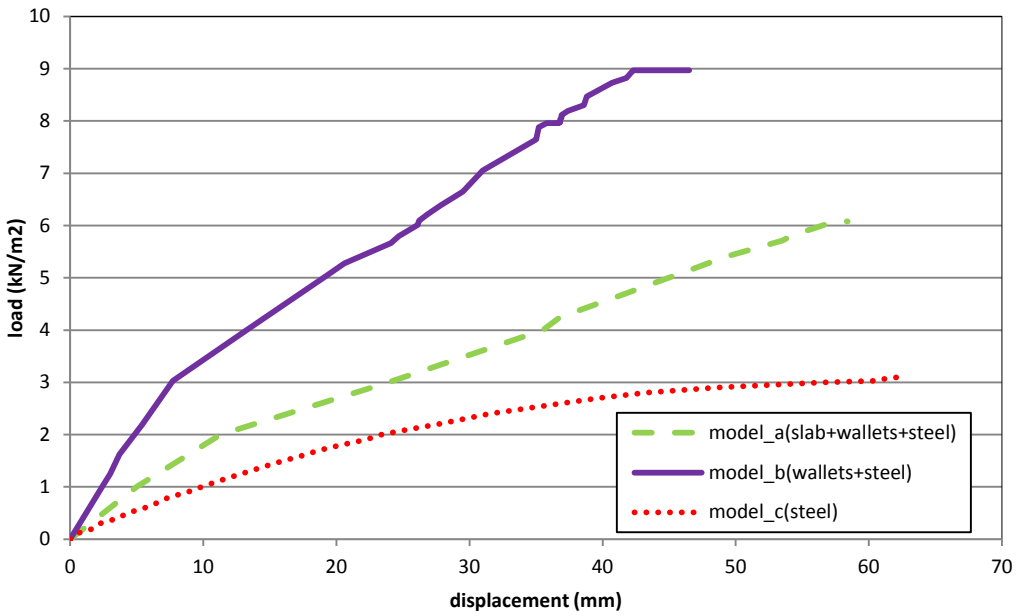

Figure 5.34 – Load-deflection curves, Large vault, at the centre of the vault.

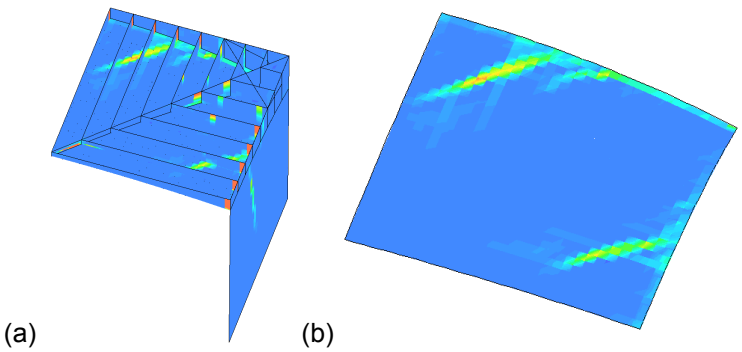

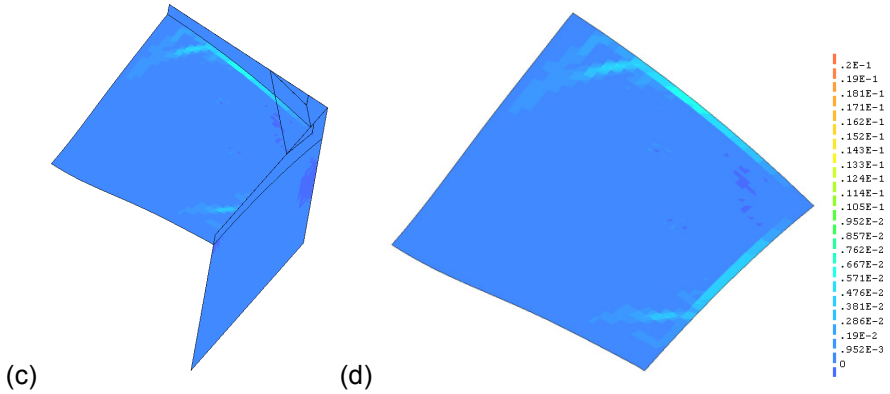

Figure 5.35 – Ultimate principal tensile strain distributions (a,b) model_b and (c,d) model_c

5.6 Discussions

Vaults in Mercé Pavilion and Administration building of Hospital Sant Pau have been studied. In this chapter, as abbreviation, only the name of the pavilion has been used to indicate it: e.g Mercè is used instead of Ntra. Sra. De la Mercé pavilion. As for the Merce, the single-curvature vault has been named Lower vault and the double-curvature vault has been named Upper vault in accordance with their location. As for the Administration building, three double-curvature vaults located in the basement floor have been studied. According to their dimension, they have been named: Small, Intermediate and Large vault, respectively. In this section, the same denotation is used. In Merce, steel profiles are located both in vertically and horizontally. While the load bearing walls do not resist loads, the steel members support the loads. Regarding the Administration building, on the other hand, steel profiles are located principally in horizontal direction and vaults are supported on load-bearing walls.

5.6.1 In-situ and laboratory tests

Different tests have been carried out on two pavilions, including an in-situ penetrometer test on mortars, a laboratory compression test on bricks, static loading tests and dynamic identification tests. The values of mechanical properties of the FEM models have been determined on the basis of these material tests. A static loading test was carried out on Sant Rafael Pavilion, which has a quasi-equal structural configuration to Mercé pavilion. In the Administration building, static loading and dynamic identification tests were conducted on the two selected vaults with different span length. A comparison of behaviour has been made between the response of the FEM models and that of the real structure, taking advantage of these experiments. In each case, the FEM models have shown good agreement with the results obtained from the static loading and/or dynamic identification tests.

5.6.2 Behaviour of the vaults in Mercé Pavilion under a uniform live load

For the Lower vault, a model has been prepared representing the vault and the existing structural elements (wallets and top slab) over the vaults. Uniform live load has been applied and gradually increased until simulating the failure.

At the ultimate state significant damage is seen at the connection between the slab and longitudinal beams. Sereious damage also has appeared transversally around the middle of the vault. This damage has been identified both in intrados and extrados, as has indicated failure of the vault. The estimated ultimate ultimate load capacity has been 13.7 kN/m^2 . A second analysis has been carried out with applied conventional safety factors over the dead load (1.35) and over the live load (1.5) and also with reduced values of the material properties (with factors of 2.5 and 1.15 applied respectively over masonry and steel). When these safety factors have been considered, the maximum acceptable live load is 9.1 kN/m^2. It must be noted that this load has been obtained assuming that the vaults and the steel beems can work together, as a composte structure, in the longitudinal direction. When it is assumed that the vaults cannot work in this direction, so that the steel profiles are the only resisting element, the resulting load capacity is even lower than that observed in the FEM analysis. From more conservative and realistic viewpoint, the ultimate capacity of the cases of cohesion equal to 0.1 MPa is also studied. As for the 1st model, the maximum obtained live load capacity is equal to 10.4 kN/m^2. At the ultimate state, damage propagates from the connections between the steel profiles and the vault, as would indicate collapse of the vault. As for the 2nd model, the maximum load is 13.2 kN/m^2. At the ultimate state, damage appears in the middle of the longitudinal masonry walls, at the connection between the slab and longitudinal beams and transversally around the middle of the intrados of the vault. When the safety factors over the loads and material properties are considered, the maximum acceptable live load is equal to 4.3 kN/m2 (1st model) 5.6 kN/m^2 (2nd model). In all the FEM analyses of the Lower vault, the steel yield limit is reached at the end and mid-span sections of the steel profiles.

The Upper vault, has been modelled with the steel framework and the masonry upper arches on which it is supported. The ultimate load capacity has been 9.4 kN/m^2. At the ultimate state, damage in the extrados of the vault has appeared in the longitudinal direction. In the intrados of the vault, similar longitudinal damage, damage has been observed. When the safety factor is considered for the live load, the maximum acceptable live load is 2.5 kN/m^2. It must be remarked that this estimation of the maximum capacity, for both the lower and upper vaults, is only based on the strength. The maximum capacity can be also limited by the local strength of the connections between the steel members, as has not been modelled into detail in the analyses.

5.6.3 Seismic behaviour of a typical bay of Mercé

Seismic assessment has been conducted on a typical bay by pushover analysis; lateral force proportional to the masses of the model has been applied. The lower portion of the structure including

the Lower vault is not considered in this model because it is considered much stiffer that the upper part. At the ultimate state, in addition to damage at the corners of the vault, the failure of part of the vault close to the walls is observed. Longitudinal cracking on the vault is also observed. The model has attained a lateral force corresponding to an acceleration of 0.095g with an ultimate displacement of 36.6 mm at the centre of the vault. However, it has to be mentioned that to calibrate seismic capacity more properly, the other bodies of the building should also be included. The inclusion of the end bodies would help to retain the lateral movement of the central area including the typical bay. Consequently, a higher capacity would be expected.

5.6.4 Behaviour of thre vaults in Administration building under uniform live load

As for Mercé pavilion, the capacity under distributed live loads has been assessed for a set of selected vaults designed as Small, Intermediate and Large vaults. The maximum live load obtained for the Small vault has been 39.0 kN/m^2: that one obtained for the Intermediate vault 9.73 kN/m^2 and that of the large vault 8.97 kN/m^2. When the safety factor is considered for the live load, the maximum acceptable live load is 23.9 kN/m^2 , 4.73 kN/m^2 and 4.83 kN/m^2. These capacities have been calculated by considering that the existing masonry wallets and the upper slab contribute to the strength of the vault. Due to their smaller dimensions, the Small vault shows a much higher capacity than the other two vaults. For the Small vault, damage at failure is seen along the connection between the slab and the walls and also around the centre of the vault. The damage distribution has been asymmetric along the diagonal wallet due to the existence of steel profiles only in the longitudinal direction. For the Intermediate vault, at the ultimate state, damage has been observed also at the connection between slab and walls and around the centre of the vault. The ultimate damage distribution pattern is asymmetric along the diagonal wallet at the ultimate state due to different thickness of the walls. Higher damage appears on the side close to the thin wall. The Large vault model has shown high concentration of damage along the connection between the diagonal wallets and the vault at the ultimate state. For this vault damage has appeared symmetrically distributed along the diagonal wallets. The Small vault has shown more extensive damage in the vault than the Intermediate vault due to its smaller dimension. On the other hand, the Large vault has shown more distributed damage on the vault than the Intermediate vault due to its larger number of wallets. Wallets have permit more equally distribution of loads to the vault. It is supposed that the vault of Small vault and Large vault reaches failure. Number of wallets and dimension of a vault has shown a noticeable influence on the behaviour.

The intrados of vaults in Hospital Sant Pau are decorated with tiles. The deflection of a vault may cause detachment of these tiles. However, in the previous research, no criteria have been discussed regarding at which load tile detachment can be assumed to start. As a tentative approach, a criterion specified by the Spanish recommendations (PIET 70 1971) is considered for the allowable maximum deflection of a floor under the serviceability limit state. It is adopted to the three vaults studied in Administration building. The corresponding allowable load is equal to 38.2 kN/m^2 for small vault, 8.60 kN/m^2 for

intermediate vault and 1.50 kN/m^2 for large vault. For the small and intermediate vault, the observed value is very close to the ultimate load capacity presented above. However this analysis is a provisional one and further research will be necessary for more accurate estimation of the capacity under this condition.

5.6.5 Influence of different structural elements on the vault capacity

A parametric study has been carried out on the Large vault model so as to examine the influence of the existing structural elements of the vault. Three different models have been created and compared by removing the slab, wallets and steel profiles. As expected, the removal of these structural elements has significantly decreased the load capacity and stiffness. Removal of the slab has decreased the capacity about 50 %. The removal of ribs has had smaller influence than the removal of the slab. As should be expected, the removal of the steel profiles has a dramatic influence on the capacity of the vault. The models with structural elements removed have shown similar damage patterns.

6. CASE STUDY 3: SAN MARCO CHURCH

6.1 Introduction

This chapter focuses on the seismic analyses of a historical masonry church. The study comprises two purposes. The first purpose is to identify and simulate the mechanisms that led to the damaged condition of the church by different seismic assessment tools. The second one is to examine the influence of different parameters and the efficacy of possible interventions.

The study is composed of three parts. The first part discusses the capability of the available methods to represent the observed seismic performance during the real earthquake. Different seismic assessment tools including pushover analysis and nonlinear dynamic analysis are applied to simulate the current damage condition, crack patterns and partial collapse mechanisms. The second part consists of the studies of the influence of different parameters by pushover analysis. Five different studies are carried out. Firstly, a parametric study is carried out on the compressive strength, the tensile strength, the Young's modulus and the tensile fracture energy of masonry. Secondly, combinations of low mechanical parameters of masonry are proposed and compared. Thirdly, the influence of a weak interlocking between bay, façade and transept is studied. Fourthly different lateral force distribution patterns are compared. Fifthly, models composed of shell elements or solid elements are compared. In the third part, possible strengthening proposals are made, considering findings gained through the above-mentioned second part. The performance of strengthened structures is evaluated by pushover analysis as in the second part.

The chosen case study is San Marco church, located in the historical centre of L'Aquila, Italy. The structure was severly damaged by the Abruzzo earthquake of 6th April 2009. After having conducted the post-earthquake emergency phases for building protection, the structure is currently under restoration.

6.2 Description of the building

6.2.1 History of the building

Comprehensive information on the building has been presented by Magi (2009), Silva et al. (2010) and Silva et al. (2011). Based on them, concise description of the history of San Marco church is presented with focus on relevant events affecting the structure.

San Marco church was one of the first churches built in L'Aquila in the latter half of the 13th century. The building went through different historical events and construction phases (Figure 6.1). Medieval trace is found in the tympanum of the south portal which was built in the 14th century. The façade seems to have been built at the beginning of the 15th century. The right side of the building dates back approximately to

the 15th century. After the earthquake in 1315, partial reconstruction was conducted. The lateral chapels were built in the 16th century. On the left side there were some buildings that were demolished after the earthquake of 1703. At that time the wall of this side was rebuilt and the presbytery rearranged. In 1750 two bell towers were constructed together with the top part of the façade.

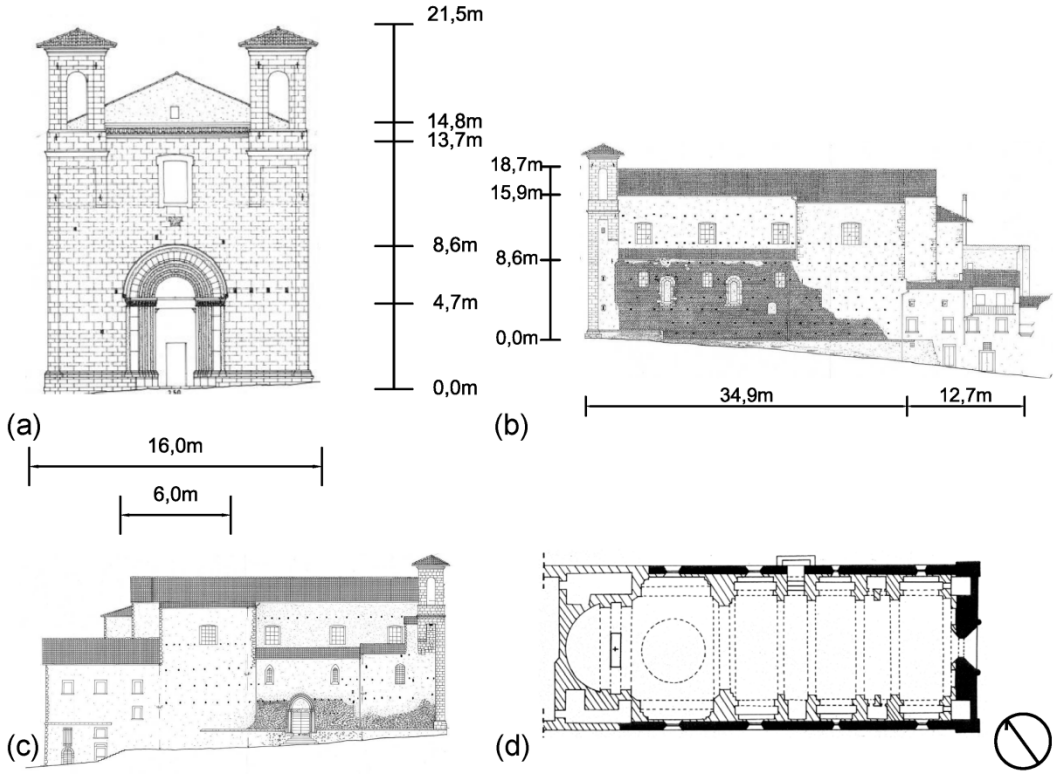

Figure 6.1 - San Marco church: (a-b-c) façade, north and south side, (d) plan (Silva et al. 2011).

The building stands in a narrow rectangular area and lays on a stone foundation. The length of the church is 41.7 m and the width is 16.0 m (Figure 6.1). The roof height is 16.7 m. The height of the two bell towers of the façade is 21.5 m. The nave is sided by three chapels at each flank. These chapels were built after the nave construction, as shown in Figure 6.1d (black parts indicate the 13th century construction). As a result, the exterior perimeter walls were not connected properly to the perpendicular walls between the chapels. This problem led to a local partial collapse of the church after the 2009 earthquake, as it will be discussed in Section 6.2.2. The nave is covered by reed vaults (Figure 6.1 d) that are supported on brick masonry arches. The lateral chapels are shielded by brick vaults. The transept area is covered by a shallow dome supported on four brick arches. The apse is roofed with a semi-dome. The dimensions of the bricks used for arches, domes and vaults are 290×150×30mm^3.

The structure underwent various interventions since the late 20th century. The main structural interventions were carried out in 1970, 2005 and 2007. The first one was rather intrusive. Two longitudinal RC beams and two transversal RC tympanums were constructed, encircling the dome

(Figure 6.2 a-b). They constitute a heavy RC box formed over the transept. The entire pre-existing timber roof was replaced with a new system with prefabricated RC beams, hollow flat bricks and steel ties (Figure 6.2 b). In 2005 the old iron ties at the top part of the bell towers were replaced with new steel ties. In 2007 carbon FRP (CFRP) strips were glued to the intrados of the arches supporting the dome (Figure 6.2 c).

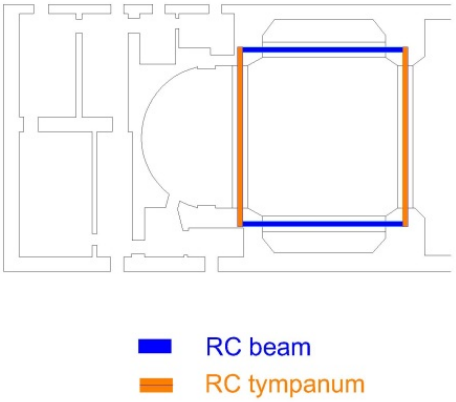

(a)

(b)

(c)

Figure 6.2 - Past interventions visible after the earthquake (Silva et al. 2011): (a) location of RC beams and tympanums, (b) RC tympanum over the transept and new roof and (c) CFRP strips installed on the intrados of arches.

6.2.2 Collapse mechanisms and damage after the 2009 earthquake

A strong earthquake hit L'Aquila early in the morning (3:32 AM, local time) on 6th of April of 2009. The magnitude was M_W = 6.3 (M_S = 6.3 and M_L = 6.2) in accordance with the Italian Institute of Geophysics and Volcanology. The epicentre was shallow (9.5 km) and very close to the historic centre of L'Aquila (approximately 7 km SW). Indirli et al. (2013) have presented a detailed discussion on the characteristics of the earthquake and an overview of damage in buildings. The earthquake was characterised by pseudo-acceleration response spectra with high peaks in the range of low periods, in spite of not very high magnitude. This may have been one of the reasons why rigid structures were subjected to strong forces (Modena et al. 2011).

Figure 6.3 a-b show the accelerograms recorded at the Spanish fort (station AQU), the closest to San Marco church. The orientations of accelerograms are EW and NS, corresponding to longitudinal (X) and transversal (Y) directions of the church. The information has been obtained from the website of ITACA (Italian Accelerometric Archive 2012). The spectra of the two records are shown in Figure 3c. They are compared with those provided by the Italian standards for the site of L'Aquila and a type B foundation, making use of the program Spettri-NTC ver 1.03 (Italian Board of Public Works 2008). Since San Marco church is a historical religious building, 10% exceeding probability in 75 years should be assumed (712 years of return period). However, the elastic spectrum with 10% exceeding probability in 50 years (475 years of return period) fits better the spectrum obtained from the accelerograms of the main shock and hence it will be considered for the analyses of this study.

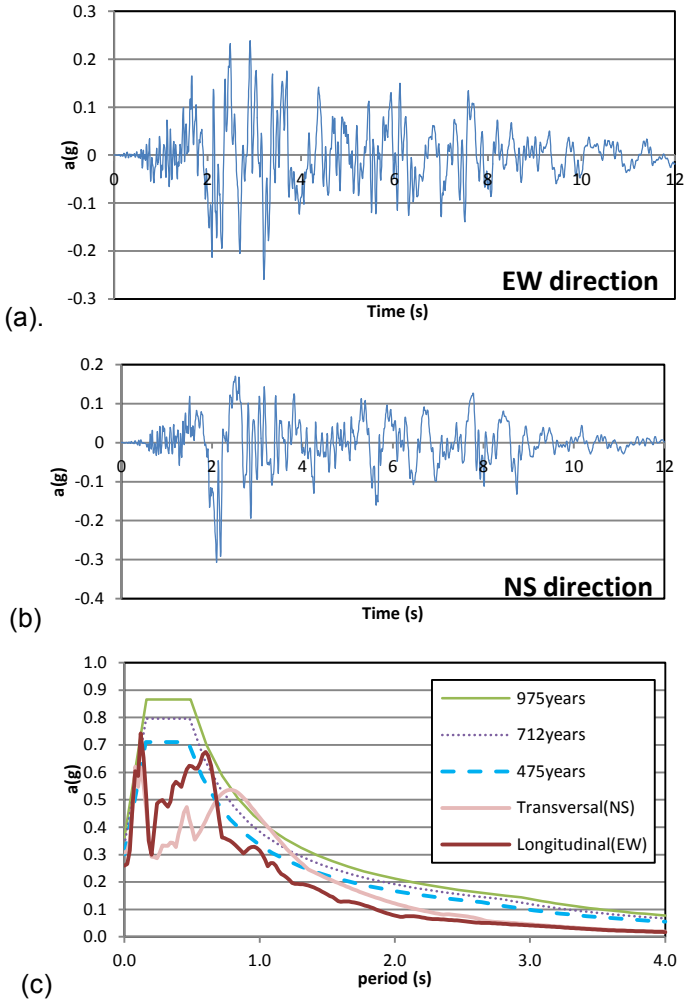

Figure 6.3 - Accelerograms of L'Aquila main shock in the EW direction (a) and NS direction (b), comparison of corresponding spectra with those provided by Italian standards for the city of L'Aquila for different return periods (c).

Today San Marco church is under restoration due to the critical state caused to it by the earthquake. The damage and cracks were surveyed after the earthquake by a careful in-situ inspection, as shown in Figure 6.4 (Magi 2009, Silva et al. 2010, Silva et al. 2010). Several types of collapse were identified.

Out-of-plane mechanisms occurred in the main façade (Figure 6.5 a), in the upper part of the main façade, in the chapel walls (Figure 6.5 b), in the transept walls and in the apse. In-plane mechanisms occurred in the façade with deep diagonal cracking across the window (Figure 6.5 c), and also in perimeter, transept and apse walls. Collapses affected the arches and reed vaults over the nave, the triumphal arch, the arches that support the dome of the transept, the semi-dome over the apse (Figure 6.5 d), the chapel vaults and the wall above them in the south side (Figure 6.5 e). The separation caused by the earthquake made it apparent the existing detachment between the buttresses and the perimeter wall (Figure 6.5 f). Severe damage was observed in the dome. The south nave wall partially collapsed together with its underneath arches and buttresses. The development of this critical mechanism is discussed in detail in Sections 6.2.2 and 6.5.3. Damage was also detected at the top of the south nave wall, in a region under the roof and next to the bell towers (Figure 6.5 g).

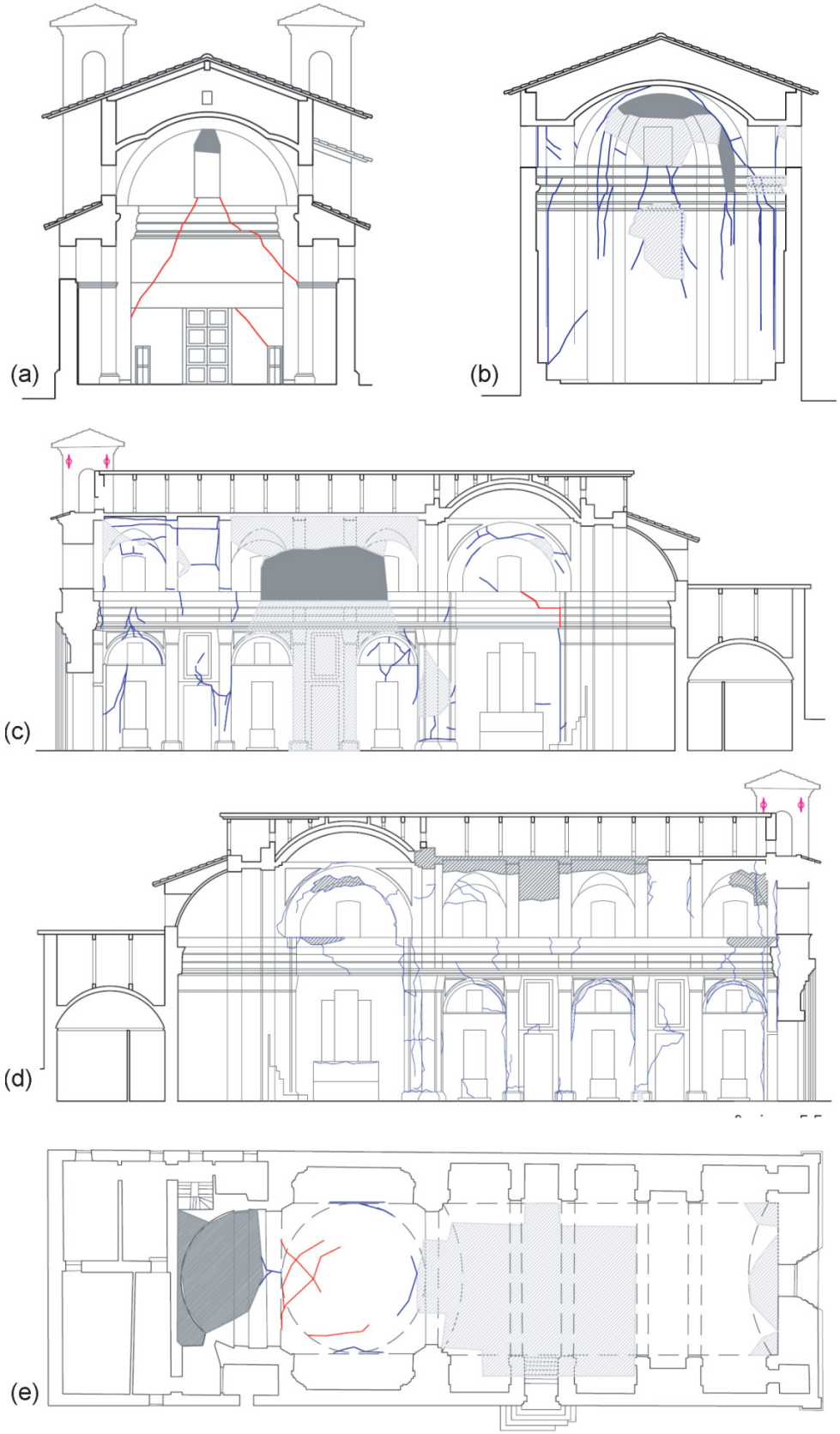

Figure 6.4 - Maps of crack patterns observed after the earthquake (Silva et al. 2011): (a) façade, (b) apse, (c-d) nave and chapels and (e) top view.

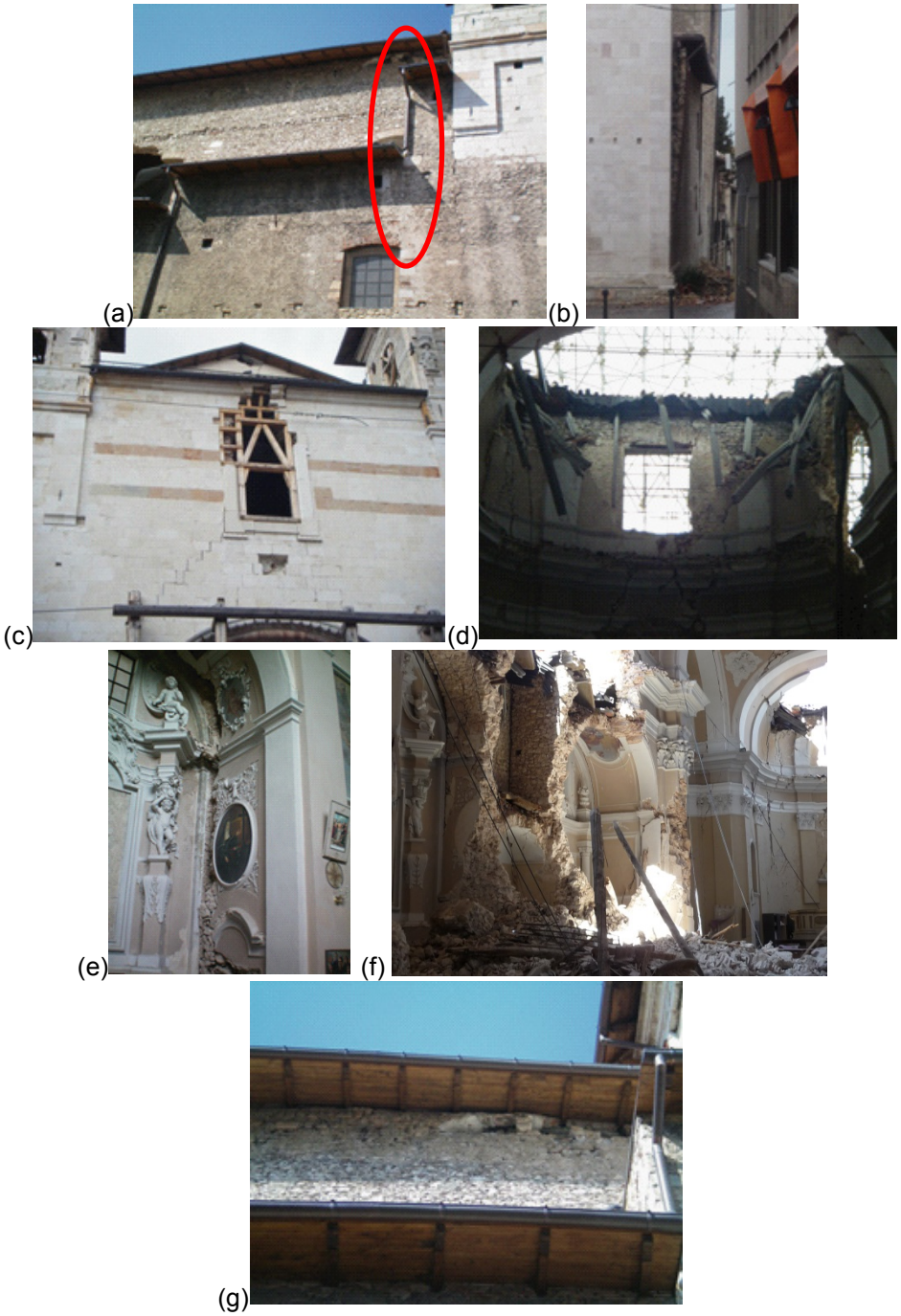

Figure 6.5 - Some mechanisms observed after the earthquake (Silva et al. 2011): (a) overturning of façade and (b) lateral chapel walls, (c) shear mechanism in the façade, (d) collapse of the semi-dome and the roof in the apse, (e) collapse of the lateral chapel and the wall above, (f) disconnection between the chapel wall and external wall and (g) damage under the roof in the south nave wall.

From a preliminary analysis of damage distribution, it emerges that partial collapses were greatly influenced by the lack of efficient connection between façade and nave walls, and among chapels and perimeter walls. This structural defect is a result of the construction history, as mentioned in Section 6.2.1. After the earthquake, it was also possible to understand that the past interventions with RC and CFRP did not improve or even worsened the seismic behaviour of the structure. The collapses of the

roof and the semi-dome in the apse, and also of the dome and the underneath arches, seem to be affected in a certain measure by the RC box introduced in 1970 over the transept. These hypotheses are supported by the FE simulations discussed in Section 6.5.2.2. CFRP strips implemented on arches did not work during the earthquake due to premature delamination resulting from their application at the intrados of the curved members.

6.3 Application of different seismic assessment tools

6.3.1 Section Introduction

In this section, the seismic assessment of San Marco church is carried out. The aim of the study is to identify and simulate the mechanisms that led to the damaged condition of the church. Kinematic limit analysis, pushover analysis and nonlinear dynamic analysis (NDA) are carried out. The results obtained through the different methods for seismic analysis (kinematic limit analysis, pushover analysis, NDA) are compared to evaluate their ability to predict the real collapse mechanisms. Both pushover analysis and NDA have been carried out using a global FE model of the church. The accelerograms of the main shock of the 6th April 2009 L'Aquila earthquake are considered for NDA. Kinematic limit analysis is carried out on representative macro-elements of the church.

The result of the different methods are compared into detail with the real evidence of damage and collapse caused by the 2009 L'Aquila earthquake on the church.

Historical research and in-situ inspection have been carried out to identify the different construction phases of the building, the geometry, the materials, the quality of the connections between the different structural elements and the possible vulnerabilities. In particular, past interventions with RC have been studied to assess their influence on the deterioration of the behaviour of the church. Lack of efficient connections among members, particularly at the intersection of the perimeter wall with the buttresses, has been carefully analysed since it affects considerably the seismic response. This first stage of the research has been useful for the preparation of the structural models for the analyses.

The damage and the partial collapses induced by the earthquake have been carefully surveyed as discussed in Section 6.2.2. The analysis of cracks has made it possible to evaluate the structural behaviour of the church during the earthquake and to identify the relevant collapse mechanisms.

6.3.2 Kinematic limit analysis

Limit analysis is one of the approaches that have been selected to study the seismic behaviour of the church. From the damage mapping of San Marco church presented in Section 6.2, it emerges that in many portions of the structure the collapse was due to the loss of equilibrium of parts behaving as rigid blocks. Applying the principle of virtual work for each chosen mechanism, it is possible to estimate the

seismic capacity in terms of maximum force (linear kinematic analysis, LKA) and ultimate displacement by evaluating finite shifts (non-linear kinematic analysis, NKKA) (Italian Ministry of Infrastructure and Transport 2009). The discussion on kinematic limit analysis has been made in Section 2.4.1.

To perform this analysis it is necessary to define the geometry, the material properties, the confidence factor and the seismic action. The geometry and the material properties of the different elements of the church were obtained from previous studies of the church of San Marco (Magi 2009, Silva et al. 2010, Silva et al. 2011). The calculation of the confidence factor, i.e. the safety coefficient taking into account the uncertainties about the properties of historical structures, was carried out as specified by the Italian Guidelines (Italian Ministry for Cultural Heritage and Activities 2011). For the structure analysed in this study the confidence factor is equal to 1.24, corresponding to a case with limited survey of materials and mechanical parameters and limited survey of foundations and foundation soil.

A detailed analysis of possible failure mechanisms has been carried out for San Marco church. For the present research, previous applications of kinematic analysis (Magi 2009, Silva et al. 2011, De Conti 2013) have been reviewed and complemented.

Figure 6.6 presents the summary of failure mechanisms considered in kinematic limit analysis with the indication of the activation coefficient α_0 The weakest mechanism is the one involving the partial overturning of the upper nave wall (Figure 6.6 a), which is activated for a coefficient α_0=0.081. Other mechanisms considered are those involving the overturning of the perimeter wall (Figure 6.6 b), the failure of the lateral buttresses and arches (Figure 6.6 c), the overturning of the entire nave wall (Figure 6.6 d), the overturning of the façade (Figure 6.6 e), the failure of the apse (Figure 6.6 f), and the in-plane failure of the façade (Figure 6.6 g). The damage and collapses experienced by the real the structure suggest that all these mechanisms were actually activated with the possible exception of those corresponding to the overturning of the nave wall (mechanism a) and the entire nave wall (mechanism d). These two mechanisms may not have occurred because of an effective connection of the walls with the façade and transept, or because of the anticipation of other mechanisms with close activation factor.

	mechanism	LKA α0 (g)	a*0(g)	Verfication	NKA Δd(m)	d*u(m)	Verfication
a) out-of-plane partial overturning of nave wall	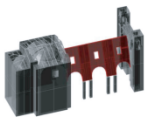	0.081	0.081	No	0.18	0.16	No
b) out-of-plane behaviour of perimeter wall	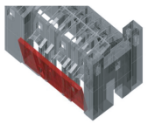	0.095	0.095	No	0.18	0.19	Yes
c) combined mechanism of arches and buttresses		0.099	0.108	No	0.19	0.17	No
d) out-of-plane overturning of whole nave wall		0.116	0.116	No	0.22	0.72	Yes
e) overturning of facade	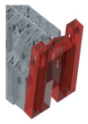	0.167	0.167	Yes	0.22	0.49	Yes
f) out-of-plane behaviour of apse		0.218	0.218	Yes	0.22	0.776	Yes
g) in-plane mechanism of facade		0.354	0.361	Yes	0.22	1.23	Yes

Figure 6.6 - Collapse mechanisms and corresponding coefficients obtained by limit analysis.

The collapse of the nave wall seems better explained by the mechanism described in Figure 6.6 c and Figure 6.7. In this case, the mechanism involves the overturning of the buttresses and the collapse of the arches supported on them. The activation coefficient α_0=0.099 has been calculated taking into account a complex mechanisms including the overturning of the buttresses and a sufficient number of hinges in the arches (Figure 6.7 d). As a result of this mechanism, the upper nave wall losses it support on the arches and detaches vertically forming the actually observed relieving arch at its upper part (Figure 6.7 a-b). This mechanism is made possible by the lack of connection between the perimeter wall and the buttresses due to the construction process, as discussed in Section 6.2.2 and shown in Figure 6.5 f. The low activation coefficient obtained (0.099) shows the likelihood of this type of failure, which is consistent with the damage and collapses observed in the lateral façades of the church. In fact, the collapse occurred because of the vertical detachment of a lower portion of the wall rather than because of its overall overturning. The overturning of the main façade is activated for a coefficient of 0.167 (Figure 6.6 e). The façade has been supposed partially connected to the orthogonal walls, according to the morphology derived from historical and on-site inspection.

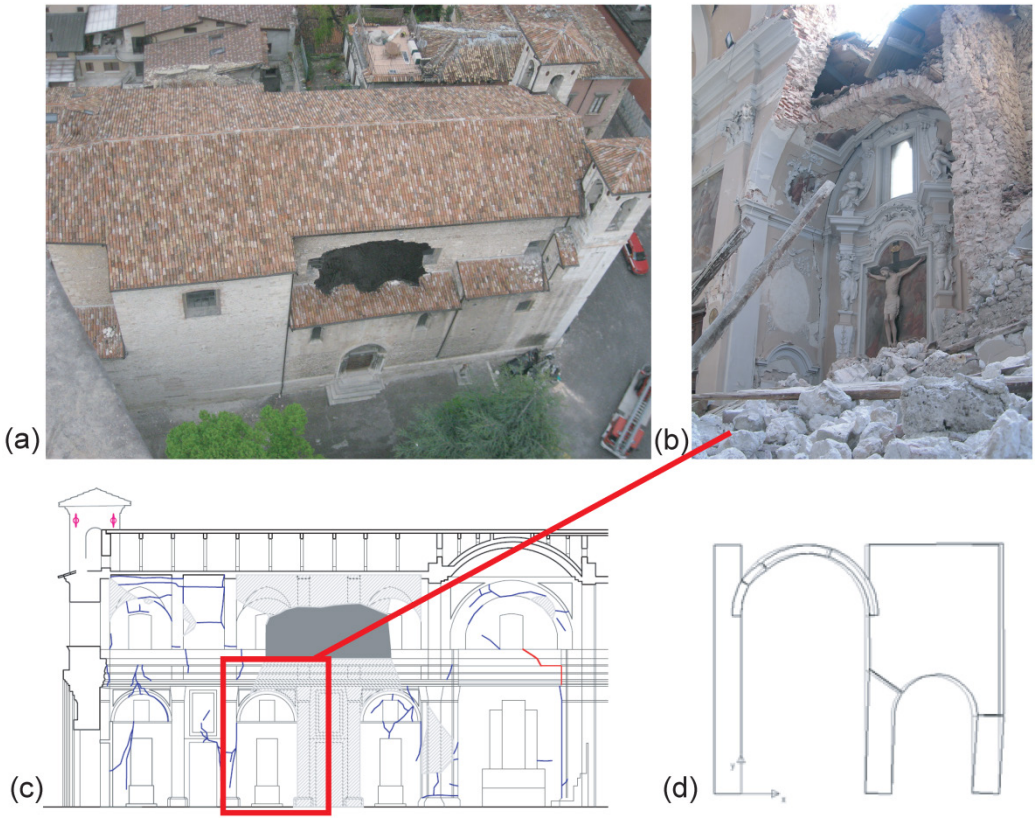

Figure 6.7 - Collapse of the chapels and upper part of the south nave wall (De Conti 2013): (a) outside and (b) inside views, (c) identification of the macro element and (d) kinematic analysis of the mechanism.

The out-of-plane overturning of the apse, assumed disconnected from the semi-dome area, corresponds to 0.217 g. When the apse and the semi-dome overturn together (Figure 6.6 f), the seismic coefficient is nearly the same (0.218 g).

The in-plane failure of the façade occurs for α_0=0.354 (Figure 6.6 g). Even though this mechanism is related to a rather high collapse coefficient, it has been actually activated as can be recognised from damage observed at both the interior and exterior paraments of the façade.

The occurrence of highly developed mechanisms and even collapse is investigated by considering the State of Life Safeguard (SLV) according to the Italian standards (Italian Ministry of Infrastructure and Transport 2009) using both linear and nonlinear kinematic analysis.

In the application of linear kinematic analysis the spectral acceleration a^*_0 of mechanism activation is compared with the demand acceleration divided by a structural factor *q* taken equal to 2. The spectral acceleration a^*_0 is computed as α_0 divided by the mass participation factor and the confidence factor FC. The mass participation factor is equal to 1 except for mechanisms c) and g), with values equal to 0.92 and 0.98 respectively. Since the aim of the study is the comparison with actually occurred mechanisms, the confidence factor is taken equal to the unit. The demand acceleration has been calculated according

to the Italian standards (Italian Ministry of Infrastructure and Transport 2009). For the factor q=2, the reference demand acceleration to be considered in the comparison is equal to 0.15g.

All mechanisms interesting the lateral walls (mechanisms a) to d) of Figure 6.6), and specifically the mechanism involving the collapse of the chapel buttresses and arches (mechanism c), are below this reference value. Conversely, the mechanisms associated to the in-plane failure of the façade and the overturning of the façade and apse show activating coefficients above the reference value, meaning that they should not be expected to attain a condition close to full collapse.

As the second step, the limit state of life safeguard (SLV) is assessed by nonlinear kinematic analysis. Following the specifications of the Italian standards, and for the different mechanisms considered, the ultimate displacement capacity d_u^* is calculated for each mechanism and compared with the value of the displacement demand Δ_d. The SLV condition is satisfied if $d_u^* \geq \Delta_d$. The calculation of both terms has been carried out with the software c-Sisma (Modena et al. 2009).

Figure 6.6 compares the values of d_u^* and Δ_d for the different mechanisms. As can be seen in the figure, the SLV condition is not verified for mechanisms a) and c), respectively corresponding to the overturning of the upper part of nave wall and the collapse of the system of arches and buttresses of the chapels which, as mentioned before, causes as well the vertical detachment of the upper part of nave wall. Both mechanisms show a similar ratio, of about 0.9, between the ultimate displacement capacity and the displacement demand. The SLV condition is verified for the rest of the mechanisms, which helps explain why some of these mechanisms (specifically, mechanisms e) and g) corresponding to overturning and in-plane failure of the façade and mechanism f), corresponding to the overturning of the apse) have been only partially activated by the earthquake. In the case of the set of mechanisms analysed, the comparison between linear and nonlinear kinematic analysis shows that the former produces more conservative results, having in all the cases yielded ratios between capacity and demand higher than the latter.

6.3.3 Description of the FE model

A FE model of the entire church (Zografou 2010) has been prepared. The model represents the state of the structure just before the 2009 earthquake. The RC members of the 1970 intervention, i.e. tympanums and beams over the transept, are included in the model. The disconnection among the buttresses supporting the chapel vaults and the external walls is properly modelled, since it is very influential on the global behaviour. Disconnection among finite elements is realised by duplicating nodes at the connections. Interface elements are not considered in order to reduce the computational cost. Since falling of roof trusses occurred during the earthquake of 2009, the roof beams are not discretised to avoid overestimation of the stiffening effect given by the flexible roof. However, their masses are lumped to the top edge of walls.

Silva et al. (2010) estimated the mechanical properties of masonry through inspection, according to the Italian standards (Italian Ministry of Infrastructure and Transport 2009). The façade is composed of dressed rectangular (ashlar) non-soft stone masonry and the north nave wall of uncut stone masonry, of variable dimensions, with prevailingly horizontal layers. The material properties that have been assumed in the analyses are listed in Table 6.1. Nonlinear properties are assigned to masonry. Discussions on failure criteria have been made in Chapter 3 and 4. Accordingly, a smeared cracking model with a Rankine failure criterion for tension and a plasticity model with Drucker-Prager failure criterion for compression are adopted. Timber members are modelled as linear elastic.

Table 6.1 - Mechanical properties for FEM analysis.

	stone masonry	**brick masonry**	**RC**	**timber**
Density (kg/m^3)	2000	1800	2400	650
Compressive strength (MPa)	4	4	15	-
Young's modulus (MPa)	500×fc (2000)	500×fc	20000	11000
Tensile strength (MPa)	5%fc (0.2)	5%fc	1	-
Poisson ratio (-)	0.2	0.2	0.2	0.2
Fracture energy (N/m)	50	50	100	-

The model is composed of 14,217 quadrilateral four-node shell elements, 1,333 triangular three-node shell elements (both shell elements possess 11 integration points in thickness), 205 straight two-node 3D beam elements and 115 one-node translational mass elements to provide the dead load over the roof beams (Figure 8). The total number of nodes is 16,976. The RC beams and tympanums in the transept are modelled with four-node quadrilateral and three-node triangular shell elements. Given the symmetry of the structure, half of the model is employed for the analysis in the longitudinal direction with appropriate boundary conditions. Both geometrical and mechanical nonlinearities are considered in the analyses.

In this chapter, certain control nodes are repeatedly used to draw load-displacement curves. Their locations are specified in Figure 6.8. They correspond to the top of the bell tower (blue square), the top of the north and south nave wall (red and green pentagon), the top of the chapel wall (orange square), the middle of the arch between the nave and transept (pink X shape), the top of the transept wall (light blue circle) and the top of the apse wall (light green triangle).

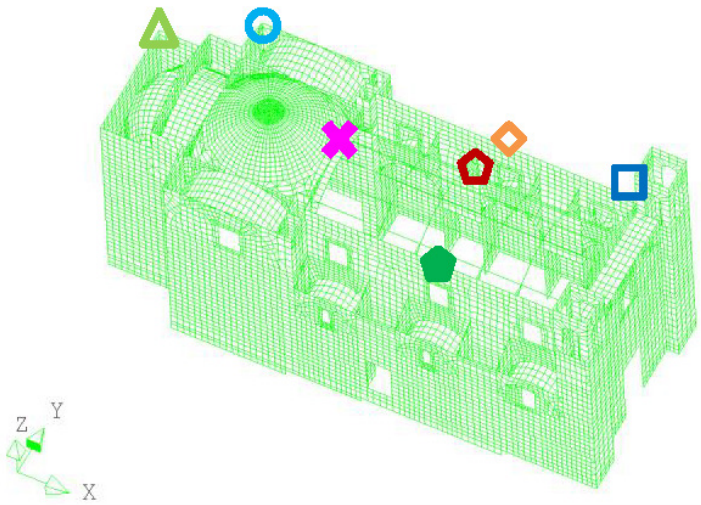

Figure 6.8 - Global model and control nodes.

6.3.4 Pushover analysis

The analyses are carried out in three directions, namely positive and negative longitudinal (±X) and transversal (Y) direction (Figure 6.9). Gravity is applied in a first loading step and then seismic forces proportional to the mass of the structure are incremented until the analysis stops due to the collapse of the model.

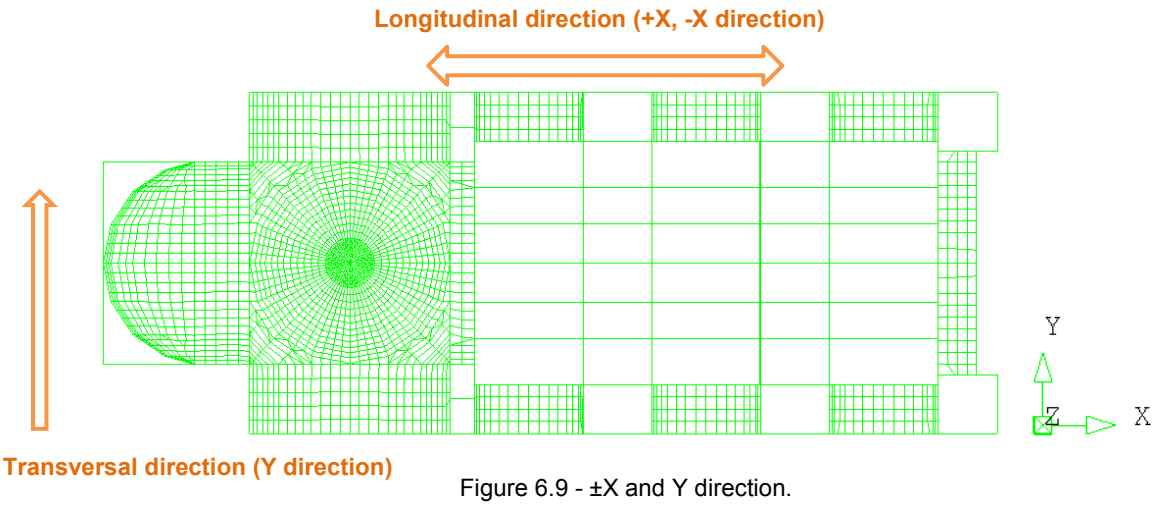

Figure 6.9 - ±X and Y direction.

6.3.4.1 Positive longitudinal direction

In the positive longitudinal direction (+X), the first horizontal branch of the load-displacement curve is seen at an acceleration of 0.085 g (Figure 6.10 a). At this point, separation of the façade from the nave and cracking in the chapel vault close to the transept starts. Damage in the arch between the nave and the transept starts to appear as well. This damage keeps developing until the ultimate condition is reached. A diagonal crack across the arch in the transept and the dome starts to appear also at this stage. The ultimate state is reached for an acceleration of 0.165g and a displacement at the top of the

bell tower of 43 mm. The failure is due to the overturning of the façade with part of the chapel wall, leading in turn to the detachment of the nave wall from the transept (Figure 6.10 b-c).

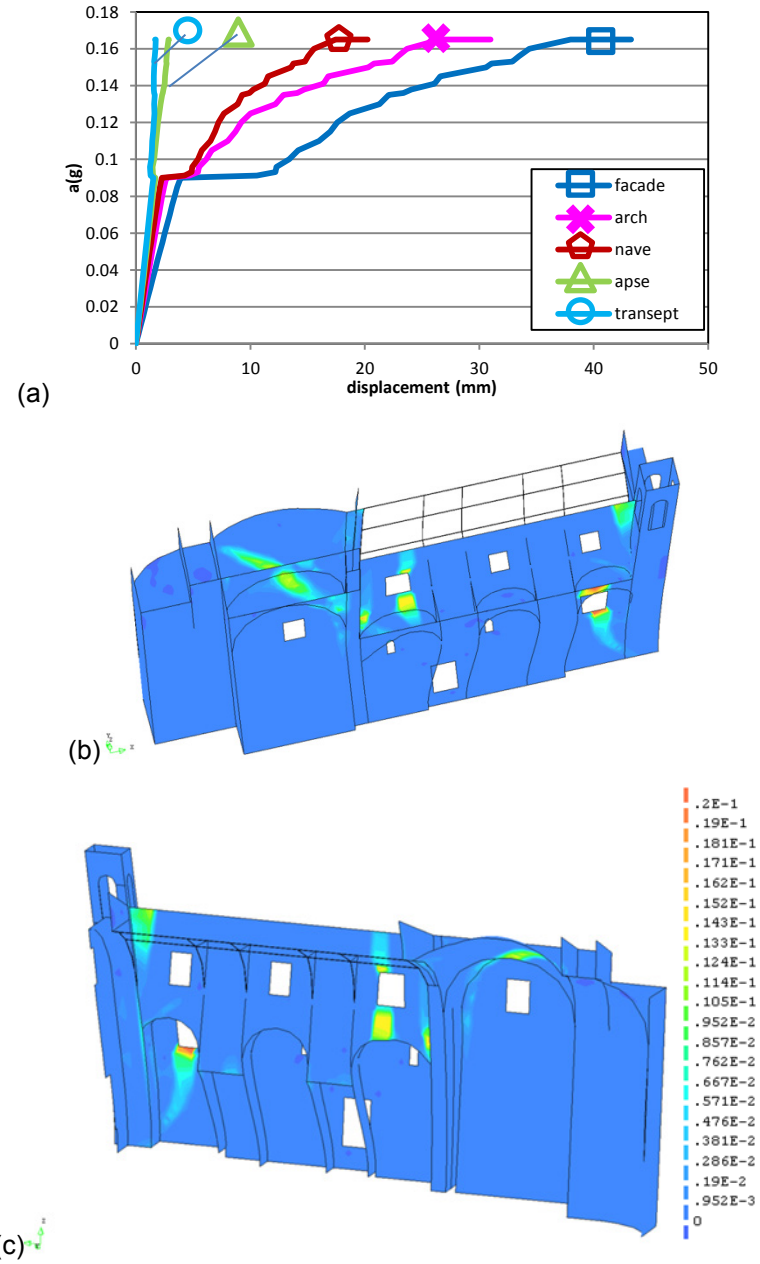

Figure 6.10 - Pushover analysis in the positive longitudinal direction (+X): (a) load-displacement curves at different control nodes and (b-c) contour of principal tensile strain at the ultimate state.

The capacity resulting from this analysis agrees well with the activation coefficient obtained for the façade overturning mechanism by kinematic analysis (0.165g vs. 0.167g). This fact may indicate that both approaches are able to represent correctly this type of failure. In the real building, the activation of the out-of-plane mechanism of the façade was recognisable from both the inside and the outside (Figure 6.11 a-b) and an urgent intervention was required for its stabilisation (Figure 6.11 c). Damage in the arch and in the dome was also observed in the real structure. However, the partial collapse of the upper part

of the south nave wall is not completely represented by the FE model. The buttresses supporting the chapel vaults are significantly deformed due to the disconnection from the perimeter wall. This problem induces the formation of damage in the vault of one of the lateral chapels, as shown in Figure 6.11 c, starting at the acceleration of 0.105g. However, the FE analysis does not afford the simulation of the loss of balance of the vaults and the consequent falling of the wall above. In spite of it, the threshold of damage formation in the structure is in a good agreement with the seismic coefficient α_0=0.099g derived from limit analysis for out-of-plane overturning of buttresses.

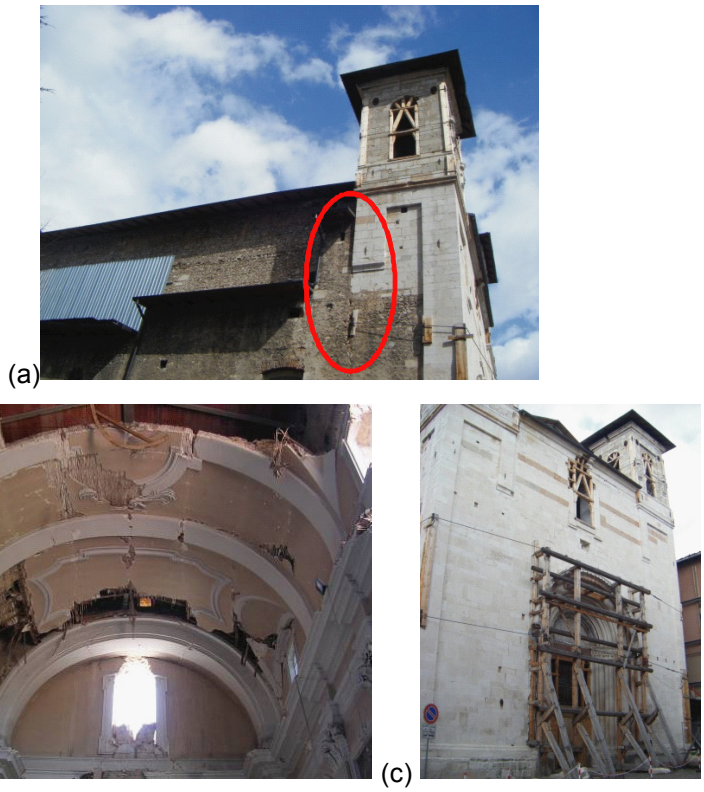

Figure 6.11 - Real collapse mechanism detected by +X direction pushover analysis: (a) overturning of the façade seen from the exterior and (b) from the interior and (c) post-earthquake urgent intervention by ties and timber propping.

6.3.4.2 Negative longitudinal direction

In the negative longitudinal direction (-X) damage starts to appear in the connection between the facade and the nave and also on the vault of the chapel next to the façade. At 0.111 g, damage appears also in the vault of one of the chapels. This value is close to that observed in the positive longitudinal direction. At 0.19 g, the first the load-displacement curve shows a first horizontal branch, corresponding to damage arising in the perimeter wall (Figure 6.12 a). When the curve reaches the second horizontal branch (0.217 g), the out-of-plane movement of the apse becomes visible and a diagonal crack across the window in the transept wall also appears (Figure 6.12 b-c). The ultimate acceleration is 0.217 g and the corresponding displacement is 19 mm at the top of the apse wall. The failure is due to the out-of-plane behaviour of the apse, leading, in turn, to the failure of a chapel vault and the in-plane failure of the transept and perimeter walls. High concentration of damage is seen in the connection

between the façade and the nave, and between the nave and the transept. Most of the failures predicted by –X pushover analysis, including the out-of-plane behaviour of the apse, were also observed in the real structure (Figure 6.13). The ultimate acceleration of FEM analysis is close to the activation coefficient α_0=0.218 g derived from limit analysis for out-of-plane overturning of the apse wall.

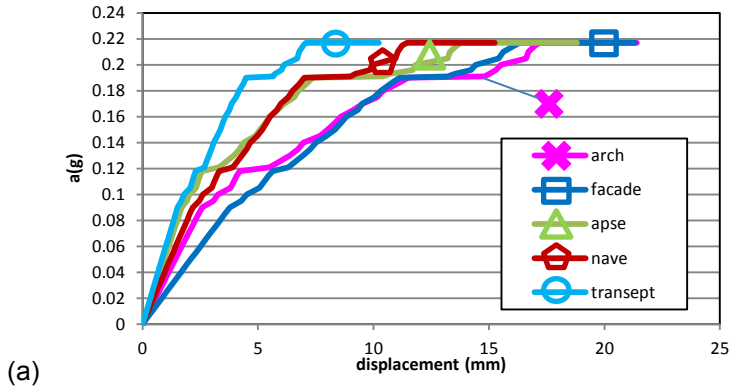

(a)

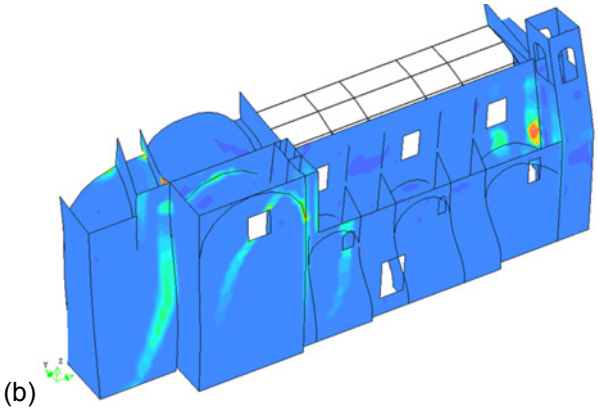

(b)

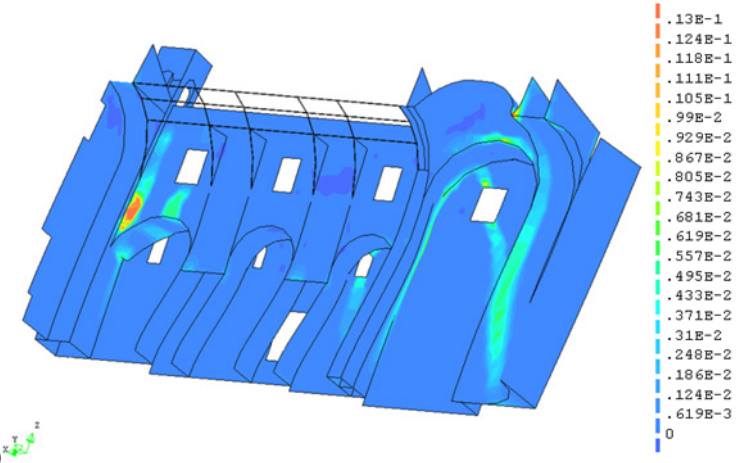

(c)

Figure 6.12 - Pushover analysis in the negative longitudinal direction (-X): (a) load-displacement curves at different control nodes and (b-c) contour of principal tensile strain at the ultimate state.

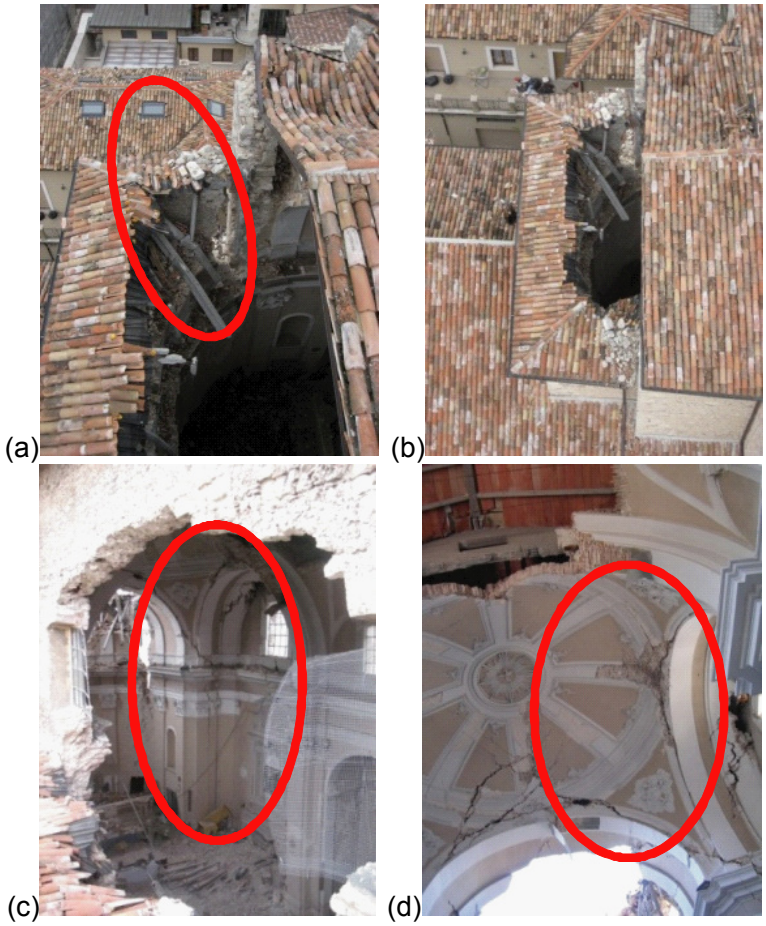

Figure 6.13 - Collapse mechanisms detected by -X direction pushover analysis: (a-b) out-of-plane overturning of the apse and (c-d) separation of the transept wall from the arch sustaining the dome.

6.3.4.3 Transversal direction

The main prediction of pushover analysis in the transversal direction is found in the global overturning of the nave wall (Figure 6.14). At the acceleration of 0.045 g some damage appears in the chapel vault and in the connection between the nave walls and the façade, and between the transept and the nave walls. At 0.08 g, damage in the arch of the transept starts to appear. The out-of-plane deformation is more noticeable in the south wall than in the north one (Figure 6.14a). This asymmetrical behaviour may be due to geometrical nonlinearity. In fact, an additional FE analysis without geometrical nonlinearity showed nearly equal ultimate displacements of both walls. Another factor to be considered for this difference is the disconnection among buttresses and chapel walls.

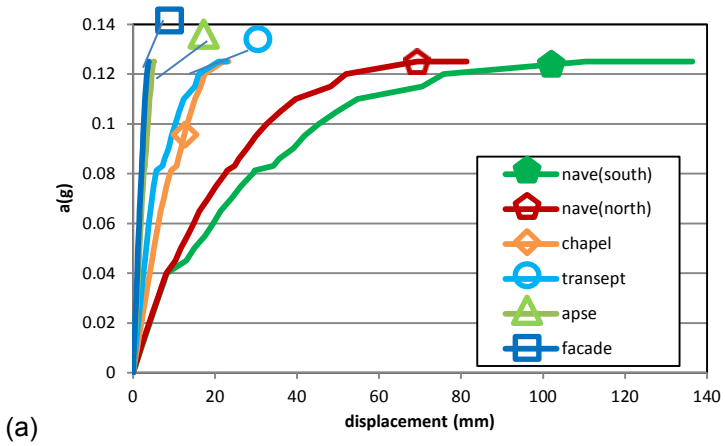

(a)

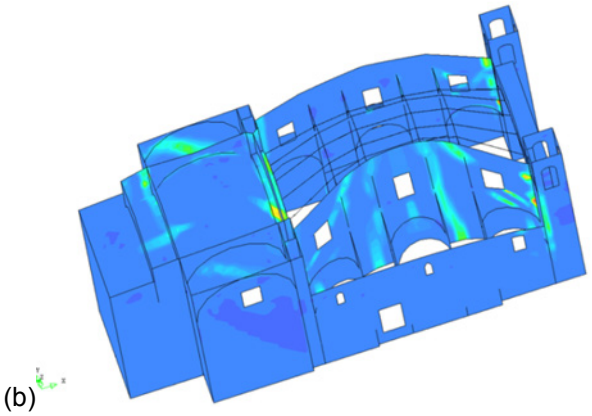

(b)

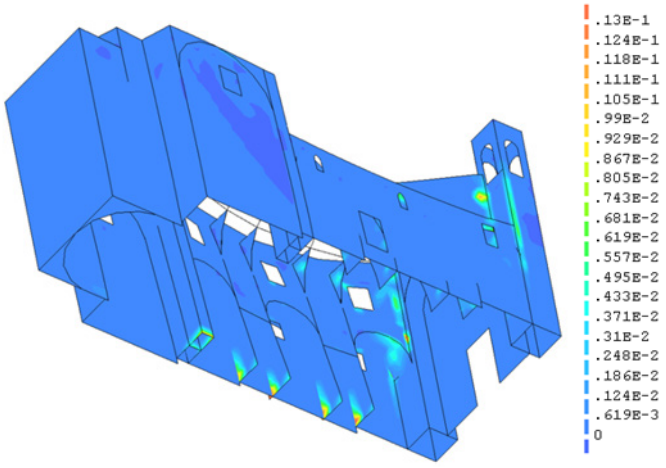

(c)

Figure 6.14 - Pushover analysis in the transversal direction (Y): (a) load-displacement curves at different control nodes and (b-c) contour of principal tensile strain at the ultimate state.

At the acceleration of 0.12 g, the damage concentrates in the middle part of the bent nave wall, and then at 0.125 g diagonal cracks arise from the middle part of the nave wall and propagate by involving the windows. Finally, the analysis stops when the whole nave wall overturns at the ultimate state (0.1254 g). This value is similar to the activation coefficient obtained for the nave wall overturning in limit analysis (0.116 g).

However, the overturning of the entire nave wall was not observed after the earthquake. As already discussed in Sections 6.2.2 and 6.5.3, the partial downfall of the upper nave wall seems to have been caused by the combined collapse of the lateral arches and buttresses under longitudinal loading (mechanism of Figure 6.6 c).

At the ultimate state, significant damage can also be observed in the FE model in the arches of the transept (Figure 6.14 b-c). In particular, the arch between the nave and the transept is seriously damaged. High damage concentration is also seen at the end of the RC tympani. The bottom of the buttresses is also damaged due to the out-of-plane behaviour of the entire nave wall (Figure 6.14 c). All the aforementioned failures were also detected in the structure after the earthquake (Figure 6.15). In turn, in-plane failure of the façade is not predicted although it was observed after the earthquake.

Figure 6.15 - Collapse mechanisms detected by Y direction pushover analysis: (a) arches in the nave, (b-c) walls and buttresses in lateral chapels, d) transept arches.

6.3.5 Nonlinear dynamic analysis

NDA is carried out with the accelerograms shown in Figure 6.3 a-b. The FE model and its material properties are the same that have been used for pushover analysis. A Rayleigh damping model is

considered, with mass-proportional and stiffness-proportional damping coefficients respectively equal to a_0=0.5789 and a_1=0.0042. The Newmark-beta method has been used for the integration in the time domain. Constant average acceleration is assumed within each time step, with parameters γ=0.5 and β=0.25. Time intervals of 0.002 seconds have been assumed. Sensitivity analyses have been carried out to assess the accuracy of the adopted time discretization. The duration of the input ground motion in each NDA depends on the considered earthquake record, with 12 seconds assumed. The N2 method (Fajfar 2002) is adopted to compare the results obtained from the pushover analysis and those from NDA in terms of the seismic performance estimations.

6.3.5.1 Longitudinal direction

The NDA along the longitudinal direction (X) stops after 2.74 seconds (Figure 6.16 a-b). Significant increase of the acceleration is seen after 2 seconds, according to the shape of the accelerogram. The maximum displacement of the structure (31 mm at the top of the bell tower) occurs at 2.6 seconds. At this moment, the principal tensile strain contours indicate the detachment of the façade. Damage can be seen under the roof in the right part of the south façade, near the connection with the tower, as actually observed after the earthquake (Figure 6.5 g). Damage can be found also in the arch of the transept, in the upper part of the south nave wall and the chapel vault adjacent to the transept (Figure 6.16 c-d), in good agreement with the real collapse. Although some damage is found at the connection between the presbytery and transept, no activation of the out of plane failure of the apse is observed.

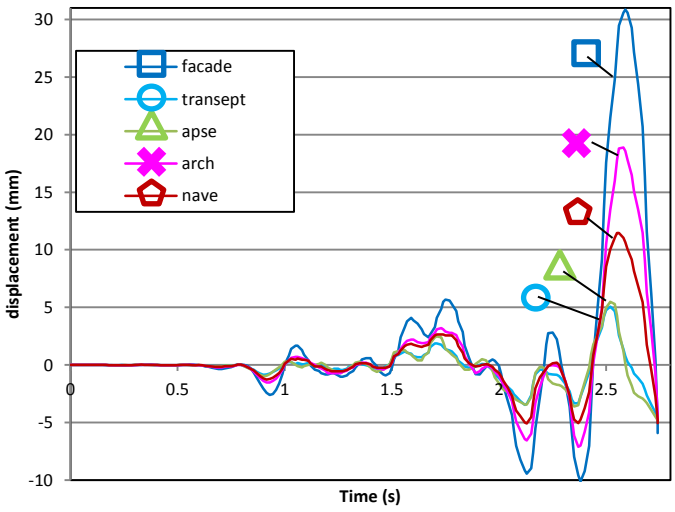

(a)

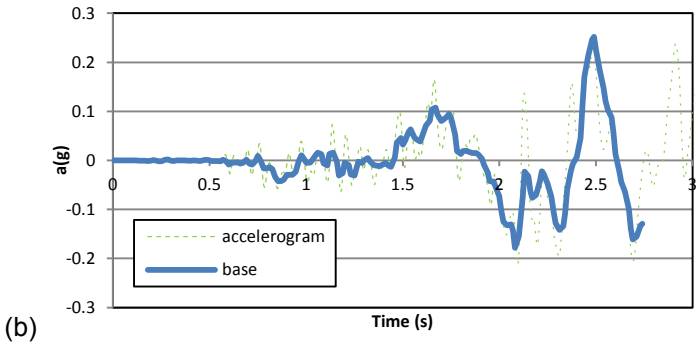

(b)

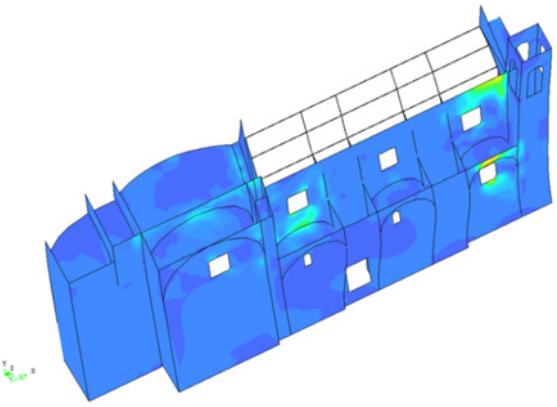

(c)

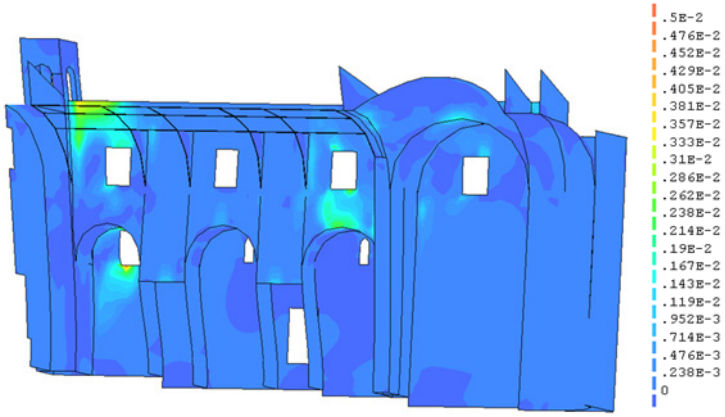

(d)

Figure 6.16 - NDA in the longitudinal direction (X): (a) time-history of displacements at different control nodes, (b) comparison accelerogram vs. acceleration at the base of the structure and (c-d) contour of principal tensile strain at 2.6 sec.

Outcomes of NDA are compared with those of the pushover analysis by N2 method. The displacement (top of the bell tower) at the performance point is 26 mm and the acceleration is 0.14 g (Figure 6.17a). In turn, the maximum displacement obtained in NDA is 31 mm and the corresponding acceleration is 0.09 g. The two analyses provide very similar estimations of the displacement due to earthquake. When the contours of principal tensile strains at the performance point of pushover analysis (Figure 6.17b) are compared with those for the maximum displacement of NDA (Figure 6.16 c-d), they both illustrate similar patterns of damage. However, in the NDA the principal tensile strains present smaller magnitude and are more distributed in walls and less concentrated in the connections. Pushover analysis describes a more critical state than NDA regarding the overturning of the façade, the shear mechanism in the wall of

the lateral chapel, the damage around the window in the south nave wall and the separation of the nave wall from the transept (Figure 6.17b).

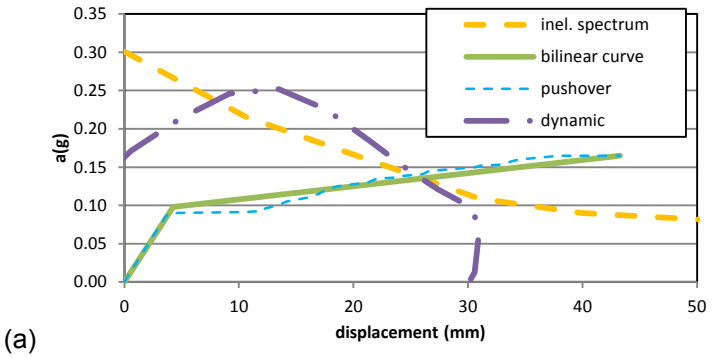

(a)

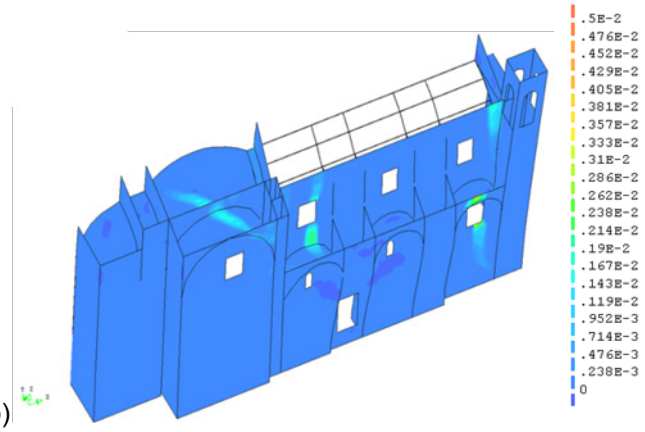

(b)

Figure 6.17 - Comparison between NDA and N2 method, longitudinal direction (X), top of the façade control node: (a) NDA acceleration-displacement envelope compared with the load-displacement curve and (b) contour of principal tensile strains at the performance point of pushover analysis.

6.3.5.2 Transversal direction

The NDA along the transversal direction (Y) stops after 2.21 seconds (Figure 6.18 a-b). Significant increase of the acceleration is seen before 2 seconds, leading to ultimate state. The maximum displacement of 102 mm is observed at the top of the north nave wall at the ultimate state. The contour of principal tensile strains at the ultimate state (Figure 6.18 c-d-e) indicates the overturning of both north and south nave walls, whereas concentration of damage is seen in the arches of the transept. The arch between the nave and the transept is significantly damaged.

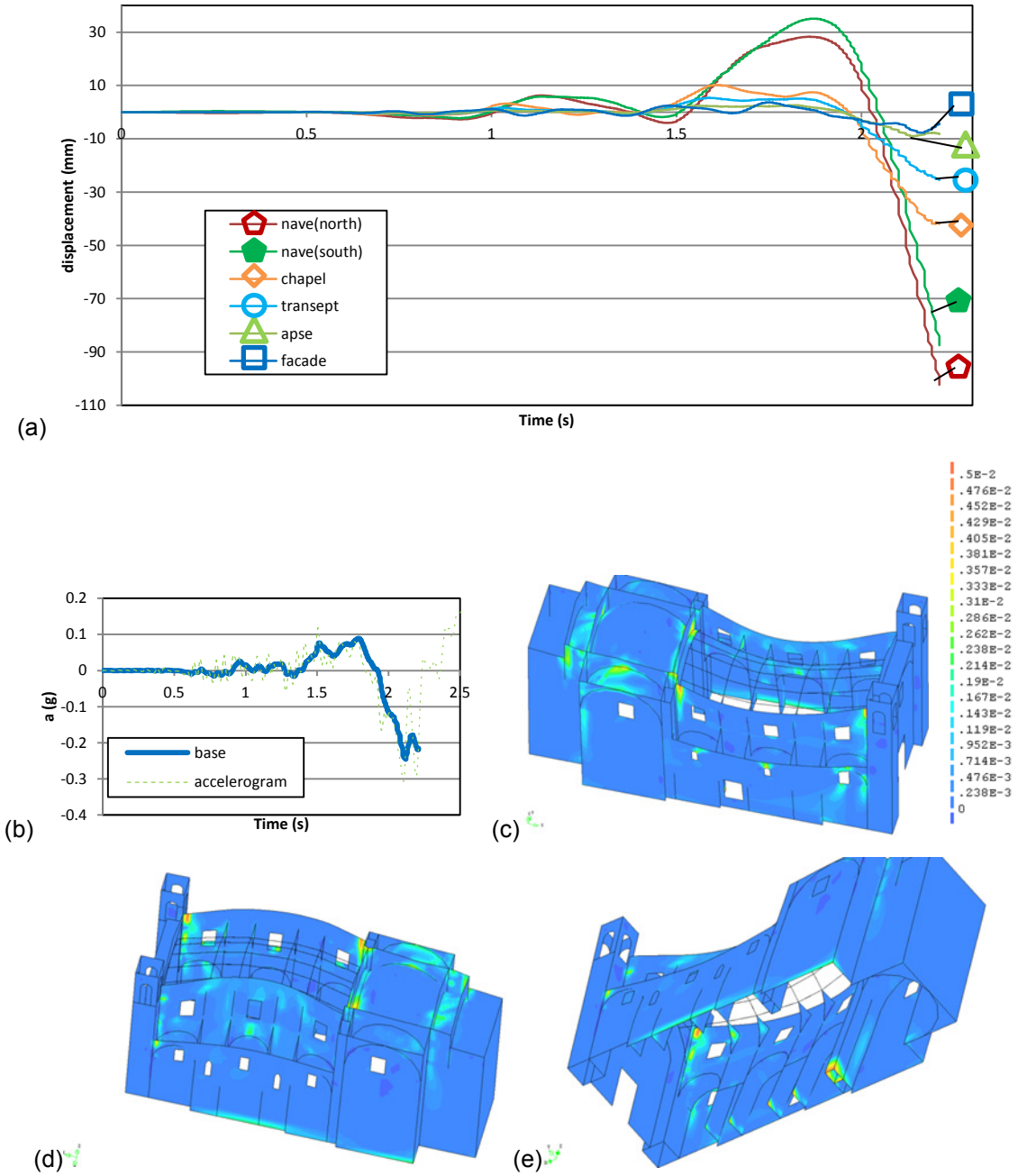

Figure 6.18 - NDA in the transversal direction (Y): (a) time-history of displacements at different control nodes (b) comparison accelerogram vs. acceleration at the base of the structure and (c-e) contour of principal tensile strain at 2.21 sec.

From the comparison between the time-histories of the nave walls it emerges that although the south wall shows the maximum positive displacement, the maximum negative displacement is observed in the north wall. The movement towards the nave results larger than the outward deformation. This is due to the effect of the buttresses and the influence of the geometrical nonlinearity.

Outcomes of NDA are compared again with those of the pushover analysis by N2 method. The displacement at the top of the nave wall at the performance point is 59 mm and the corresponding

acceleration is 0.125 g. This displacement is lower than that from NDA (87.5 mm) (Figure 6.19 a). The maximum acceleration predicted by NDA (0.245 g) is also higher. Principal tensile strain values at the performance point are more moderate in NDA than in pushover analysis. Damage appears more distributed in NDA than in pushover analysis, especially in the transept area (Figure 6.19 b-c).

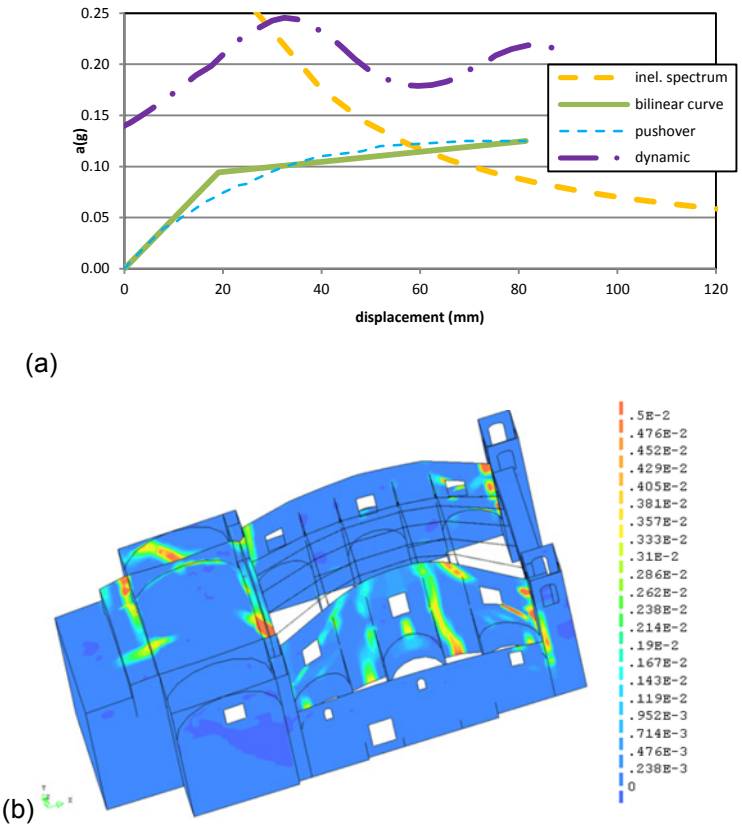

Figure 6.19 - Comparison between NDA and N2 method, transversal direction (Y), top of the nave wall control node: (a) NDA acceleration-displacement envelope compared with the load-displacement curve and (b-c) contour of principal tensile strain at the performance point of pushover analysis.

6.3.6 Study of structure before the RC intervention carried out in 1970

In this section, a study focuses on an influence of the RC intervention carried out in 1970. In this year, an intrusive intervention was carried out by using RC as discussed in Section 6.2.1. A new model is prepared and compared with the model presented in Section 6.3.3. The new model represents the state of the structure just before the RC intervention was conducted. There are no RC beams and tympanums in the transept area. The roof is composed of a timber traditional roof instead of the RC prefabricated one. However, like in the previous model, the roof beams are not discretised and their masses are lumped to the top edge of walls. The model before the intervention is named as *timber model* and the model after the RC intervention (the same one as presented in Section 6.3.3) is named *RC model*. Comparison of the behaviour between timber and RC model is made by means of pushover and nonlinear dynamic analysis.

6.3.6.1 Pushover analysis

6.3.6.1.1 Positive longitudinal direction

The load-displacement curves (control node at the top of the arch) are compared (Figure 6.20). The two models represent similar load and displacement capacity (0.165g, 31.0 mm for RC model vs. 0.169g, 30.3 mm for timber model). When the Principal tensile strain distributions in the ultimate state are compared, very similar damage distribution patterns are observed (Figure 6.21, Figure 6.10 b-c).

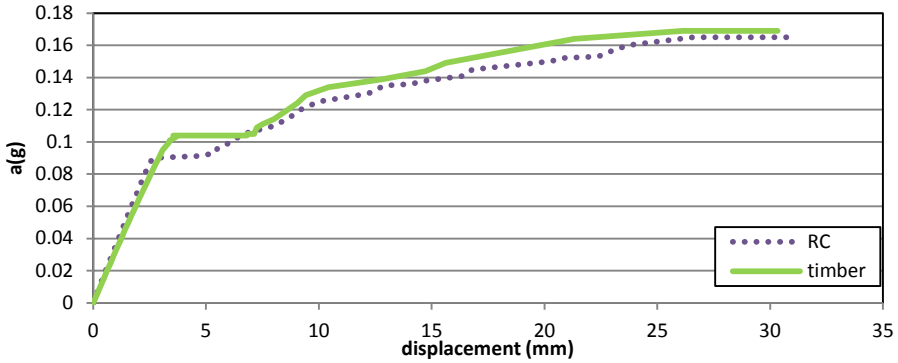

Figure 6.20 - Load-displacement curves, +X direction, control node at the top of the arch.

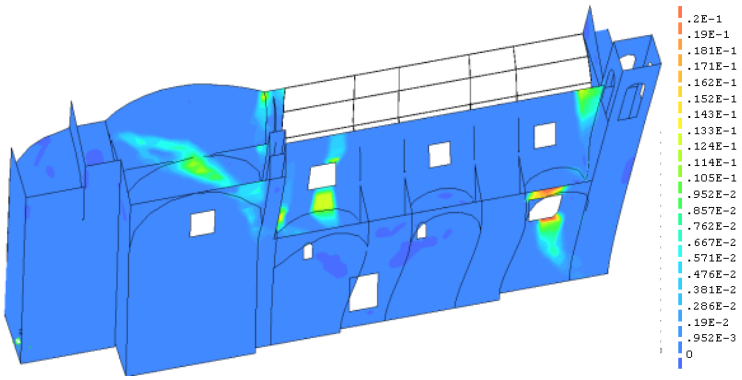

Figure 6.21 - Principal tensile strain distributions in the ultimate state, +X direction, timber model.

6.3.6.1.2 Negative longitudinal direction

In the –X direction, the two models shows similar load capacity (0.217g for RC model vs. 0.229g for timber model). When the load-displacement curves at the top of the apse wall are compared, the timber and RC model show much higher displacement capacity (21.4 mm vs. 18.8 mm) (Figure 6.22). When the Principal tensile strain distributions in the ultimate state are compared, similar damage distribution patterns are observed apart from the state of damage intensity in the transept area (Figure 6.23, Figure 6.12 b-c).

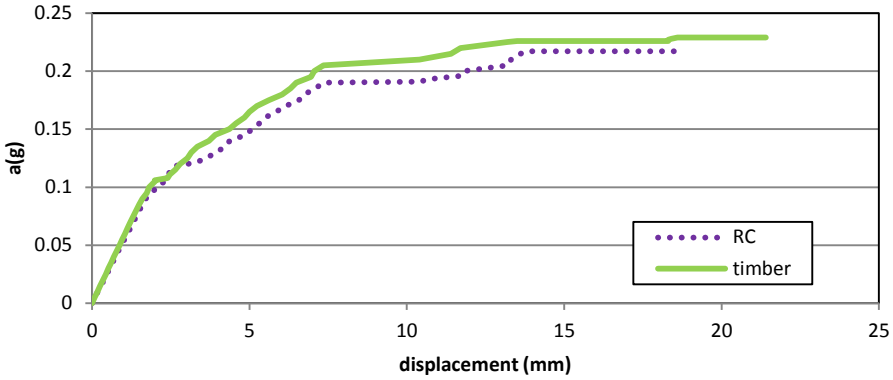

Figure 6.22 - Load-displacement curves, -X direction, control node at the top of the apse wall.

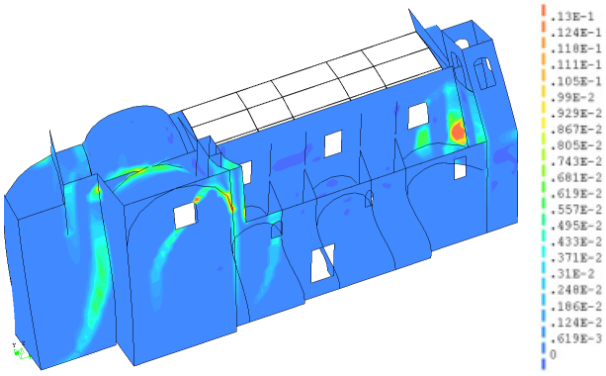

Figure 6.23 - Principal tensile strain distributions in the ultimate state, -X direction, timber model.

6.3.6.1.3 Transversal direction

In the transversal direction, the timber model shows higher load and displacement capacity (0.14g, 27.6 mm) than the RC models (0.125g, 22.9 mm) (Figure 6.24). A noticeable difference of damage distribution patterns is observed than in the other two directions. The RC model shows much higher damage in the nave area than the timber model (Figure 6.25, Figure 6.14 b-c). This is clearly due to the large weight of RC roofs over the nave wall in the RC model.

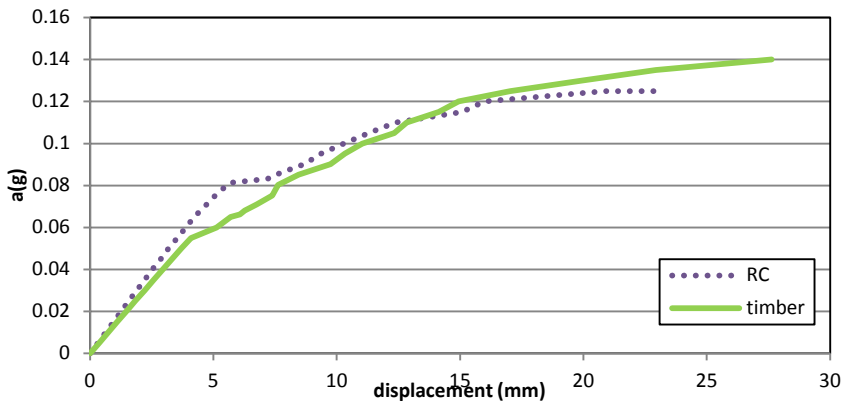

Figure 6.24 - Load-displacement curves, Y direction, control node at the top of the transept wall.

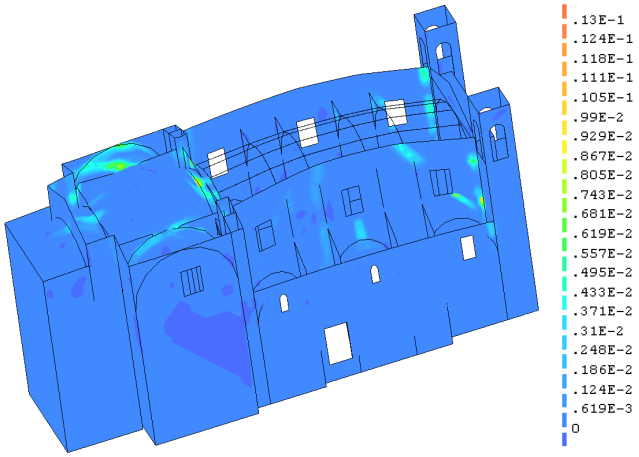

Figure 6.25 - Principal tensile strain distributions in the ultimate state, Y direction, timber model.

6.3.6.2 Nonlinear dynamic analysis

6.3.6.2.1 Longitudinal direction

In the longitudinal direction, the timber model analysis stops at 2.72 seconds against while the RC model does at 2.75 seconds. When time histories of the displacement at the middle of the arch are compared (Figure 6.26 a), the timber model shows a slightly higher maximum displacement (20.2 mm at 2.55 seconds) than the RC model (19.1 mm at 2.55 seconds). On the other hand, the RC model demonstrates a higher maximum base acceleration (0.252g) than the timber model (0.229g). When the maximum principal tensile strain distributions are compared, the two models show similar damage patterns around the façade (Figure 6.27 and Figure 6.16 c-d). However, the RC model shows less damage in the transept area than the timber model.

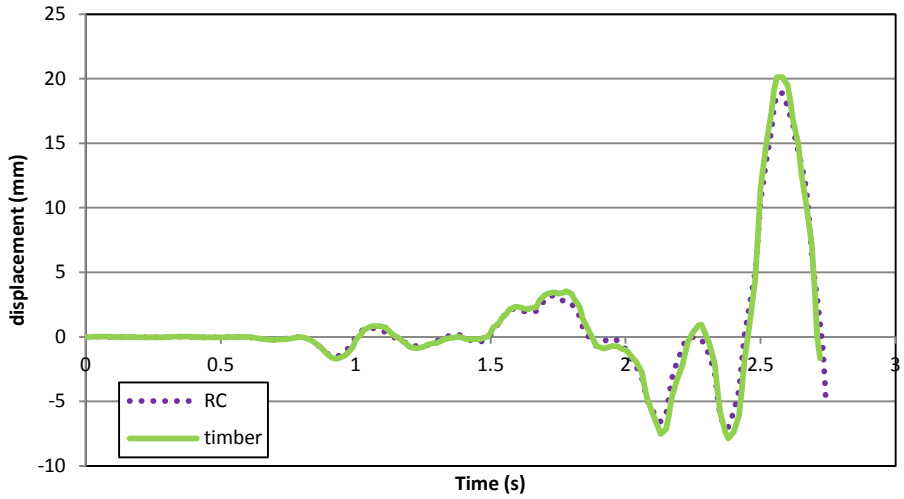

Figure 6.26 - NDA in the X direction, time-history of displacements at the top of the arch between the nave and transept.

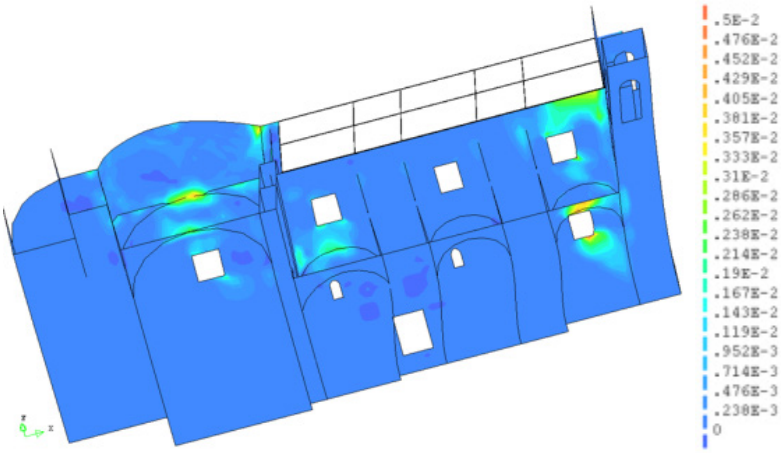

Figure 6.27 - NDA in the X direction, contour of principal tensile strain at 2.6 sec, timber model

6.3.6.2.2 Transversal direction

The time histories of the displacement at the top of transept and nave wall are presented (Figure 6.28). The timber model (2.38 seconds) lasts longer than RC model (2.23 seconds). It has to be mentioned that NDA of the timber model continues after it reaches the maximum absolute displacement for both control nodes. On the other hand, NDA of RC model stops when it reaches the maximum absolute displacement. As for the time history of the top of the transept wall (Figure 6.28 a), the RC model shows the absolute maximum displacement (25.2 mm) at its ultimate state while the timber model shows the absolute maximum displacement (32.2 mm) at 2.25 seconds. As for the time history of the displacement at the top of the nave wall (Figure 6.28 b), they show the absolute maximum displacement at different moments (102.3 mm at 2.23 seconds for the RC model vs. 124.9 mm at 2.34 seconds for the timber model). The RC model (0.245g) shows the same maximum base shear acceleration as the timber model. When the damage distribution patterns are compared (Figure 6.29, Figure 6.18 c-e), they two show similar patterns in spite of the difference of damage intensity.

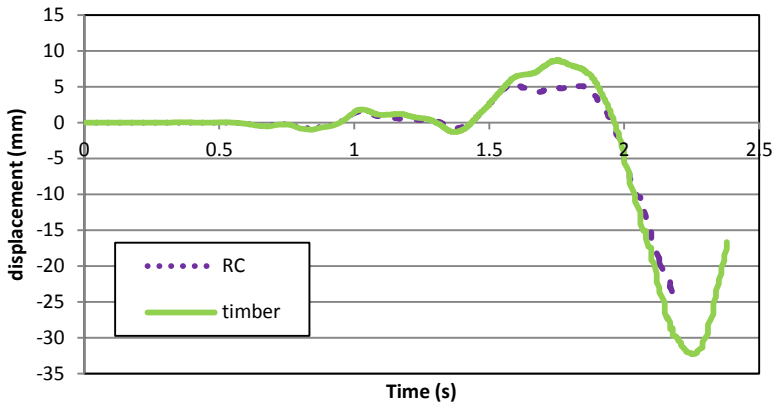

(a)

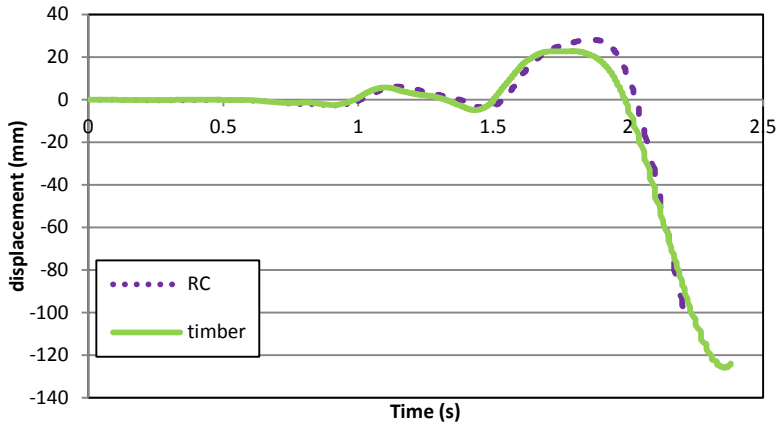

(b)

Figure 6.28 - NDA in the Y direction, time-history of displacements: (a) transept wall and (b) at the top of the nave wall.

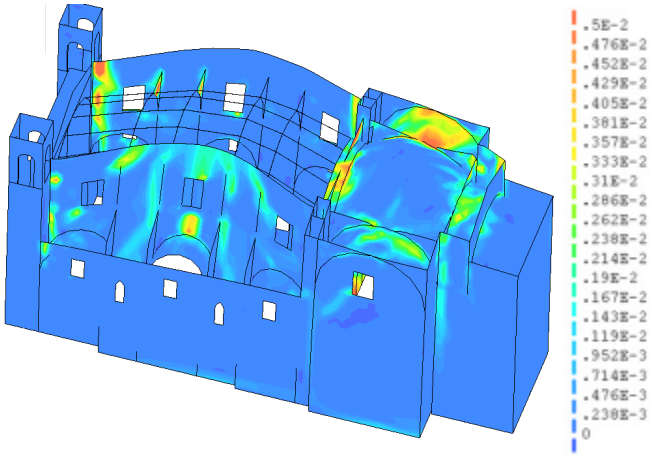

Figure 6.29 - NDA in the Y direction, contour of principal tensile strain, timber model at 2.26 seconds.

6.4 Study of the influence of different parameters

6.4.1 Section introduction

The influence of different parameters, including the mechanical parameters of masonry, are studied. The reference model in this section is different from the model presented in Section 6.3. It is prepared based on the geometry of San Marco church before the RC intervention was installed in 1970. The roof trusses are discretised with beam elements. In addition full connection is assumed between the buttresses and perimeter wall. The model is composed of 13,818 quadrilateral four-node shell elements, 1,202 triangular three-node elements, 1013 straight two-node 3-D beam elements and 555 one-node translation mass elements which apply the dead load over the roof trusses. The total number of nodes is 16,817. The model is similar to the “timber model” presented in Section 6.3.6.1 except for the assumption of the connection between the buttresses and perimeter wall and existence of the roof trusses. The reason why this model is considered as the reference model is to study more representative state of a church-type structure.

The reference mechanical properties of masonry and timber are the same as those presented in Section 6.3.3. As for the masonry, compressive strength is equal to 4 MPa, 0.2 MPa (5% of f_c), Young's modulus is 2000 MPa (500 times f_c) and tensile fracture energy is 50 N/m. As for the timber, Young's modulus is equal to 11,000 MPa. For masonry, a smeared cracking model with a Rankine failure criterion for tension and a plasticity model with Drucker-Prager failure criterion for compression are adopted. Timber members are modelled as linear elastic.

Firstly, the reference model is analysed. Secondly, parametric studies are carried out. The mechanical parameters whose influence on the response is examined, are the compressive and the tensile strength, the Young's modulus and the tensile fracture energy. In accordance with the results of the parametric study, different combinations of lower values of mechanical parameters are proposed and examined. Models with weak interlocking are also analysed. These models are examined on the basis of the assumption that the structure may have poor interlocking between structural elements (façade, nave, transept). Then different seismic-force distribution patterns are compared with that of mass-proportional distribution. Comparison of a shell-element and a solid-element model is also made. For this last comparison, partial models (façade and typical bay) are used to reduce the computational effort required by the analysis of the solid-element models.

All the analyses are carried out by pushover analysis. The used force distribution pattern is proportional to the masses of the structure except for the analyses of Section 6.4.5 where different force distribution patterns are compared. As in the Section 6.3, considering the symmetry, half of the model is utilised for the analysis in the longitudinal direction with the appropriate boundary conditions.

6.4.2 Pushover analysis on the reference model

6.4.2.1 Positive longitudinal direction

In the +X direction, the first branch is observed in the load-displacement curve (Figure 6.30) for a load factor of 0.155g. At this load factor, concentration of damage appears involving the windows of the nave and chapels and the connection between the façade and nave walls (Figure 6.31 a). The obtained maximum capacity, of 0.211g, is determined by the collapse mechanism of the out-of-plane behaviour of the façade. The overturning of the façade involves part of the nave wall (Figure 6.31 b). The ultimate displacement is 31 mm at the top of the bell tower and 4.5 mm at the top of the nave wall. The comparison of the load-displacement curves obtained for the control node at the top of the bell tower and that at the nave wall shows that the nave wall exhibits higher stiffness than the façade. This result agrees with the response observed in the real structure, which experienced out-of-plane behaviour of the façade as presented in Section 6.2.2 (Figure 6.5 a).

Compared to the "timber model" presented in Section 6.3.6.1.1, the load capacity is increased by 19.9 %. However the displacement capacity, at the top of the bell tower, is not changed. The reference model

shows damage mostly related to the overturning of the façade while the timber model shows damage also in the transept area and in the nave wall close to the transept.

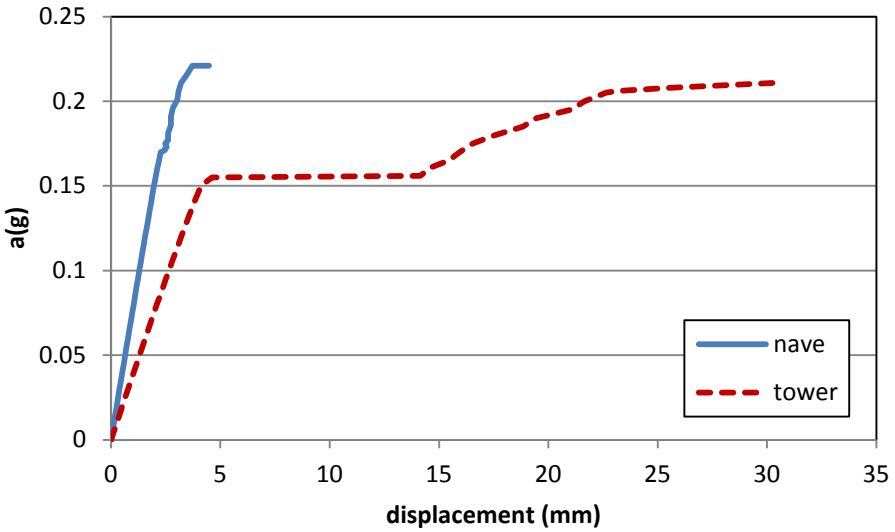

Figure 6.30 - Load-displacement curves, control nodes at the top of the bell tower and the nave wall, +X direction.

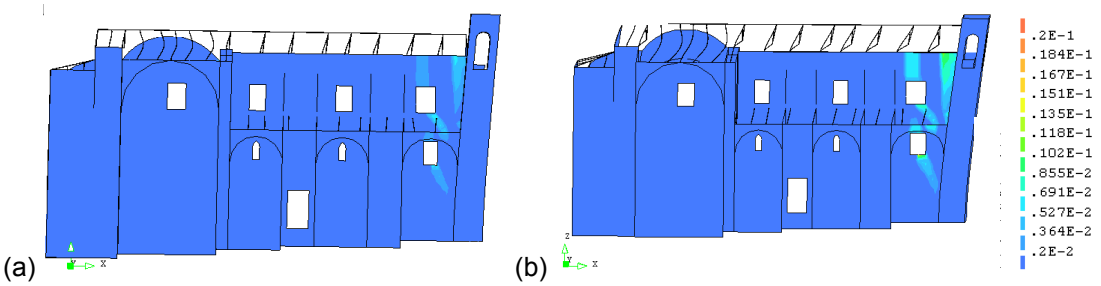

Figure 6.31 - Principal tensile strain distributions: (a) 0.171g and (b) at the ultimate state.

6.4.2.2 Negative longitudinal direction

In the –X direction, the ultimate acceleration (0.294g) is the highest among the three cases considered (+X, -X and Y). The corresponding displacement is 19.9 mm at the top of the apse wall. The load-displacement curves at the control points of the apse and the nave wall present similar elastic stiffness (Figure 6.33 a). The change of the stiffness in the load-displacement curve of the top of the apse wall is observed at an acceleration of 0.19g. At this load factor, damage becomes evident in the vaults of the lateral chapels. At an acceleration of 0.25g, the apse separation starts. At the ultimate state, the collapsing mechanisms are the shear mechanism of the perimeter wall, the out-of plane behaviour of the apse and the collapse of the vaults of the lateral chapels and the transept (Figure 6.33 b-c). The first mechanism can be identified as diagonal damage appearing around the window of the perimeter wall. Significant damage between the apse and the transept indicates the second mechanism. The real structure also exhibited the out-of-plane behaviour of the apse after the 2009 earthquake (Figure 6.13 a b). On the other hand, in the real structure most part of the roof fell off in the apse and the total collapse

of the semi-dome also occurred (Figure 6.5 d). These two mechanisms are not predicted by the FEM model.

Comparison is made between the reference model and timber model presented in Section 6.3.6.1.2. The load capacity is increased by 22.1% while the displacement capacity, at the top of the apse wall, is decreased by 12.6 %. Except for the damage observed in the transept wall of the timber model, similar damage distributions are observed between two models.

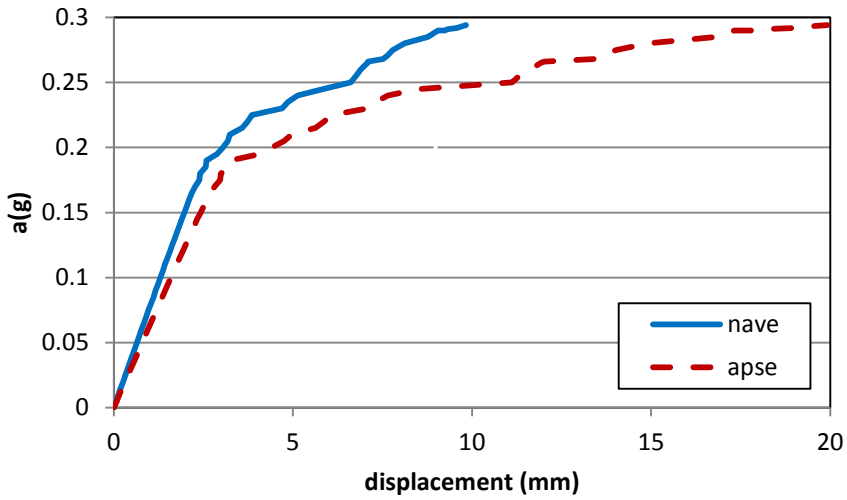

Figure 6.32 - Load-displacement curve, control nodes at the top of the apse and nave wall, -X direction.

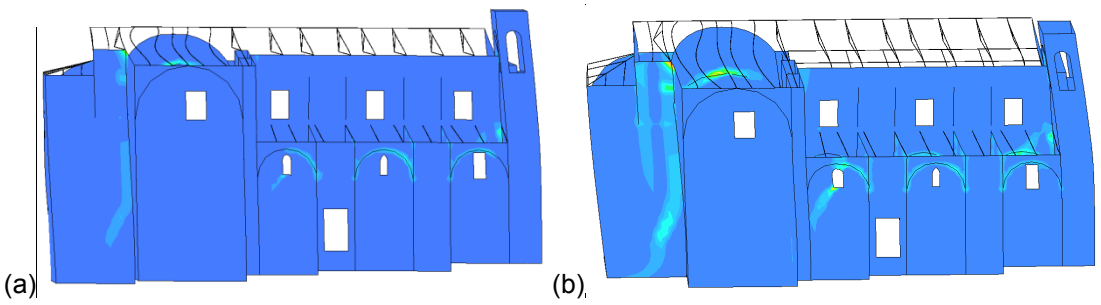

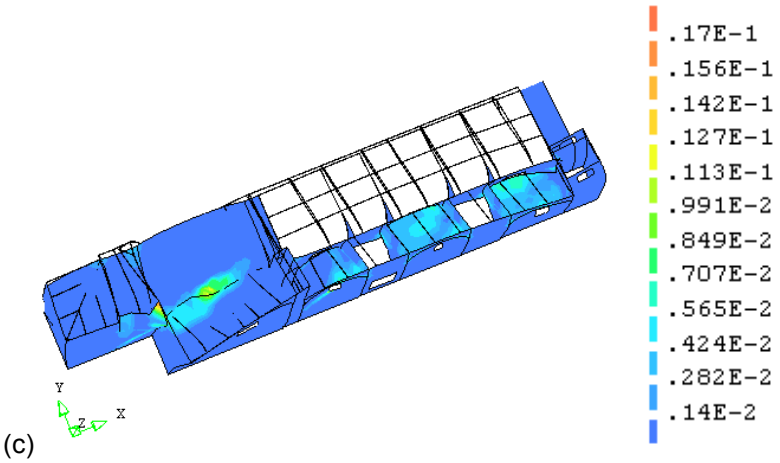

(c)

Figure 6.33 - Principal tensile strain distributions at the load factor of: (a) 0.25g and (b-c) ultimate state.

6.4.2.3 Transversal direction

In the Y direction, the model shows the lowest capacity among the three cases, with a maximum acceleration of 0.178g (Figure 6.34). At an acceleration of 0.16g, a horizontal large crack appears in the connection between the dome and the arch between the dome and the transept along with a diagonal crack crossing the arch (Figure 6.35 a). At the ultimate state, the observed collapse mechanisms are the collapse of the vaults in the transept and in the lateral chapel (Figure 6.35 b). The real structure actually developed these mechanisms presented by this FEM model during the 2009 earthquake (Figure 6.2 e and Figure 6.5 d).

The comparison is made between the timber model presented in Section 6.3.6.1.3. The load capacity is increased by 29.8%. The displacement capacity is decreased by 61.7 % at the top of the nave wall and increased by 8.0 % at the top of the transept wall.

In the three directions the reference model shows the lower load capacity than the timber model. However, more evident difference of the behaviour between the two models is seen in the transversal direction. When the ultimate displacement at the top of the nave wall is compared, the reference model shows much lower value than the timber model (42.6 mm vs. 68.9 mm). This is clearly due to the difference of the model: that is to say, the disconnection of the buttresses and the perimeter wall and also the existence of the roof trusses.

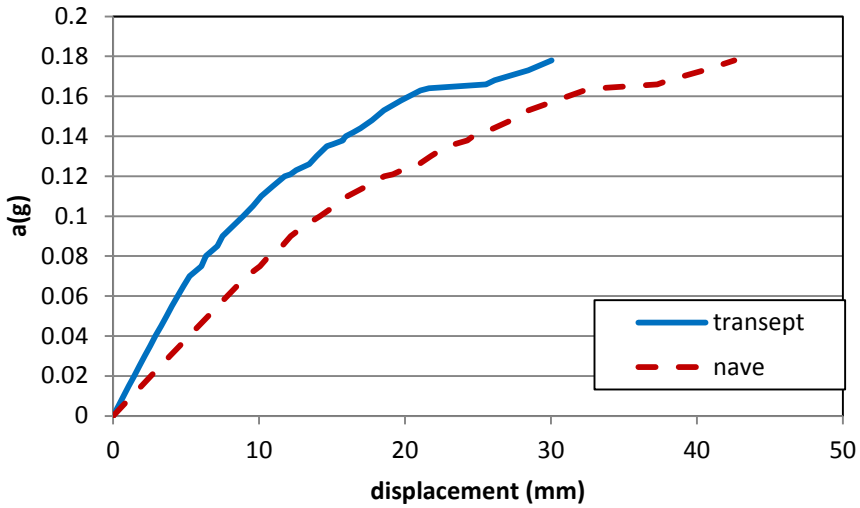

Figure 6.34 - Load-displacement curves, control nodes at top of the nave and transept wall, Y direction.

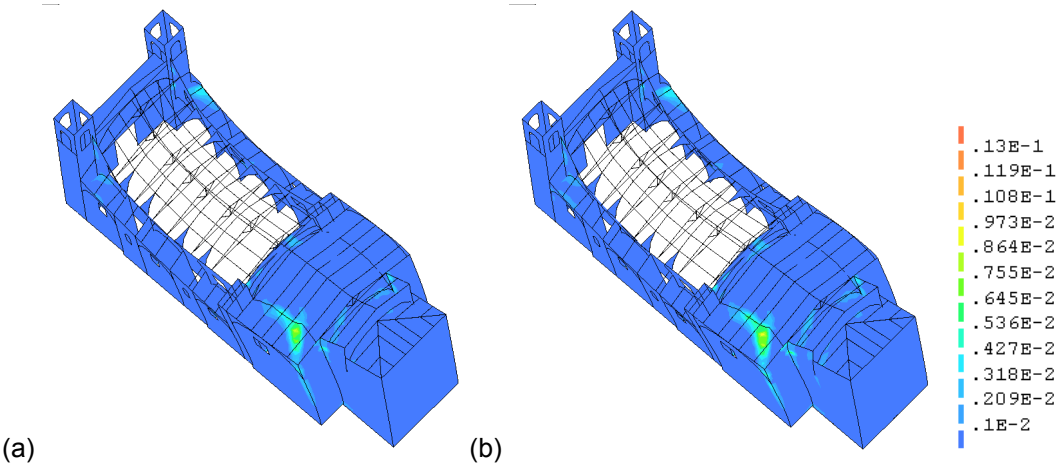

(a) (b)

Figure 6.35 - Principal tensile strain distributions, Y direction at the load factor of: (a) 0.166g and (b) ultimate state.

6.4.3 Parametric studies

6.4.3.1 Combination of parameters to analyse

Parametric studies are carried out for tensile strength (f_t), Young's modulus (E), tensile fracture energy (G_{ft}) and compressive strength (f_c). The values to be tested are determined by considering possible values of the mechanical parameters of masonry of stone masonry historical churches. The mechanical parameters of masonry have been discussed in Section 2.1.1.

In total, 10 FEM analyses are carried out (Table 6.2). The values in the squared boxes with the thick line are the parameters changed from the reference values. Most of the analyses are carried out in the +X direction since a more evident collapse mechanism is seen than in the other two directions, as discussed in Section 6.4.2. However, selected representative parameters are also examined in Y direction. As for the tensile strength, values of 5% (reference model), 1% and 0.1% of f_c are examined. Tensile fracture energy is adjusted properly in each case by assuming it linearly proportional to tensile

strength so that the same ductility is obtained. Thus, the value is reduced to 50 N/m, 10 N/m and 1 N/m according to the tensile strength. For Young's modulus, 500 (reference model), 250 and 100 times f_c are compared in the +X direction. In the Y direction, E=100xf_c is examined. For tensile fracture energy, 100, 50 (reference model) and 25 N/m are compared in the +X direction. As for compressive strength, 4 (reference model), 2 and 1 MPa are considered in the +X direction.

Table 6.2 – List of the parameter combinations

Parameter to study	-	***Tensile strength, f_t***		
Pushover direction	-	***+X direction***		***Y direction***
Case	**reference**	**1**	**2**	**3**
f_c **(MPa)**	4	4	4	4
E **(MPa)**	500xfc (2000)	500xfc (2000)	500xfc (2000)	500xf_c (2000)
f_t **(MPa)**	5%fc (0.2)	1%fc (0.02)	0.1%fc(0.002)	0.1%f_c (0.002)
G_{ft} **(N/m)**	50	10	1	1

Parameter to study	***Young's modulus, E***		
Pushover direction	***+X direction***		***Y direction***
Case	**4**	**5**	**6**
f_c **(MPa)**	4	4	4
E **(MPa)**	250xfc (1000)	100xfc (400)	100xf_c (400)
f_t **(MPa)**	5%fc (0.2)	5%fc (0.2)	5%f_c (0.2)
G_{ft} **(N/m)**	50	50	50

Parameter to study	***Tensile fracture energy, G_{ft}***		***Compressive strength, f_c***	
Pushover direction	***+X direction***		***+X direction***	
Case	**7**	**8**	**9**	**10**
f_c **(MPa)**	4	4	2	1
E **(MPa)**	500xf_c (2000)	500xf_c (2000)	500xf_c (2000)	500xf_c (2000)
f_t **(MPa)**	5%f_c (0.2)	5%f_c (0.2)	5%f_c (0.2)	5%f_c (0.2)
G_{ft} **(N/m)**	25	100	50	50

6.4.3.2 Influence of tensile strength (case 1, 2, 3)

6.4.3.2.1 Positive longitudinal direction

The case of f_t=1% and 0.1% of f_c is compared with f_t=5% of f_c. In case of f_t=1% of f_c, the load capacity is decreased from the reference case (f_t=5% of f_c) from 0.211g to 0.135g. However, the displacement capacity at top of the bell tower (30.5 mm) is similar to the reference case (30.6 mm) (Figure 6.36). The damage distribution pattern at the ultimate state indicates out-of-plane behaviour of the façade (Figure 6.37a). Although it is similar to the reference model discussed in Section 6.4.2.1 (Figure 6.31 b), part of the nave or perimeter wall is not taken by the façade (Figure 6.31 b). In the case of f_t=0.1% of f_c, the

model reaches nearly the state of collapse under the self-weight and the analysis stops at very low load factor (0.03g) (Figure 6.36). The ultimate state shows failure of the arch between the apse and the dome (Figure 6.37 b-c).

For the façade overturning, limit analysis is carried out to compare the capacity with FEM analysis. For San Marco church, the comparison of the results between limit analysis and pushover analysis has been also carried out in Section 6.3. The observed capacity by limit analysis is similar to that identified by FEM analysis when sufficiently low tensile strength is assumed in the FEM model. However, a local stress problem limits the capacity and keeps a full collapse mechanism from appearing when extremely small tensile strength is applied to a FEM model.

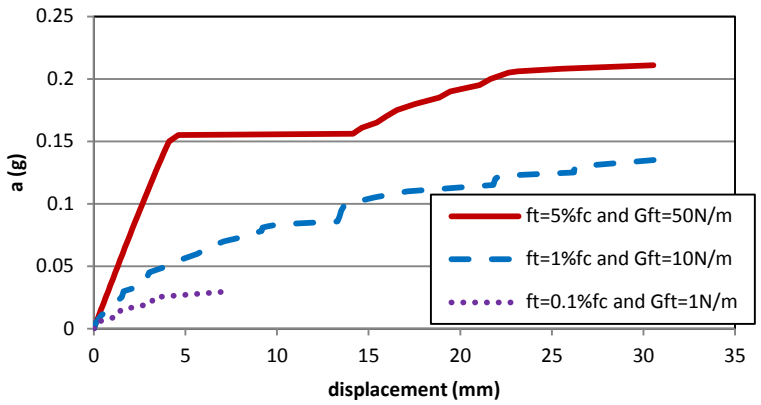

Figure 6.36 - Load-displacement curves, +X direction, control node at the top of the bell tower for different tensile strengths.

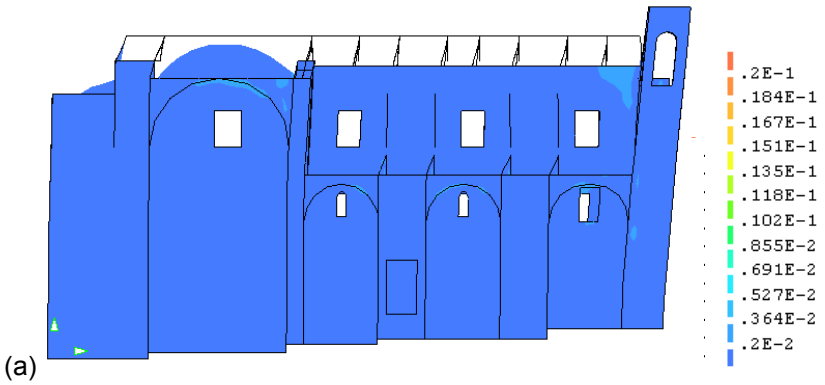

(a)

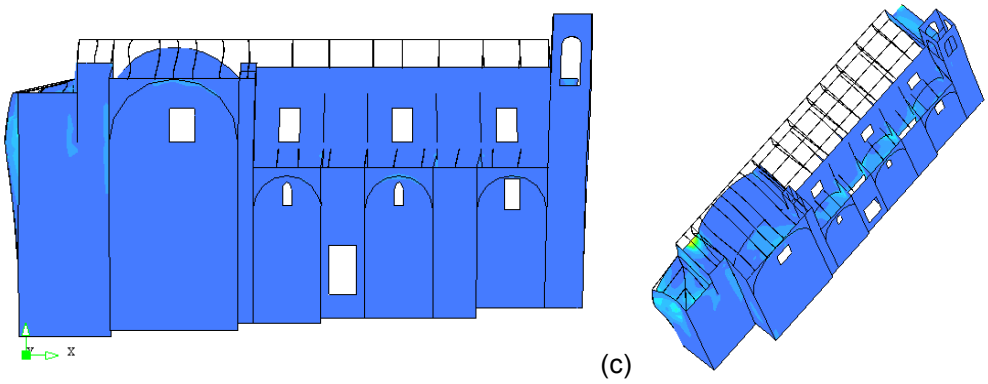

(b) (c)

Figure 6.37 - Principal tensile strain distributions in the ultimate state for different tensile strengths, +X direction: (a) f_t=1% of f_c and (b-c) f_t=0.1% of f_c.

6.4.3.2.2 Transversal direction

In the Y direction, the case of f_t=0.1% of f_c is compared with the reference case (f_t=5% of f_c). Compared to the reference case, a similar displacement capacity (30.0 mm vs. 30.7 mm) is observed while the load capacity is significantly decreased (from 0.178g to 0.068g) (Figure 6.38 a). The mechanism is different from the reference case that has been presented in Section 6.4.2.3 (Figure 6.35 b). Out-of-plane bending of the transept wall is seen with horizontal flexure failure due to a three-hinge arch mechanism in the thickness of the wall. The out-of-plane bending is observed also in the apse wall (Figure 6.38 b). Tensile strength is considerably influential on structural performance. The reduction of tensile strength implies reduction of displacement capacity, elastic stiffness and load capacity.

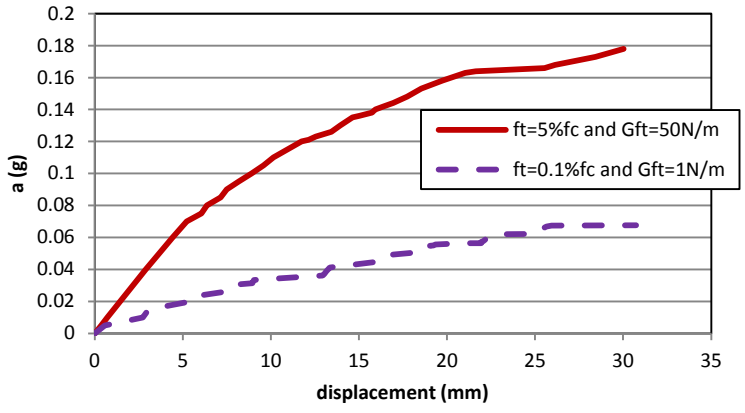

(a)

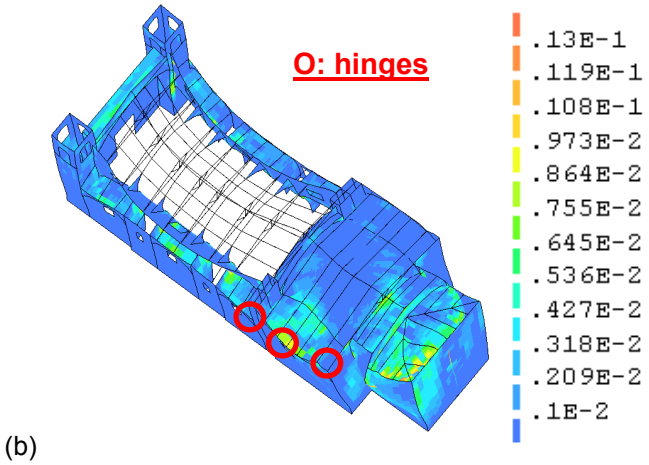

(b)

Figure 6.38 - (a) Load-displacement curves for different tensile strengths, Y direction, control node at the top of the transept wall and (b) Principal tensile strain distributions in the ultimate state (f_t=0.1% of f_c).

6.4.3.3 Influence of Young's modulus (case 4,5,6)

6.4.3.3.1 Positive longitudinal direction

Two cases (E=250x f_c, E=100x f_c) are compared with the reference case (E=500xf_c). A proportional relation between Young's modulus and load capacity is observed while an inversely proportional relation between Young's modulus and displacement capacity is seen (Figure 6.40). In the case of E=250xf_c, the mechanism is the overturning of the façade and the shear mechanism of the perimeter wall (Figure 6.41 a). In addition, noticeable damage is seen around the window of the nave wall although it does not seem to reach the ultimate mechanism. These damage distribution patterns are similar to those of the reference model as presented in Figure 6.31b. As for the model of 100xf_c, the mechanisms are overturning of the façade and shear mechanism in the perimeter wall like the case of 250xf_c (Figure 6.41b). In this case, damage is not observed around the window of the nave wall.

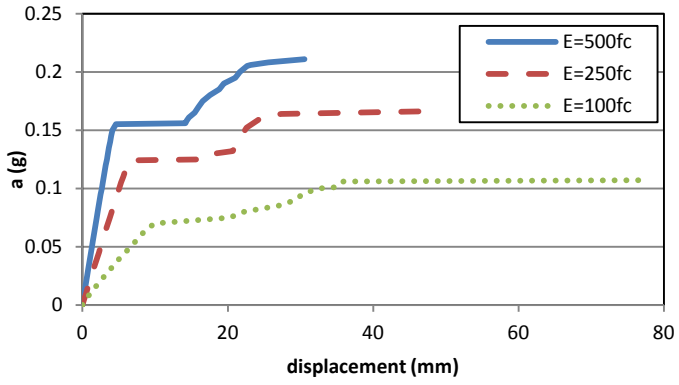

Figure 6.39 - Load-displacement curves, +X direction, control node at the top of the bell tower with different Young's moduli.

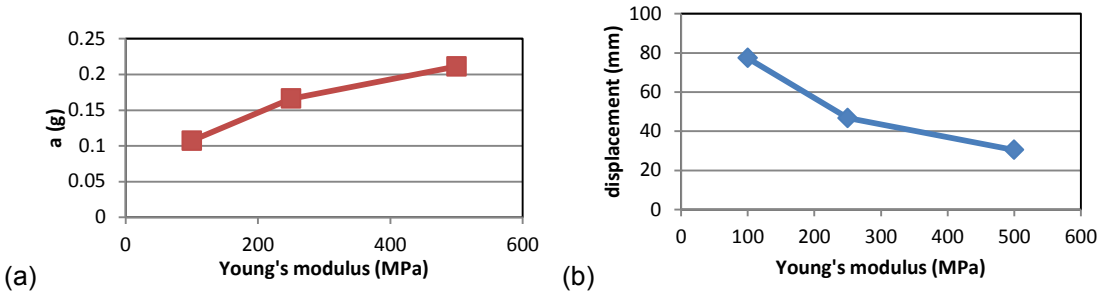

Figure 6.40 - Comparison of: (a) load capacity and (b) displacement capacity.

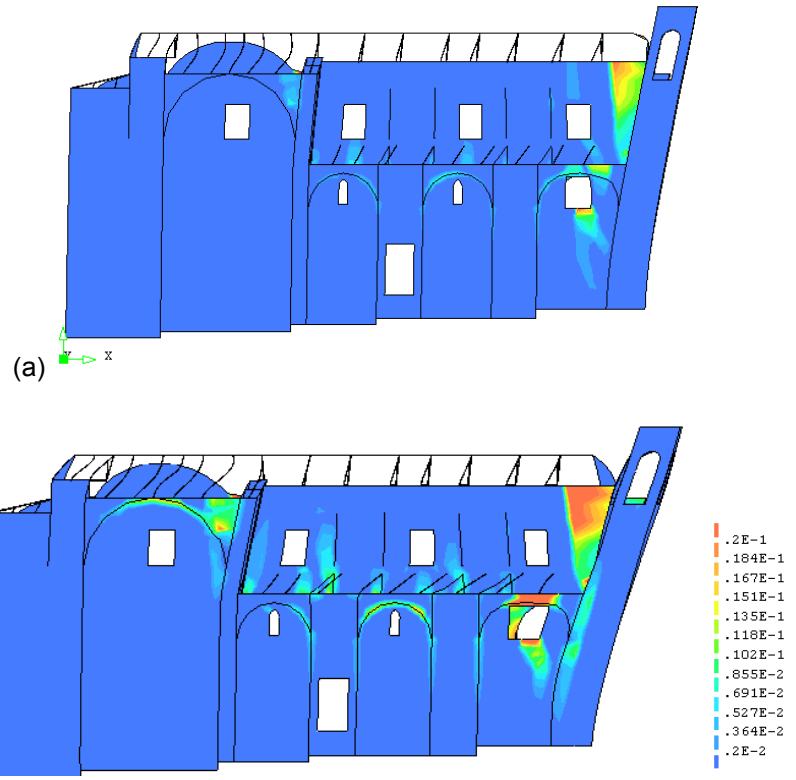

Figure 6.41 - Principal tensile strain distributions in the ultimate state, +X direction: (a) E=250xf_c and (b) E=100xf_c.

6.4.3.3.2 Transversal direction

In the Y direction, the model with E=100xf_c is analysed. The load capacity (0.125g) is decreased from the reference case (0.178g) (Figure 6.42). The mechanisms are overturning of the nave wall, collapse of the arch between the nave and the dome, collapse of the arch between the transept wall and the dome, out-of-plane bending of the apse wall and collapse of the vault of the lateral chapel (Figure 6.43). While the reference model shows concentration of damage especially in the transept area (Figure 6.35 b), the model of E=100xf_c shows damage distributed in the entire structure.

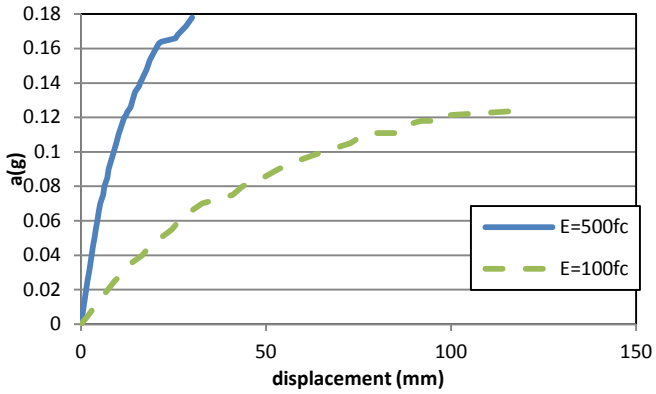

Figure 6.42 - Load-displacement curves, Y direction, control node at the top of the transept wall, different Young's moduli.

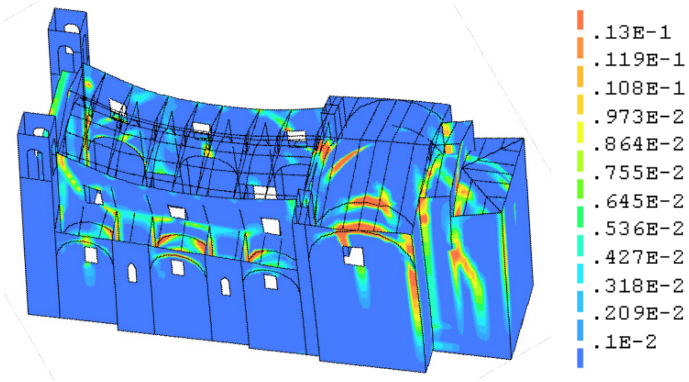

Figure 6.43 - Principal tensile strain distributions in the ultimate state, Y direction, E=100xf_c with a reduced deformation scale of 20.

6.4.3.4 Influence of tensile fracture energy (case 7, 8)

In the +X direction, 100, 50 and 25 N/m are compared. The value of tensile fracture energy does not have influence on elastic stiffness although Increase of the fracture energy causes increase of both load and displacement capacity (Figure 6.44). In fact, the relation between the capacity and tensile fracture energy is nearly linear proportional (Figure 6.45). In both cases, the mechanisms are not changed from the reference cases presented in Section 6.4.2.1 (Figure 6.31 b). They are the overturning of the apse and the shear mechanism in the apse wall and in the perimeter wall (Figure 6.46).

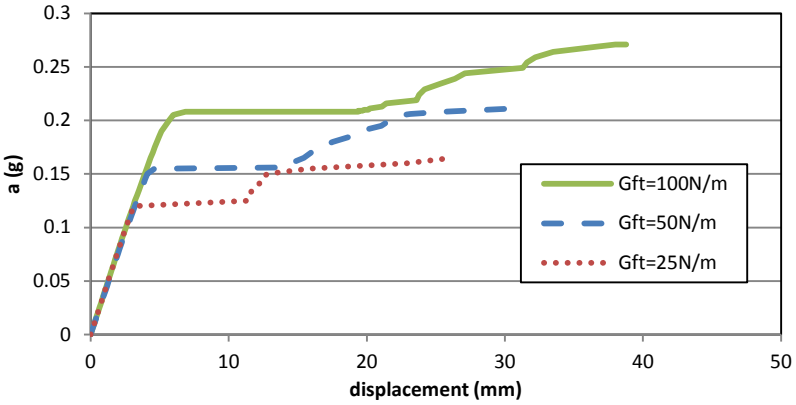

Figure 6.44 - Load-displacement curves, +X direction, control node at the top of the bell tower, for different fracture energies.

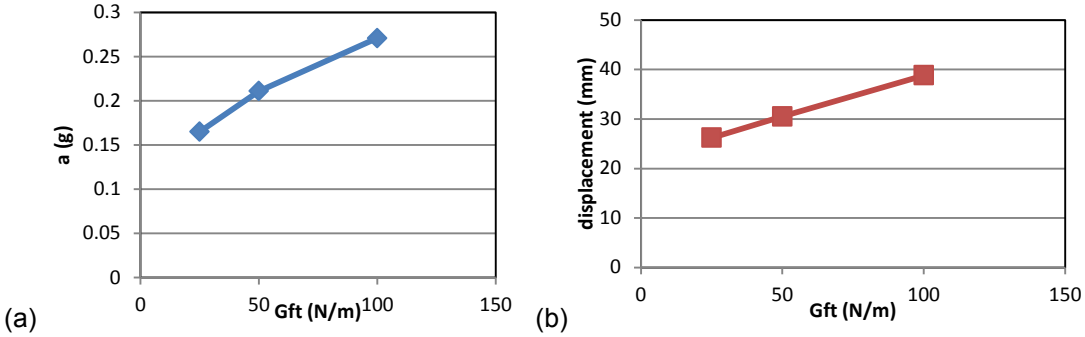

Figure 6.45 - Comparison of: (a) load capacity and (b) displacement capacity.

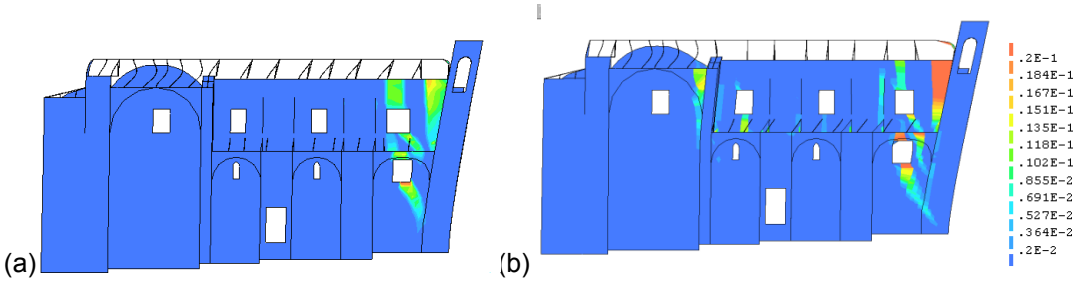

Figure 6.46 - Principal tensile strain distributions in the ultimate state, +X direction,: (a) G_{ft} =100 N/m and (b) G_{ft} =25 N/m.

6.4.3.5 Influence of compressive strength (case 9, 10)

In the +X direction, compressive strength of 2 and 1 MPa are compared with 4 MPa (reference case). Reduction of compressive strength from 4 MPa to 2 MPa shows some reduction of the load and displacement capacity (from 0.211g, 30.5 mm to 0.182g, 28.8 mm) (Figure 6.47). In these two cases, very similar damage patterns are seen; the collapse mechanism is overturning of the façade taking the part of the nave and perimeter wall (Figure 6.48 and see, Figure 6.31 b).

The reduction of compressive strength from 4 MPa to 1 MPa results in significant reduction of load capacity (from 0.211g to 0.115g). When the load-displacement curve at the top of the facade is observed (Figure 6.47), the model with f_c =1 MPa shows brittle behaviour. In fact different mechanism is observed from the reference case. The failure is due to crushing at the bottom of the façade.

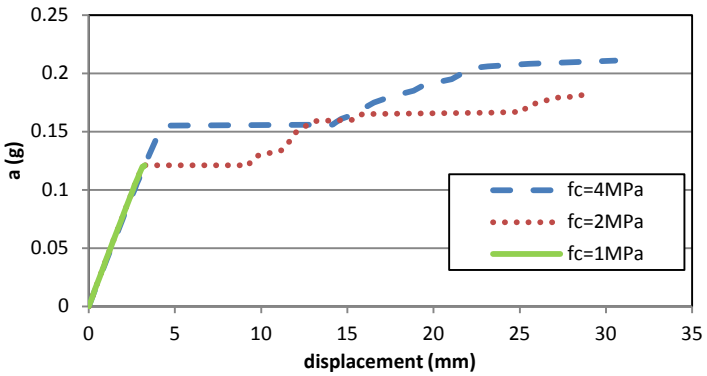

Figure 6.47 - Load-displacement curves for different compressive strengths, +X direction, control point at the top of the bell tower.

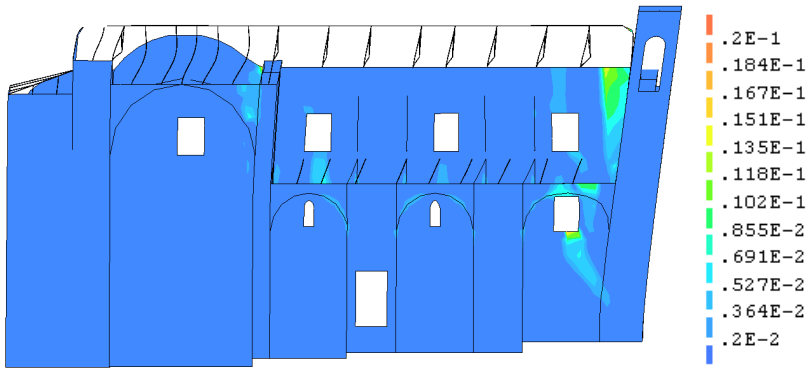

Figure 6.48 - Ultimate principal tensile strains, +X direction, f_c =2 MPa.

6.4.4 Assumption of weak interlocking

In this section, weakening interlocking is realised by applying lower values of mechanical properties to the corresponding connections. This assumption permits to simulate a structure which possesses weak interlocking between structural elements, as frequently observed in historical masonry structures. Damage and collapse mechanisms of masonry have been discussed in Section 2.2.2. This is a simplified procedure, compared to disconnecting structural elements and applying interface elements to their connections.

The considered parts with weak interlocking are indicated with the red lines in Figure 6.50. They are the connection between facade and nave (1), transept and nave (2) and transept and apse (3). Lower values are assigned to the width equal to 1 m in each side of the connection from the bottom to the top.

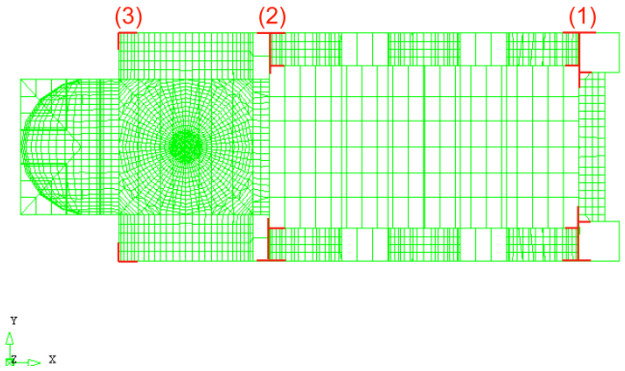

Figure 6.49 - Locations of the weakened connections.

Four combinations (type A, B, C, D) of properties are examined (Table 6.3). Except the compressive strength, the values of each parameter are reduced accordingly from type A to D. As for compressive strength it is set 2 MPa except for type C, for which a value of 0.5 MPa is used. . Regarding tensile strength and Young's modulus, type A and C possess the same proportion to the compressive strength (f_t=1% of fc and E=100x f_c). Type B has lower proportion of those values than type A and C. In terms of the values of tensile strength and Young's modulus, type B is an intermediate case between Type A and C. Type D is the case where the connections have extremely limited values of tensile strength and Young's modulus. The remaining part of the model maintains the reference values assumed for the masonry (f_c =4 MPa, f_t=5% of f_c, E=500x f_c and G_{ft}=50 N/m).

Table 6.3 – Combination of the values for the weakened connections.

	Type A	Type B	Type C	Type D
Compressive strength (MPa)	2	2	0.5	2
Tensile strength (MPa)	1% f_c (0.02)	0.5% f_c (0.01)	1% f_c (0.005)	0.1% f_c (0.002)
Young's modulus (MPa)	100× f_c (200)	50× f_c (100)	100× f_c (50)	10× f_c (20)
Fracture energy (N/m)	5	2.5	1.25	0.5

6.4.4.1 Positive longitudinal direction

The load capacity is decreased accordingly from type A to D (0.186g, 0.168g, 0.156g, 0.07g, respectively) compared to the reference case (0.211g) (Figure 6.51). When the load-displacement curves at the top of the façade are compared, the type A shows higher displacement capacity (60.6 mm) than the reference case (30.5 mm) (Figure 6.51 a). The type B and C show similar values (30.5 mm, 27.1 mm) to the reference case while the type D shows much lower value (7.6 mm). As for the load-displacement curves at the top of the nave wall, the type A (12.9 mm) shows higher displacement capacity than the reference case (4.5 mm) while type B, C, D show lower values (4.3 mm, 3.6 mm. 1.4 mm, respectively) (Figure 6.51 b). The elastic stiffness is not influenced by changing the properties of the connections from type A to type D. For type A, B and C, the collapse mechanism is the overturning of the façade (Figure 6.52 a-c). In these cases, the upper part of the nave wall is not drawn together unlike

the reference case (Figure 6.31 b). This means that lower tensile strength causes the overturning of the sole façade. As for type A, separation crack of the nave wall is also seen. For type D, the model is collapsed due to the local failure of the connection between the transept and apse (Figure 6.52 d).

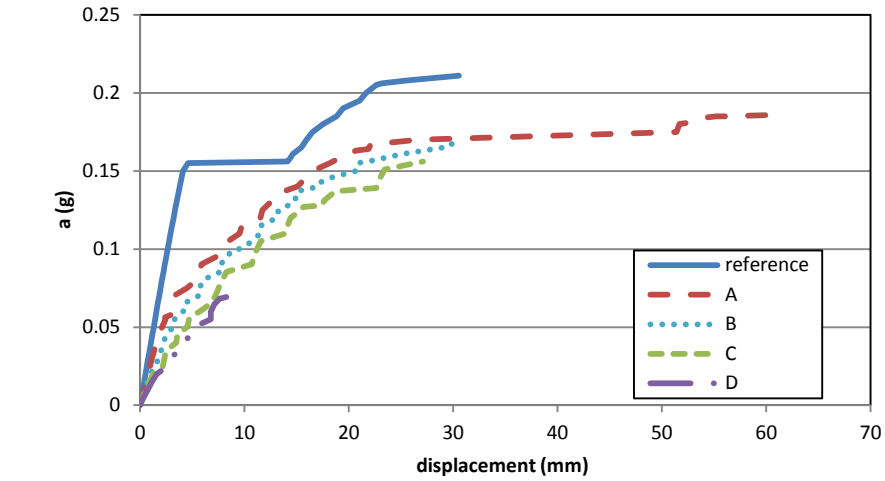

(a)

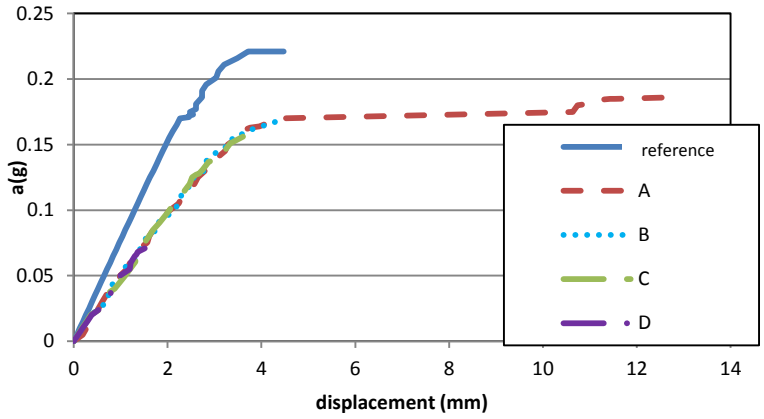

(b)

Figure 6.50 - Load-displacement curves for weakened connections between structural elements, +X direction, control node of: (a) at the top of the bell tower and (b) at the top of the nave wall.

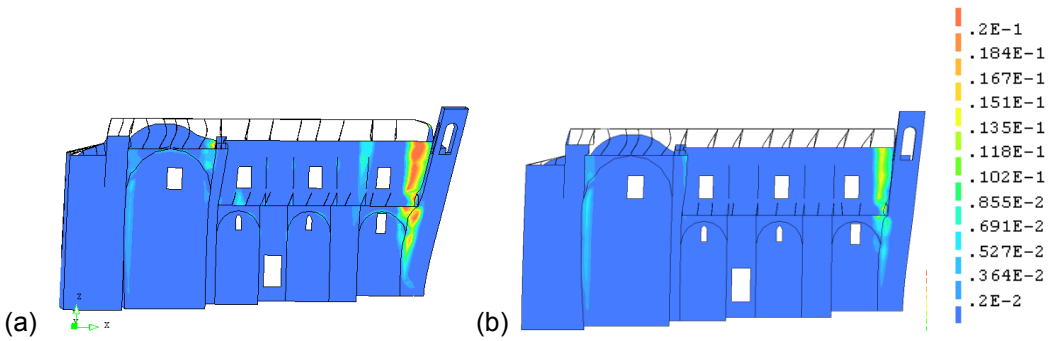

(a) (b)

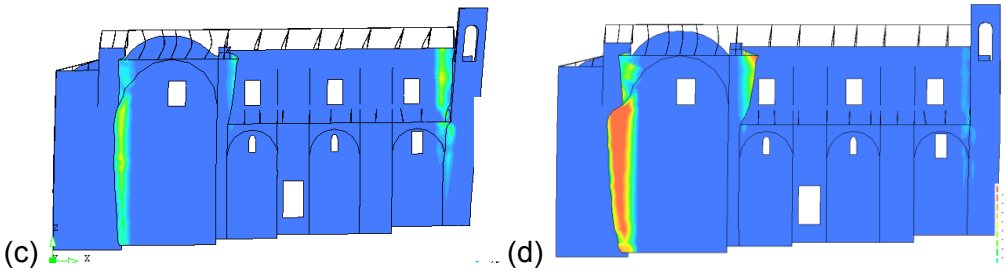

Figure 6.51 - Principal tensile strain distributions in the ultimate state, +X direction: (a) type A, (b) type B, (c) type C and (d) type D.

6.4.4.2 Negative longitudinal direction

In the -X direction, the models with weakened connections (type A, B, C, D) show much lower load capacity (0.187g, 0.135g, 0.135g, 0.131g, respectively) than the reference case (0.294g) (Figure 6.53). The load-displacement curves with the control node of the top of the apse wall show similar elastic stiffness for type B, C and D (Figure 6.53a). The load-displacement curve of the connection at the top of the transept wall represents different elastic stiffness (Figure 6.53 b). While the reference case (19.9 mm) shows much higher displacement capacity than the models with weakened connections (type A, B, C, D) (7.5 mm, 4.9 mm, 5.2 mm, 5.5 mm, respectively) at the top of the apse wall, the models with weakened connections (12.7 mm (type A), 9.4 mm (type D)) show higher value than the reference case (7.7 mm) at the top of the transept wall. Although the reference case has shown separation of the apse from the transept area at the ultimate state (Figure 6.33 b-c), local failure of the connection between the transept and apse wall is seen in each type (type A, B, C, D) (Figure 6.54 a-b). The figure of type B and C are not presented since they are very similar to that of type A.

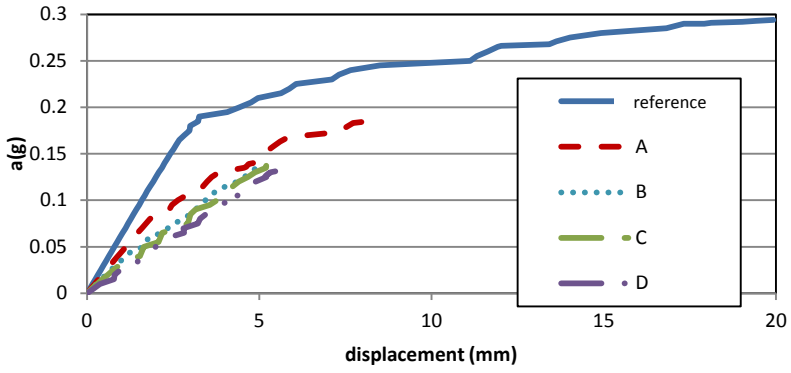

(a)

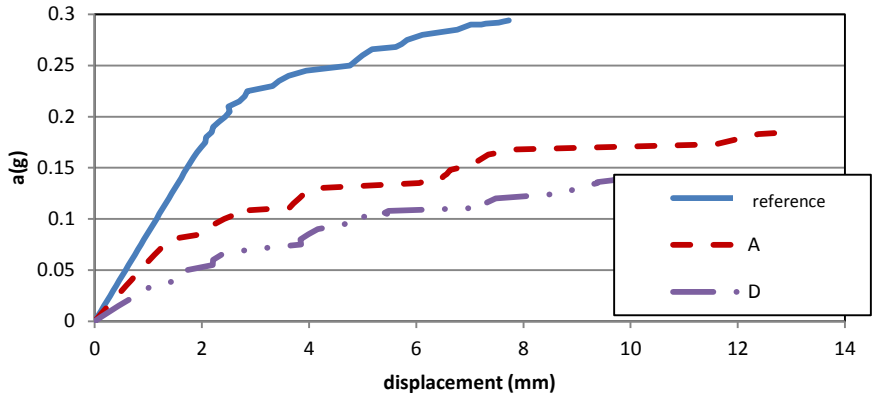

(b)

Figure 6.52 - Load-displacement curves for weakened connections between structural elements, -X direction: (a) at the top of the apse wall and (b) at the top of the transept wall.

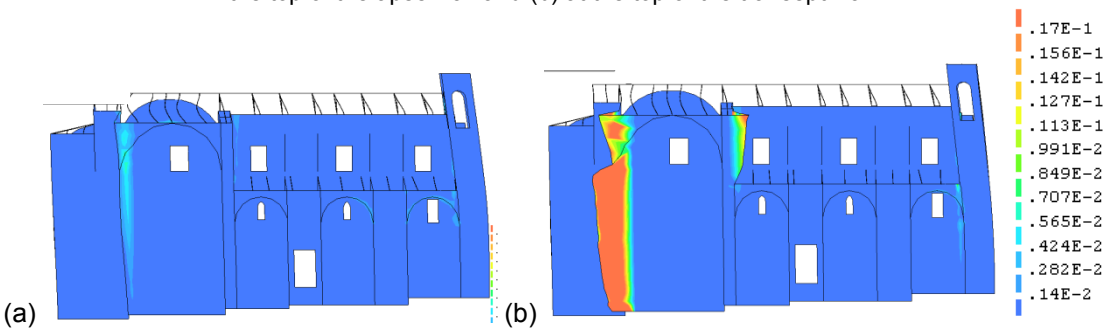

(a) (b)

Figure 6.53 - Principal tensile strain distributions in the ultimate state, -X direction: (a) type A and (b) type D.

6.4.4.3 Transversal direction

In the Y direction, the load capacity is decreased accordingly from type A to D (0.140g, 0.126g, 0.117g, 0.061g, respectively) (Figure 6.55). When the load-displacement curves at the top of the transept wall are compared, the type A, B, C (29.5 mm. 30.4 mm. 29.9 mm) show displacement capacity nearly equal to the reference case (30.0 mm) from type A to C while the type D represents lower value (23.0 mm). As for the load-displacement curves at the top of the nave wall, the type A, B, C show similar values (34.0 mm, 33.8 mm, 34.2 mm). They are lower than the reference case (40.5 mm). Type D demonstrates much lower value (15.1 mm) than the reference case. Collapse of the arch between the dome and the transept wall occurs in case of type A (Figure 6.56 a) like the reference case (Figure 6.35 b). The figure of type B and C are not presented since they are very similar to that of type A. As for type D, at the ultimate state, local failure is observed in the connection between the apse and the transept area (Figure 6.56 b).

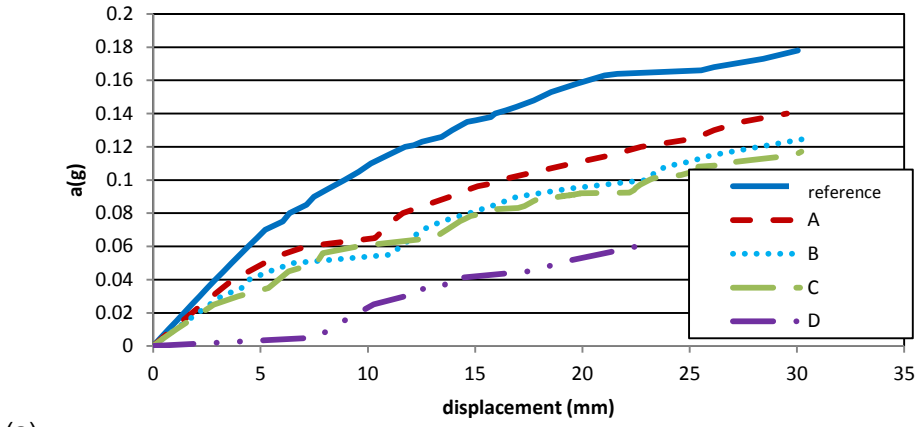

(a)

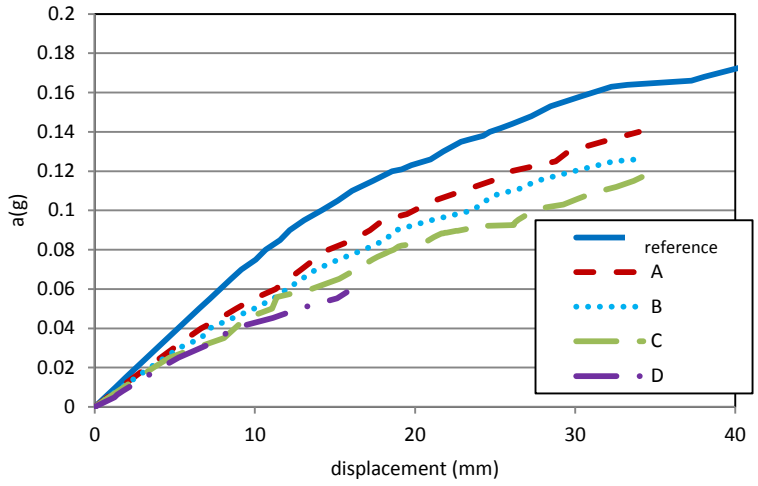

(b)

Figure 6.54 - Load-displacement curves, Y direction, control node at: (a) top of the transept wall and (b) top of the nave wall.

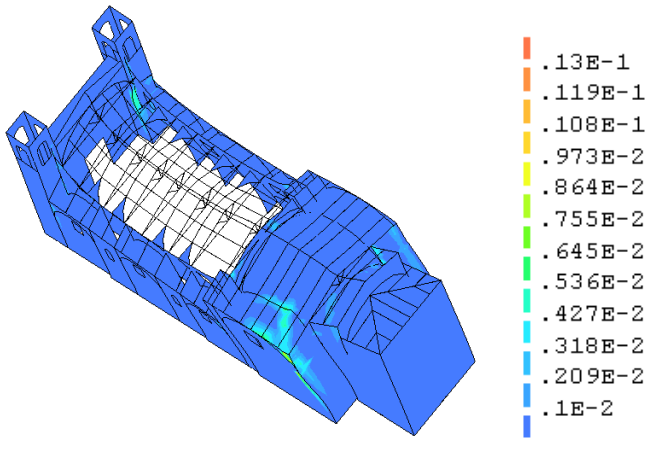

(a)

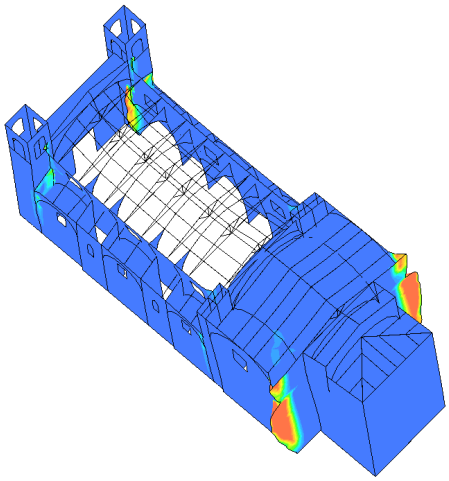

(b)

Figure 6.55 - Principal tensile strain distributions in the ultimate state, Y direction: (a) type A and (b) type D.

6.4.5 Comparison of different seismic-force-distribution patterns

From Section 6.4.2 to Section 6.4.5, the used force distribution pattern for pushover analysis has been proportional to the masses of the structure. In this section, two different force patterns (triangular and uniform distribution) are compared with the reference case (mass proportional pattern). Triangular load distribution is proposed as a simplified representation of a lateral load pattern proportional to the fundamental mode. The mechanical parameters for masonry and timber are equal to those of the reference case discussed in Section 6.4.2. The weakened connection discussed in Section 6.4.4 is not considered in this section. The analyses are carried out in the +X and Y directions.

6.4.5.1 Positive longitudinal direction

Comparison of the force distributions of the +X direction is presented in Figure 6.57. As for the mass-proportional distribution, concentration of the seismic forces is seen where the dome and the arches of the lateral chapels are located. In this figure, the mass-proportional force distribution has been presented by calculating the sum of the masses at the height of each 0.5 m.

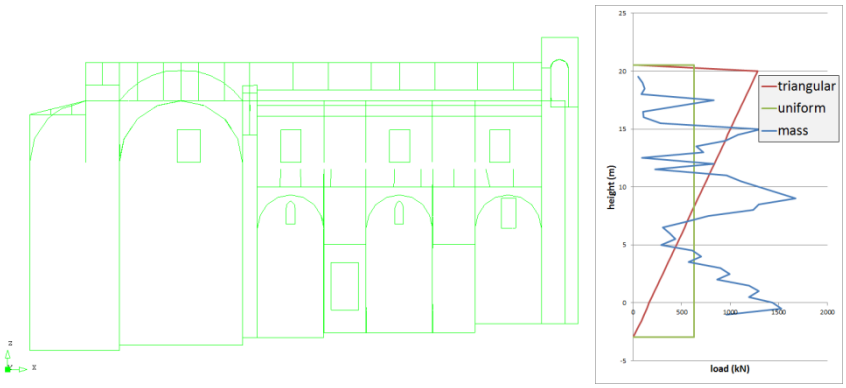

Figure 6.56 - Comparison of three seismic-force-distribution patterns in the +X direction.

The ultimate base shear-force of the triangular distribution (1,395 kN) is decreased to a great deal, compared to that of the mass-proportional case (6,674 kN) (Figure 6.58). As for the triangular distribution, the collapse mechanism is the overturning of the top part of the bell tower (Figure 6.59 a). It is probably due to the concentration of the seismic force at the top part of the model as discussed above (Figure 6.57). Regarding the uniformly-distributed case, the collapse occurs in the arch of the lateral chapel next to the transept area, instead of the overturning of the façade (Figure 6.59 b-c). This is due to higher concentration of the seismic force around the height of the arches of the lateral chapels than the uniformly-distributed case (Figure 6.57). This failure pattern is not observed in the mass-proportional lateral force pattern (Figure 6.31 b).

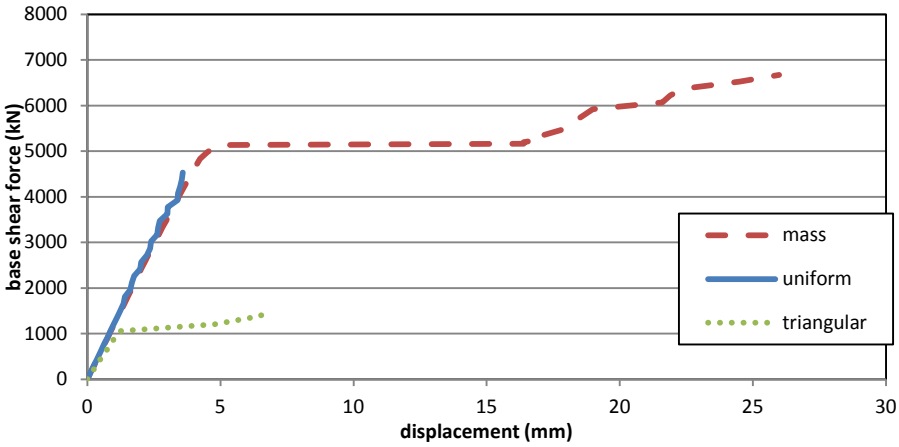

Figure 6.57 - Load-displacement curves, +X direction, control node at the middle of the tower, for different seismic force distributions

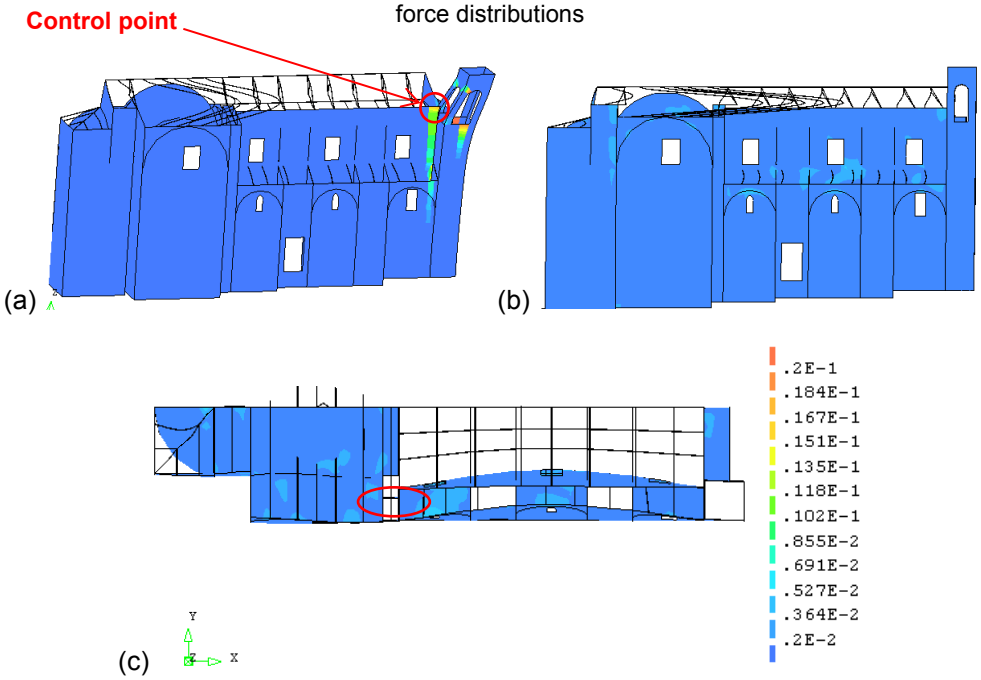

Figure 6.58 - Principal tensile strain distributions in the ultimate state, +X direction: (a) triangular and (b-c) triangular load distributions.

6.4.5.2 Transversal direction

In the Y direction, the case of uniform distribution is compared with the mass-proportional case. The former case represent lower load capacity (8758 kN) than the reference case (10751 kN), as seen in Figure 6.60. For the uniform distribution, the collapse mechanisms are the collapse of the arch, collapse of the dome and out-of-plane bending apse wall (Figure 6.61). Also noticeable damage is seen over the semi-dome and the arches around the dome. The entire apse and transept area is damaged since the seismic force is distributed equally over those areas compared to the reference case (mass-proportional distribution case) (Figure 6.35 b).

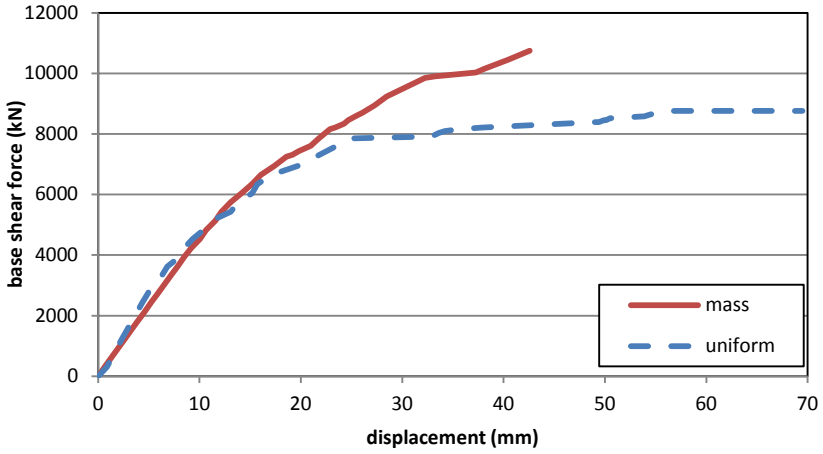

Figure 6.59 - Load-displacement curves, control node at the top of the nave wall, Y direction for different seismic force distributions.

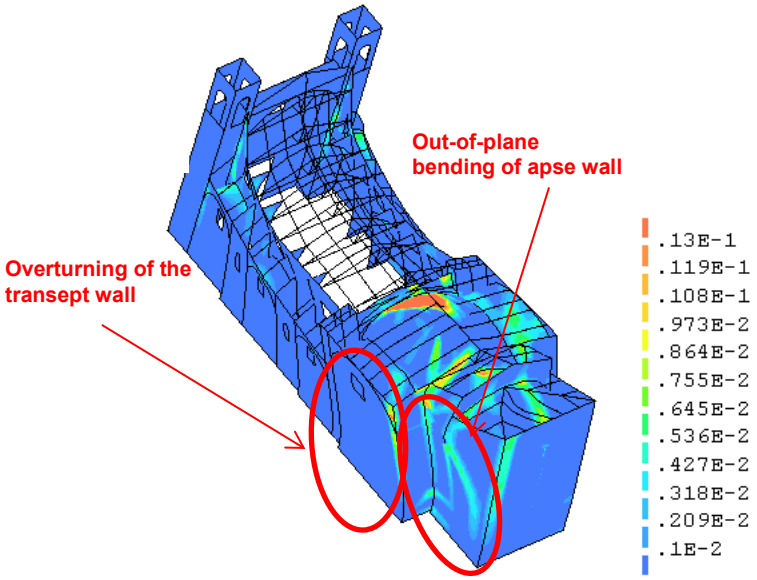

Figure 6.60 - Principal tensile strain distributions in the ultimate state, Y direction, for uniform distributions.

6.4.6 Comparison of models composed of shell and solid elements

From Section 6.4.2 to Section 6.4.6, the entire model composed of shell and beam elements has been used. In this section, comparison of the model is made between shell and solid elements. The analysis is carried out in the +X and Y direction. Partial models are used to save computational effort. For the analysis in the +X direction, a partial model representing the façade is used. For the analysis in the Y direction, a partial model representing a typical bay is considered.

6.4.6.1 Positive longitudinal direction

A partial model of the facade is prepared in shell or solid elements and compared. As for the shell-element model, the number of nodes is 1,011 and that of elements is 1,089. This model is taken from the entire model presented in Section 6.4.1. For the solid-element model, four-node tetrahedral elements with five integration points are considered. The number of nodes is 54,013 and that of elements is 264,347.

The solid-element model shows the load capacity equal to 0.255g while the shell-element one shows the capacity equal to 0.235g (Figure 6.62). The two models show a very similar distribution of damage (Figure 6.63). Damage is observed in the connection between the façade and the nave wall, around the window in the nave and perimeter wall and at the bottom of the perimeter wall. The damage in the connection between the façade and the nave wall indicates out-of-plane movement of the façade. In fact, the overturning of the façade also was observed in the real structure after the 2009 earthquake as discussed in Section 6.2.1 (Figure 6.5 a).

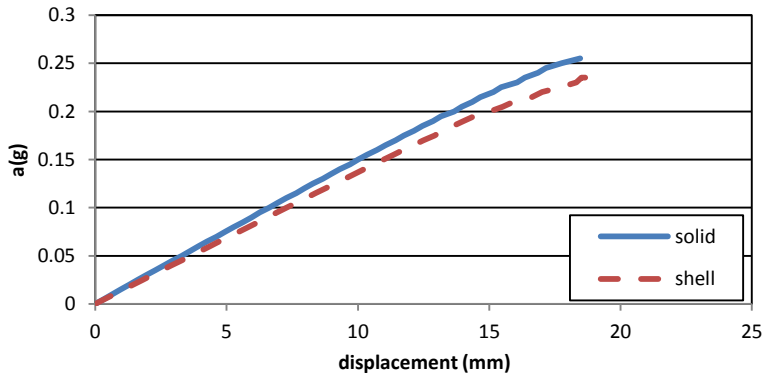

Figure 6.61 - Load-displacement curves, control node at the top of the tower, +X direction.

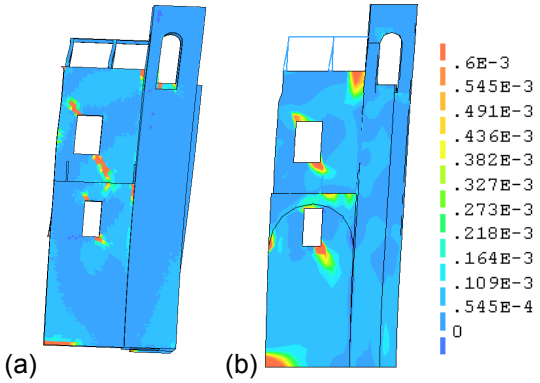

Figure 6.62 - Principal tensile strain distributions in the ultimate state: (a) solid- and (b) shell-element model.

6.4.6.2 Transversal direction

In the transversal direction, a partial model of a typical bay is used for the comparison. For, the shell-element model, the number of nodes is 1799 and that of elements is 1883. This model is taken from the entire model presented in Section 6.4.1. For the solid-element model, four-node tetrahedral elements with five integration points are considered. The number of nodes is 41,567 and that of elements is 191,940.

The load-displacement curve at the control point of the middle of the wall shows similar elastic stiffness (Figure 6.64). The ultimate acceleration is 0.185g for the solid element model and 0.16g for the shell element model. Although the difference is slightly larger than the case of the previous analyses of the façade, also in this case two models show similar failure pattern, consisting of the out-of-plane behaviour of the nave wall (Figure 6.65). The partial models indicate generation of hinges of the arch at its springing points. The hinges of the arches were placed almost at the same locations in the real structure after the 2009 earthquake, as presented in Section 6.3.4.3 (Figure 6.15 a). In addition, the base of the chapel wall shows high tensile strains due to the overturning of the nave wall. The actual structure also shows noticeable cracks at the base of the lateral chapels (Figure 6.15 b-c).

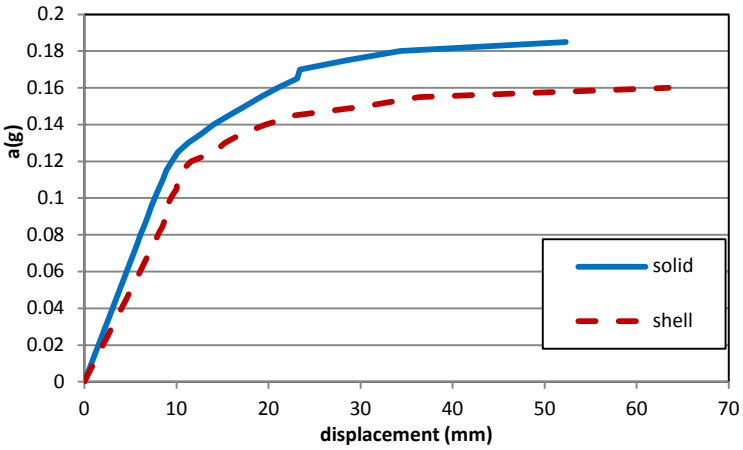

Figure 6.63 - Load-displacement curves in the Y direction, control node at the top of the buttress.

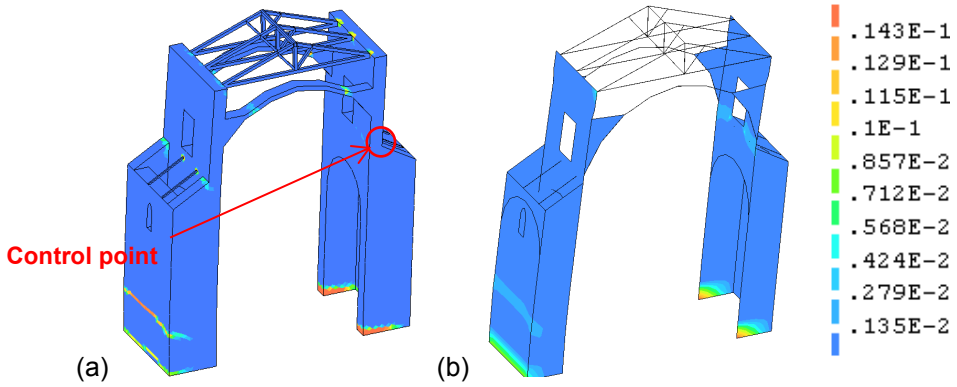

Figure 6.64 - Principal tensile strain distributions in the ultimate state: (a) solid- and (b) shell-element model.

6.5 Assessment of possible interventions

6.5.1 Introduction

In this section, possible interventions are proposed and examined. The proposals are made considering the damage and mechanisms observed after the earthquake as discussed in Section 6.2. The model with weakened interlocking, which has been studied in Section 6.4.5, is considered for the reference model (model before the intervention is installed). For the mechanical properties of the weakened interlocking, those of type A is assumed (f_c=2 MPa, f_t=0.01 MPa, E=200 MPa, G_{ft}=5 N/m).

In this study, two interventions are considered. They are tie system and combination of ties with improving interlocking. The improvement of the interlocking can be done through techniques such as injection, tie anchor or scuci-cuci. These intervention techniques have been investigated and executed extensively by various researchers and professionals such as Modena et al. (2002) and Valluzzi et al. (2004). The strengthening proposals are examined by pushover analysis. The used force distribution is proportional to the masses of the structure. As in the Section 6.3, considering the symmetry, half of the model is utilised for the analysis in the longitudinal direction with the appropriate boundary conditions introduced.

6.5.2 Tie system

The intervention with ties is evaluated. The locations and dimensions of the ties are determined considering the seismic behaviour of the reference model discussed in Section 6.4.5. In the +X direction overturning of the façade is considered (Figure 6.52a), in the –X direction, the local failure of the connection between the apse and transept wall and also the overturning of the apse (Figure 6.54 a) and in the Y direction, overturning of the transept wall (Figure 6.56 a).

The location of the ties is presented in Figure 6.66. Different colours are used to specify the function of each tie. Different numbers (8, 12 and 16) of longitudinal ties are located to avoid the overturning of the façade (blue lines in Figure 6.66 a-b). Different numbers (0, 3 or 6) of transversal ties are installed horizontally in the transept wall to constrict the connection between the apse and the transept (purple lines in Figure 6.66 c). The other ties are the same number in all the analyses as presented below. 7 transversal ties are for prevention of overturning of the nave wall (pink lines in Figure 6.66 b). 6 transversal ties are located to avoid the overturning of the transept wall (pink lines in Figure 6.66 c). 4 ties encircling the semi-dome are positioned in order to avoid its out-of-plane movement (green lines in Figure 6.66 a-b). 2 ties surrounding the apse wall are located to prevent out-of-plane movement (green lines in Figure 6.66 a-b). The diameter of the ties is assumed to be 70 mm. As for the semi-dome, instead of the tie, steel sheet is installed around the semi-dome to fit the steel well around its round shape. The section of the sheet is 20x200 mm^2. These design values are obtained through linear kinematic limit analysis on each mechanism (out-of-plane behaviour of the façade, transept and apse). Application of kinematic limit analysis has been discussed in Section 2.4.1.

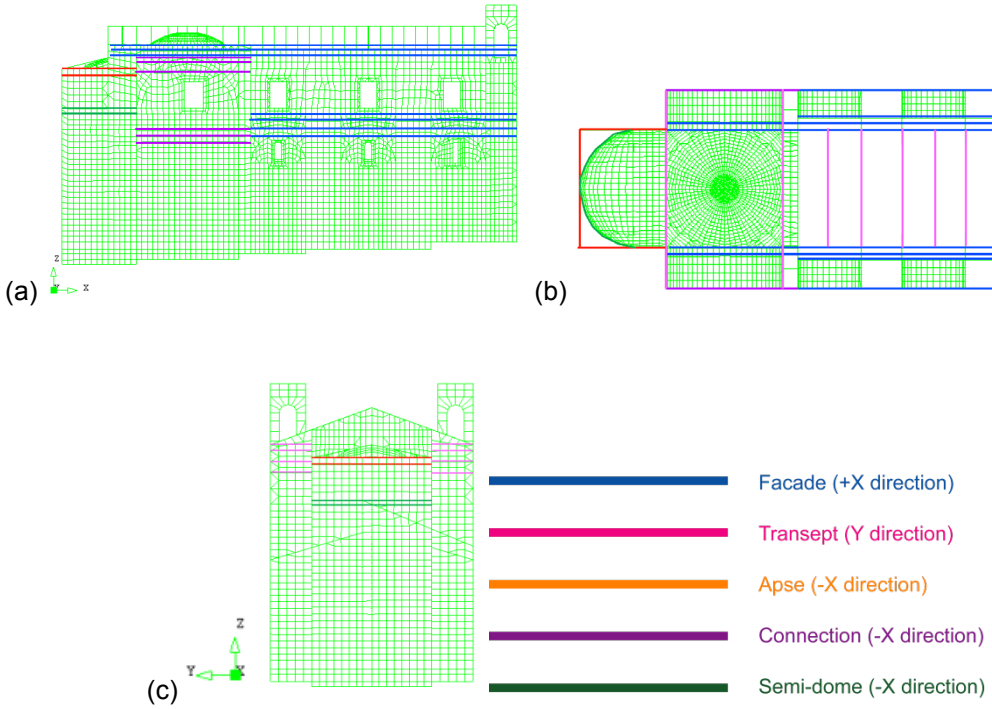

Figure 6.65 - Tie locations in FEM model (a) north elavation (b) plan and (c) east elevation.

The mechanical properties of the steel ties are presented in Table 6.4. Parameters of steel are determined as specified in the Spanish code (Spanish ministry of development 2011). Von Mises yield criterion is assumed. The ties are discretised with 3-D straight truss element.

Table 6.4 - Mechanical properties of steel tie.

Parameter	value
Density (kg/m^3)	7850
Compressive strength (MPa)	280
Young's modulus (GPa)	200
Tensile strength (MPa)	280
Poisson's ratio (-)	0.3

The connection between the ties and masonry walls is only made at the ends of the tie. The ties are represented by one element from one connection to another. Thus for instance, the tie between the façade and the transept is only constrained at the façade and the transept and is modelled with one FEM element. Linear elastic properties are assigned to the shell elements sharing the nodes with the ends of the ties to avoid local failure of those shell elements. For example, as for the tie connected to the top of the façade, the elements shown in light-blue-colour are assigned linear elastic properties (Figure 6.67). This assumption is justified since in principle an anchorage plate would be installed at the connection of the tie and the masonry wall.

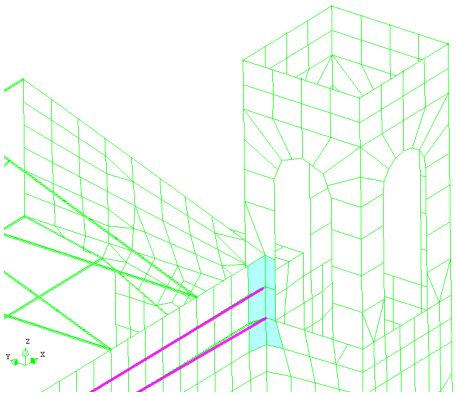

Figure 6.66 - Shell elements of linear elastic property at the connections with the tie.

6.5.2.1 Positive longitudinal direction

Three different cases (named 8, 12 and 16 ties) are studied. The name corresponds to the number of ties installed for the prevention of overturning of the façade. In the 8-tie case, 4 ties are put along the top of each longitudinal wall (blue lines in Figure 6.66 a-b). In the 12-tie case, in addition to the 8 ties, 2 ties are located along the top of each lateral chapel wall. In the 16-tie case, additional 2 ties are inserted along the top of each chapel roof. The Figure 6.66 a shows 16-tie case.

When the load-displacement curves at the top of the bell tower are compared, the three cases show the same stiffness to the reference case up to the load factor of 0.065g (Figure 6.68). The 8-tie case shows a horizontal branch at the load factor of 0.186g. Then the analysis stops at the same load factor. This case shows a lower displacement capacity (43.3 mm) than the reference case (61.6 mm). The 12-tie case

shows the same load capacity as the 8-tie and reference case although its displacement capacity (12.8 mm) is much lower than the reference case. The 16-tie case reaches higher load capacity (0.219g) than the reference case by 17.8 %. Its displacement capacity is equal to 21.3 mm. The 8-,12-tie and 16-tie cases represent the overturning of the façade (Figure 6.69 a-c), as seen in the reference case (Figure 6.52a). The 16-tie case also shows failure in the arches in the chapels (Figure 6.69 c-d).

Limit analysis is carried out to compare the capacity observed by FEM analysis. The application of limit analysis has been discussed in Section 2.4.1. For the façade overturning, the observed capacity by limit analysis is 0.151g, 0.183g and 0.216g, for 8-tie, 12-tie and 16-tie case respectively. Both limit analysis and FEM analysis have reported similar values.

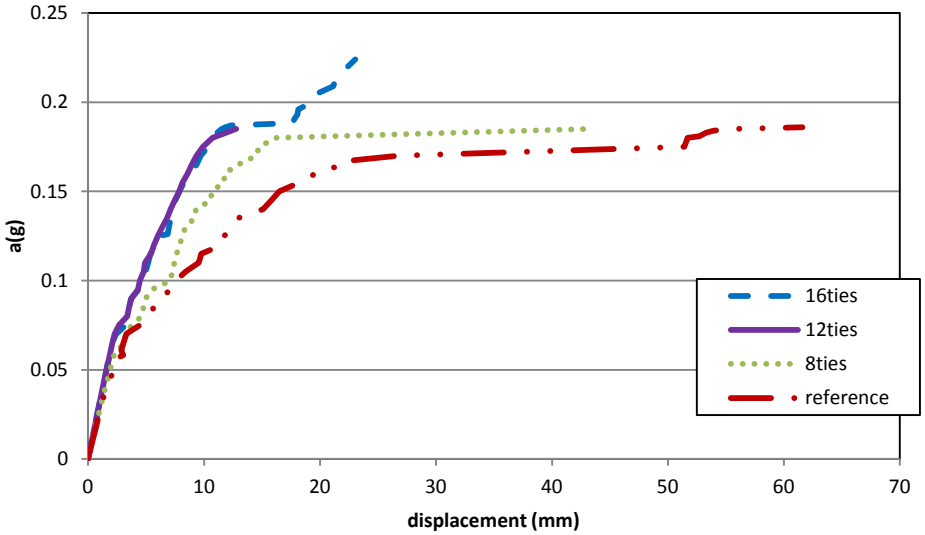

Figure 6.67 - Load-displacement curves, control point at the top of the bell tower, +X direction.

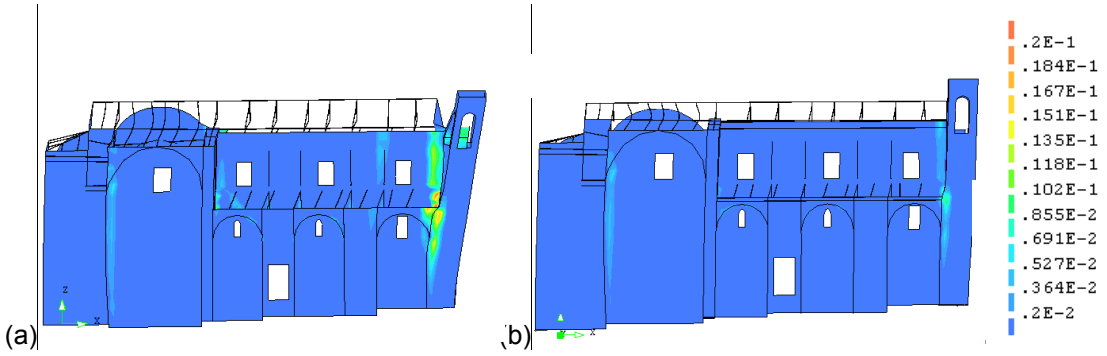

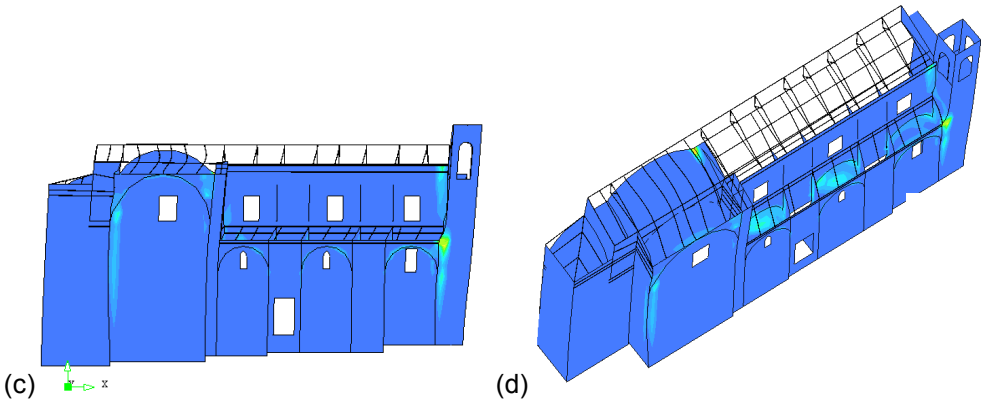

Figure 6.68 – Principal tensile strain distributions in the ultimate state, +X direction: (a) 8 ties, (b) 12 ties and (c-d) 16 ties.

6.5.2.2 Negative longitudinal direction

In the -X direction, three cases (0, 3 and 6 ties) are studied. They are different according to the number of ties located horizontally in the transept wall (purple lines in Figure 6.66 a). In the 0-tie case, no ties are located in the transept wall. The 3-tie case means that 3 ties are located along the top of the transept wall. In the 6-tie case, additional 3 ties are put in the middle of the transept wall. The Figure 6.66 a shows 6-tie case.

Two cases (0-, 3-tie case) represent similar load and displacement capacity at the top of the apse wall to the reference case (0.183g, 7.5 mm) (Figure 6.70). In the 3-tie case, the capacity is slightly increased (0.185g, 7.7 mm). These cases demonstrate local failure of the connection between the apse and transept wall (Figure 6.71 a-b), as is similar failure to the reference case (Figure 6.54 a). The 6-tie (0.234g, 11.1 mm) case shows higher capacity than the reference case by 27.9 %. More damage is seen in the 6-tie case at the ultimate state (Figure 6.71 c). Failure is observed in the arches of the lateral chapels (Figure 6.71 d).

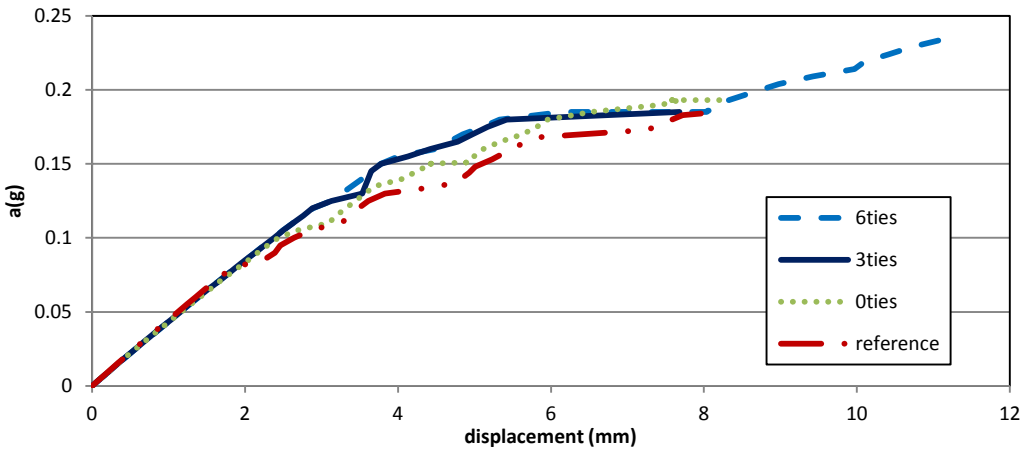

Figure 6.69 - Load-displacement curves, -X direction, control nodes (a) at the top of the apse wall and (b) at the top of the arch of the chapel 6 ties case.

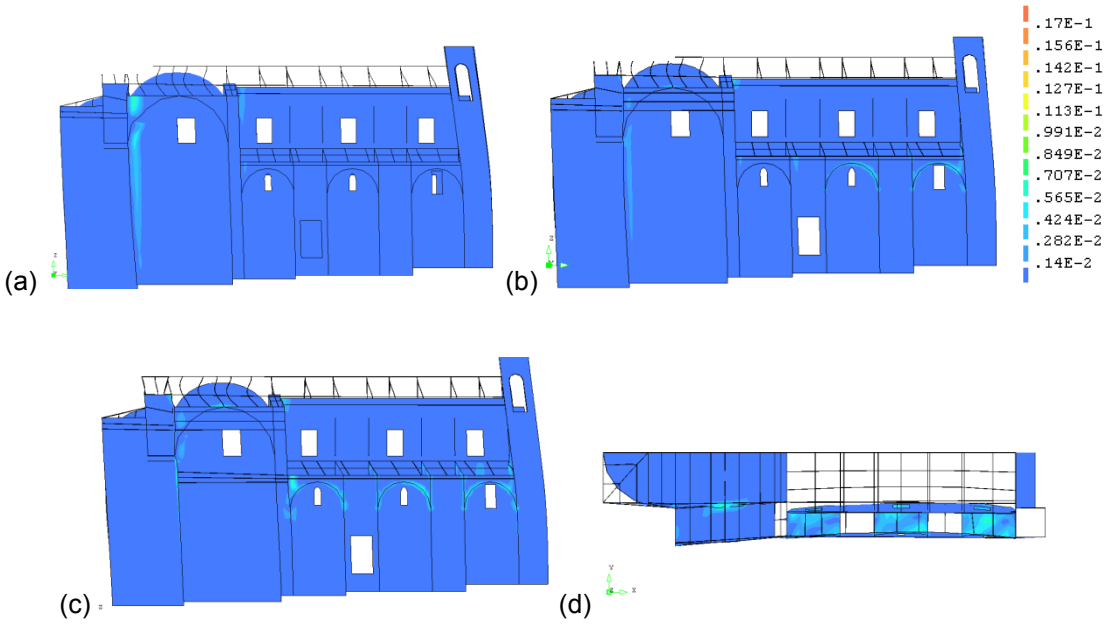

Figure 6.70 – Principal tensile strain distributions in the ultimate state, -X direction (a) 0 tie, (b) 3 ties and (c-d) 6 ties.

6.5.2.3 Transversal direction

In the Y direction, one case is studied. The tie intervention increases the capacity by 18.4 % (from 0.141g to 0.167g) (Figure 6.72). As for the load-displacement curves at the control node of the transept wall (Figure 6.72 a), similar stiffness is observed up to the load factor of 0.035g. At this load factor the reference case reaches nonlinear stage while the strengthened model reaches nonlinear stage at 0.06g. As for the load-displacement curve at the top of the nave wall (Figure 6.72 b), a similar shape is seen up to the load factor of 0.141g. The curve of the reference case stops at this load factor but that of the strengthened model continues till 0.167g. Decrease of the displacement capacity of the transept wall (from 29.5 mm to 23.4 mm) is observed from the reference case while increase of the displacement capacity of the nave wall occurs (from 34.0 mm to 47.0 mm). The same collapse mechanism is observed as in the reference case: collapse of the arch between the dome and the transept wall (Figure 6.73, Figure 6.56a). However, more damage in the nave wall is observed than in the reference case.

It has to be mentioned that the ties present working stresses lower than the yield value (280 MPa) in all the cases. For instance, 30 MPa is observed for the ultimate tensile stress of the tie between the façade and transept of 8-ties case in the +X direction.

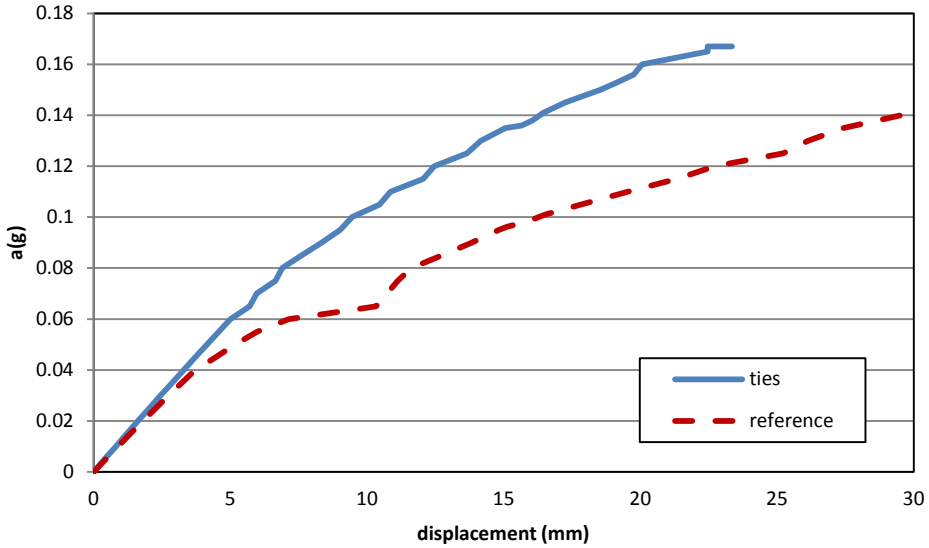

(a)

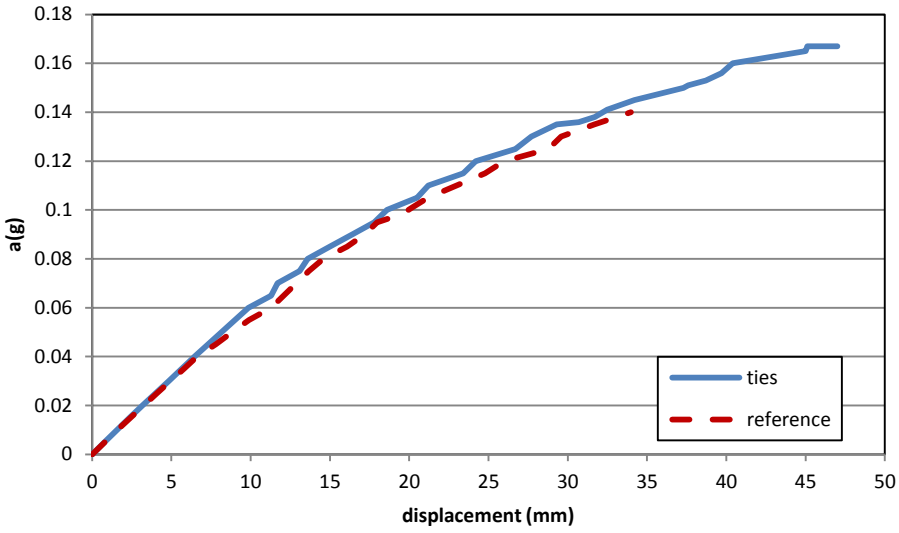

(b)

Figure 6.71 - Load-displacement curves, Y direction, control nodes (a) at the top of the transept wall and (b) at the middle-top of the nave wall.

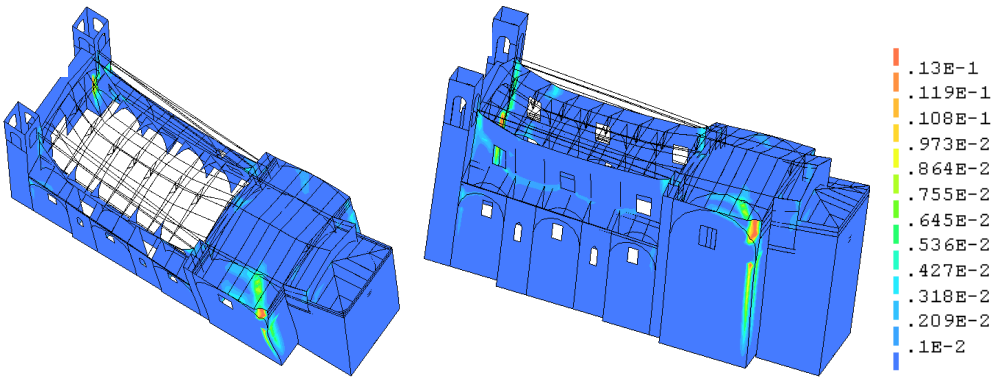

Figure 6.72 – Principal tensile strain distributions in the ultimate state, Y direction.

6.5.3 Combination of strengthening techniques (tie system and improvement of interlocking)

In this section, the combination of tie and improved connection technique is considered. The mechanical properties of the strengthened interlocking are assumed as 4 MPa in compressive strength, 2000 MPa (500 times f_c) in Young's modulus, 0.2 MPa (5% of f_c), and 50 N/m in fracture energy. These values are the same as those of the masonry of the rest parts of the structure.

The dimensions of mechanical properties of the ties are the same as those discussed in Section 6.5.2. The locations and numbers of ties are also the same as presented in Figure 6.66. As for the longitudinal ties against the overturning of the facade and longitudinal ties in the transept wall, the maximum number studied in Section 6.5.2.1 and 6.5.2.2 are considered. Thus, 16 longitudinal ties are located so as to avoid the overturning of the façade (blue lines in Figure 6.66 a-b). 6 transversal ties are installed along each side of the transept wall to constrict the connection between the apse and the transept (purple lines in Figure 6.66 c).

Behaviour of the model strengthened with combination of the two techniques is compared with that of the reference model (discussed in Section 6.4.5) and of the model strengthened with the tie system (discussed in Section 6.5.2).

6.5.3.1 Positive longitudinal direction

Compared to the reference case, the combination of the techniques increases the load capacity by 74.8 % (from 0.186g to 0.325g) (Figure 6.74). Compared to the tie-strengthened case (0.219g), the capacity is increased by 48.4 %. On the other hand, displacement capacity (24.1 mm) is decreased from the reference case (60.6 mm) and the tie-strengthened case (21.4 mm). At the ultimate state, out-of-plane behaviour of the façade and part of the nave wall from the nave is identified (Figure 6.75). This mechanism is similar to the reference case (Figure 6.52 a) while the tie-strengthened model represents the collapse of the arches in the chapels (Figure 6.69 c-d).

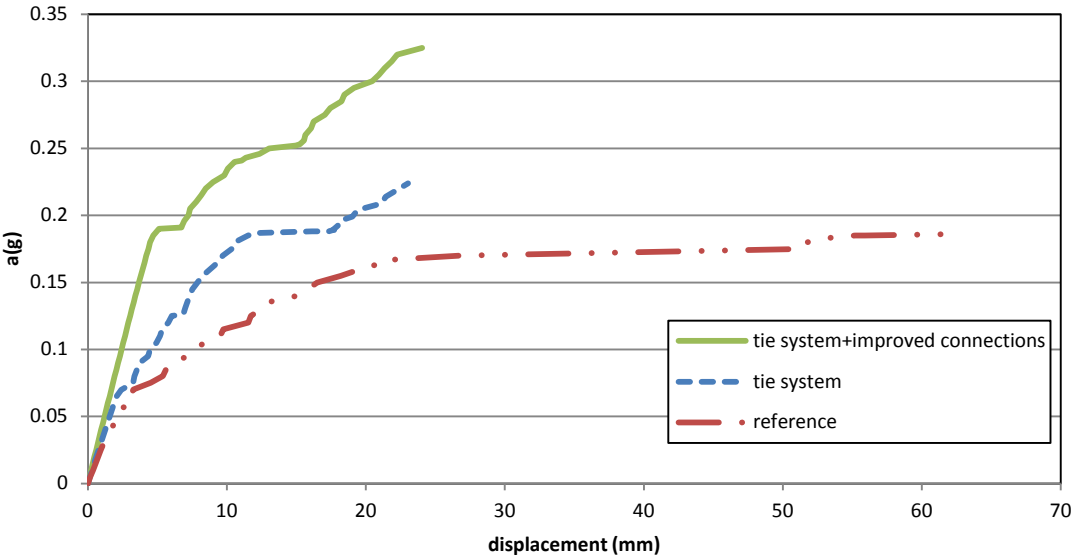

Figure 6.73 - Load-displacement curves, +X direction, control nodes at the top of the bell tower.

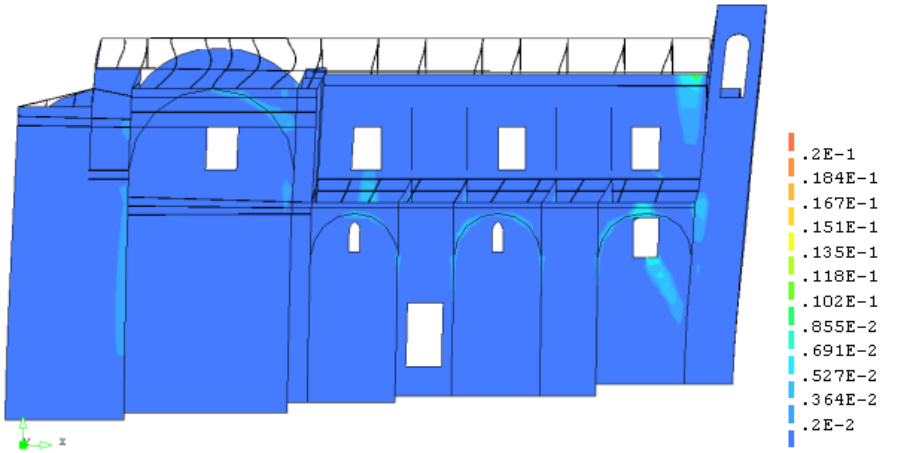

Figure 6.74 - Principal tensile strain distributions in the ultimate state, +X direction (a) basic tie with improved connections and (b) complete tie with improved connections.

6.5.3.2 Negative longitudinal direction

In the -X direction, the combination of the technique increases the capacity to 0.353g (Figure 6.76). Increase is observed from the reference case (0.187g) by 92.9 % and the tie-strengthened case (0.234g) by 50.9 %. As for the displacement capacity at the top of the apse wall, increase (16.3 mm) is seen from the reference case (8.7 mm) and tie-strengthened case (11.1 mm). At the ultimate state, the model shows overturning of the apse, collapse of the arches of the chapel and shear mechanism in the perimeter walls (Figure 6.77). Local failure of the connection is not observed unlike the reference case (Figure 6.54 a) and the tie-strengthened model (Figure 6.71 d).

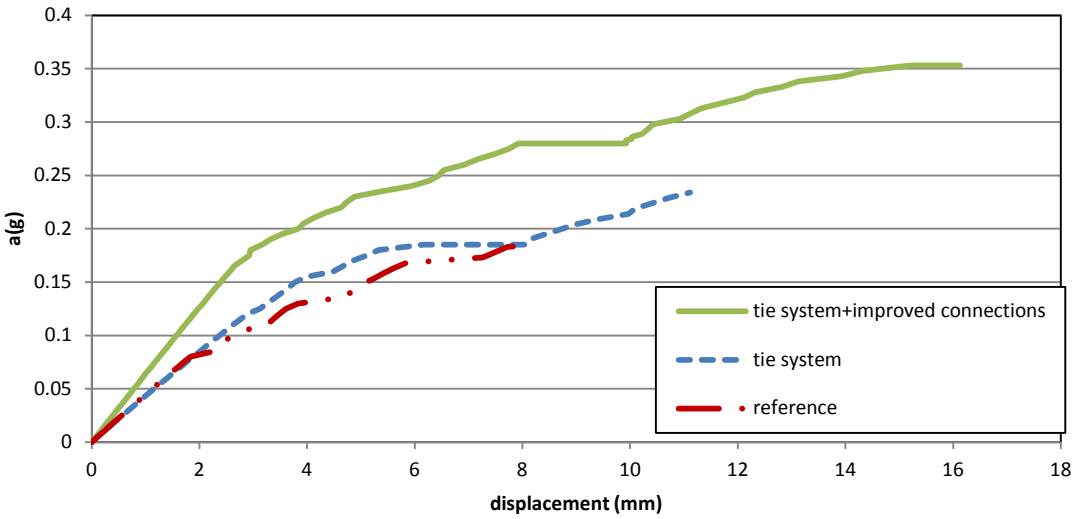

Figure 6.75 - Load-displacement curves, -X direction, control nodes at the top of the apse wall.

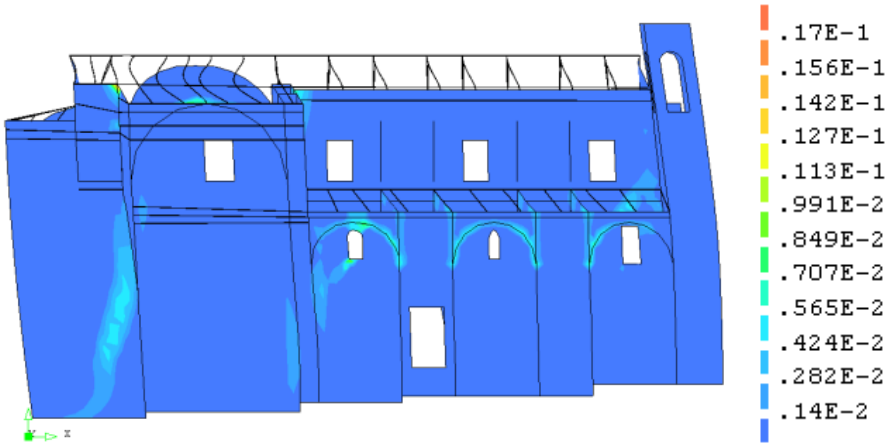

Figure 6.76 - Principal tensile strain distributions in the ultimate state, -X direction (a) basic tie with improved connections and (b) complete tie with improved connections.

6.5.3.3 Transversal direction

In the Y direction, the capacity of the combined technique model is equal to 0.221g (Figure 6.78). Compared to the reference case whose capacity is equal to 0.140g and the tie-strengthened case whose capacity is equal to 0.167g, it is increased by 56.7 % and by 32.3 %, respectively.

At the top of the transept wall, the combined technique model shows the displacement capacity equal to 31.0 mm. It is close to that of the reference case whose capacity is equal to 29.5 mm and is higher than that of the tie-strengthened model whose capacity is equal to 23.4 mm. At the top of the nave wall (Figure 6.78 b), the displacement capacity of the combined model is equal to 55.3 mm. It is higher than that of the reference case (34.0 mm) and of the tie-strengthened case (47.0 mm). At both control nodes, higher elastic stiffness is observed than the reference and tie-strengthened case. The technique-combined case (Figure 6.79) shows failure in the arch between the dome and the transept

wall which is also seen in the reference case (Figure 6.56 a) and also tie-strengthened case (Figure 6.73).

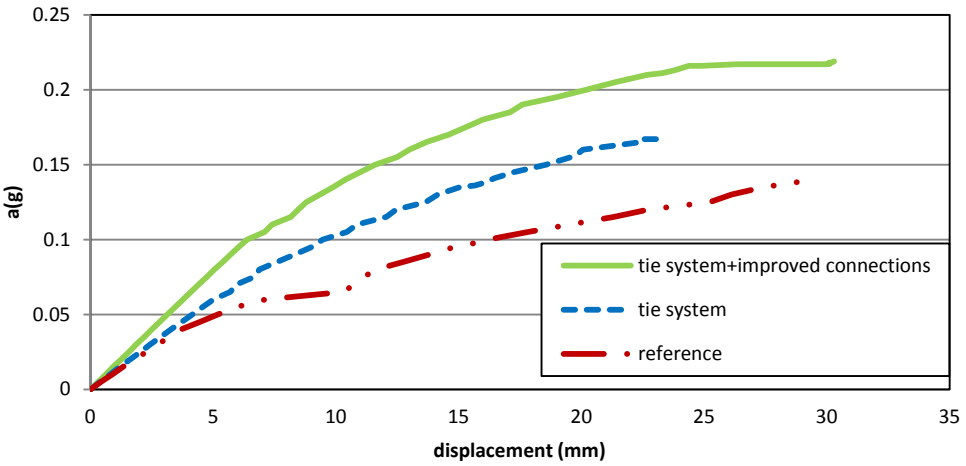

(a)

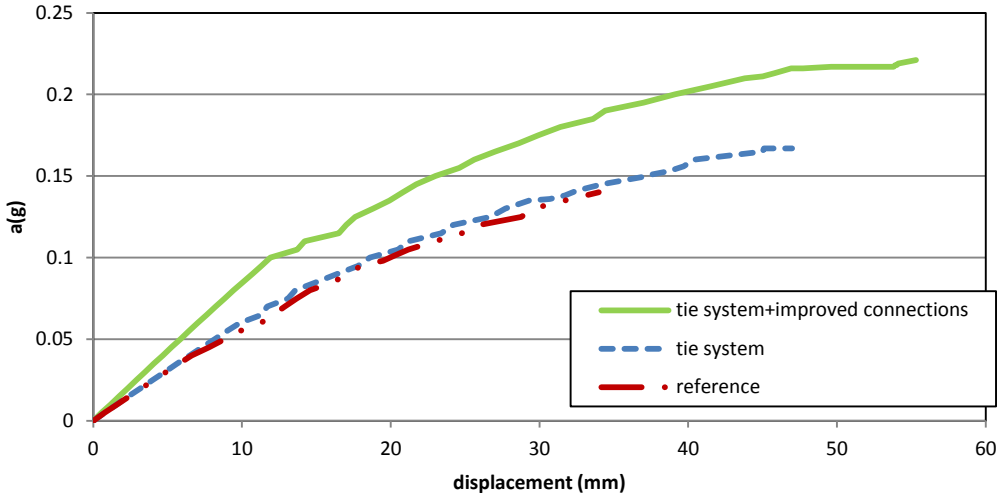

(b)

Figure 6.77 - Load-displacement curves, Y direction, control nodes at the top of: (a) transept wall and (b) nave wall.

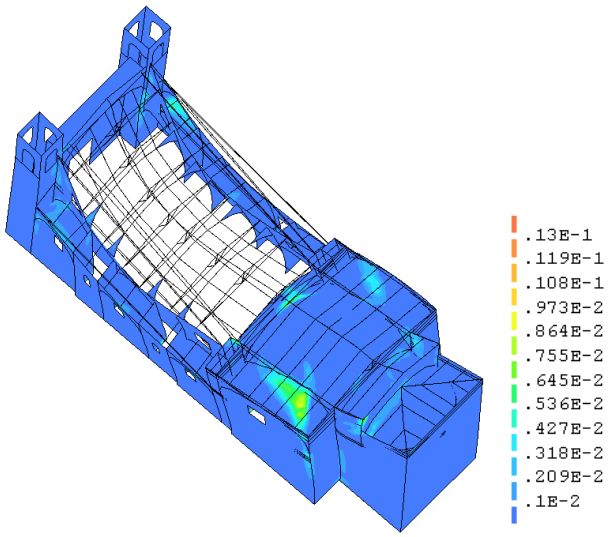

Figure 6.78 - Principal tensile strain distributions in the ultimate state, Y direction (a) basic tie with improved connection and (b) complete tie with improved connection.

6.6 Discussions

6.6.1 Prediction of real damage and collapse

The comparison of the results by the different methods permits some considerations on their performance and ability to predict the actually observed damage and collapse mechanisms. In fact, all the methods tested (limit analysis, FEM pushover analysis and NDA) have been able to predict most of the observed damage and collapse for a seismic demand similar to that caused by the real earthquake of 2009. The comparison among different methods has contributed to the understanding of the real performance of the structure and the collapse mechanisms actually activated. All methods satisfactorily predict, for a similar demand level, the overturning of the façade, the separation of the nave wall from the transept, the collapses of the chapel vaults, and the failure of arches of the transept, of the dome and the apse. FEM pushover and limit analysis have estimated similar maximum accelerations for most of the collapse mechanisms analysed, as in particular for the chapel vaults and nave wall (0.105 g vs. 0.099 g), the façade overturning (0.165 g vs. 0.167 g), overturning of the entire nave wall (0.125 g vs. 0.116 g) and the apse wall overturn (0.217 g vs. 0.218 g).

However, some of the collapses observed after the earthquake, as in particular that of the upper part of the south nave wall, have been only indirectly inferred from the outcome of these methods. In this particular case, all methods predict the failure of the chapel vaults on which the mentioned wall is supported. The failure of the wall can be understood, in all cases, as a logical consequence of the collapse of its supporting elements (the vaults). This understanding is consistent with the generation of the relieving arch at the upper part of the wall that can be recognised in the damaged structure (Figure 6.7 a). Nevertheless, the numerical methods utilised do not afford the simulation of the collapse of the wall itself because the structure already reaches an ultimate condition at the failure of the arches,

causing the analysis to stop at this point. A detailed simulation of the collapse of the wall would require a more sophisticated approach (such as DEM) overcoming the limitations of continuous mechanics in the description of realistic masonry collapsing mechanisms.

Limit analysis predicts the possibility of a full overturning of the whole nave wall which, in fact, did not occur. Also in this case, the failure of the lower portion of the wall (below the reliving arch) can be understood as a consequence of the failure of the supporting arches, which happens, according to this analysis, for a lower activation coefficient (0.099 g for the chapel vaults collapse against 0.116 g for the entire nave wall overturning). In the real structure, the whole nave wall overturning seems to have been prevented by the connections with the façade and transept walls. Hence, it should be noted that the decomposition of the structure into fully disconnected macro-elements may in some cases lead to predict mechanisms not actually occurring in the structure.

Comparison between pushover predictions through N2 method and NDA yields also some meaningful conclusions. Although pushover analysis represents similar damage distributions, compared to NDA, for both longitudinal and transverse earthquakes, NDA causes a more distributed damage pattern which, in some places, is more in agreement with the cracking observed in the real structure. Some of the mechanisms, such as those involving the collapse of the chapel vaults, the nave wall and the arches of the transept are better represented by NDA than by pushover analysis.

The maximum displacement values provided by NDA are close to the ones yielded by pushover analysis at the performance point by N2 method for the façade overturning (31 mm for NDA and 26 mm for pushover). However, a significant discrepancy has been obtained for the displacements associated to the nave wall collapse which, as mentioned, is in fact a mechanism not adequately simulated by these methods.

6.6.2 Influence of wall-wall connections

In spite of the agreement obtained between the pushover and the limit analysis results, in general, limit analysis shows to be more conservative. This fact can be understood as a consequence of the decomposition of the structure into fully disconnected macro-elements, while for the FEM approaches the analysis have been carried out on global models with assumed initially intact connections. The comparison with the real damage and collapse mechanisms suggests that the real situation may be an intermediate one between those described by the macro-elements and the global models. In reality, the connections of the structure (as in particular those between the different perpendicular walls) may have been showing some degree of imperfection due to construction defects or initial cracking and deterioration. The results of the FEM analysis might be improved by artificially weakening these connections in the models. Application of weakened connections has been discussed in Section 6.4.5. However, this possibility brings out the need for a detailed characterisation and accurate mechanical

modelling of the imperfect connections, which in practice are hardly attainable in an objective way. Actually, some additional analysis were carried out with initially weakened connections, and it was obtained, as expected, that the results tended to become more similar to the limit analysis' ones.

In any case, the above considerations highlight the need for a previous detailed inspection and recognition of the construction features and condition of the connections. Specifically, lack of connection (or weak connection) linked to architectural alterations or different construction phases should be carefully assessed. In the case of San Marco, one of the aspects having largely influenced on the simulated response of the building is found in the disconnection between the buttresses and the perimeter north and south walls. It has been observed that neglecting this construction feature leads to largely unsafe results. As should be expected, FEM analyses on a model with perfect buttress-wall connection produce more optimistic results on the seismic response of the building. For instance, +X direction pushover analysis of the model with perfect connection provides a load capacity of 0.193 g that is higher than that obtained by the model with disconnections (0.165 g).

Nonlinear geometric effects have been found significant for the study of the earthquake in the transverse direction. This influence is due to the deformation of the nave walls with respect to the buttresses on which they are supported. According to the pushover analysis performed, considering geometric nonlinearity caused a reduction of 15 % on the displacement capacity in the transverse direction, while it did not sensibly affect the load capacity. Therefore, and even if the structure does not show significantly slender members, considering geometric nonlinear analysis seems advisable in the seismic assessment of similar structures.

6.6.3 Study of the RC interventions carried out in 1970

Comparison of the state before and after the RC intervention of 1970 has been carried out. The former model has been named *timber model* and the latter has been *RC model*. Comparison of the two models has been conducted by pushover analysis and NDA. It has been found that the RC intervention produced a decreased capacity. The large weight of RC has resulted in the decrease of the capacity rather than improving structural performance. NDA has shown this effect of the RC elements more clearly than pushover analysis. By pushover analysis, the two models have shown similar performance in the negative and positive longitudinal direction. However, in the transversal direction, the timber model has shown more optimistic results than the RC model. The RC model has shown higher concentration of damage in the nave area than the timber model. It is due to the larger mass of the roof of the RC model. By NDA, in both longitudinal and transversal directions, the timber model has shown higher displacement capacity than RC model. In the transversal direction, the analysis of the RC model (2.23 seconds) has stopped earlier than that of the reference model (2.38 seconds). It also has to be added that NDA of the timber model continues after it reached the maximum absolute displacement while that of the RC model stops at the maximum absolute displacement.

A brief comment is made on the properties of RC. The properties of the RC members in masonry structures need to be determined carefully since the parameters of RC may be crucial for the performance of the entire structure. To study this influence, a parametric study has been carried out. Four cases have been studied. They were three cases of different compressive strength (30 MPa, 20 MPa, 10 MPa) and one case of linear elastic property. The study has been carried out by pushover analysis and NDA. The compressive strength equal to 20 MPa has shown behaviour more similar to that observed in the real structure than the other three cases. The case of linear elastic property particularly has overestimated the capacity.

6.6.4 Influence of different parameters

The influence of different parameters on the seismic performance has been analysed in the frame of a sensitive analysis. The mechanical parameters examined are the compressive and tensile strength, the Young's modulus and tensile fracture energy. In accordance with the results of the parametric study, different combinations of lower values of mechanical parameters have been also proposed and examined. Models with weakened interlocking have been also analysed. These models have been examined on the basis of the assumption that the structure may have poor interlocking between structural elements. Then different seismic-force distribution patterns have been compared with that of mass-proportional distribution. Comparison of a shell-element and solid-element model has been also made. All the analyses have been carried out by pushover analysis.

6.6.4.1 Influence of mechanical parameters of masonry

The parametric study has been carried out on tensile strength (f_t), Young's modulus (E), tensile fracture energy (G_{ft}) and compressive strength (f_c). For the study of tensile strength, a linear correlation of values has been considered between tensile strength and tensile fractural energy. It was considered to maintain the same ductility in each case. When sufficiently low tensile strength is considered in a FEM model, FEM analysis shows similar capacity to limit analysis. However, a local stress problem limits the capacity and prevents a full collapse mechanism from appearing when extremely small tensile strength is applied to a FEM model. As for Young's modulus, its reduction leads to reduction of the capacity and of the stiffness. A comment should be added for the study of Young's modulus. A FEM element used in this study represents brittle behaviour when the crack strain at its maximum tensile stress is the same or bigger than its ultimate crack strain according to the considered softening behaviour (linear tension softening function as discussed in Section 3.1.5.1.2). In this FEM element, this occurs when E=100xf_c (400 MPa) is considered. Tensile fracture energy has to be increased to 120 N/m in order to maintain the same ductility as the case where Young's modulus is equal to 500xf_c (2000 MPa). However, when the tensile fracture energy was increased, the observed capacity became inadequately high. Through the comparison of fracture energy, its reduction reduces load and displacement capacity linear-proportionally. Controlling of compressive strength does not alter the behaviour substantially.

However, with relatively low compressive strength (1 MPa in this study) failure has occurred due to compressive mechanism such as crushing of materials instead of tensile cracking. The collapse mechanisms observed in the parametric studies have not been changed from those seen in the reference case, except for the cases in which low tensile strength or compressive strength were adopted.

6.6.4.2 Comparison of seismic force patterns for pushover analysis

Comparison of three different lateral load distribution patterns has been made. The studied load distribution patterns have been mass-proportional, uniform and triangular ones. The distribution of seismic force proportional to masses has shown clearer collapse mechanisms than the other two patterns attempted in this study. In the +X direction, overturning of the façade with part of wall of the nave and the lateral chapel has been seen in the mass-proportional case. The collapse of the top part of the bell tower has been found for the triangular distribution case and the arch of one of the lateral chapels has been collapsed in the mass-proportional case. As for the uniform case in the +X direction, no simple interpretable collapse mechanisms have been observed. On the other hand in the Y direction, mechanisms and damage have been seen all over the transept and apse, although the mass-proportional case has shown just the collapse of the arch in the transept. In this study, the lateral load distribution pattern proportional to the masses of the structure shows more evident behaviour of the structure than the other two patterns examined.

6.6.4.3 Studies on models with weak interlocking

Models with weakened interlocking between façade, nave and transept have been considered. These models have been studied on the basis of the assumption that the structure may have poor interlocking between structural elements. Four different types have been compared. They have shown certain influence on the performance of the entire structure. When inappropriately small values were applied to connections, the analysis has not permitted the development of the global collapse mechanisms. As mentioned in Section 6.6.2, this application of weakened interlocking requires a detailed characterisation and accurate mechanical modelling of the imperfect connections, which are not easily obtained in an objective way.

6.6.4.4 Comparison of models composed of solid or shell elements

Two different partial models (façade and typical bay) have been considered. They were composed of shell or solid elements. Both models have shown similar capacity (0.235g (shell) vs. 0.255g for facade) (0.16g (shell) vs. 0.185g for a typical bay). Both models (façade and a typical bay) have shown very similar distribution of damage to the real structure. As for the two models of the façade, the damage in the connection between the façade and the nave wall has indicated out-of-plane movement of the façade. The two models of the typical bay have shown similar failure pattern, showing the out-of-plane

behaviour of the nave wall. In this study, the model composed of shell element and that of solid element have shown similar behaviour.

6.6.5 Study of possible strengthening interventions

Two different possible interventions have been proposed and studied. They were the insertion of ties and the combination of the improved-interlocking and the insertion of ties. For the study of the effect of possible interventions, the model with weakened interlocking studied in Section 6.4.5, has been considered. The properties of the connections have been f_c=2 MPa, f_t=0.01 MPa, E=200 MPa, G_{ft}=5 N/m.

Firstly, the ties system has been studied. The structural behaviour has been improved when sufficient number of ties were installed. The tie system has increased the capacity by 17.7 % in the +X direction, by 27.9 % in the –X direction and by 18.4 % in the Y direction. In the -X direction, different collapse mechanisms from the reference case have been observed. In this direction, failure has been observed in the arches of the lateral chapels instead of local failure of the connection between the transept and the apse which was seen in the reference model. Secondly, the combination of technique (tie system and interlocking improvement) has been studied. The mechanical properties of the improved interlocking have been considered the same as the rest of masonry. The combination of two techniques has increased capacity more effectively than the above-mentioned tie system, by 74.7 % in the +X direction, by 92.9 % in the –X direction and by 56.7 % in the Y direction. Also by this intervention, different failure mechanism from the reference case has been observed only in the –X direction. The model has shown overturning of the apse, collapse of the arches of the chapel and shear mechanism in the perimeter walls.

6.7 Conclusions

6.7.1 Comparison of seismic assessment techniques

A seismic assessment by different analysis methods of an historical church struck by 2009 L'Aquila earthquake has been presented. The real damage and the collapse mechanisms produced by the earthquake have been directly compared with the mechanisms derived from the structural analysis. Three different methods have been considered and compared: nonlinear static (pushover) analysis, nonlinear dynamic analysis (NDA) and limit analysis. FE analysis combined with the limit analysis has been shown, with some limitations, as a suitable approach for the study of a typical church structure (a building without box-behaviour). However, FEM analysis must be applied on a realistic model of the structure adequately taking into account the nonlinear material properties, the construction features and the real connection between the different parts. In the case of San Marco church, modelling the existing lack of connection between certain parts (buttresses and perimeter walls), built at different construction phases, has been important to attain an adequate simulation of the real collapse mechanisms. An

adequate modelling of the alterations and the RC additions of 1970 has been also necessary to realistically simulate their influence on the structure's performance. All this highlights the importance of historical research and in-situ inspection for this type of studies.

Pushover analysis and NDA have afforded the simulation of the major real collapse mechanisms activated in the structure. These include the overturning of the façade, the collapse of the dome, the failure of the arches of the transept and the partial collapse of the nave wall. The simulation of the latter has required the modelling of the disconnection between the external walls and the buttresses in the chapel. It must be noted, however, that the numerical approaches have failed to predict some of the mechanisms actually activated by the earthquake, such as the in-plane mechanism of the façade. A specific limitation of the methods utilised has been found in the numerical simulation of mechanisms involving the loss of balance of walls set over collapsing arches. Such types of failures are difficult to simulate in continuum mechanics FE models and may require alternative approaches such as the DEM.

In FEM-based nonlinear seismic analyses of complex buildings, it is important to choose different control nodes and to compare their load-displacement curves in order to identify which are the most vulnerable elements and to understand the sequence of local failures during the earthquake.

In spite of the observed limitations, pushover analysis on a model of the entire structure has revealed to be a practical tool for seismic assessment of a historical church. This approach seems a good compromise between limited computational cost and accuracy of results. However, the interpretation of pushover analysis results may pose some difficulties. For this reason, it is advisable to combine distinct analysis methods in order to cover the limitations of each one.

As for the ultimate capacity, pushover and limit analysis have shown good agreement for some mechanisms. In the present study, NDA has produced a higher value of maximum acceleration than pushover analysis for earthquakes acting either in the longitudinal or transverse direction.
The N2 method has been used to compare NDA and pushover analysis results in terms of structural capacity and seismic performance. It is worth noting that N2 approach still requires further investigation for the case of irregular structures.

6.7.2 Influence of the RC intervention carried out in 1970

Comparison of the state before and after the intervention of 1970 has been carried out. Comparison of the two models has been conducted by pushover analysis and NDA. The analyses have shown that the strengthening with RC beams and tympanums carried out in San Marco church may have resulted in the certain decrease of the seismic capacity. This effect has been represented more evidently by NDA than by pushover analysis.

6.7.3 Influence of parameters

The parametric studies haves allowed to identify the influence of different mechanical parameters. It has been found that Young's modulus, tensile strength and tensile fracture energy have more influence to the studied model than the compressive strength. Application of weakened interlocking has been an effective simplified method to represent poorly interlocked connections between structural elements. A lateral load patterns has been a determinative factor of representation of mechanisms. In the study, the load distribution pattern proportional to masses has produced collapsing mechanisms more similar to the real structure than the other methods (triangular and uniform pattern). Two partial models consisting of solid elements (the façade and a typical bay) are compared with those of shell elements. The study has shown that shell- and solid-element models simulate similar behaviour.

6.7.4 Assessment of possible interventions

The conducted analyses have shown that tie system and combination of tie system and connection improvement have been effective for the seismic strengthening of the studied model. The seismic capacity is increased by 21% with a tie system and 75% by combination of a tie system and improvement of interlocking. Both techniques have been more effective in the –X direction than the +X, Y directions.

7. Conclusions

7.1 Introduction

The present research has analysed the applicability of existing nonlinear FEM approaches to the study of masonry historical structures. The FEM analysis has been adopted and applied to the analysis of real and complex structures including mixed steel and masonry vaulted systems belonging to the Hospital de Sant Pau in Barcelona and a large single-nave church damaged by the 2009 Abruzzo earthquake. In the present chapter, the main conclusions drawn from this research are presented. The conclusions presented include some considerations on the state of the art on the modelling and analysis of masonry historical structures, on the numerical modelling techniques adopted for the present research, and specific conclusions on the analysis of vaulted structures and large entire structures. As a final outcome of the research, criteria and guidelines are provided for the analysis of these types of structures under vertical loading and seismic forces. Finally, some proposals for future research in the field are presented.

7.2 Conclusions on the state of the art

- Many historical masonry structures show significant seismic vulnerability due to lack of horizontal stiffening diaphragms and limited material strength. Consequently, most of the collapse mechanisms under seismic actions derive from local out-of-plane behaviour. As for churches, the collapse mechanisms involving a façade are the most representative. Triumphal arches, domes and vaults are also vulnerable members.
- For pillars and columns under seismic forces, overturning and crushing are the typical collapsing mechanism. As for columns, drum shifting may also occur.
- Pillars under dead load may experience long-term damage related to creep. This long-term phenomenon can occur under stresses lower than the nominal material strength identified by means of static compression tests. Pillars affected by long term damage may develop vertical cracks due to lateral expansion. This dilatation phenomenon, an evident increase in volume, might lead to collapse due to crack propagation.
- Some authors have stated that Catalan vaults composed of good-quality mortar are resistant enough in tension not to experience cracking under normal service conditions. Other authors have mentioned that they experience cracking in a similar way to other types of masonry vaults. However, the real advantage of Catalan vaults to other types of vaults is seen only in the construction process. They can be constructed without centring or with light supplemental supports due to the cohesiveness derived from mortar between the layers. Once completed, they should be considered to tend to experience cracking and develop failure modes in a similar way to other types of masonry vaults.

- Many structures were strengthened with modern materials, and specifically with reinforced concrete, during the last century. Collapses and damage occurred during recent earthquakes have shown that the inadequate use of these materials may cause negative effects on the seismic behaviour of the structures due to the increase of mass and the alteration of the distribution of the stiffness.
- Nonlinear FEM analyses may permit a sufficiently accurate study of the response of the structure. However, the results provided by an FEM model have to be validated and eventually improved by comparison with available empirical evidence such as experimental results and/or the damage observed in the real structure (e.g. crack locations).
- Limit analysis is frequently used for safety assessment and for the design of seismic strengthening. One of the advantages of this method is that it can be carried out without requiring excessive calculation effort and input data. However, it only permits the study of the ultimate state condition and the choices of mechanisms to be analysed are dependent on the practitioner's experience. The determination of the most vulnerable mechanisms may not be straightforward when a large variety of mechanisms are possible in the structure.
- For pushover analysis, the distribution pattern of the seismic equivalent load is a dominant factor to the result. Frequently-used distribution patterns are those defined in proportion to the mass of the structure and to the first modal shape. In the studies carried out as part of the present research, the former load distribution pattern has resulted in more extensive damage while the latter one has led to larger damage on the higher parts of the structure.
- Although pushover analysis with predefined invariant forces has been used frequently for seismic assessment, significant limitations are observed. For instance, it is known that it cannot detect changes caused in the nonlinear dynamic response of the structure due to higher mode effects. It is advisable to compare the results of pushover analysis with more accurate approaches (such as nonlinear dynamic analysis [NDA]).
- With a set of carefully chosen ground records, NDA provides an accurate evaluation of structural seismic response. However, its practical application still poses difficulties due to its complexity and high computer effort demand. NDA is suggested to be used when a detailed vulnerable assessment is required. For the analysis of complex buildings, partial models are typically used, involving, for instance, a bell tower or a façade.

7.3 Conclusion on the numerical strategies adopted in the present research

- The numerical model utilised in the present research have considered a fixed smeared cracking model with a Rankine failure criterion in tension and a plasticity model with Drucker-Prager failure criterion in compression. However, it has to be mentioned that this model holds a limitation both in tension and compression. As for the limitation in tension, the maximum allowable tensile stress temporarily may become larger than the tensile strength of the material due to a threshold angle condition. Regarding the limitation in compression, the plasticity model adopted has considered the

compressive fracture energy infinite. As a result, the plastic yielding continues once the material reaches its maximum allowable compressive stress.

- Considering the limitations discussed in the previous paragraph for the smeared cracking model, other models such as a total-strain crack one, can be considered to represent material behaviour more accurately. The total-strain crack model does not hold these limitations since it is controlled by a uniaxial equation both in tension and compression. However it can be significantly more costly. Since most of the case-study structures in the research are large and complex (i.e. an entire single-nave church and combination of a vault and steel profiles), and since it was intended to carry out detailed parametric studies requiring a large number of analysis, it was decided to use the model referred to in the first paragraph. The analyses have been carried out under quasi Newton Raphson method. This method is more stable and robust than the full Newton-Raphson method. The analysis of a historical masonry structure is sometimes interrupted by numerical instability derived from its low tensile strength. For this reason, the quasi Newton Raphson method has been considered for most of the analyses carried out.
- In the present study, it has been possible to analyse complex Catalan vaults by discretising the structure into four node quadrilateral shell elements. As for the number of integration points across the thickness, a number equal to 11 has been found adequate. With a smaller number of integration points, the analysis, in some cases, stops due to numerical instability while a larger number of integration points require additional unnecessary computational effort without improving the result.
- A finite element with a size in surface equal to 125x125 mm^2 is normally satisfactory for the meshing of a typical Catalan vault of a thickness of about 10 cm. Therefore, shell elements with a ratio between their side length and thickness of about 10 to 12.5 seem to be adequate for the purpose of modelling the vaults. Using elements of this size, damage is adequately simulated and distributed in the structure. Elements of a larger size tend to show excessively smeared damage while those of a smaller size just increase the computational effort.
- Beam elements have been used to represent linear horizontal elements such as masonry arches and steel profiles and slender vertical elements such pillars. They can be discretised properly with two-node beam elements. Regarding the integration points in the depth of the beam elements, a sufficient number needs to be adopted. They are similar to those found adequate for shell elements. In the present research, for instance, and in the case of steel profiles, a beam element representing an I-shape steel profile, a total of 11 integration points was adopted, of which 7 were located in the web and 2 in each of the flanges.
- A large-scale historical masonry structure can be represented with satisfactory accuracy by the combination of four-node quadrilateral shell elements, three-node triangular shell elements and two-node beam elements. The first two can be used for the discretisation of walls and curved structural systems such as domes and vaults. The last one is employed for the representation of relatively narrow structural systems such as arches and roof trusses, as also mentioned in the previous paragraph.

7.4 Conclusions on the analysis of masonry vaulted systems including Catalan vaults

- Secondary construction members of a vault, including an upper slab and the wallets that sustain the slab can be an influential factor to the structural behaviour and strength of the vault. If the analysis of a vault is carried out without taking into account these elements, the result may significantly underestimate its stiffness and strength. In the studied case, the inclusion of such secondary elements was necessary for the simulation of the behaviour identified in the experiments previously carried out.
- As mentioned in the previous paragraph, in the cases analysed, the consideration of the secondary construction members has shown noticeable influence on the capacity. In the analysis of the lower vault of the Nostra Sra. De la Mercé Pavilion in Hospital Sant Pau, the inclusion of the upper slab, wallets and longitudinal beams has increased the capacity by 26.9%. In the models prepared, these elements were connected to each other by means of frictional interface elements. As for the large vault of the Administration building, the capacity was increased by 94.8 % (addition of the upper slab) and by 288 % (addition of the upper slab and wallets).
- The three studied double-curvature Catalan vaults in the Administration building of Hospital Sant Pau consist of a floor slab. For those vaults, the capacity numerically predicted under uniform load has attained satisfactory levels allowing modern uses. However, these satisfactory capacities are achieved only when the upper slab and the wallets are considered as part of the resisting structure.
- A sensitive analysis on tensile strength of a single double-curvature Catalan vault has shown noticeable influence on the capacity. Decrease of tensile strength by 60 % (from 0.2 MPa to 0.12 MPa) has reduced the load capacity by 37.5 %. Therefore, the tensile strength can be regarded as an important parameter having significant influence on the numerical results even for very small adopted values.
- It is suggested to include the frictional behaviour of masonry-steel contact in case a masonry vault structure is supported on steel profiles. In addition to a more realistic description, it reduces the likelihood of possible numerical problems. Without the use of frictional joint elements to model the masonry-steel contact, a local failure caused from stress concentration may prevent global mechanisms from occurring. However, it is not straightforward to determine the parameters for the frictional behaviour of masonry-steel contact due to lack of specific previous research.
- The geometrical modelling of a double-curvature vault may be done more accurately and efficiently by means of a computer-aided design (CAD) software, particularly if oriented to the design of curved structures, than by a standard pre-processor of a numerical-analysis software. In fact, some of the pre-processors examined were not capable of modelling correctly the double-curvature vaults analysed in the present study.

7.5 Conclusions on the seismic analysis of large masonry structures. Modelling

- An accurate structural model should take into account the real state of interlocking between different walls or parts of the structure, as the connection between parts may actually be weaker than the one that is represented by a standard description using a FEM model. Moreover, real structural parts may be very weakly connected, or totally disconnected due to construction events or alterations. In the study of San Marco church, the lack of connection linked to architectural alterations or different construction phases has been found to be very influential on the seismic response of the structure. Modelling the absence of connection between certain parts can be a crucial factor to attain an adequate simulation of real collapse mechanisms.
- In a FEM model, and as a possible simple approach, the above-mentioned possible weak interlocking may be modelled by defining decreased mechanical parameter values for finite elements around the connections. However, when extremely low values are applied to these connections, numerical instability may prevent the full development of collapse mechanism. Modelling of weak interlocking requires a detailed characterisation and accurate mechanical modelling of the imperfect connections. However, it may not be easy to identify and describe the behaviour of weakly interlocked parts accurately.
- The adopted compressive strength of RC additions such as RC tie beams or arch enlargements has shown to have significant influence on the resulting seismic response of the masonry structure. Therefore, it is necessary to specifically inspect and experimentally characterise the compressive strength of such RC members.
- In the parametric studies carried out, the Young's modulus, tensile strength and tensile fracture energy have been the main parameters influencing on the response and strength of the structure. Their influence has been found, in the cases analysed, to be significantly larger than that of the masonry compressive strength.
- Unless excessively low values have been adopted to the above-mentioned parameters of masonry (Young's modulus, tensile strength and tensile fracture energy and compressive strength), in spite of the consideration of different values, the vulnerability to out-of-plane behaviour have been found in specific structural elements including the façade and nave wall. Failure has been also seen in curved structural elements such as vaults and arches. When very low compressive strength was applied, compressive mechanism such as crushing of materials can be observed instead of tensile cracking. On the other hand, with extremely small tensile strength, local concentration of high stress keeps a full collapse mechanism from appearing.

  The description of roof and floor slabs on masonry walls may require some specific numerical treatment. A simple description as a perfect connection may result in a too simplistic modelling and may cause an overestimation of the real seismic capacity of the structure. It may be convenient, when possible, to describe such support by means of interface elements allowing separation in tension and frictional sliding. However, such modelling may significantly increase the cost of the analysis. As a compromise between accuracy and efficiency, the roof trusses may be ignored as

resisting elements (therefore ignoring both their stiffness and strength) while lumping their mass to the supporting walls.

7.6 Conclusions on the seismic analysis of large masonry structures. Seismic assessment strategies

- Linear kinematic analysis (LKA) can be used to estimate the acceleration of mechanism activation by applying the principle of virtual work for each chosen mechanism. LKA permits the verification of the mechanism by comparison with the demand acceleration of the site of the structure. When 10 % exceeding probability in the reference life period of the structure is considered for the demand acceleration, the verification considers the limit state of life safeguard (SLV). In the case study of San Marco Church analysed in the present research, good agreement has been seen between the results of LKA under SLV and the mechanisms actually occurred in the real structure struck during earthquake.
- The application of LKA is straightforward. However, when a large variety of collapsing mechanisms are possible in the structure, the determination of the governing mechanisms may not be simple. In the studied case, these difficulties were seen in the analysis of the nave wall. Different possible mechanisms could be assumed, including the partial failure of the nave wall due to the collapse of the underneath arches, for earthquake in the longitudinal direction, and overturning of the nave wall for earthquake in the transversal direction. In this case, it was concluded that the former mechanism is actually more probable than the latter. However, in some cases it may be more difficult to determine the collapse mechanisms that may be produced by a real earthquake.
- Regarding the comparison of the seismic capacity predicted by LKA and FEM pushover analysis, LKA tends to show more conservative results than FEM analysis since the tensile strength is not taken into account in LKA. When a sufficiently low tensile strength is considered in the FEM model, both FEM analysis and LKA predict a similar capacity.
- Nonlinear kinematic analysis (NLKA) permits a direct comparison between the displacement ultimate capacity and the displacement spectrum demand. The comparison between LKA and NLKA in the cases analysed has shown that LKA produces more conservative results regarding the seismic capacity.
- In the FEM analysis of a large-scale structure, it may be convenient to carry out analysis on both entire and partial models. The analysis on the entire model may be useful to characterise the global response of the structure and the interactions between structural elements. However, the occurrence of local failures affecting certain parts of the model may cause the analysis to stop prematurely, therefore preventing the possibility of prediction of damage patterns that may appear in other parts of the building and that may be better related with a more global failure. For that reason, it is suggested to use partial to characterise certain damage patterns that the entire model may not detect.

- Considering geometrical nonlinearity is advisable. For instance, the influence of geometrical nonlinearity was found significant in the study of San Marco church in the transversal direction. This influence is due to the deformation of the nave walls with respect to the buttresses on which they are supported. According to the pushover analysis performed, considering geometric nonlinearity caused a reduction of 15 % on the displacement capacity. However, it did not affect the load capacity in a significant way.
- For pushover analysis, the distribution pattern of seismic forces has a significant influence on the resulting seismic capacity. In the case of the large church analysed, the force pattern providing the results more similar to those observed in reality, in terms of damage and collapse mechanisms, was the one proportional to the masses of the structure.
- It is suggested to apply the N2 method to results obtained from pushover analysis. The N2 method combines pushover analysis with the capacity spectrum approach. It correlates the displacement capacity of the structure to the displacement demand of the expected earthquake. More specifically, it identifies the performance point in the capacity curve obtained from pushover analysis. This performance point represents the capacity of the structure under the expected earthquake. In the present study, in most of the cases, the displacement capacity at the performance point has been closer to the maximum displacement obtained from NDA than the ultimate displacement from pushover analysis. In the case study of San Marco church, particularly this was seen for the overturning of the façade and the failure of the arches of the transept. However, in some cases, the displacement capacity at the performance point is relatively far from the maximum displacement obtained from NDA. In the study of San Marco church, this was seen in the partial collapse of the nave wall. The N2 method still has to be further investigated for more accurate prediction of the performance point, regarding the study of irregular-shaped structures such as many large historical churches.
- For the simulation of the influence of RC elements in historical masonry structures, NDA may be able to simulate relevant effects that may not be adequately described by a pushover analysis. In the case of the church analysed, NDA afforded the description of the decrease of the capacity due to the additional mass and stiffness caused by the RC elements. On the other hand, pushover analysis failed to detect this negative effect and overestimated the capacity of the reinforced structure.
- In spite of the limitations observed in the present research, pushover analysis, especially with the mass-proportional force distribution pattern, has been reliable and efficient seismic assessment tool in the applications analysed. However, it has to be added that limit analysis sometimes represents seismic behaviour more accurately than pushover analysis, as for instance in the case of in-plane mechanism of the facade. NDA is more accurate than the other two above-mentioned methods, its main drawback being that it requires excessive computational effort. For these reasons, it is preferable to combine distinct analysis methods so as to overcome the limitations of each one.
- A specific limitation of all the methods utilised has been found in the simulation of the loss of balance and failure of large structural parts caused by the collapse of other structural members on which

they are supported. In the present study, this was observed in the case of the failure of part of the nave wall of San Marco church resulting by the collapse of the arches on which it was supported. Such types of failures are difficult to simulate in continuum mechanics FE models and may require alternative approaches such as the DEM.

7.7 Recommendations for further research

In this section, further study possibilities are discussed. The two main applications of the study carried out, including mixed steel and masonry vaulted systems belonging to the Hospital de Sant Pau in Barcelona and a large single-nave church damaged by the 2009 Abruzzo earthquake, suggest possible future researches oriented to improve the knowledge attained on these cases and also to improve the application of FEM and related analysis tools. The first applications allow some suggestions for the further study of Catalan-vaulted structures. The second allows suggestions the related seismic assessment on large-scale structures. In addition to the suggestions related to the above two topics, proposals are made for numerical models that permit more detailed and precise description of the response of a historical masonry structure than those employed in the present research. Although at the moment the computational cost of the models proposed may be very high and even prohibitive, it may become affordable in the near future due to future further progress in computer calculation speed.

1) Regarding the study of the vaults in Hospital Sant Pau, for the conducted FEM analysis, the estimation of the maximum capacity has been only based on the strength of the vaults and steel profiles. This has been carried out as a first approach to the capacity assessment of the vaults. However, the maximum capacity might be limited by the local strength of the connections between steel members, that have not been modelled. The connections were not modelled into detail to limit the computational demand. However, it is suggested to include the local behaviour of the connections by means of a detailed modelling including interface elements in the future.
2) As for the analysis of the vaults in Hospital Sant Pau, the detachment of tiles located at extrados has not been considered. As a matter of fact, a provisional verification was carried out by considering the maximum allowable deflection of the floor defined by the Spanish code. However, this approach may not be sufficiently accurate to examine the tile detachment and a different approach has to be investigated.
3) Carrying out an experiment on existing or laboratory-built Catalan-vaulted structures would allow a deeper understanding of the structural behaviour and strength of this type of structures. A detailed FEM analysis should be also conducted, in combination with the experiment, to simulate the behaviour and better characterise the limitations of this type of numerical approach.
4) In the analyses by NDA, a Rayleigh damping model has been assumed. The damping ratio for this model has been determined according to engineering judgement. On the other hand, the value of the damping ratio was shown to have a certain influence on the results. Further

research would be advisable for estimating the damping ratio of masonry historical structures in a more objective way.

5) Adaptive pushover analyses (APO) and multi-mode pushover analysis (MMP) have been adopted and compared with NDA and invariant-force pushover analysis. However, in the cases analysed, these two techniques have not shown much improvement with respect to the invariant-force pushover analysis. As for APO, it has been found that the results are highly influenced by the choice of the initial force distribution pattern and the updating method of the force distribution. Appropriate choice of these two factors has not been identified and therefore further research is suggested. In the cases analysed, MMP was not entirely successful probably due to the fact that the response was very much determined by a dominant first mode.
6) In the present research, comparison of seismic assessment tools has been carried out on a large single-nave church. A similar type of a study would be recommended on a different structure such as a large multiple-nave church.
7) Regarding the material behaviour of masonry, in the present research the numerical model has considered a fixed smeared cracking model with a Rankine failure criterion in tension and a plasticity model with Drucker-Prager failure criterion in compression. The model has shown certain limitations both in tension and compression as discussed in Section 7.3. A total-strain crack model, on the other hand, does not hold these limitations since it is governed by a uniaxial equation in tension and compression. For this reason, the total-strain crack model may be preferred to smeared cracking model, although it would be less efficient in terms of computational cost.
8) When a Rankine failure criterion is considered in tension for a smeared crack model, a rotating crack model may be more appropriate than a fixed crack model. Under the rotating crack model, the threshold angle condition is not considered since a crack continuously changes its orientation. Therefore, the above-discussed limitation regarding the maximum allowable tensile stress does not have to be taken into account. However, this model requires more computational effort than the fixed crack model.
9) An accurate description of the imperfect connection between the structural elements such as vertical (e.g. walls, pillars), horizontal (floors, roof trusses) and curved ones (arches, vaults) should be achieved. This description would require the modelling of the disconnection or partial connection between the structural elements and the definition of interface behaviour at the connections. The interface behaviour should have the capability of simulating crushing, sliding and cracking of the material.

8. REFRERENCES

Abbaneo S, Baronio G, Binda L, Tiraboschi C (1993) Murature in pietra: classificazione ed indagini preliminari per la scelta e la progettazione delle miscele per l'iniezione. Convegno Murature, Sicurezza, Recupero Trento, Italy: 185-222

Adam JP (2005) Roman building: materials and techniques. Routledge: London

Anzani A, Binda L, Roberti G M (2008). Experimental researches into long-term behavior of historical masonry. Learning from Failure: Long-term Behaviour of Heavy Masonry Structures WIT Press: 29-56

Albanesi T, Biondi S, Petrangeli M (2002) Pushover analysis: An energy based approach. In Proc. of the Twelfth European Conference on Earthquake Engineering, London, United Kingdom, Paper No. 605

Andreu A, Gil L, Roca P (2007) Computational Analysis of Masonry Structures with a Funicular Model. Journal of Engineering Mechanics 133(4): 473-480

Andreu A, Gil L, Roca P (2010) Analysis of masonry structures by funicular networks.
Engineering and Computational Mechanics 163: 147-154

Antoniou S, Pinho R (2004a) Advantages and limitations of adaptive and non-adaptive force-based pushover procedures. Journal of Earthquake Engineering 8(04): 497-522

Antoniou S, Pinho R (2004b) Development and verification of a displacement-based adaptive pushover procedure. Journal of Earthquake Engineering 8(05): 643-661

Anzani A, Binda L, Melchiorri G (1995) Time dependent damage of rubble masonry walls. In 4th International Masonry Conference, British Masonry Society, London: 341-351.

Apostolopoulos C, Sotiropoulos P (2008) Venetian churches of Lefkada, Greece Construction documentation and seismic behaviour “Virgin Mary of the Strangers”. Constr and Build Mater 22(4): 434-443

Araguas P (1999) Voute a la rousillon. Butlleti de la Reial Academia Catalana de Selles Arts Sant jordi 13: 173-185

Arias J (2013) Structural Analysis of a vault of the Administration building of the Hospital Sant Pau. Master thesis, Barcelona: Technical University of Catalonia

ASTM C270 (2007) standard specification for mortar for unit masonry. West Conshohocken, PA, USA: ASTM International

ASTM C803 (2010) Standard test method for penetration resistance of hardened concrete. West Conshohocken, PA, USA: ASTM International

Augenti N, Parisi F (2010) Constitutive models for tuff masonry under uniaxial compression J. Mater. Civ. Eng 22(11): 1102–1111

Augenti N, Romano A (2007) Preliminary experimental results for advanced modelling of tuff masonry structures. ReLUIS “Rete di Laboratori Universitari Ingegneria Sismica” in the context of the activities of “Linea 1 – Valutazione e Riduzione della Vulnerabilita’ di Edifici in Muratura”. II year scientific account rendering (Enclosure 4.3-UR03-2)

Aydinoğlu MN (2003) An incremental response spectrum analysis procedure based on inelastic spectral displacements for multi-mode seismic performance evaluation. Bulletin of Earthquake Engineering 1(1): 3-36

Backers HP (1985) On the behavior of masonry under tension in the direction of the bed joints PhD Dissertation, Aachen: Aachen University of Technology

Baggio C, Trovalusci P (1998) Limit analysis for no-tension and frictional three-dimensional discrete systems. Mech Struct Mach 26(3): 287–304

Barthel R (1993) Rissbildung in gemauerten Kreutzgewölben. Structural Preservation of the Architectural Heritage, Zürich Switzerland: IABSE

Bazant ZP, Oh BH, (1983) Crack band theory for fracture of concrete. *Materials and Structures,* RILEM, 16(93), 155-177

Berto L, Saetta A, Scotta R, Vitaliani R (2002) An orthotropic damage model for masonry structures. Int J Numer Methods Eng 55:127–157

Bates W (1991) Historical structural steelwork handbook. British Constructional Steelwork Association(BCSA), 76

Bathe KJ (1986) Finite element procedures for solids and structures—nonlinear analysis. Video-Course Study Guide Centre for Advanced Engineering Study, MIT

Bathe KJ (1996). Finite element procedures. Englewood Cliffs: Prentice hall

Bayraktar A, Şahin A, Özcan DM, Yildirim F (2010) Numerical damage assessment of Haghia Sophia bell tower by nonlinear FE modeling. Appl Math Model 34(1): 92-121

Benfratello S, Caiozzo G, D'Avenia M, Palizzolo L (2012) Tradition and modernity of Catalan vaults: Historical and Structural analysis. Meccanica dei Materiali e delle Strutture 3: 44-54

Benfratello, S Palizzolo, L Giambanco, F D'Avenia, M (2010) On the analysis of Catalan thin vaults High Performance Structures and Materials V 112: 453-464

Bennett RM, Boyd KA, Flanagan RD (1997) Compressive properties of structural clay tile prisms. J. Struct. Eng. 123 (7): 920–926

Benvenuto E (1981) La scienza delle costruzioni e il suo sviluppo storico. Florence, Italy: Sansoni

Bernuz-Fernández Arquitectes SLP (2010) Report on the loading capacity of the existing floor slab of the San Rafael in Hospital de Sant Pau Barcelona, Spain. Bernuz-Fernandez Arquitectes SLP

Betti M, Bartoli G, Orlando M (2010) Evaluation study on structural fault of a Renaissance Italian palace. Eng Struct 32(7):1801-1813

Betti M, Galano L (2012) Seismic Analysis of Historic Masonry Buildings: The Vicarious Palace in Pescia (Italy). Buildings 2(2):63-82

Betti M, Vignoli A (2008) Modelling and analysis of a Romanesque church under earthquake loading: Assessment of seismic resistance. Eng Struct 30(2):352-367

Betti M, Vignoli A (2011) Numerical assessment of the static and seismic behaviour of the basilica of Santa Maria all'Impruneta (Italy). Constr Build Mater 25(12):4308-4324

Bicanic N, Ponniah D, Robinson J (2001) Discontinuous deformation analysis of masonry bridges. Comput ModelMason:177–196

Binda L (2000) Caratterizzazione delle murature in pietra e mattoni ai fini dell'individuazione di opportune tecniche di riparazione. CNR-Gruppo Nazionale per la Difesa dai Terremoti, Rome, Italy

Binda L, Baronio G, Penazzi D, Palma M, Tiraboschi C (1999) Caratterizzazione di murature in pietra in zona sismica: DATA-BASE sulle sezione murarie e indagini sui materiali. 9° Convegno Nazionale «L'ingegneria sismica in Italia», Torino

Binda L, Cardani G, Saisi A, Valluzzi M R (2006) Vulnerability analysis of the historical buildings in seismic area by a multilevel approach. Asian Journal of Civil Engineering (Building and Housing) 7(4):343-357

Binda L, Gatti G, Mangano G, Poggi C, Sacchi L G (1992) The Collapse of the Civic Tower of Pavia. a Survey of the Materials and Structure, Masonry International:11-20

Binda L, Lualdi M, Saisi A (2007) Non-Destructive Testing Techniques Applied for Diagnostic Investigation: Syracuse Cathedral in Sicily, Italy. International Journal of Architectural Heritage, Conservation, Analysis and Restoration 1(4): 380-402.

Binda L, Penazzi D, Saisi A (2003b) Historic Masonry Buildings: Necessity of a Classification of Structures and Masonries for the Adequate Choice of Analytical Models. VI International Symposium Computer Methods in Structural Masonry - STRUMAS, Rome, Italy: 168-173

Binda L, Saisi A (2001) State of the art of research on historic structures in Italy. Dept. of Structural Engineering, Politecnico of Milan, Italy

Binda L, Saisi A, Messina S, Tringali S (2001a) Mechanical damage due to long term behaviour of multiple leaf pillars in Sicilian Churches. In: III int seminar: historical constructions 2001. Possibilities of numerical and experimental techniques, Guimaraes, Portugal: 707–718

Binda L, Tiraboschi C, Baronio G (2003a) On site investigation on the remainings of the Cathedral of Noto. Constr Build Mater 17:543–55

Binda L, Tiraboschi C, Tongini F R (1998) On site and laboratory investigation on materials and structure of a bell-tower in Monza. 2nd International Conference RILEM on Rehabilitation of Structures, Melbourne: 542-556

Binda L, Valluzzi MR, Michielon E, Modena C (2001b) Modellazione del comportamento di Edifici in Muratura sotto Azioni Sismiche: l'Esperienza Umbria-Marche. X National Congress "L'ingegneria Sismica in Italia", Potenza-Matera 9-13

Black EF, Aschheim M (2000) Seismic Design and Evaluation of Multistory Buildings using Yield Point Spectra. CD Release 00-04, Mid-America Earthquake Center, University of Illinois, Urbana

Boothby TE (2001) Analysis of masonry arches and vaults. Structural Engineering and Materials 3:246-256

Boothby TE, Atamtürktür SH, Erdogmus E (2006) Manual for the Assessment of Load-Bearing Unreinforced Masonry Structures. Louisiana, USA: National Center for Preservation Technology and Training

BOMA (2007) Dictamen relatiu a la capacitat estructural del Pavelló d'Administració, pertanyent al recinte hospitalari de L'Hospital de la Santa Creu i Sant Pau, Barcelona. 10574-ADM-V01 Barcelona Spain: Brufau, Obiol, Moya & Ass, S.L.P.

BOMA (2008) Dictamen relatiu a la capacitat estructural del Pavelló de Ntra. Sra. De La Mercè al recinte hospitalari de L'Hospital de la Santa Creu i Sant Pau, Barcelona. Barcelona Spain: Brufau, Obiol, Moya

& Ass, S.L.P.

Borri A, Avorio A, Cangi G (1999) Riparazione e consolidamento degli edifici in muratura Regione dell'Umbria, F. Gurrieri, Manuale per la riabilitazione e la ricostruzione postsismica degli edifici. Rome, Italy: DEI Tipografia del Genio Civile

Borri A, Cangi G (2004a) Vulnerabilità ed interventi di prevenzione sismica nei centri storici umbri dell'alta Val Tiberina. XI Congresso Nazionale "L'ingegneria Sismica in Italia", ANIDIS, Genoa, Italy

Borri A, Grazini A (2004b) Criteri e metodologie per il dimensionamento degli interventi con FRP nel miglioramento sismico degli edifici in muratura. XI Congresso Nazionale "L'ingegneria Sismica in Italia", ANIDIS, Genoa, Italy

Boscato G, Pizzolato M, Russo S, Tralli A (2014) Seismic Behaviour of a Complex Historical Church in L'Aquila. Int J Archit Herit 8(5):718-757

Bow RH (2014). Economics of construction in relation to framed structures. Cambridge University Press

Bracci JB, Kunnath SK, Reinhorn AM (1997) Seismic performance and retrofit evaluation of reinforced concrete structures. Journal of Structural Engineering, 123: 3-10

Brameshuber W, Graubohm M, Meyer U (2012) Druckfestigkeit von Ziegelmauerwerk – aktuelle Auswertungen zur Festlegung von charakteristischen Mauerwerksdruckfestigkeiten in DIN EN 1996. Mauerwerk 16(1): 10–28

Cagnan Z (2012) Numerical models for the seismic assessment of St. Nicholas Cathedral, Cyprus. Soil Dyn and Earthq Eng 39:50-60

Casals A, González JL, Onecha B, Sanmartí C (2011) Las razones del uso masivo de la bóveda tabicada en el Hospital de Sant Pau de Barcelona. Una hipótesis para el debate. Simposio Internacional sobre Bóvedas Tabicadas**.** Valencia

Carbone I, Fiore A, Pistone G (2001) Le costruzioni in muratura. Interpretazione del comportamento statico e tecniche di intervento Milano, Italy: Hoepli

Cardani G (2004) La vulnerabilità sismica dei centri storici: il caso di Campi Alto di Norcia. Linee guida per la diagnosi finalizzata alla scelta delle tecniche di intervento per la prevenzione dei danni. PhD Dissertation Milan, Italy: Technical University of Milan

Cardani G, Binda L (2013) Guidelines for the masonry quality evaluation in built heritage. Built Heritage: Monitoring Conservation Management. Springer International Publishing

Carocci C, Ceradini V, Cremonini I, Panzetta M. (2004) Recupero e riduzione della vulnerabilità dei centri storici danneggiati dal sisma del 1997. Regione Marche, Italy

Casarin F, Modena C (2008) Seismic Assessment of Complex Historical Buildings: Application to Reggio Emilia Cathedral, Italy. Int J Archit Herit 2:304–327

Castellazzi G (2012) Cultural heritage preservation: seismic assessment of a church façade. Proceedings of the 3rd International conference on Urban Sustainability, Cultural Sustainability, Green Development, Green Structures and Clean Cars:145–150

Casolo S, Uva G (2013) Nonlinear analysis of out-of-plane masonry façades: full dynamic versus pushover methods by rigid body and spring model. Earthq Eng Struct D 42:499-521

Cauvin A, Stagnitto G (1993) Problems concerning strength assessment and repair of Historical Vaulted Structures Public Assembly Structures from Antiquity to the Present. Istanbul, Turkey: IASS

Cauvin A, Stagnitto G (1995) Criteria of design and methods of structural analysis of Gothic ribbed vaults using traditional and computer methods Spatial Structures Heritage. Present and Future Padua, Italy: SGE Editoriali

Cedolin L, Dei Poli S, (1977) Finite element studies of shear-critical RIC beams. J. Engrg. Mech.Div. 103(3): 395-410

Cervera M, Chiumenti M, Valverde Q, de Saracibar CA (2003) Mixed linear/linear simplicial elements for incompressible elasticity and plasticity.Computer Methods in Applied Mechanics and Engineering 192(49): 5249-5263

Cennamo C, Bernardino M, Chiaia BM, D'Angelo S, Ferretti D (2011) Seismic Assessment and Rehabilitation of a Historical Theater Based on a Macro-Element Strategy. Int J Archit Herit 5:264–295

Chopra AK (2001). Dynamics of structures: theory and applications to earthquake engineering. Englewood Cliffs, NJ: Prentice Hall

Chopra AK, Goel RK (2002) A modal pushover analysis procedure for estimating seismic demands for buildings. Earthquake Engineering & Structural Dynamics, 31(3): 561-582

Chopra AK, Goel RK (2004) A modal pushover analysis procedure to estimate seismic demands for unsymmetric-plan buildings. Earthquake engineering & structural dynamics, 33(8): 903-927

Cocta s.a. (2010) Informe sobre el ensayo de carga estatica realizado en el forjado planta baja del pabellon administrativo del hospital de sant pau – barcelona. Barcelona Spain: Cotca s.a.

Collins GR (1968) The Transfer of Thin Masonry Vaulting from Spain to America. Journal of the Society of Architectural Historians 27(3): 176-201

Cope RJ, Rao PV, Clark LA, Norris P, (1980) Modelling of reinforced concrete behaviour for finite element analysis of bridge slabs. Numerical Methods for Nonlinear problems 1, Taylor C. et al. (Eds.) Pineridge Press Swansea: 457-470

Corradi M, Grazini A, Borri A (2007) Confinement of brick masonry columns with CFRP materials. Composites science and technology, 67(9): 1772-1783

Croci G (1998) The Basilica of St. Francis of Assisi after the September 1997. Earthquake Structural Engineering International 8(1):56-58

Croci G, Carluccio G, Viskovic A (1998a) Análisis estructural de la Catedral de Santa María Vieja de Vitoria. Primer Congreso Europeo sobre Catedrales Góticas Vitoria, Spain: Diputación Foral de Alava

Croci G, Taupin JL, Viskovic A (1998b) Análisis matemático del derrumbamiento de bóvedas en la catedral de San Pedro de Beauvais. Primer Congreso Europeo sobre Catedrales Góticas Vitoria, Spain: Diputación Foral de Alava

Cundall PA, Hart P (1971) A computer model for simulating progressive large scale movements in blocky rock systems. In: Proc of the symposium of the society of rock mechanics. Nancy, France, vol 1, paper No II-8

Da Porto F, Valluzi M R, Modea C (2003) Investigations for the knowledge of multi-leaf stone masonry walls. Proceedings of the First International Congress on Construction History, Madrid

Dall'Asta A, Zona A (2002) Non-linear analysis of composite beams by a displacement approach. Computers & structures 80(27): 2217-2228

D'Ayala D (2004) Unreinforced brick masonry construction EERI. World Housing Encyclopedia, 2004, world-housing.net

D'Ayala D, Tomasoni E (2008) The Structural Behaviour of Masonry Vaults: Limit State Analysis with Finite Fiction. International Seminar on Structural Analysis of Historical Constructions- SAHC08 Bath, the UK: 47-61

Dayaratnam P (1987) Brick and reinforced brick structures New Delhi, India: Oxford and IBH

De Borst R (1997) Some recent developments in computational modelling of concrete fracture. International journal of fracture 86(1-2): 5-36

De Borst R, Crisfield MA, Remmers JJC, Verhoosel CV (2012) Non-linear finite element analysis of solids and structures second edition. New York: John Wiley & Sons

De Borst R, Sluys LJ, Muhlhaus HB, Pamin J (1993) Fundamental issues in finite element analyses of localization of deformation. Engineering computations 10(2): 99-121

De Cesaris F (1996) Le murature. In Restauro Architettonico. By Giovanni Carbonara. UTET Ed.Torino 2: E2:15-82

De Conti A (2013) Seismic analysis and simulation of collapse mechanism of a masonry church. Master thesis Technical University of Catalonia, University of Padova

D'Espie C (1754) Maniere de rendre toutes sortes d'édifices incombustibles. Paris, France: Duchesne

Dhanasekar M, Kleeman PW, Page AW (1985) Biaxial Stress-Strain Relations for Brick Masonry. Jr. of Structural Engineering 111(5):1085-1100

Doglioni F. (1999) Codice di pratica (linee guida) per la progettazione degli interventi di riparazione, miglioramento sismico e restauro dei beni architettonici danneggiati dal terremoto umbro-marchigiano del 1997. A cura di F. Doglioni, Bollettino Ufficiale Regione Marche, Italy

Doglioni F, Moretti A, Petrini V (1994) Le chiese ed il terremoto. Trieste, Italy: LINT

D'Olivier (1837) Relatif à la construction des voutes en briques posées de piat, suivi du recherehes expérimentales sur la poussée de ces sones des voutes. Annales des Ponts et Chaussées, ler série:292-309

Drougkas A, Roca P, Molins C (2014) Numerical micro-modeling simulation of masonry in compression. 9th International Masonry Conference 2014 in Guimarães

Dvorkin EN, Bathe KJ (1984) A continuum mechanics based four-node shell element for general non-linear analysis. Engineering computations 1(1): 77-88

Eddy HT (1878) Researches in Graphical Statics. New York, USA: Van Nostrand

Elnashai AS (2001) Advanced inelastic static (pushover) analysis for earthquake applications. Structural engineering and mechanics, 12(1):51-70

Elnashai AS (2002) Do we really need inelastic dynamic analysis?. Journal of Earthquake Engineering 6(1): 123-130

European Committee of Standardization (CEN) (1996) Eurocode 6: Design of masonry structures Part 1-1: General rules for buildings -Reinforced and unreinforced masonry. Brussels, Belgium

European Committee of Standardization (CEN) (2002) Eurocode 1: Actions on structures - Part 1-1: General actions -Densities, self weight, imposed loads for buildings. Brussels Belgium

European Committee of Standardization (CEN) (2004) Eurocode 8: Design Provisions for Earthquake Resistance of Structures, Part 1.1: General rules, seismic actions and rules for buildings. Brussels Belgium

Fajfar P, Fischinger M (1987) Non-linear seismic analysis of RC buildings: Implications of a case study. European Earthquake Engineering 1:31-43

Fajfar P, Fischinger M (1988) N2–A method for non-linear seismic analysis of regular buildings. In Proceedings of the Ninth World Conference in Earthquake Engineering 5:111-116

Fajfar P (2002) Structural analysis in earthquake engineering - a breakthrough of simplified nonlinear methods. Proceeding of 12th European conference on earthquake engineering

Fajfar P, Kilar V, Marusic D, Perus I, Magliulo G (2005) The extension of the N2 method to asymmetric buildings. Proceedings of the 4th European workshop on the seismic behaviour of irregular and complex structures

Federal Emergency Management Agency (2004) Improvement of inelastic seismic analysis procedures, FEMA 440, Federal Emergency Management Agency, Washington, D.C.

Ferrini M, Melozzi A, Pagliazzi A, Scarparo S (2003) Rilevamento della vulnerabilità sísmica degli edifici in muratura. Manuale per la compilazione della Scheda GNDT/CNR di II livello. Versione modificata dalla Regione Toscana, Regione Toscana, Italy

Fontaine H (1865) Expériences faites sur la stabilité des Voutes en briques Nouvelles Annales de la Construction 11: 149-159

Galasco A, Lagomarsino S, Penna A (2006) On the use of pushover analysis for existing masonry buildings. Proceedings of first european conference on earthquake engineering and seismology (a joint event of the 13th ECEE and 30th general assembly of the ESC) 3-8

Gambarotta L, Lagomarsino S (1997a) Damage models for the seismic response of brick masonry shear walls part I. Earthquake Engineering and Structural Dynamics, Vol. 26 New York, USA: 423-439

Gambarotta L, Lagomarsino S (1997b) Damage models for the seismic response of brick masonry shear walls part II. Earthquake Engineering and Structural Dynamics, Vol. 26 New York, USA: 441-462

Geoff (2014) Committee for European Standardisation: Technical Committee125. Test Method Development: The First 25 Years. 9th International Masonry Conference 2014 in Guimarães

Ghaboussi J, Barbosa R (1990) Three-dimensional discrete element method for granular materials. Int J Numer Anal Methods Geomech 14:451–472

Giordano A, Mele E, De Luca A (2002) Modelling of historical masonry structures: comparison of different approaches through a case study. Engineering Structures 24(8): 1057-1069

Giuffrè A (1993) Safety and conservation of historical centers: the case of Ortigia. Bari: Laterza. Editori Laterza: Bari

González JL (1999) La bóveda tabicada. Su historia y su futuro. Teoría e historia de la rehabilitación. Teoría e historia de la restauración 1: 237-259

González JL (2005) La bóveda tabicada: entre la conservación y la destrucción. Informes de la Construcción 56(496): 67-72

González JL, Balagué AC, Martínez CS, Pérez BO (2011) Los sistemas de estribado de las bóvedas tabicadas del hospital de Sant Pau Barcelona: tirantes, zunchos y pórticos. In Actas del Séptimo Congreso Nacional de Historia de la Construcción, Santiago de Compostela, 26-29 octubre de 2011 Instituto Juan de Herrera:583-592

González R, Caballé F, Domenge J, Vendrell M, Giráldez P, Roca P, González JL (2008) Construction process, damage and structural analysis. Two case studies. Structural Analysis of Historical Constructions- SAHC08 Bath, the UK: 643-651

González JL, Casals A, Dotor A, García E, Onecha B (2012) A masonry tile dome restoration in Catalonia. Construction History Society of America 3rd Biennial Meeting

Gregory D (1697) Catenaria Philosophical Transactions of the Royal Society vol.19 pp. 637-652

Grieve N (2008) The urban conservation glossary
http://www.trp.dundee.ac.uk/research/glossary/glossary.html
last accessed on 10th of February 2015

Guastavino R (1893) The theory and history of cohesion system. Boston, USA: Ticknor and company

Guinea GV, Hussein G, Elices M, Planas J (2000) Micromechanical modeling of brick-masonry fracture. Cement and concrete research 30(5): 731-737

Gulkan P, Sozen M A (1974) Inelastic response of RC structures to earthquake motion. ACI, 71: 609-614

Gulli R, Mochi G (1995) Bovedas tabicadas: Architeaura e cosrruzione. Rome: COI' Editrice

Gupta AK, Akbar H (1984) Cracking in reinforced concrete analysis. J. Struct. Engng. 110(8): 1735-1746

Gupta B, Kunnath S K (2000) Adaptive spectra-based pushover procedure for seismic evaluation of structures. Earthquake Spectra 16(2): 367-391

Hernandez-Montes E, Kwon OS, Aschheim MA (2004) An energy-based formulation for first-and multiple-mode nonlinear static (pushover) analyses. Journal of Earthquake Engineering 8(01): 69-88

Heyman J (1966) The stone skeleton. International Journal of Solids and Structures, 2:270-279

Heyman J (1982) The masonry arch. Chichester, the UK: EllisHorwood

Hooke R (1676) A Description of Helioscopes and Some Other Instruments London: J. Martyn

Hube MA, Mosalam KM (2009) Experimental and Computational Evaluation of Current and Innovative In-span Hinge Details in Reinforced Concrete Box-girder Bridges: Experimental Findings and Pre-test Analysis. Pacific Earthquake Engineering Research Center

Huerta S (2001) Mechanics of masonry vaults: The equilibrium approach. Historical Constructions Minho, Portugal: University of Minho: 47-70

Huerta S (2003) The Mechanics of Catalan Vaults: A Historical Outline. Essays on the History of Mechanics Berlin, Germany: Birkhauser Verlag: 89-134

Huerta S (2008) The analysis of masonry architecture: a historical approach. Architectural Science Review Sydney, Australia: University of Sydney: 297-328

Huerta S, López MG, Redondo ME (2001). Bibliografía seleccionada y comentada sobre Guastavino y la construcción tabicada. In Las bóvedas de Guastavino en América. S. Huerta (ed.). Madrid: Instituto Juan de Herrera, CEHOPU: 373-393

Indirli MS, Kouris LA, Formisano A, Borg RP, Mazzolani FM (2013) Seismic Damage Assessment of Unreinforced Masonry Structures After The Abruzzo 2009 Earthquake: The Case Study of the Historical Centers of L'Aquila and Castelvecchio Subequo. Int J Archit Herit 7:536–578

International Code Council (2012) International Building Code http://publicecodes.cyberregs.com/icod/ibc/2012/, last accessed on 10th of February 2015

ITACA (2013) Italian Accelerometric Archive http://itaca.mi.ingv.it/ItacaNet/ last accessed on 27th of June 2013

Italian Ministry of Public works (1987) Norme tecniche per la progettazione, esecuzione e collaudo degli edifici in muratura e per il loro consolidamento, D.M. del 20/11/87, Gazzetta Ufficiale 5/12/1987, n. 285

Italian Board of Public works (2008) Spettri-NTC ver 1.03. www.cslp.it last accessed on 27th of June 2013

Italian Ministry for Cultural Heritage and Activities (2011) Guidelines for Evaluation and Mitigation of Seismic Risk to Cultural Heritage. Gangemi, Rome

Italian Ministry of Infrastructure and Transport (2009) Circolare 2 febbraio 2009, n. 617 Istruzioni per l'applicazione delle «Nuove norme tecniche per le costruzioni» di cui al decreto ministeriale 14 gennaio 2008

Jäger W, Pech A (2014) Background of the values for compressive strength of masonry accodring to EC 6–evaluation of data. Mauerwerk, 18(3-4): 229-238

Jan TS, Liu MW, Kao YC (2004) An upper bound pushover analysis procedure for estimating the seismic demands of high rise buildings. Engineering Structures, Vol. 26, pp. 117-128

Jirásek M, Zimmermann T (1998) Analysis of rotating crack model. Journal of engineering mechanics 124(8): 842-851

Kaushik HB, Rai DC, Jain SK (2007) Stress-strain characteristics of clay brick masonry under uniaxial compression J Mater Civ Eng, 19(9): 728–739

Kim S, D'Amore E (1999) Push-over analysis procedure in earthquake engineering. Earthquake Spectra 15(3): 417-434

Kolmar W, Mehlhorn G (1984) Comparison of shear stiffness formulations for cracked reinforced concrete beams. Computer-Aided Analysis and Design of Concrete Structures Damjanic et al. (eds.), Pineridge Press, Swansea: 133-147

Konstantinidis D, Makris N (2005) Seismic response analysis of multidrum classical columns. Earthquake engineering & structural dynamics, 34(10): 1243-1270

Krawinkler H (1995) New trends in seismic design methodology. In: Proceedings of 10th European Conference on Earthquake Engineering, Vienna, Austria, vol. 2. Rotterdam: AA Balkema: 821–830

Krawinkler H, Seneviratna GDPK (1998) Pros and cons of a pushover analysis of seismic performance evaluation. Eng Struct 20(4):452-464

Krenk S (2009) Non-linear modeling and analysis of solids and structures. Cambridge University Press

Kupfer H, Hilsdorf HK, Rusch H (1969) Behaviour of concrete under biaxial stresses J. Am. Concrete Inst. 66(8): 656-666

Lefort T (2000) Advanced pushover analysis of RC multi-storey buildings. Master thesis Engineering

Seismology and Earthquake Engineering Section Imperial College London UK

Lemos JV (1995) Assesment of the ultimate load of a masonry arch using discrete elements. Comput Methods Struct Mason: 294–302

Lemos JV (1998) Discrete element modeling of the seismic behavior of stone masonry arches. In: Pande G et al (eds) Computer methods in structural masonry, 4. E& FN Spon, London: 220–227

Lemos JV (2007) Discrete element modeling of masonry structures. Int J Archit Herit 1(2):190-213

Liberatore D, Marotta A, Sorrentino L (2014) Estimation of clay-brick unreinforced masonry compressive strength based on mortar and unit mechanical parameters. 9th International Masonry Conference 2014 in Guimarães

Litton RW (1975) A contribution to the analysis of concrete structures under cyclic loading. PhD dissertation University of California: Berkeley

Llorens M (2013) Caracterització del comportament de les voltes de l'edifici de l'administració de l'hospital de la santa creu i sant pau, GMK associats, SLP: Barcelona

Lofti HR, Shing PB (1994) Interface model applied to fracture of masonry structures. Journal of Structural Engineering ASCE 120 (1): 63–80

Lourenço PB (1994) Analysis of Masonry Structures with Interface elements, Theory and Applications. Delft, Netherlands: Delft University of Technology

Lourenço PB (1997) An anisotropic plasticity model for quasi-brittle composite shells Computational Plasticity: Fundamentals and Applications. London, the UK: Pinteridge Press

Lourenço PB (1998) Experimental and Numerical Issues in the Modelling of the Mechanical Behaviour of Masonry Structural Analysis of Historical Constructions Barcelona, Spain: CINME

Lourenço PB (2002) Computations on historic masonry structures. Progress in Structural Engineering and Materials 4(3):301-319

Lourenço PB (2005) From Fracture Mechanics to Case Studies: The issue of Cultural Heritage

Lourenço PB, Mendes N, Ramos LF, Oliveira DV (2011) Analysis of Masonry Structures Without Box Behaviour. Int J Archit Herit 5:369–382

Lourenço PB, Ramos LF (2004) Characterization of cyclic behavior of dry masonry joints. Journal of Structural Engineering, 130(5): 779-786

Lourenço PB, Rots JG, Blaauwendraad J (1995) Two approaches for the analysis of masonry structures: micro and macro-modelling HERON, vol. 40 No 4 Delft, Netherland: TNO Building and Construction Research Delft University of Technology pp.314-340

Lourenço PB, Rots JG (1997) A multisurface interface model for analysis of masonry structures. Journal of engineering mechanics, 123(7): 660-668

Lourenço PB, Trujillo A, Mendes N, Ramos LF (2012) Seismic performance of the St. George of the Latins church: Lessons learned from studying masonry ruins. Eng Struct 40:501-518

Lorenzo de San Nicholas F (1639) Arte y Uso de Architectura Primera parte. Madrid: Spain

Macdonald AJ (2007) Structure and architecture. Routledge: London

Magi J (2009) Seismic Vulnerability of Historical Structure Case study: San Marco church in the sequence of 2009 Abruzzo earthquake. Dissertation University of Padova

Mallardo V, Malvezzi R, Milani E, Milani G (2008) Seismic vulnerability of historical masonry buildings: A case study in Ferrara. Engineering Structures, 30: 2223–2241

Manie and Kikstra (2012) Diana Finite Element Analysis User's Manual Version 9.4,4. Deflt: TNO Building and Construction Research

Marini A, Giardina G, Riva P, Giuriani E (2008) Seismic Behaviour of Barrel Vault Systems. VIII International Seminar on Structural Analysis of Historical Constructions - SAHC08, Bath, the UK: 413-421

Martínez G, Roca P, Caselles O, Clapés J (2006) Characterization of the Dynamic Response for the Structure of Mallorca Cathedral. In: Lourenço PB, Roca P, Modena C, Agrawal S (eds) Structural Analysis of Historical Constructions, New Delhi, India

Masonry Standards Joint Committee (MSJC) (2002) Building code requirements for masonry structures, ACI 530-02/ASCE 5-02/TMS 402-02 Detroit: American Concrete Institute, Structural Engineering Institute of the American Society of Civil Engineers, The Masonry Society

Maxwell JC (1864) On reciprocal figures and diagrams of forces Phil. Mag. Series 27: 250–261

McNary WS (1981) Basic properties of clay-unit masonry in compression. Master thesis Colorado, USA: University of Colorado

McNary WS, Abrams DP (1985) Mechanics of masonry in compression. Jr. of Structural Engineering: 857-870

Milani G, Casolo S, Naliato A, Tralli A (2012) Seismic Assessment of a Medieval Masonry Tower in Northern Italy by Limit, Nonlinear Static, and Full Dynamic Analyses. Int J Archit Herit 6:489–534

Milankowitch M (1907) Theorie der Druckkurven Zeitsch für Mathematik und Physik, 55: 1-27

Miltiadou-Fezans A (2008) A multidisciplinary approach for the structural restoration of the Katholikon of Dafni Monastery in Attica Greece. Structural Analysis of Historical Constructions- SAHC08 Bath, the UK: 71-87

Modena C, Valluzzi MR, da Porto F, Casarin F (2011) Structural Aspects of The Conservation of Historic Masonry Constructions in Seismic Areas: Remedial Measures and Emergency Actions. Int J Archit Herit 5:539–558

Modena C, Valluzzi MR, Folli R, Binda L (2002) Design choices and intervention techniques for repairing and strengthening of the Monza cathedral bell-tower", Construction and Building Materials, Special Issue 16(7): 385-395

Modena C, Valluzzi MR, Zenere M (2009) c-Sisma 3.0 PRO Procedura automatica per il calcolo e la verifica di meccanismi di pareti in muratura. User manual. University of Padova, Padova

Mosalam K, Glasco L, Bernier J (2009) Mechanical Properties of Unreinforced Brick Masonry, Section1 Lawrence Livermore National Laboratory

Moseley H (1835) On the equilibrium of the arch. Cambridge Philosophical Transactions 5:293-313

Moya LB (2000) Bóvedas tabicadas. Madrid, Spain: Ministerio de Fomento, Centro de Pubilicaciones

Murcia-Delso J, Das AK, Roca M, Cervera M. (2009) Seismic safety analysis of historical masonry structures using a damage constitutive model. Thematic Conference on Computational Methods in Structural Dynamics and Earthquake Engineering

Mwafy AM, Elnashai AS (2001). Static pushover versus dynamic collapse analysis of RC buildings. Engineering structures 23(5):407-424

Naraine K, Sinha SN (1989) Behavior of brick masonry under cyclic compressive loading Jr. of Structural Engineering 115(6):1432–1445

Naraine K, Sinha SN (1991) Cyclic Behavior of Brick Masonry under Biaxial Compression. Jr. of Structural Engineering 117(5):1336-1355

Ngo D, Scordelis AC (1967) Finite element analysis of reinforced concrete beams. ACI Journal Proceedings 64(3)

NIKER report (2010) Inventory of earthquake-induced failure mechanisms related to construction types, structural elements, and materials (Deliverable 3.1). Padua, Italy: project NIKER

NIKER catalogue (2013) http://www.niker.eu last accessed on 27th of June 2013

Nuroji, Besari, Irman I (2010) Rotated discrete crack model for reinforced concrete structures. 35th Conference on OUR WORLD IN CONCRETE & STRUCTURES: 25 - 27 August 2010, Singapore

Ochsendorf J, Block P (2008a) Lower-bound Analysis of Masonry Vaults. Structural Analysis of Historic Construction London, the UK: Taylor & Francis Group:593-600

Ochsendorf J, Block P (2008b) Lower-bound Analysis of Masonry Vaults. Structure (lecture note) Structural Analysis of Historical Constructions- SAHC08 Bath, the UK

O'Dwyer D (1999) Funicular analysis of masonry vaults. Computer and Structures vol. 73 Amsterdam, Netherlands:187-197

Olivito RS, Stumpo P (2001) Fracture mechanics in the characterisation of brick masonry structures. Materials and Structures 34(4):217-223

Oñate E, Hanganu A, Barbat A, Oller S, Vitaliani R, Saetta A, Scotta R (1995) Structural analysis and durability assessment of historical constructions using a finite element damage model. Structural Analysis of Historical Constructions Barcelona, Spain:189-224

Page AW (1978) Finite element model for masonry. J. Struc. Div. vol.104 Issue 8 Virginia, USA: American Society of Civil Engineers (ASCE):1267-1285

Page AW (1981) The biaxial compressive strength of brick masonry. Proc. Intsn. Civ. Engrs. Part 2:893-906

Page AW (1983) The strength of brick masonry under biaxial compression-tension. Int. J. Masonry Constr 3(1):26-31

Pagnoni T (1994) Seismic analysis of masonry and block structures with the discrete element method. In: Proc 10th European conference on earthquake engineering, vol 3, pp 1674–1694

Pande GN, Kralj B, Middleton J (1994) Analysis of the Compressive Strength of Masonry Given by the Equation $f_k = K*f_b^a*f_j^b$ The Structural Engineer 71(1):7-12

Papa E, Taliercio A (2000) Prediction of the evolution of damage in ancient masonry towers. In: Proc int symposium 'Bridging Large Spans from Antiquity to the Present'. Istanbul:135–144

Papanikolaou VK, Elnashai AS (2005) Evaluation of conventional and adaptive pushover analysis I: Methodology. Journal of Earthquake Engineering 9(06):923-941

Papastamatiou D, Psycharis I (1993) Seismic response of classical manuments—a numerical perspective developed at the Temple of Apollo Bassae, Greece. Terra Nova 5:591–601

Psycharis I, Lemos JV, Papastamatiou D, Zambas C, Papantonopoulos C (2003) Numerical study of the seismic behaviour of a part of the Partenón Pronaos. Earthq Eng Struct Dyn32:2063–2084

Pagnoni T, Vanzi I (1995) Experimental and numerical study of the seismic response of block structures. In: Computer methods in structural masonry:213–222

PCI Industry Handbook Committee. (2004) PCI Design Handbook: Precast and Prestressed Concrete

Pelà L, Aprile A, Benedetti A (2009) Seismic assessment of masonry arch bridges. Eng Struct; 31(8):1777–88

Pelà L. Aprile A. Benedetti, (2013a) Comparison of seismic assessment procedures for masonry arch bridges, Constr Build Mater 38:381-394

Pelà L, Benedetti A, Aprile A, Mangoni E (2013b) Seismic assessment of the Milano Centrale railway station. Int J Archit Herit 7:609-627

Pelà L, Bourgeois J, Roca P, Cervera M, Chiumenti M (2014) Analysis of the Effect of Provisional Ties on the Construction and Current Deformation of Mallorca Cathedral. Int J Archit Herit, DOI: 10.1080/15583058.2014.996920

Peña F, Prieto F, Lourenço PB, Campos Costa A, Lemos JV (2007) On the dynamics of rocking motion of single rigid–block structures. In: Earthquake engineering and structural dynamics: 36(15), 2383-2399

PIET 70 (1971) Obras de fábrica. Prescripciones del Instituto Eduardo Torroja. Consejo Superior de Investigaciones Científicas Madrid: Spain

Pina-Henriques J, Lourenço PB (2006). Masonry compression: a numerical investigation at the meso-level. Engineering Computations, 23(4):382-407

Plujim RVD (1992) Material properties of masonry and its components under tension and shear. Proc. 6th Canadian Masonry Symp., Ed. V.V. Neis, Saskatoon, Saskatchewan:.675-686

Plujim RVD (1993) Shear behavior of bed joints. Proc. 6th North American Masonry Conf., Ed. A.A. Hamid and H.G. Harris, Philadelphia, Pennsylvania:125-136

Plujim RVD (1997) Non-linear behaviour of masonry under tension. Heron vol. 42 No.1 Delft, Netherland: TNO Building and Construction Research Delft University of Technology:25-54

Palizzolo L, Benfratello S, Caffarelli A, Giambanco F, Urso R, (2008) Bòvedas tabicadas: experimental and numerical analysis. High Performance Structures and Materials IV 97: 503-512

Poleni G (1748) Memorie istoriche del/a gran cupo/a del tempio Vaticano. Padova, Italy: N ella Stamperia del Seminario

Ramage MH (2004) Building a Catalan Vault. Massachusetts, USA:MIT press

Rahman MA, Anand SC (1994) Empirical Mohr-Coulomb failure criterion for concrete block-mortar joints. Journal of Structural Engineering 120(8): 2408-2422

Rashid YR (1968) Ultimate strength analysis of prestressed concrete pressure vessels. Nuclear engineering and design 7(4): 334-344

Ramos LF, Lourenço PB (2004) Modeling and vulnerability of historical city centers in seismic areas: a case study in Lisbon. Eng Struct 26(9):1295-1310

Ramos LF, Lourenço PB, Costa AC (2005) Operational modal analysis for damage detection of a masonry construction. “International Operational Modal Analysis Conference 1, Copenhagem, 2005 : proceedings” Aalborg: Aalborg University, ISBN 87-81606-00-1:495-502

Reinhorn A (1997) Inelastic techniques in seismic evaluations. in Seismic Design Methodologies for the Next Generation of Codes, Fajfar P, and Krawinkler H, eds, Bled, Slovenia

Reyes E, Gálvez JC, Casati MJ, Cendón DA, Sancho JM, Planas J (2009) An embedded cohesive crack model for finite element analysis of brickwork masonry fracture. Engineering Fracture Mechanics 76(12): 1930-1944

Roca P (2009) Study of Gothic churches: inspection, monitoring and structural analysis. Tecnología de la rehabilitación y gestión del patrimonio construido, Bilbao Spain: 1-19

Roca P, Cervera M, Gariup G Pelà L (2010) Structural Analysis of Masonry Historical Constructions. Classical and Advanced Approaches. Arc Comput Methods E:17:299–325

Roca P, Cervera M, Pelà L, Clemente R, Chiumenti, M (2012) Viscoelasticity and Damage Model for Creep Behavior of Historical Masonry Structures. The Open Civil Engineering Journal; 6 (Suppl 1-M7):188-199

Roca P, Cervera M, Pelà L, Clemente R, Chiumenti M (2013) Continuum FE models for the analysis of Mallorca Cathedral. Engineering Structures, 46:653-670

Roca P, Massanas M, Cervera M, Arun G (2004) Structural analysis of Küçük Ayasofya Mosque in Ístanbul. In: Structural analysis of historical constructions IV. Balkema, Amsterdam: 679–686

Rots JG (1988) Computational Modeling of Concrete Fracture. PhD thesis, Delft University of Technology

Rots JG (1991) Numerical simulation of cracking in structural masonry Heron vol. 36 Issue 2 Delft, Netherland: TNO Building and Construction Research Delft University of Technology:49–63

Rots JG, Blaauwendraad J (1989) Crack models for concrete, discrete or smeared? Fixed, multi-directional or rotating?. HERON 34(1)

Rots JG, Nauta P, Kusters GMA (1984) Variable reduction factor for the shear stiffness of cracked concrete *Rep. B/-84-33,* Inst. TNO for Building Mat. and Struct., Delft

Rots JG, Nauta P, Kusters GMA, Blaauwendraad J (1985) Smeared crack approach and fracture localization in concrete. *HERON* 30(1):1-48

Saiidi M, Sozen MA (1981) Simple nonlinear analysis of RC structures. ASCE. Struct. Div.. 107(5):937-951

Saloustros,S Pelà L, Roca P, Portal J (2015) Numerical analysis of structural damage in the church of the Poblet Monastery. Engineering Failure Analysis 48:41–61

Sasaki K, Freeman SA, Paret TF (1998) Multimode pushover procedure (MMP)—A method to identify the effects of higher modes in a pushover analysis. In Proceedings of the 6th US National Conference on Earthquake Engineering, Seattle, Washington

Schlegel R, Rautenstrauch K (2004) Failure analysis of masonry shear walls. Numer Model Discrete Mater:15–18
Schubert P (1988) The influence of mortar on the strength of masonry. Proc. 8th Int. Brick and Block Masonry Conf., Ed. J.W. de Courcy, Applied Science:162-174

Selby RG, Vecchio FJ (1993) Three-dimensional Constitutive Relations for Reinforced Concrete. Tech. Rep. 93-02, Uniiversity of Toronto, Department of civil engineering, Canada

Silva B, Magi J, Casarin F, Modena C, Condoleo P, Cardani G, Binda L (2010) Assessment of the San Marco church structural behaviour in sequence of the April 2009 earthquake in Abruzzo (Italy). 8th International Symposium on the Conservation of Monuments in the Mediterranean Basin Patras, Greece

Silva B, Magi J, Casarin F, Modena C, Valluzzi MR, Binda L, Condoleo P (2011) Chiesa di San Marco all'Aquila. Valutazione preliminare dei danni. L'università e la ricerca per l'Abruzzo – Il patrimonio culturale dopo il terremoto del 6 aprile 2009:78-85

Sincraian GE (2001) Seismic behaviour of blocky masonry structures. A discrete element method approach. PhD Dissertation Lisbon: Technical University of Lisbon

Spanish ministry of development (2002) Norma de construccion sismoresistente NCSE-02 BOE No 244 Madrid: Spain

Spanish ministry of development (2009) Documento basico SE-AE Seguridad Estructural Acciones en la edificación Madrid: Spain

Suter GT, Margaret LT, Fontaine L (1998) Mortar Study of Mechanical Properties for the Repointing of the Canadian Parliament Buildings. APT Bulletin 29(2):51-58

Sutcliffe DJ, Yu HS, Page AW (2001) Lower bound limit analysis of unreinforced masonry shear walls. Comput Struct 79(14):1295–1312

Tesarik DR, Seymour JB, Yanske TR (2009) Long-term stability of a backfilled room-and-pillar test section at the Buick Mine, Missouri, USA. International Journal of Rock Mechanics and Mining Sciences 46(7):1182-1196.

Theodossopoulos D, Sinha BP (2004) Function and technology of historic cross vaults. Structural Engineering and Materials, 6:10-20

Theodossopoulos D, Sinha BP Usmani AS, Macdonald AJ (2002) Assessment of the structural response of masonry cross vaults., Journal of the British Society for Strain Measurement 38(3):119–127

Truñó Á (2004) Construcción de bóvedas tabicadas. Madrid, Spain: Instituto Juan de Herrera Escuela Técnica Superior de Arquitectura

Valluzzi MR (2007) On the vulnerability of historical masonry structures: analysis and mitigation. Materials and structures 40(7):723-743

Valluzzi MR, da Porto F, Casarin F, Monteforte N, Modena C (2009) A contribution to the characterization of masonry typologies by using sonic waves investigations. In Proc., 7th Int. Symp. in Non Destructive Testing in Civil Engineering (pp. 713-718). Nantes, France: LCPC

Valluzzi MR, da Porto F, Modena C (2004) Behavior and modeling of strengthened three-leaf stone masonry walls. RILEM Materials and Structures, MS 267, Vol. 37, April 2004:184-192

Vasconcelos G, Lourenco PB (2009) Experimental characterization of stone masonry in shear and compression. Constr Build Mater 23:3337–45

Vecchio FJ, Collins MP (1986) The modified compression-field theory for reinforced concrete elements subjected to shear. ACI J. 83(2): 219-231

Vermeltfoort AT (2005) Brick–mortar interaction in masonry under pressure. PhD Dissertation Netherlands: Eindhoven University of Technology

Vintzileou E, Miltiadou-Fezans A (2008) Mechanical properties of three-leaf stone masonry grouted with ternary or hydraulic lime-based grouts. Engineering Structures 30(8): 2265-2276

Virdi K.S. and Rossen D. Rashkoff, R. D. (2013) Low-rise residential construction detailing to resist eatthquakes available at http://www.staff.city.ac.uk/earthquakes/MasonryAdobe/index.php (assessed on the 13th of Febrary, 2014)

Windsor Pin Test system (2010) Windosr Pin System Instructions available at http://www.ndtjames.com/Windsor-Pin-System-p/w-p-2000.htm#Instructions (assessed on the 13th of Febrary, 2014)

Wright GR (2009) Ancient Building Technology, Volume 3: Construction (2 Vols). Brill

Zienkiewicz OC, Taylor RL (2005) The finite element method for solid and structural mechanics. Butterworth-heinemann

Zijl van GPA.G (2000) *Computational Modelling of Masonry Creep and Shrinkage*. PhD thesis, Delft University of Technology

Zografou A (2010) Structural Modeling of masonry structures severely damaged by earthquake Case study of St.Marco's church in L'Aquila. Master thesis Padova: University of Padova

Zucchini A, Lourenço PB (2002) A micro-mechanical model for the homogenization of masonry. Int J Solids Struct 39:3233–3255